Application of Concurrent Development Practices to Petrochemical Equipment Design

Franklin D. Lomax, Jr.

Virginia Polytechnic Institute and State University

Doctor of Philosophy
Mechanical Engineering

Graduate Committee
D. J. Nelson, PhD., Chair
M.W. Ellis, PhD
Y.A. Liu, PhD
M.R. von Spakovsky, PhD
U. Vandsburger, PhD

March 16, 2001
Blacksburg, Virginia, USA

Keywords: fuel cell, steam reformer, concurrent engineering, hydrogen

Application of Concurrent Development Practices to Petrochemical Equipment Design

Franklin D. Lomax, Jr.

Abstract

Principles of concurrent development are applied to the design of a small-scale device for converting natural gas or liquefied petroleum gas into hydrogen. The small hydrogen generator is intended for serial production for application in the production of industrial hydrogen, fueling stationary fuel cell power systems and refueling hydrogen-fueled fuel cell electric vehicles. The concurrent development process is contrasted with the traditional, linear development process for petrochemical systems and equipment, and the design is benchmarked against existing small hydrogen generators as well as industrial hydrogen production apparatus. A novel system and hardware design are described, and a single cycle of concurrent development is applied in the areas of catalyst development, thermodynamic optimization, and reactor modeling and design. The impact of applying concurrent development techniques is assessed through economic modeling, and directions for future development work are identified.

Acknowledgements

The work described in this study was wholly funded by, and is the intellectual property of Directed Technologies Inc.. Special thanks are thus due to Ira F. Kuhn, Jr., president of Directed Technologies Inc., who possessed the vision to commission this work beginning in 1996. Because of the unusual circumstances surrounding commercially-funded doctoral research, my advisor, Doug Nelson, also deserves special recognition for helping to navigate this process without compromising my legal and ethical responsibilities. Likewise, the other members of my committee have made special efforts to facilitate this process, and I am in their debt. The text of this study is subject to binding confidentiality agreements between the members of my committee, the author, and Directed Technologies Inc. until March 16, 2006.

Like all students, I am indebted to many persons who have inspired, consoled, encouraged and assisted me throughout the process of conducting the research described in this study. Eric Kruszewski and Stephen Gurski provided invaluable assistance in building and operating the test apparatus at Virginia Tech. Jonathan Ho, Jason Barbour, John Reardon and Stephen Waide of Directed Technologies Inc. all assisted in invaluable ways in the development and implementation of the chemical process and reactor described here. Jon Wagner and his colleagues at Sud-Chemie, Inc. provided valuable cooperation in the catalyst development effort, and provided samples for testing described herein. All of my colleagues at Directed Technologies Inc. have assisted at various times by providing their valuable insight and commentary, not the least in proofreading this document. Throughout my life, and especially during the past few years, the unswerving support of my friends and family have formed the bedrock foundation upon which I have built all that I've accomplished, or will accomplish in the future. Without them, I'd be but a pale reflection of myself.

Table of Contents

Chapter 1 Introduction....1
Chapter 2 Literature review and foundations 8
2.1 Industrial-scale catalytic steam reforming....8
2.2 Current small-scale reforming technology 16
2.3 The DTI steam reforming process, concurrent design in action....24
2.3.1 Product requirements and design philosophy 24
2.3.1 General process selection considerations 27
2.3.1 The DTI steam reforming process 33
Chapter 3 Catalyst development and testing 37
3.1 Catalyst design....37
3.1.1 Metal and support effects on activity....38
3.1.2 Catalyst aging 44
3.1.3 Sulfur tolerance of candidate catalysts 47
3.1.4 Conclusions on Catalyst Design....53
3.2 Catalyst testing....54
3.2.1 Test apparatus and methodology 54
3.2.2 Catalyst test results 60
3.3 Catalyst conclusions 69
Chapter 4: Thermodynamic Modeling 70
4.1 Model architecture and parameters....72
4.2 Thermodynamic modeling results and discussion....75
4.2.1 Impact of reactor parameters on system efficiency....75
4.2.2 Impact of burner temperature on system efficiency....77
4.2.3 Detailed modeling using version 3.4 81
4.3 Thermodynamic modeling conclusions 82
Chapter 5 Reactor Design, Costing, Build and Test....83
5.1 Chemical reactor modeling....83
5.1.1 Model formulation and structure....83
5.1.2 Reactor modeling results 90
5.2 Mechanical design and manufacturing cost....99
5.2.1 Selection and sizing of the reformer tubes 99
5.2.2 1/3rd-scale pilot reactor design and fabrication....107
5.2.3 Manufacturing cost estimates for the integrated reformer....108
5.3 1/3rd-scale pilot reactor test system, results and observations 120
Chapter 6 Economic analysis 125
Chapter 7 Conclusions and Recommendations 132
7.1 Conclusions....132
7.2 Recommendations....135
References 137
Appendix 143
Vita 181

List of Figures

Figure 1.1: Cost of hydrogen from various sources 2
Figure 1.2: Air Product's Carson, CA hydrogen plant, 237 tonnes per day of hydrogen 3
Figure 1.3: Existing small hydrogen generation technology 4
Figure 1.4: Traditional, linear development process for chemical plants 4
Figure 1.5: Proposed concurrent development process for chemical engineering 5
Figure 2.1: Typical industrial cost and performance of hydrogen production technologies 9
Figure 2.2: Typical modern industrial catalytic steam reformer process flowsheet from Encyclopedia of Chemical Technology, 1995 11
Figure 2.3: Topsoe primary reformer furnace from Rostrup-Nielsen, 1984 14
Figure 2.4: Metal membrane performance 31
Figure 3.1: Turnover frequency vs. temperature for water-gas shift catalysts 42
Figure 3.2: "Volcano" plots for methanation and water-gas shift on different metals 43
Figure 3.3: Correlation between hydrogen sulfide heat of adsorption and bulk sulfide heat of adsorption (from Wise, *et al*, 1985, p. 45) 48
Figure 3.4: Equilibrium P_{H2}/P_{H2S} for bulk metal sulfide reactions 50
Figure 3.5: Metal sulfide equilibria for important steam reforming metals 51
Figure 3.6: Sulfide equilibria for important water-gas shift metals 52
Figure 3.7: Flow schematic for laboratory micro-reactor catalyst test stand 55
Figure 3.9: Curve fits to activity (k_{CH4}) data for screened catalysts 62
Figure 3.10: Arhennius plot of screening test data 63
Figure 3.11: Arhennius plot of mixed gas activity (k_{CH4}) results for FCR-10 64
Figure 3.12: Comparison of the mixed-gas test results for FCR-10 and FCR –9a 65
Figure 3.14: Results of endurance testing of FCR-10 68
Figure 4.1: Thermodynamic process model flowsheet, version 3.4 71
Figure 4.2: HyQuestor 600-series PSA recovery map 73
Figure 4.3: Model version 3.1 trade study results 76
Figure 4.4: Blower airflow versus reactor temperature and burner exhaust temperature 78
Figure 4.5: Steam reformer LMTD versus burner temperature for a 775C reformer outlet 79
Figure 4.6: Energy consumption of the air blower 80
Figure 5.1: Typical temperature profiles generated by the steam reforming model 90
Figure 5.2: Impact of tube diameter and baffle spacing on reactor performance 91
Figure 5.3: Impact of shell diameter and tube spacing on reactor performance 93
Figure 5.4: Impact of burner and reformer temperature on reactor performance 95
Figure 5.5: Typical water-gas shift model temperature profiles 97
Figure 5.6: Concentration profiles (kPa) in the water-gas shift reactor 98
Figure 5.7: Allowable stress versus temperature for candidate alloys 100
Figure 5.8: ASME wall thickness allowables for 12.7 mm o.d. reformer tubes 101
Figure 5.9: Raw oxidation data for candidate superalloys 103
Figure 5.10: Estimated corrosion allowances for 10-year continuous operation 103
Figure 5.11: Total tube wall thickness versus burner temperature for candidate alloys 104
Figure 5.12: Reformer tube material cost per unit length for different alloys 105
Figure 5.13: Line drawing of the 1/3rd-scale pilot reactor 106

Figure 5.14: Estimated reformer tube cost per linear foot vs. reformer and combustor peak temperatures (2000US$) 111
Figure 5.15: Reactor assembly process flow diagram 115
Figure 5.16: Relative cost contribution to example reformer cost 118
Figure 5.17: Reactor cost versus combustor temperature, reformer temperature and tube diameter (2000US$) 118
Figure 5.18: 1/3rd-scale reactor installed in test chamber w/o insulation 121
Figure 5.19: Predicted and measured temperature profiles in the reactor 123
Figure 6.1: Results of the baseline economic trade study at 10-year lifetime for various reformer and combustor peak temperatures 129
Figure 6.2: Results of the energy price trade study at 10-year system lifetime 130

List of Tables

Table 2.1: Simplified molar balances for steam reforming and autothermal reforming 29
Table 2.2: Comparison of hydrogen purification techniques 30
Table 3.1: Relative activity of noble metals for steam reforming hydrocarbons 39
Table 3.2: Temperature ranges for the onset of sintering 45
Table 3.3: Data recorded in catalyst tests 56
Table 3.4: Composition of the catalyst feedstreams 58
Table 4.1: detailed simulation results from version 3.4 81
Table 5.1: Parameter space for reactor design optimization 91
Table 5.2: Preliminary steam reformer trade study results 92
Table 5.3: Final steam reformer cases for cost estimation 96
Table 5.4: Final water-gas shift cases for cost estimation 96
Table 5.5: Example bill of materials for the reactor assembly 109
Table 5.6: Calculation of tube manufacturing costs from supplier quotations 110
Table 5.7: Estimated manufacturing cost at a life volume of 500 units 112
Table 5.8: Representative reactor bill of materials with materials and manufacturing costs and markup 114
Table 5.9: Reactor cost estimates 119
Table 5.10: Laboratory flow capabilities relative to design values on January 7, 2001 122
Table 6.1: Projected balance of plant costs for the steam reformer system 126
Table 6.2: Economic parameters employed 127
Table 6.3: Example economic calculation results using the baseline assumptions 128
Table 6.4: Alternate energy case assumptions 128

Nomenclature

a_i	activity of the species i
A	area
C_p	constant-pressure specific heat
D_{part}	diameter of a catalyst particle
D	tube outer diameter
e	tube factor from ASME code
G_i^0	Gibb's energy of formation for the species i
H	enthalpy
H_i^0	enthalpy of formation of the species i
J	hydrogen permeability
k_i	reaction rate coefficient for the consumption of species I
K, K_i, K_{eq}	equilibrium constant
L	length
LHV_i	lower heating value of the species i
MW_i	molecular weight of the species i
$\dot{n}_i$	molar flowrate of species i
p_i	partial pressure of the species i
P	total pressure
P^0	standard pressure
P_i	power of the i^{th} process
r_p	pressure ratio
r_t	residence time
R_i	thermal resistance of the i^{th} component
R_u	universal gas constant
t	time
t, t_w	thickness of membrane and tube wall respectively
T, T_i	temperature
U	superficial velocity
U_{oa}	overall heat-transfer coefficient
V	volume
y_i	mole fraction
θ	fractional surface coverage of the catalyst
ν_i	stoichiometric number of the i^{th} species
Φ	bed void fraction
γ	ratio of gas specific heats
ρ	density
η, η_i	efficiency

Chapter 1 Introduction

Fuel cell electric vehicles (FCEV's) utilizing polymer electrolyte (or proton exchange) membrane (PEM) fuel cells are now recognized as a potential replacement for internal combustion engine vehicles. The shift towards FCEV's is motivated by the potential reduction in tailpipe emissions, climate change gases, and reliance upon imported petroleum. It has been suggested that hydrogen-fueled FCEV's will maximize these benefits, and will provide the lowest vehicle cost[1] of all potential FCEV configurations. Unfortunately, market penetration of hydrogen-fueled FCEV's will be very slow unless an adequate hydrogen infrastructure is in place to refuel the vehicles at a cost per vehicle mile competitive with other alternative fueled vehicles and conventional vehicles. In order to facilitate market penetration, previous studies have established that mass-manufactured hydrogen refueling appliances could offer a viable alternative to hydrogen delivered through the conventional infrastructure. This result is illustrated in Figure 1.1, which shows the results of an industry-government hydrogen infrastructure study conducted under the aegis of the Ford Motor Company and the U.S. Department of Energy[2].

The data of Figure 1.1 show that small, mass-produced hydrogen generators offer the most attractive economics of all the potential option studied for delivering hydrogen to FCEV's. However, the calculations assume that high volume manufacturing will reduce the cost of the hydrogen generators. For this to happen, it will be necessary to apply the techniques of the commercial manufacturing sector to the established business of generating hydrogen. It will be posited below that this represents a major change in the standard practices of the chemical engineering industry, and requires a shift from traditional practices to concurrent engineering.

Traditional chemical engineering projects are approached in a roughly linear fashion. To some extent, this is a result of the disparate skills involved in the development of a complete, field-fabricated, industrial-scale chemical plant such as the hydrogen generation plant pictured in Figure 1.2. As evidenced in the figure, a traditional plant is comprised of numerous individual elements, each of which is far too large to be transported by rail or road transport, which must be fabricated on site after a detailed engineering site design. Often, the cost of the field fabrication alone equals the cost of all of the process components. The construction of the plant in Figure 1.2 required over 17 months, and $80 million for a plant capable of delivering 237 tonnes per day.

This approach contrasts sharply with a manufacturing environment producing even a few hundred hydrogen appliances a year. In this environment, each refueling appliance would

---

[1] James, B.D., Lomax, F.D., Thomas, C.E., Colella, W.G., PEM Fuel Cell Power System Cost Estimates: Sulfur-Free Gasoline Partial Oxidation and Compressed Direct Hydrogen, 10/17/97

[2] Thomas, C.E., James, B.D., Kuhn, I.F., Lomax, F.D., Baum, G.N., Hydrogen Infrastructure Report, July 1997.

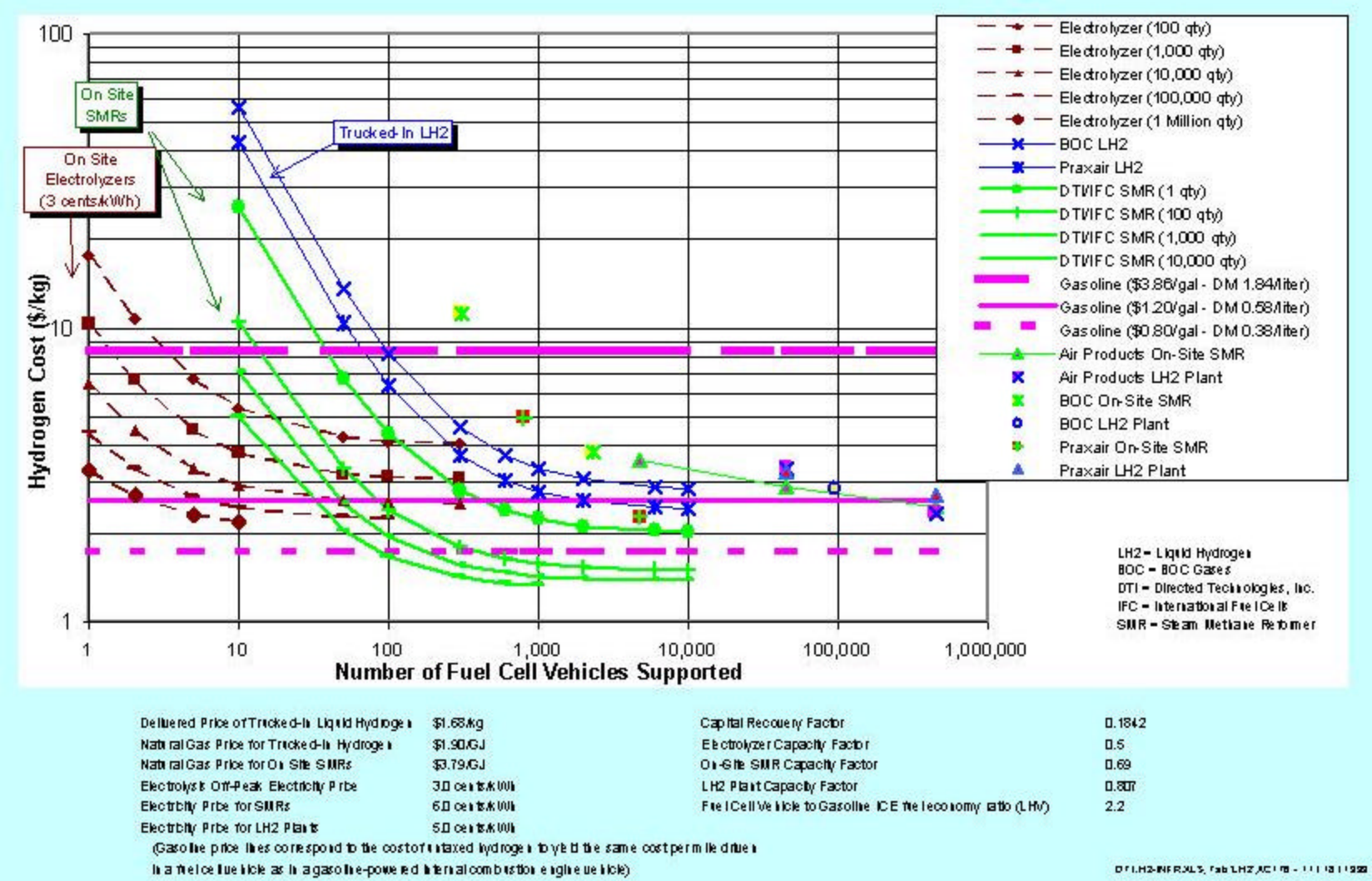

Figure 1.1: Cost of hydrogen from various sources

Figure 1.2: Air Product's Carson, CA hydrogen plant, 237 tonnes per day of hydrogen

require a day or less to manufacture, and perhaps a day to test. Then, the turn-key unit would be freighted to the customer who could install the plant on a simple concrete pad, connect to local utilities, and be operational in a few working days. This clearly represents a paradigm shift in the chemical process industry, a point further emphasized when existing small-scale hydrogen generators are considered. An example of an existing small system is shown in Figure 1.3, which illustrates a Hydrogen Burner Technologies (also known as Phoenix Gas) system installed at the Sunline Transit Authority.

Figure 1.3: Existing small hydrogen generation technology

The small system depicted in Figure 1.3 obviously shares much in common with its far larger cousin in Carson, CA. Both require extensive field plumbing and site preparation, both employ many obvious unit processes, and neither is obviously oriented towards manufacture in volume. These features are somewhat necessary in the industrial plant with enormous subsystems, but cannot be tolerated if a low-cost product is to be obtained. The traditional process development cycle for industrial chemical engineering projects is illustrated in Figure 1.4.

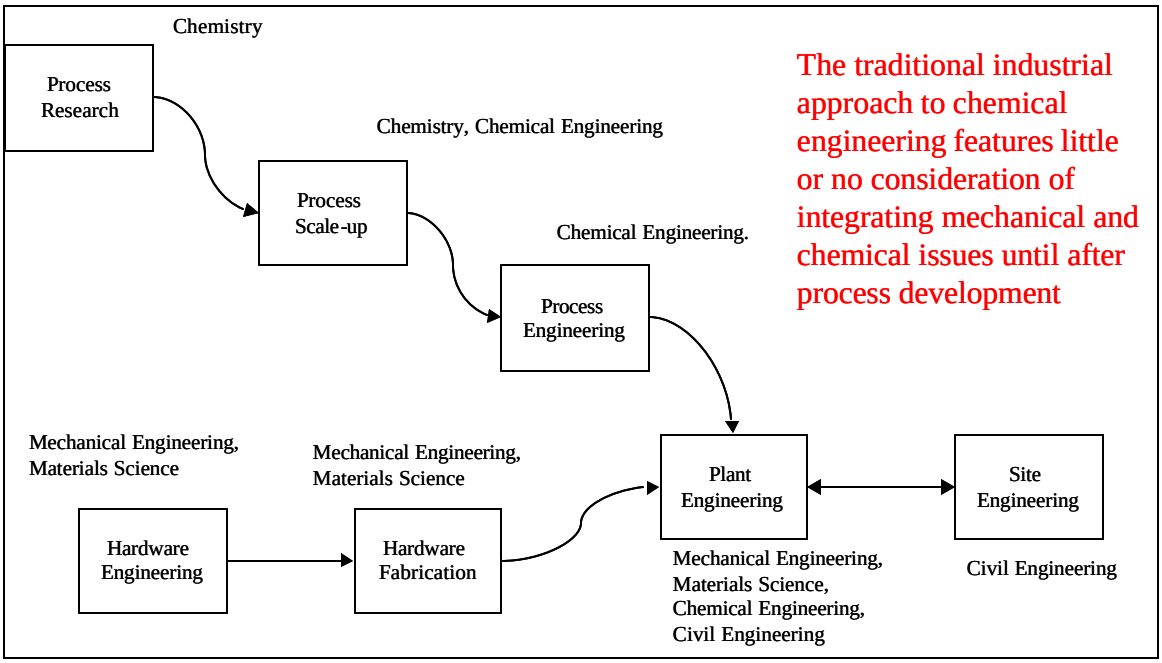

Figure 1.4: Traditional, linear development process for chemical plants

In the traditional process development cycle, the actual chemical process involved in generating the hydrogen is fixed long before the plant design is ever considered. Industrially in the hydrogen business, the basic catalytic chemistry is developed by catalyst manufacturer's such as Haldor-Topsoe, ICI or Sud-Chemie, Inc. The chemical engineering of the reactor in which the chemical process is conducted is then handled by a separate group. In the hydrogen industry, this is done either by Haldor-Topsoe, KCI or Krupp-Udahl. These reactor developers then work with the actual customer to design the overall plant implementation. Commonly, hydrogen plants are actually owned by a specialty gas supplier such as Air Liquide, British Oxygen, Praxair or Air Products. Often, these specialty gas suppliers design the gas purification systems, transmission networks and liquefaction systems if required. All of the significant mechanical subsystems are designed and supplied by outside vendors, including heat exchangers, compressors, pumps, pressure vessels and the like. These components, which may themselves be too large to ship unassembled, are then erected in the field. Only when the actual field erection is considered does a team of engineers representing the various companies work together to implement the design. The worst feature of this system is that although the core design may be re-used, the site engineering and implementation change every time a system is implemented. Further, the site engineers have little ability to simplify the system through innovations in chemistry or chemical engineering, as these activities are already completed when the actual field implementation is being considered.

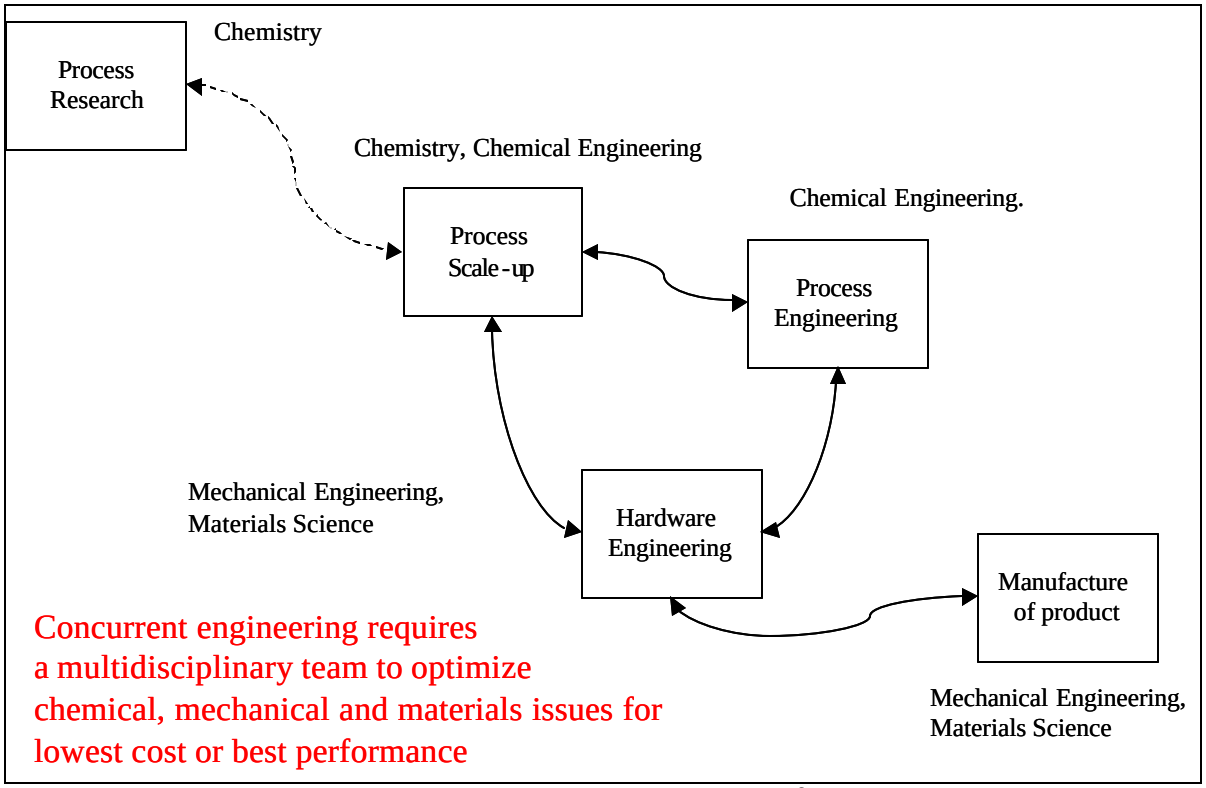

Figure 1.5: Proposed concurrent development process for chemical engineering

An alternative to the linear, or "over-the-wall" system described above has gained increasing acceptance in businesses where a large volume of similar components are to be

manufactured[3]. This approach, which is at it's heart multidisciplinary and team-based, has been referred to under many pseudonyms. Perhaps the most popular is concurrent engineering or concurrent development. This approach is widely credited with the reduction in development time for U.S. car manufacturers for new models from 6 years to 3 years, and has yielded similar successes in other product-oriented businesses[4]. Schey's textbook on manufacturing describes the process of concurrent development as follows:

> …succeeds only when the team has a clear mandate and the full support of management. Within the team, each member has a different expertise, but the team functions best if all members have at least a general appreciation of problems and solutions. Smaller companies may not even have a sufficient number of experts to create formalized teams, and then a small group or even an individual may have to provide all input. In view of the vast range of manufacturing processes available, this may seem an impossible task. Fortunately, there are physical principles that can be invoked across a wide range of processes[5]…

Though Schey is describing a conventional product development environment where mechanical engineering, materials science and possible electrical engineering skills intersect, there is no reason to believe that the same philosophy of design cannot be applied to the more diverse problems inherent to the design of a chemical process plant. Indeed, all that would be required is to include the required chemistry and chemical engineering skills in the concurrent design team.

The application of the concurrent development strategy to the chemical engineering process would fundamentally alter the flow diagram shown in Figure 1.4, and a proposed process flow schematic is shown in Figure 1.5. The major changes envisioned are closer integration of the mechanical and chemical engineering portions of the design process, with a clear and early interaction between the engineering implementation and the fundamental process chemistry as well as the actual product manufacture. It may seem premature to consider manufacturing issues during the development phase of a project, however it has been shown in manufacturing industries that over 70% of the final product cost is determined in the early design phase[6].

The application of the proposed concurrent development process to the problem of the design of a hydrogen refueling appliance is the goal of this project. This study details the first complete iteration of the concurrent design process, and details the various parts of the process independently, then synthesizes the elements into an overall set of conclusions. Directed Technologies Inc. has formed a spin-off company named H2Gen Innovations, to complete the latter iterations of this concurrent development process and to bring the hydrogen refueling appliance technology to market. Thus, the design activities described in this study are the foundation for the formation of the type of multi-disciplinary team envisioned by Schey, and hopefully point the way towards a speedy and cost-effective product development.

---

3 Boothroyd, G., Dewhurst, P., Knight, W., Product Design for Manufacture and Assembly, 1994, p. 3.
4 Schey, J.A., Introduction to Manufacturing Processes: Third Edition, 2000, p. 29.
5 Schey, 2000, p.30.
6 Boothroyd, et al, 1994, p. 2.

The study presented here first reviews current and historical industrial practice for hydrogen production, then reviews extant work on small-scale hydrogen generators by other workers. Then, a new system and improved hardware for small-scale hydrogen generation is formulated based on the application of concurrent engineering principals. This novel system and hardware was developed by the author while working for Directed Technologies, Inc., and is the subject of a pending U.S. patent applications which is attached as an appendix to this study. The concurrent development of this improved system and hardware is detailed in three areas: catalyst development, thermodynamic optimization, and chemical reactor simulation and design. As indicated by Schey, this concurrent development effort involved only the author, and thus the complete thought process involved is related in this document. The results of the three parallel research efforts are then synthesized through an economic analysis to identify design choices which yield the lowest realized cost for the delivered hydrogen, thus completing what is defined in this study as a single cycle of the continuous development process. Finally, directions for research in the next cycle of the concurrent development process are identified. It will become clear in reading this study that the ability to consider all of the aspects of the system and hardware design does yield rather impressive benefits relative to the linear approach typically employed in chemical process design.

Chapter 2 Literature review and foundations

As of 1995, the annual U.S. consumption of hydrogen was 1.2 ExoJoules, or 1.1 quad. Of this hydrogen, 94% was used for petroleum refining, ammonia synthesis and methanol synthesis. Of the hydrogen used in ammonia plants in the U.S., which was 49% of the total hydrogen generated and consumed, 97% was generated using catalytic steam reforming of natural gas[7]. The enormous scale of hydrogen production and use certainly suggests that the technology of hydrogen production is highly evolved.

Indeed, the technology for the large, centralized, industrial production of hydrogen is extremely refined, and several excellent literature reviews are available[8]. Therefore, an exhaustive description of all of the available industrial hydrogen production technologies will not be attempted here. Instead, the evolution and current practice of industrial catalytic steam reforming will be described. Then, a review of the pertinent patent literature of small-scale hydrogen generation will be conducted, in order to establish a baseline understanding of current trends in the design of small-scale hydrogen generators. Finally, a scoping analysis will be conducted which will show qualitative and quantitative factors involved in the development of a novel steam-reforming process for small scale hydrogen production devised by the author with the support of Directed Technologies Inc.. This novel process will form the basis for the concurrent engineering process described in this study, and is described in detail in the pending U.S. patent application shown in Appendix.

2.1 Industrial-scale catalytic steam reforming

Hydrogen has long been an important industrial chemical, and its production predates the widespread use of catalytic processes for chemical synthesis. In the 19th and early part of the 20th century, hydrogen was extensively produced by steam quenching of coal in coke manufacture, resulting in a hydrogen-bearing mixture referred to as coke oven gas or town gas. In the past, this gas was used extensively for domestic heating and cooking, and was actually conveyed in caulked wooden piping systems. Coke oven gas manufacture and the reaction of iron with steam were the two main routes for hydrogen synthesis well into 20th century[9].

In the first half of the 20th century, rapid progress in the application of catalytic processes to chemical synthesis began to yield dividends for hydrogen production, and the first catalytic steam reforming plant was installed by Standard Oil in Baton Rouge, LA in 1930[10]. After this point, the steam reforming process expanded rapidly in markets where light feeds were available economically, such as North America. For markets where heavy feeds are the norm, partial

---

7 "Hydrogen," Encyclopedia of Chemical Technology: 4th edition, 1995, pp. 878-884.

8 See above and "Hydrogen," Ullmann's Encyclopedia of Industrial Chemistry: 5th edition, 1989, pp. 297-442.

9 "Hydrogen," 1995, p.866.

10 Rostrup-Nielsen, J.R., Catalytic Steam Reforming, Reprint from Catalysis-Science and technology, 1984, pp. 11.

oxidation reformers of either the Texaco or Shell process are employed. In countries where coke production is still an economically important activity, hydrogen is still generated as a byproduct of coke manufacture. Finally, water electrolysis accounts for a small fraction of worldwide capacity. As of 1995, the worldwide production split for hydrogen was 77% from natural gas and petroleum, 18% from coal, 4% by water electrolysis and 1% by other means[11]. Of the natural gas/petroleum fraction, steam reforming is undoubtedly the world-wide leader in converting light feed fractions. This trend can be better understood when comparative cost and efficiency figures for the competing processes are considered, these are shown here in Figure 2.1

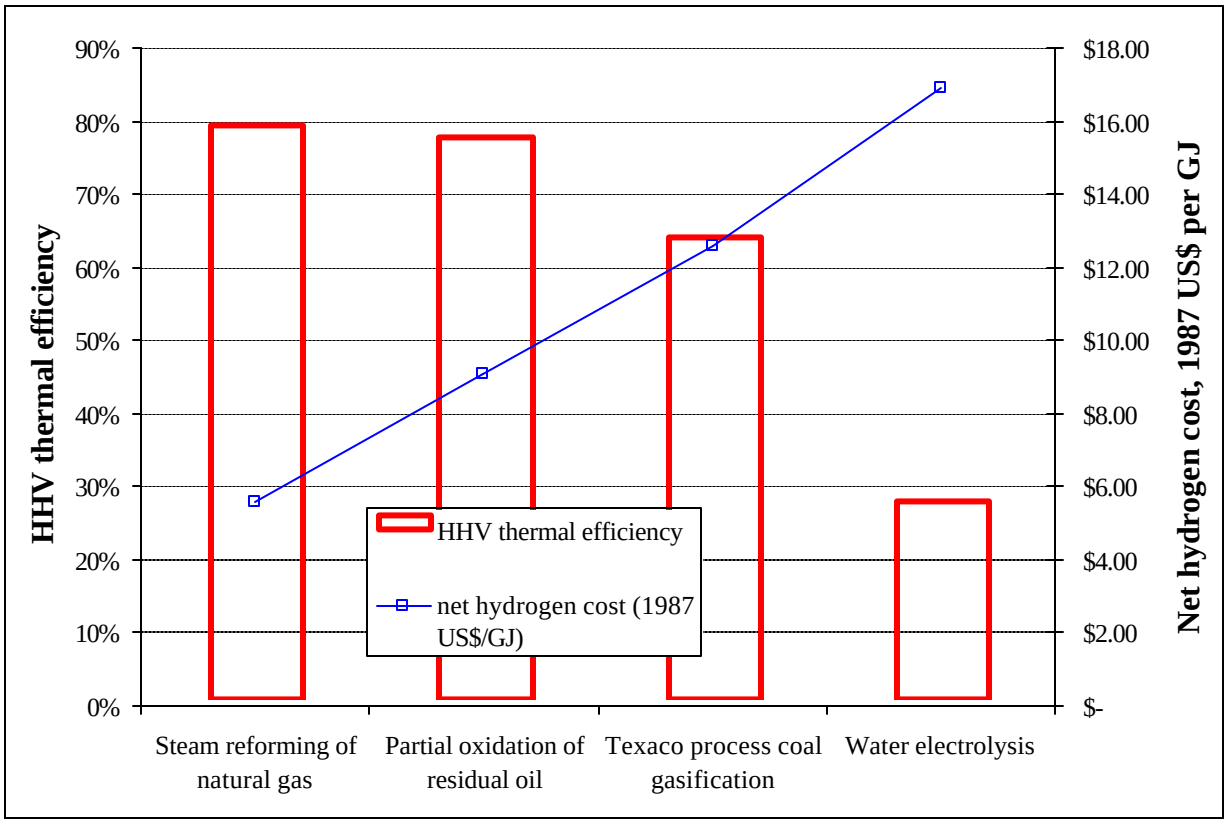

Figure 2.1: Typical industrial cost and performance of hydrogen production technologies[12]

Thus, the predominance of catalytic steam reformers in industrial practice is driven by high thermal efficiency and low overall product cost. It is interesting that the partial oxidation process results in more expensive hydrogen, as it does not generally use a catalyst in the main reactor, uses very inexpensive residual oil feedstock, and has a fairly good thermal efficiency. These are all factors which should reduce cost. The difference in cost is accrued because air separation is required to achieve the thermal efficiency noted in Figure 2.1, and air separation plant capital and operating costs make the economics of the partial oxidation process less attractive[13]. The same may be said of coal gasification, which likewise requires air separation for effective performance.

---

11 "Hydrogen," 1995, p.852.
12 "Hydrogen," 1995, p.853.
13 "Hydrogen," 1989, p. 314-318.

Although catalytic steam reforming has been the preferred industrial synthesis route for many years, the means of purification for the hydrogen produced has changed radically in the last half of the 20th century. Originally, no means of hydrogen purification was available, and the only route to producing relatively pure hydrogen was through steam-iron or steam-zinc reactions. Eventually, two fairly complicated routes for hydrogen purification emerged, and served as the only commercial means for hydrogen purification until the 1960's.

The first of these methods was cryogenic distillation, and relied upon the refrigeration of the process product gas with liquefied nitrogen or air to effect condensation of the heavy components. This process can achieve purities of 90% to 99%, depending upon the inlet compositions and the final condensation temperature. Clearly, complete cryogenic distillation of hydrogen produced from natural gas is an energy-intensive business because of the preponderance of permanent gas constituents in the product gas. Thus, cryogenic distillation has fallen out of favor for purification in all but specialty application such as petrochemical streams with only high boiling point diluents[14].

The second purification route, sometimes referred to as the classic process, was a complicated combination of physical scrubbing and catalytic upgrading. The general process flowsheet involved first reduces the carbon monoxide to the lowest feasible value (between 1% and 0.1%) through the water-gas shift reaction, which is described below. Then, the product gas is quenched to as low a temperature as is practical, and often below ambient conditions, at which point carbon dioxide is physically scrubbed from the gas by absorption into a liquid solvent or onto hot potassium carbonate. Commercial processes using the former approach include the Selexol, Sulfinol and Rectisol processes, and can also simultaneously remove sulfur compounds. The scrubbed gas typically contains less than 2% of impurities, mainly carbon oxides and methane. The remaining carbon oxides are converted to methane in a catalytic methanation reactor, according to the following equations:

$$CO_{(g)} + 3H_{2(g)} \longleftrightarrow CH_{4(g)} + H_2O_{(g)}$$
$$CO_{2(g)} + H_{2(g)} \longleftrightarrow CO_{(g)} + H_2O_{(g)}$$

The overall process is exothermic, and care is exercised to prevent thermal runaway in the catalytic methanator. This reaction network can greatly reduce the hydrogen yield if the carbon oxide concentrations are high, and thus care must be exercised in the design and execution of the preceding process steps. The resulting process gas is then cooled and the water vapor condensed, yielding a product with a purity of 92% to 98.2%.

Both of these processes are obviously quite complicated, require numerous, large heat exchangers, and are subject to very high energy expenditure in operation. However, for many years the only alternative processes were based on metal membrane purification with costly palladium metal membranes, which has never achieved anything beyond niche market penetration. This situation was fundamentally changed by the commercialization of the Pressure

[14] "Hydrogen," 1995, p.876.

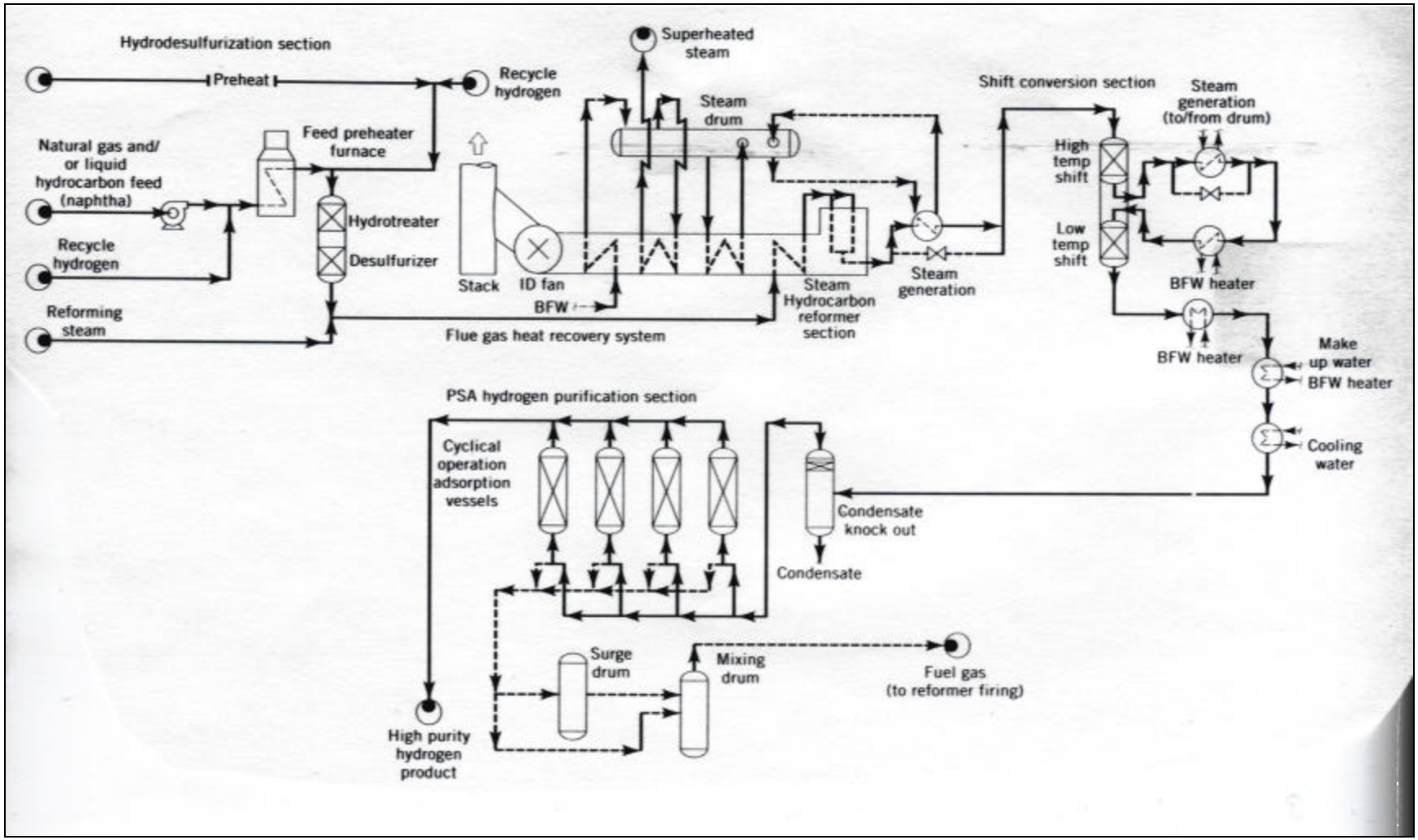

Figure 2.2: Typical modern industrial catalytic steam reformer process flowsheet from Encyclopedia of Chemical Technology, 1995

Swing Adsorption (PSA) process during the 1960's. PSA was first commercialized for air separation and drying around 1960 with the competing commercialization of the processes of Skartsrom of Esso and Guerin de Montgareuil and Domine of Air Liquide, the patents for both of which were filed in 1958[15]. These simple adsorptive processes for air separation gave way to far more complex variations, including the first industrial hydrogen PSA system installed near Toronto in 1966. The PSA system quickly became the favored hydrogen purification process because of its simplicity and high performance. Using only the pressure of the reformate feed, hydrogen recoveries exceeding 70% are achieved in 3 or 4 bed processes based on the patent of Batta, and recoveries in excess of 80% are possible using variations of the polybed process developed by Fuderer and Rudelstorfer[16]. Both of these processes can yield product purities in excess of 99.999%, values technically infeasible using the prior-art techniques.

Since the advent of the PSA process, the competing cleanup processes have been almost completely replaced by the newer, more efficient process[17]. A typical catalytic steam reforming plant process flow diagram excerpted from the literature is shown in Figure 2.2[18]. This process includes the following subsystems:

1. Feed delivery
2. Feed hydrodesulfurization (HDS)
3. Feed preheat and mixing
4. Primary steam reforming
5. High and low temperature water-gas shift with gas cooling
6. Process gas cooling
7. PSA

These steps will be described briefly below, as they also form the core processes found in existing small-scale hydrogen generators discussed in Section 2.2. One point which should be mentioned is that the conventional reformer process of Figure 2.2 has 10 separate heat exchange cores, a heat-exchange reformer, pumps and/or compressors for fuel feed, hydrogen recycle and water feed, and at least four catalytic reactors. The discussion below will show that many industrial reformers have at least one more reactor. None of these components is physically integrated with the others, a fact illustrated in Figure 1.2. Thus, extensive plumbing runs are erected, and must be insulated to reduce heat losses. Despite these shortcomings, such industrial plants are robust and economical for large-scale hydrogen production. The shortcomings of this approach for small-scale generation will be discussed below.

Feed delivery to the inlet of the process is accomplished using standard industrial compressors and pumps. These are supplied for the water, fuel and hydrogen recycle feeds. The latter is a necessary feedstock for the hydrodesulfurization (HDS) reactor described below, and to keep certain industrial reforming catalysts in the reduced state. If the fuel feed is supplied from the wellhead, from a refinery stream, or from liquefied gas, then the degree of oxygen entrained is very low. If, however, line natural gas is employed, air added for peak shaving can

---

15 Yang, R.T., Gas Separation by Adsorption Processes, 1987, p. 237.
16 Yang, R.T., 1987, p. 256.
17 "Hydrogen," 1989, p. 374.
18 "Hydrogen," 1995, p. 857.

destroy the activity of the base metal catalysts employed in the HDS and steam reformer. In this case, a catalytic partial oxidation reactor is employed to react di-oxygen with the fuel prior to the other catalytic reactors. This is an almost universal feature in small hydrogen generators described in Section 2.2, as they almost universally employ line natural gas as a feedstock.

The preheated dry fuel feed and the recycled hydrogen are combined in the HDS reactor, where a sulfided cobalt-molybdenum catalyst or a nickel tungsten catalyst is used to react the organic sulfur compounds to form hydrogen sulfide. The general hydrodesulfurization reaction is as follows, where R is a general hydrocarbon group:

$$R - S + H_2 \longrightarrow R + H_2S$$

This overall mechanism is a gross simplification, and there is a wide disparity among organic sulfur compounds in the ease with which the HDS reaction may proceed[19]. Typical natural gas feeds contain few refractory compounds, and HDS can reduce essentially all of the sulfur present to hydrogen sulfide. Depending upon the feed sulfur level and composition, this may require a hydrogen recycle of 5% to 25% by volume[20].

Once the hydrogen sulfide is formed, the dry feed gas is passed over zinc oxide absorbent, which reacts with the hydrogen sulfide to produce zinc sulfide and water. This exothermic reaction, which is equilibrium limited, is generally conducted near 350 C to ensure complete hydrogen sulfide removal. The usual level of desulfurization is less than 1 ppm total sulfur. Steps are taken to reduce sulfur content to 100 ppb or less if low temperature water-gas shift catalysts of the mixed oxide type are employed. The zinc oxide material is replaced as needed, and utilizations of 20% by mass are not uncommon[21].

Subsequent to the HDS, where the feed gases must be as dry as possible to encourage the hydrogen sulfide absorption, the feed steam is mixed with the fuel and remaining hydrogen feed. This gas is preheated to 400 C to 500 C before being admitted to the steam reformer.

Steam reforming of natural gas can be idealized as the reforming of methane:

$$CH_{4(g)} + H_2O_{(g)} \longleftrightarrow 3H_{2(g)} + CO_{(g)} \qquad \text{steam reforming}$$

Steam reforming is highly endothermic, and in the case of thermodynamically stable methane, has a very high activation barrier against homogeneous reaction. Industrially, a nickel catalyst supported on either α-alumina, magnesium aluminate spinel, or calcium aluminate is used to lower the activation barrier, while the reaction is carried out at temperatures in excess of 800 C to shift the equilibrium towards hydrogen production. Some nickel catalysts are highly susceptible to oxidation by steam, and hydrogen must be recycled to the reactor inlet to maintain them in the reduced state. This is especially true of catalysts employing a magnesium-aluminate

---

19 "Presentation of Topsoe Technologies for the Refining Industry," September 17-19, 1997, p. 9.

20 "Hydrogen," 1989, p. 326.

21 G-72D Sulfur Removal Catalyst Product Bulletin, United Catalysts, Inc., Louisville, KY.

spinel support[22]. On shutdown, nickel catalysts must be protected from di-oxygen, which will oxidize the catalyst, thus requiring a lengthy reduction in hydrogen to restart the process train[23]. In the worst case, addition of large amounts of oxygen can result in a pyrophorric reaction of the catalyst, which can damage the reactor vessel and cause a significant safety hazard. Nickel catalysts are also highly susceptible to sulfur poisoning through the chemisorption of hydrogen sulfide[24]. Because the steam-reforming reaction is endothermic, it is conducted in heat-exchange reactors with inlet conditions for the feed of about 500 C. This lower inlet temperature as well as the low hydrogen concentration in the feed both favor sulfur poisoning at the reformer inlet. Typical reformer feeds must contain less than 1 ppm of hydrogen sulfide to avoid catalyst poisoning.

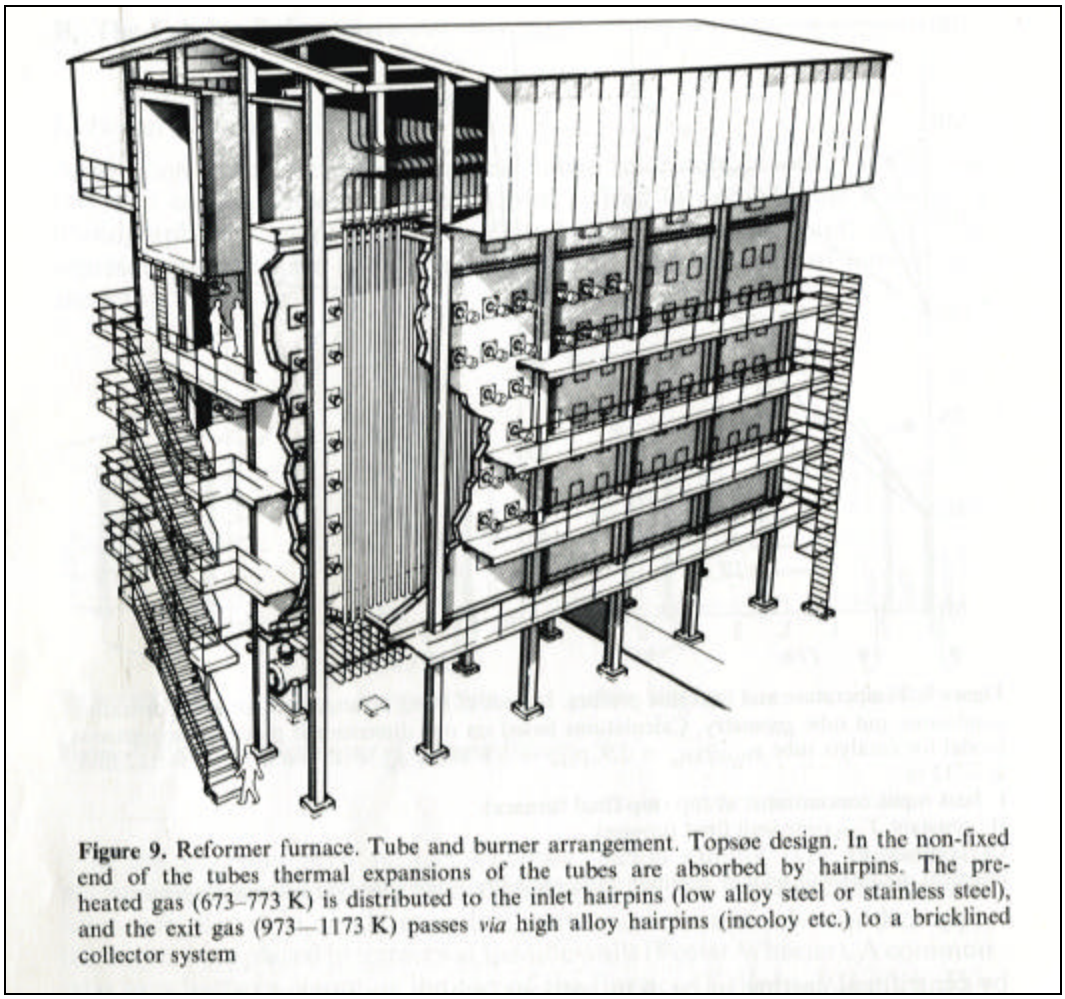

Figure 9. Reformer furnace. Tube and burner arrangement. Topsøe design. In the non-fixed end of the tubes thermal expansions of the tubes are absorbed by hairpins. The pre-heated gas (673–773 K) is distributed to the inlet hairpins (low alloy steel or stainless steel), and the exit gas (973—1173 K) passes *via* high alloy hairpins (incoloy etc.) to a bricklined collector system

Figure 2.3: Topsoe primary reformer furnace from Rostrup-Nielsen, 1984

Industrial steam reformers rely on radiant heat transfer from burners for the supply of the thermal energy for the reaction. Several overall flow geometries have been employed and burner

22 Personal communication with Jon Wagner, Sud-Chemie, Inc, February 2000.
23 Rostrup-Nielsen, J.R, 1984, pp. 33-36.
24 Rostrup-Nielsen, J.R., 1984, pp. 95-106.

placement is dictated by the design firm employed. Kellogg, ThyssenKrupp[25] and ICI employ top firing by long flame burners. Foster Wheeler employs terraced burners on the side of the furnace. Bottom firing is employed by Exxon, and radiant sidewall burners are employed in Haldor-Topsoe designs[26]. In all of these designs, the tubes are subject to hot-spotting should the catalyst deactivate due to oxidation, coking or sulfur poisoning. This is because the radiant burners are generally at a temperature above the alloy service temperatures. Therefore, careful monitoring of the tubes is conducted, and failed tubes are noted and taken out of operation.

The industrial tubular reformer furnace is typically a rectangular structure, with tubes in excess of 10 m in length. A schematic drawing is shown in Figure 2.3, which illustrates the truly enormous scale of these structures. Perusal of Figure 1.2 also clearly shows the rectangular furnace structure of the KCI-designed reformer employed at modern Air Products plants. These enormous industrial furnaces obviously are ill-suited to direct scaling to much smaller capacities, and alternative designs currently in use are discussed in Section 2.2.

Additional hydrogen can be recovered from the fuel feed through the water-gas shift (WGS) reaction:

$$CO_{(g)} + H_2O_{(g)} \longleftrightarrow H_{2(g)} + CO_{2(g)} \qquad \text{water gas shift}$$

This reaction is mildly exothermic, and is thus conducted at significantly lower temperatures to attain acceptable levels of equilibrium conversion. Generally, a two-stage conversion process is implemented. The first stage employs a chromium promoted iron oxide catalyst, commonly referred to as a ferrochrome catalyst. Ferrochrome catalysts of one form or another have been in service since before 1920, when they were first employed in a BASF hydrogen plant in Oppau, Germany[27]. These catalysts, which are physically robust and quite inexpensive, also exhibit relatively modest activity below 350 C. Typical industrial operation involves space velocities as high as 4000 bed volumes per hour on a total gas volume basis, with lower volumes used at lower temperatures[28].

The ferrochrome catalyst does require reduction to an active Fe_3O_4 from the ambient condition form of α-Fe_2O_3, however this is a relatively facile conversion which does not require careful control. Thus, the ferrochrome catalysts are not pyrophorric, although rapid oxidation can reduce active area through sintering. Perhaps the most interesting feature of the ferrochrome catalyst is that it has a good tolerance to sulfur poisoning, and can operate successfully in feeds with as much as 2,000 ppm of hydrogen sulfide, albeit at reduced activity. This sulfur tolerance is in strong contrast to the steam reforming and low temperature shift catalysts described here, both of which are extremely susceptible to sulfur adsorption. The insensitivity to sulfur may be because of the oxide nature of the ferrochrome catalyst, which contrasts strongly with the reduced metallic character of the other catalysts. Resistance to sulfur poisoning explains the

---

[25] "Hydrogen Production: Krupp Uhde technology with top-class performance," ThyssenKrupp Engineering, 9/99, pp. 12-13.

[26] Rostrup-Nielsen, J.R., 1984, p. 20.

[27] Bohlbro, H., An Investigation of the Kinetics of the Conversion of Carbon Monoxide with Water Vapour over Iron Oxide Based Catalysts, 1966, p. 9.

[28] "Hydrogen," 1995, p. 856.

early success of the ferrochrome material, and its early use in "depoisoning" coke oven gas for domestic use, despite the highly contaminated nature of the coke oven gas feedstock.

Copper-based "mixed oxide" catalysts have been shown to have the highest activity for the WGS reaction[29]. Such catalysts are also highly susceptible to sulfur adsorption followed by irreversible bulk metal sulfide formation. This tendency is exacerbated by the nominally 225 C to 250 C operating conditions in the water-gas shift reactors. Further, the mixed-oxide water-gas shift catalysts exhibit exotherms during both the activation (reduction) and oxidation processes, and require close process control to avoid pyrophorric "events.[30]" Also, in industrial process trains the water-gas shift reaction is separated into a high temperature and a low temperature section because the highly active copper catalysts sinter at temperatures above 300 C. The less-active ferrochrome catalysts are typically employed in the high temperature reactor to achieve a rapid initial conversion of carbon monoxide before the gas is fed to the low temperature shift reactor. This both limits the size of the more expensive low temperature shift reactor, and prevents large exotherms in the adiabatic packed bed. These exotherms can sinter the copper mixed-oxide catalyst, thus ruining its activity. Thus, the carbon monoxide concentration entering the low temperature shift reactor is often as low as 1% by volume, rather than the 6% or higher entering the high temperature reactor from the steam reformer.

After the low temperature shift reactor, the reformate gas is cooled by contact with the process feedstocks, and possibly with ambient air, prior to a water knockout vessel where the condensed liquid is separated from the gas prior to feed to the PSA system. The PSA system, which may employ a variety of process manifestations as described previously, then recovers as much as 85% of the hydrogen from the reformate. The balance of the reformate is delivered to the primary reformer furnace where it is mixed with raw fuel and used to fire the process burners.

This type of industrial-scale catalytic steam reforming process train based on the unit operation concept of design can be designed and field fabricated wherever a large hydrogen production capacity is required. Typically, these plants are sited as the front end of ammonia or methanol synthesis plants, or near petroleum refineries to supply hydrogen needs for refinery operations. Economically viable plants as small as 6 tons (7.6 MW on a LHV basis) per day are operated in the U.S., although much larger plants are more common. When hydrogen requirements are small, such as for fuel cell power plants or in the case of vehicle refueling, much less than 1 ton per day of hydrogen is needed. For this small requirement, an entirely different kind of process equipment is needed.

2.2 Current small-scale reforming technology

The technology for small-scale chemical fuel reforming has developed during the past forty years, and is largely derived from previous and concurrent developments in the industrial steam reforming and partial oxidation reforming *milieu*. The genesis of the interest in small-scale

---

[29] Grenoble, D.C., Estadt, M.M., Ollis, D.F., "The Chemistry and Catalysis of the Water Gas Shift Reaction, 1: The kinetics over Supported Metal Catalysts,", vol 67, 1981.

[30] Personal communication with Dr. Shabbir Ahmed of Argonne National Laboratory.

reformer development was the development of fuel cell powerplants for aerospace, military and more recently, commercial applications. In the early years of fuel cell development, only phosphoric acid and solid oxide fuel cells made much headway. Because these fuel cells do not require high purity hydrogen to operate, the emphasis on early reformer work was not on pure hydrogen production. Focus has only recently been shifted by the emergence of commercially important PEM fuel cells, which require very high purity fuel gas. Thus, the design goals of fuel reformers have slowly shifted, although it can be convincingly argued that an evolved design optimized for hydrogen production has not yet been synthesized.

The most relevant source of data regarding existing hydrogen generation technologies is the patent literature. For small-scale reforming systems, in particular, the patent literature provides a rich record of developments dating to 1969, when United Aircraft Corporation's team began developing the technology which culminated in the current PC-25c steam methane reformer system. The relevant reformer patents granted since then are described briefly below, including a discussion of the careers of the most prolific designers, who often have played roles in more than one company. Only the patents pertaining to the processing of methane and higher hydrocarbons such as naphtha, kerosene, etc. are discussed, as methanol and ammonia processors operate under conditions so disparate from those employed for the regular hydrocarbon feeds as to be unrelated to the former.

US 3,446,594, May 27, 1969, United Aircraft Corporation, Buswell, R.F., Sederquist, R.A., Setzer, H.J., Snopkowski, D.J.: This expired patent, the earliest-referenced patent involved in the UTC/IFC/ONSI reformer development program, outlines the construction of a rack-mounted steam reformer system for the conversion of high molecular weight logistic fuels to a reformate stream which is subsequently separated into pure hydrogen and a raffinate stream in a Pd-Ag metal membrane separator. The relevance of this patent is several-fold. First, it demonstrates the basic tenets of steam reformer system design, including the separation of the system into a high temperature reformer and a lower temperature water-gas shift reactor. It also demonstrates a degree of thermal integration superficially similar to the current DTI reformer concept, but executed in a fashion not amenable to mechanical scale-up. Finally, this patent reveals the basic concept of membrane-based separation systems, which are being pursued by many current commercial entities.

US 3,477,832, Nov 11, 1969, Girdler Corporation, Mayland, B.J., Trimarke, C.R., Harvin, R.L., Brandon, C.S.: This expired patent to the Girdler Corporation, which has subsequently been acquired by the Sud-Chemie, Inc., is the earliest patent to reference the now standard practice of hydrocarbon treatment by hydrodesulfurization (HDS) to remove sulfur which poisons common nickel reforming catalysts. This HDS step followed by steam reforming is the central process feature of the subsequently patented reforming systems of IFC and Ballard. This patent also is the first disclosure of sulfided cobalt-moly as an HDS catalyst. Of crucial relevance is the fact that the Girdler patent discloses that hydrocarbon/steam mixtures tend to coke at high temperatures when no catalyst is present, in the case of this patent at temperatures above 650F (343C) are specifically referenced for neat naphtha vapors.

US 3,485,746, December 23, 1969, United Aircraft Corporation, Setzer, H.J.,Whiting, R.W.: This expired patent, the first advance of the aforementioned UAC reformer, incorporates a HDS

reactor and a hydrogen recycle, features later to be evidenced in all competitors' reformer systems. In this early effort, the thermodynamic disadvantage of operating ZnO sulfur absorbents in the presence of steam had not yet been realized by what later became IFC's development team. Thus, the steam and fuel boilers were located upstream of the ZnO absorption bed. Thus, this patent is mainly a historical curiosity, but shows the continued activity of Setzer in IFC's development program.

US 3,541,729, November 24, 1970, General Electric, Dantowitz, P.: This expired patent is the first revelation of what has since evolved to the heat-exchange reformer (HER) concept, later duplicated by Gerald Voecks at NASA and Haldor Topsoe. The central tenet of the HER concept is the provision of an annular-flow, serpentine flow path reactor wherein the hottest fluids are introduced at the center of the reactor and subsequently made to flow through a number of annular passages, exchanging heat, reacting, etc. during their transit. It may, in fact, be argued that the Nuevera gasoline partial oxidation reformer is a direct copy of this early G.E. patent to Dantowitz, who in fact suggested its employment as a partial oxidation reactor. Of importance to DTI's intellectual property, this patent is one of several disclosing a water-gas shift zone with heat transfer means, although in this case the heat transfer is to a separate sealed boiler and is used to maintain isothermality rather than the non-isothermal operation desired in the DTI system which is described in Section 2.3.

US 3,551,124, December 29, 1970, Japan Gasoline Co., Lmtd., Iwaki, T., Eqashira, S., Okagami, A.,: This expired patent is the first revelation of sulfided nickel catalysts for HDS of naphtha feeds. The overall steam reforming process is conventional, with the only notable feature being heat recovery from the reformate to raise process steam and vaporize the fuel.

US 3,655,448, April 11, 1972, United Aircraft Corporation, Setzer, H.J.,: This expired patent is the first disclosure by IFC's team of a reformer coupled with a fuel cell wherein the fuel cell is fed an impure hydrogen stream. The process includes the original process of Buswell and the desulfurizer of Setzer. This patent also discloses the first use of an ejector to recycle hydrogen to the reformer inlet, a feature of all subsequent IFC designs. This patent does state that operation without any shift converters is contemplated, but further elaborates that this is because the focus of the patent is desulfurization, not the balance of the process.

US 3,909,299, September 30, 1975, United Technologies Corporation, Corrigan, T.J.: This expired patent is the first disclosure by IFC's team of the ganged array of large-diameter reformer tubes later to become characteristic of their PC25 product range. Further, this patent discloses the thermal flow concept wherein the reacted, hot reformate is used to regeneratively heat the incoming cold stream of reformate. This thermal management approach is evidenced in subsequent patents including their planar reformer patent to Lesieur in 1998. Importantly for DTI, the patent discusses air-cooling of a shift reactor. The geometry of the water-gas shift bed is annular, like the Dantowitz design, and exchanges heat with air on its inner surface only. Once again, the stated purpose of this practice is the control of isothermality within a bed of low temperature shift catalyst specifically to prevent catalyst sintering. It is interesting to note that this patent is the earliest contribution of Corrigan to the IFC team, he figures significantly in many of their later PC25 designs.

US 4,004,947, January 25, 1977, United Technologies Corporation, Bloomfield, D.P.: This expired patent marks one of the earliest and most significant contributions of Dave Bloomfield to the fuel cell arena. The patent discloses and claims the advantages accrued through the implementation of a turbo-compounded fuel cell and its associated reformer systems. These advantages are smaller fuel cell and reactor size and cost, an improved ability to recover product water so as to maintain water balance, and the possibility of higher system efficiency due to energy recovery from the turbine. This patent is a watershed as it marks the delineation between the ambient-pressure approach subsequently adopted by IFC and the pressurized operation strategy subsequently pursued by all other fuel cell manufacturers. Dave Bloomfield eventually left IFC to form Analytic Power, and several other disgruntled engineers eventually left to design Ballard's reformer and fuel cell systems. The patent sets the stage for the scission of IFC's fuel cell team.

US 4,554,223, November 19, 1985, Hitachi, Yokoyama, E., Kaneko, T., Amano, Y., Sugimoto, S.: This patent pertains to a water-cooled water-gas shift reactor which may be used as a steam generator or an absorptive chiller in addition to its function as a shift reactor. The patent seems superficially similar to the cooled water-gas shift section of DTI's reformer device described later except for the following: the reactor is a unit-process with a discrete inlet and outlet zone, the purpose of the cooling is to maintain substantial isothermality, the cooling fluid is pressurized water. Though the physical manifestation is different than that in the design of Dantowitz, it may be argued that the purpose is the same and that thus much of the patent is unenforceable.

US 4,781,241, November 1, 1988, IFC, Misage, R., Scheffler, G.W., Setzer, H.J., Margiott, P.R., Parenti, E.K.: This patent describes an elaborate finned-tube heat exchanger combining intercooling of the reformate with boiling the feed water and preheating the fuel. This patent typifies the unit-process approach wherein the separate heat exchange functions require an elaborate heat exchanger array separate from the reaction vessels. This approach is inherently more costly, less compact, and has inherently higher heat loss than the integrated DTI approach. It is interesting to note the ongoing role of Setzer at this stage in IFC's development program.

US 4,909,808, Mar 20, 1990, NASA, Voecks, G.E.: This patent describes what is referred to in the literature as a heat-exchange reformer, an integrated annular combination of a burner and a catalytic steam reformer. This NASA-developed unit is substantially identical to the unit developed by Haldor-Topsoe, AG and sold by them, and quite similar to the even earlier design of Dantowitz. This type of reformer can yield high efficiencies, but is fairly complicated to construct. It also does not integrate the water-gas shift functionality, thus requiring a separate reactor to accomplish the shift function. These heat-exchange reformers also use mixed-mode heat transfer (radiant and convective), which can result in local hot-spotting if the reforming catalyst deactivates. Gerald Voecks continues in the employ of the government, and is no longer actively involved in reformer design.

US 4,921,680, May 1, 1990, IFC, Bonk, S.P., Morganthaler, G.F., Miura, Y.: This IFC patent discloses an improved sealing arrangement for their radiantly-fired reformer array employed in the PC25. This mechanical improvement is an evolutionary, rather than revolutionary step compared to the original PC25a design. The extremely complex nature of the PC-25 reactor

array is evidenced in this patent very clearly. Also extremely important to note is that this patent involves none of the original IFC reformer design team, all of whom except Sederquist had left for retirement or work for Ballard by this point.

US 4,976,747, December 11, 1990, IFC, Szydlowski, D.F., Lesiur, R.R.: This IFC patent discloses a very significant improvement in their fuel pretreatment system, representing the most important advance since the original process patents of Setzer and Buswell, *et al*. The thermodynamically unfavorable HDS of water-laden fuel is here abandoned in favor of HDS of dry fuel, as practiced in industrial installations and described in the aforementioned Girdler patent as well as others. This patent also clearly articulates the need for a fuel partial oxidation step to remove di-oxygen from the fuel feed. This same arrangement is later evidenced in Ballard's very similar steam reforming system patents to Buswell, *et al*.

US 5,110,559, May 5,1992, Hitachi, Kondo, Y., Amamo, Y., Kimura, S., Horiuchi, S.: This Hitachi patent discloses a low-pressure reformer with a conventional unit-process design. The most important novel feature is the use of a flow diverter valve and a convectively heated water-gas shift reactor to improve startup speed.

US 5,186,859, Feb 16, 1993, Shell Oil Company, Sie, S.T.: This Shell patent is the first of a series of process and device patents concerning catalytic autothermal reforming of natural gas and other hydrocarbons. This particular patent discloses a fluidized bed reactor system to achieve ATR of natural gas over group VIII metal catalysts. This patent covers a wide range of process conditions and stoichiometries.

US 5,207,185, May 4, 1993, Greiner, L., Moard, D.M., also US 5,299,536 April 5, 1994: This patent, much infringed since, is the basis for HBT's hydrogen generation business. The device and process described are the non-catalytic partial oxidation of gasoline and other hydrocarbons to form a hydrogen-rich synthesis gas for the reduction of NOx in IC engines. This process was later employed by Moard to deliver the first non-catalytic HBT/Phoenix gas reformers, precursors of the unit shown in Figure 1.3. The non-catalytic POx system is inherently less efficient than ATR, as described in Shell's patents and much less efficient than the steam reforming process described in most other patents. The sole advantage being insensitivity to fuel composition and a low cost of the primary reactor (although the balance of plant remains costly.) This system is functionally identical to the Texaco HyTex process, and may represent an infringement thereof, though Texaco has made no move to claim such an infringement.

US 5,284,717, February 8, 1994, Japanese Petroleum Energy Center, Yamase, O.,Miura, T., Kubota, H.: This Japanese-held patent covers old ground in the description of conventional naphtha and kerosene reforming with HDS, a primary reformer, and two shift reactors with a variety of post-shift cleanup strategies. The only new ground broken is the use of zeolite base-metal catalysts for the steam reforming. This technology uses a chemistry which is actually thermodynamically unstable under the quoted operating conditions.

US 5,360,679, November 1, 1994, Ballard Power Systems, Inc., Buswell, R.F., Clausi, J.V., Cohen, R., Louie, C., Watkins, D.S.: This Ballard patent is the first solid evidence of the contribution of the former IFC engineers Buswell, Clausi and Cohen to Ballard's reformer design

effort. The referenced patent list also illustrates the lasting influence of Dave Bloomfield, also formerly of IFC, on thinking in the fuel cell system design arena. It is interesting to note that all of the influential thinkers on fuel cells at IFC had left by the early 1990's, and Sederquist, the last of IFC's original team filed his last IFC patent in 1994. Thus, none of IFC's original design team is still in place, with follow-on work being conducted by Lesieur, Corrigan and other, more recent hires. In any event, this Ballard patent combines the features of IFC's system patents which were pursued at low pressures, but combines the unused ideas of Bloomfield on pressurized and turbo-compounded systems for increased power density. Discussions with former Ballard employees suggest that Cohen and Buswell left IFC dissatisfied with the corporate insistence on low pressure systems, confirming this with Buswell is impossible, as he passed away several years ago, ending a notable career as one of the most gifted reformer design engineers in history. The resulting Ballard system employs a pressure in excess of 2 bar, allowing higher power densities to be realized in the fuel cell and reformer than possible with IFC's ambient pressure PC25 series. Otherwise the system is conventional, employing partial oxidation and HDS fuel pretreatment followed by reforming, and a high-temperature shift reactor. A selective oxidizer is employed, as is a two-stage low temperature shift reactor described in a later patent. Interestingly, the most important difference between the Ballard and IFC systems is the use of a compressor in place of IFC's ejector to recirculate hydrogen for the HDS reactor. This patent discloses a totally traditional, unit-process reforming system functionally identical to much of current industrial steam reforming plants.

US 5,464,606, November 7, 1995, Ballard Power Systems, Inc., Buswell, R.F., Clausi, J.V., Louie, C.: This Ballard patent covers the two-stage, low temperature water-gas shift reactor developed for their powerplant system. This reactor employs a non-isothermal second stage with a mechanical structure akin to Buswell's 1969 UAC reformer system. This patent would present a challenge to the DTI non-isothermal water-gas shift concept except that it is specifically restricted to low temperature applications whereas the DTI system is aimed towards high-temperature shift.

US 5,470,360, November 28, 1995, IFC, Sedequist, R.A.: This IFC patent pertains to an improved baffling system to distribute burner gas to evenly heat the three concentric banks of large-diameter reformer tubes in the PC25b reformer. This patent reveals the mechanical complexity and large size of the PC25-style, low-pressure reformer.

US 5,484,577, January 16, 1996, Ballard Power Systems, Inc., Buswell, R.F., Cohen, R., Clausi, J.V., Leavitt, S.L., Watkins, D.S.: This Ballard patent covers their version of a large diameter, radiantly/convective heated steam reformer tube, and their array of these tubes in a PC-25 analog structure with seven individual tubes.

US 5,486,313, January 23, 1996, Shell Oil Company, DeJong, K.P., Lednor, P.W., Oud, A.E.M., Schoonebeek, R.J., Vonkeman, K.A., VanDerZwet, G.P.: This Shell patent covers the application of noble metal catalysts on ceramic supports to the autothermal reforming of natural gas and other gaseous light hydrocarbons. In particular, catalysts containing Rhodium, Platinum and Iridium are claimed as especially advantageous because of their selectivity against ammonia and hydrogen cyanide formation. The process conditions claimed cover all super-ambient applications to partial oxidation and autothermal reforming. This patent makes it essentially

inconceivable that any non-infringing improvement to HBT or Neuvera's reformer systems could be made without royalties being paid to Shell.

US 5,510,056, April 23, 1996, Shell Oil Company, Jacobs, L.L.G., Lednor, P.W.,Limahelu, A.G.G., Schoonebeek, R.J., Vonkeman, K.A.: This Shell patent extends the previously-referenced patent to cover porous foam supports of cell density higher than 750 pores per square inch. These very high pore density foams enhance mixing, and thus the reaction rate of the autothermal reforming.

US 5,516,344, May 14, 1996, IFC, Corrigan, T.J.: This IFC patent by Corrigan, the original innovator of the large diameter, tubular array reformer of the PC25, improves upon the performance of the PC25 by integrating all of the reformer elements into a single insulated rack. This mirrors the early patent to Buswell, *et al*. It is interesting to note that the reformer depicted in this patent departs from the tiered array of the previous PC25-related patents, and moves towards a Ballard-like employment of five "fat" steam reformer tubes. This mounting rack separates the very high temperature reactor tubes from the much lower temperature shift zone by means of a division plate. All of the reactor components other than the steam reformer tubes are arrayed below the division plate in an annular array which owes much to the patents of Dantowitz, Buswell, and Voecks. This packaging concept comes closest to the spirit of the DTI integrated reactor, with one critical difference, the components are individually plumbed and mounted, yielding higher complexity and cost than the DTI approach which is described in Section 2.3.

US 5,628,931, May 13, 1997, US 5,639,401, June 17, 1997, US 5,658,497, August 19, 1997, US 5,720,901, February 24, 1998, all to Shell Oil Company, Kumar, K.N.P., Lange, J.P., Searcy_Roberts, K., Van der Zwet, G.P., Van Leon, P.J.M., Oosterveld, M., Senden, M.M.G., Jacobs, L.L.G., Lednor, P.W., Limahelu, A.G.G., Schoonebeek, R.J., Vonkeman, K.A.: These more recent patents to the prolific Shell team cover further advantageous methods applied to autothermal reforming of light hydrocarbons for producing synthesis gas. Much of the emphasis is towards methanol and Fischer-Tropsch synthesis, and is thus concerned with controlling Hydrogen to carbon ratios, etc.. These areas are not truly germane to reformers for pure hydrogen production. More crucial are claims relating to the advantageous use of thermal shock tolerant supports such as Zirconia foams, the advantages of applying a high area washcoat to support the catalyst, particularly active combustion catalyst oxides such as lanthides and barium hexa-aluminate. These claims further restrict the ability of competing companies to use advanced catalysts, as the claims in the patents are quite broad, and cover many of the known catalyst design techniques. A most interesting aside relates to the last of these patents, which claims sulfur addition to the autothermal reformer feed to suppress ammonia and hydrogen cyanide formation. In this patent sulfur content ranges for reforming operability for supported noble metal catalysts. These ranges correspond to the tested ranges employed in our development program described in Chapter 3. The sulfur-tolerance of the catalysts, however, is not claimed. Nor is the operation in a steam reforming mode claimed.

US 5, 733,347, March 31, 1998, IFC, Lesieur, R.R.: This IFC patent applies a brazed, planar heat transfer matrix design to the flow and thermal geometry originally devised and described by Corrigan. The resulting planar units may be washcoated with a catalyst and employed in place

of the "fat tubes" common to previous IFC and Ballard designs. Washcoated catalysts have poor durability, and planar reactors of brazed construction are not useful at elevated pressures, thus confirming IFC's reliance on ambient-pressure reformer systems.

Review of the existing patents reveals several unifying themes in current small-scale reformer design. These common threads may be largely due to the fact that a small community of engineers were responsible for the development of most of the small hydrogen generators extant.

- Industrial catalysts have been almost exclusively used for steam reformer development
- Thermal integration has been more widely practiced for partial oxidation and autothermal reforming than for steam reforming
- Catalyst innovation has been largely restricted to autothermal reforming catalysts developed by Shell
- All of the existing processes and hardware are functionally similar to their large-scale, industrial counterparts

The first of these points is relatively easy to understand. When Buswell, *et al* began developing the United Aircraft and later International Fuel Cells steam reforming processes, the fundamental understanding of catalysis was in its infancy. Although many engineers today still falsely claim that catalysis is "black art," in the 1960's it largely was a business of trial and error. The exciting findings of Temkin, Boudard, Bodrov and the other early catalyst researchers were still not widely disseminated, nor even fully accepted, and the design of catalysts based on first principles was limited to an elite few in the employ of the catalyst manufacturers and university research groups. Therefore, these early developers, who actually have dominated the field in terms of units designed and in the field, could hardly have been expected to investigate or synthesize new catalyst materials. Instead, they focused on mechanical designs, which for the processes they were implementing were perfectly adequate, if not entirely revolutionary.

The second point probably has more to do with the fact that partial oxidation reformers require little heat exchange area at high temperature, and have higher peak temperatures, than any other technology. This allows more elegant structural designs to be executed. Further, the very high peak temperatures demand either strong integration or truly heroic insulation to prevent catastrophic heat loss.

Shell's CPO team has taken the lead in developing partial oxidation catalysts based on noble metals. This commercial development is related to the fact that most base metal catalysts for autothermal reforming are rather tricky to operate successfully, whereas noble metal oxidation catalysts have been known since the 19^{th} century. Because the use of noble metal catalysts is not required in industrial steam reformers, and because it would drastically increase the price of hydrogen from these processes at the industrial scale, no incentive to develop such catalysts has existed until the present day, and previous research efforts have been extremely limited.

This last point is natural. The reformer development groups worked from the process flowsheets which are published in the patent and review literature for large plants, they were

constrained to use existing catalysts, and they were not constrained by cost or even thermal efficiency in many cases. Thus, they were conservative process designers and adventuresome mechanical innovators, a fact evidenced in the mechanical orientation of most of the patented innovations described above. Within the constraints of the feedstock purity requirements of the existing catalysts, the existing processes were already essentially optimal, and the hardware developed to this point is generally very clever and complete in implementing the industrial processes in a space and energy efficient manner.

2.3 The DTI steam reforming process, concurrent design in action

The first step in the design of a new product is the determination of system level requirements. These requirements are determined solely by the marketplace, and are not dependent upon the characteristics of existing processes or products to meet the requirements. At first, this exercise may seem facetious, and in traditional, incremental product improvement it is anethema. In that case, the question is "how can we evolve what we have to make it more desirable to the customer?" This incremental development process is evident in the existing small-scale hydrogen generators, and is arguably the reason for their current form.

After the system-level requirements are established, opportunities for fulfilling the requirements using existing technology or new technology must be investigated. This process is described in Section 2.3.2, which evaluates existing purification and hydrogen generation technologies at a simple level to select an appropriate set of technologies best suited to meeting the customer requirements. Finally, a complete product concept is formulated. This conceptual basis is then the starting point from which the concurrent engineering activities begin. In this study, the conceptual basis is detailed in Directed Technologies Inc.'s patent application shown in Appendix, and summarized in Section 2.3.3.

2.3.1 Product requirements and design philosophy

When the customers for a small-scale hydrogen generator are considered, three major groups are evident. These customers include industrial users, fuel cell manufacturers, and refueling stations for vehicles. All of these customers have the following common requirements:

- Logistic fuel/infrastructure
- Safety
- Reliability
- Low capital cost
- Low operating cost

Hydrogen purity is not a fixed requirement, and some applications can tolerate higher impurity levels than others. The strictest purity standards are probably for some industrial processes such as semiconductor manufacture. For PEM fuel cells, the standard adopted here is 5 ppm of CO or less and essentially zero hydrogen sulfide. This purity goal will satisfy most users, with the

exception of semiconductor manufacturers, metal powder producers and some corrosion prevention applications[31].

For vehicle refueling, additional requirements exist. The first is the ability to deliver hydrogen to the vehicle tank for storage at an appropriate pressure, probably 340 bar. The second is the ability to meet a reasonable vehicle demand pattern and to refuel vehicles quickly, probably in less than 3 minutes. Finally, the hydrogen must be generated with a minimum attendant production of climate change gases. This implies a high thermal efficiency, which is consistent with the low operating cost goal above.

The first product requirement is the use of a logistic, or infrastructure fuel. This means that boutique feeds such as methanol and neat ammonia are poor candidates, as these are not widely available. The best chemical fuels to consider are natural gas and liquefied petroleum gas (LPG). The infrastructure for these fuels is widely developed in industrialized countries, and even to some extent in the less developed world. Further, the fuel composition is generally controlled within specified limits in the interest of public safety and corporate accountability. Thus, the heating value and sulfur content of these feeds are controlled within prescribed limits in many countries of interest. In addition to these common fuels, water, ambient air and electricity are other widely available feedstocks.

Safety concerns dictate the method of construction and the design manifestation of the mechanical and electrical aspects of systems for handling fuels and electricity. Codes and standards, which have traditionally been nationally based, are beginning to be unified across international boundaries. The design of the reforming system must comply with the applicable national and international codes in order to be accepted as a commercial product. Opportunities within the scope of the codes to reduce costs through design must be exploited fully to realize a low-cost product.

This consideration relates to the capital cost of the hydrogen generator. In large industrial plants, the fabrication, inspection and maintenance of extensive piping systems and numerous reactor vessels and heat exchangers is an accepted aspect of operation. In an appliance-style hydrogen generator, regular maintenance must be minimized to facilitate customer acceptance and low recurring costs. Further, each joint in a code-compliant system must be fabricated and inspected according to prescribed practices. Each separate reactor vessel and heat exchanger must further be designed, tested and inspected in accordance with the applicable codes. Thus, additional components and complexity are directly correlated with increased cost in a small-scale system. In analyzing opportunities to reduce cost in manufactured products, several design rules may be considered as guidelines for reducing the number of parts[32].

- During the operation of the product, does the part move relative to the other parts assembled?
- Must the part be of a different material than or isolated from all of the other parts already assembled?

---

[31] Heydorn, B., Zuanich, J., Market Assessment: Small Scale Hydrogen Generators, SRI consulting for Gas Research Institute, #5096-930-3902, January, 1998.

[32] Boothroyd, G., *et al*, 1994, p. 7.

- Must the part be separate from all the other parts already assembled because otherwise assembly would be impossible?

If the answer to all three questions is no, then it is feasible to combine the disparate parts into a single part.

The application of these rules to a chemical process is new, and the results achievable are not proven. However, there is no fundamental reason to expect that the application of the rules will not yield benefits in both reduced cost and increased safety and reliability. Indeed, there are many factors which suggest that reducing parts count could dramatically improve small reformer system performance.

- Each separate pressure vessel and heat exchanger must be code compliant, adding a cost premium per individual component in the system. Further, each pressure vessel must be provided with attendant relief valves and fittings, which further increase cost.
- Each plumbing connection introduces added manufacturing costs, and poses a safety risk due to leakage, blockage or failure
- Heat loss per unit volume is proportional to one over the radius for spherical components, and can be worse for irregularly shaped parts, thus, small components will lose relatively more heat than larger ones
- Reducing the parts count reduces required component inventories, and streamlines the manufacture of the hydrogen appliance

Given these considerations, it is imperative to consider reducing the complexity of the hydrogen generator by combining component functionalities and eliminating unnecessary components. This is especially true for small-scale systems, where the cost of valves, fittings, pressure vessels and other mechanical features can be substantial. The author and a number of colleagues have previously shown that the cost contribution of mechanical components and assembly in a scaled-down industrial steam reformer would account for more than 95% of the total cost[33].

Operating costs for the hydrogen appliance comprise fuel costs, electricity costs, and operation and maintenance (O&M) costs. Reducing the first two depends upon maximizing the overall thermal efficiency of the hydrogen generator, a goal which helps attain the lowering of climate change gases as well. The degree to which efficiency can be increased must be traded against the resulting system capital cost, an activity which is addressed beginning in Section 2.3.3. Reducing O&M cost is a more complicated subject. At one level, reducing the parts count and complexity will naturally reduce the number of components subject to failure, and should improve reliability and reduce O&M costs. Once the number of components is minimized, improvements in O&M costs can only be realized through the selection of highly reliable and fault-tolerant components. This means that proven components are desirable, and that a capital cost premium may be allowable for especially robust components. This aspect of the system design is highly commercial in nature, and is not extensively addressed in this study.

[33] Thomas, C.E., James, B.D., Lomax, F.D., Kuhn, I.F., "Integrated Analysis of Hydrogen Passenger Vehicle Transportation Pathways," prepared for the National Renewable Energy Laboratory, March 1998.

For vehicle refueling applications where the average capacity factor[34] is 69%[35], and a fast refueling capability is required, both hydrogen compression and storage may be desired. This capability can be provided by using commercially available pressure vessels and compressors, and the hydrogen compression and storage component of the hydrogen appliance will therefore not be addressed extensively in this document. The fact that the system must interact with compressors and storage tanks is taken into consideration though in the thermodynamic analysis of Chapter 4.

The final customer requirement is the sizing of the capacity of the hydrogen appliance. The final capacity of the appliance could be optimized for many different applications, and involves consideration of application requirements and system economics. The calculations which determine the preferred capacity are thus somewhat sensitive commercial information. For the purposes of this study, the capacity of the hydrogen appliance is set at 56 standard cubic meters of hydrogen product per hour (or 4.5 kg/hr) based on internal Directed Technologies Inc. calculations. This capacity is dictated by market requirements and system cost factors. One of the chief factors involved in the optimization is the fact that many system ancillaries are only available in a single, minimum capacity. Thus, the ancillary cost scales very poorly with capacity below some minimum value consistent with the maximum capacity of the ancillaries. For many of the ancillaries envisioned for the hydrogen appliance, maximum capacity is about 50% higher than the design capacity selected here, which reveals that other market factors are involved in the capacity optimization.

2.3.1 General process selection considerations

Section 2.2 showed that a variety of technologies are being evaluated for use in small scale hydrogen generators. The most important technology considerations revolve around the selection of the primary fuel reforming process and the hydrogen purification technology. The selection of the appropriate purification processes depends critically upon the selection of the reforming process. Therefore, the primary reforming processes are described first below.

The two general reforming processes which must be considered are steam reforming and autothermal reforming. The latter can be further segregated into catalytic and non-catalytic processes, although non-catalytic processes offer far worse efficiency and are thus not considered here in detail. The simplified equations for methane steam reforming and combustion are shown below.

steam reforming $\quad CH_4 + H_2O \xleftrightarrow[K_{eq}]{} CO + 3H_2 \qquad \Delta H_r^o = 250.15 \ {}^{kJ}/_{mol}$

combustion $\quad CH_4 + 2(O_2 + 3.78N_2) \longrightarrow CO_2 + 2H_2O + 7.56N_2 \qquad \Delta H_c^o = -890.36 \ {}^{kJ}/_{mol}$ HHV

[34] Capacity factor is defined here as the average daily vehicle refueling requirement divided by the peak requirement.

[35] Thomas, *et al*, 1997, p. 2.

In earlier studies, it was often assumed that a direct catalytic partial oxidation of methane to carbon monoxide occurred, but recent consensus holds that complete oxidation, followed by steam reforming is the more likely mechanism. When this is considered, and a very simple energy balance across these two reactions is conducted. We see that at least 0.28 moles of methane must be combusted to facilitate the steam reforming of a single mole of methane. Resolved to the basis of a single mole of methane, at least 22% of the incoming fuel must be combusted to facilitate reforming if no other irreversibilities exist (i.e. perfect intercooling, adiabatic reactors, complete steam reforming conversion, etc.). These ideal assumptions yield the following overall equation for ideal "partial oxidation."

$$CH_4 + 0.78H_2O + 0.44(O_2 + 3.78N_2) \longrightarrow 0.78CO + 0.22CO_2 + 0.88H_2O + 2.34H_2 + 1.66N_2$$

This ideal equation is used here to represent autothermal reforming. Although the simplified equation ignores most of the real effects, it results in an overall feed and product mix similar to that employed in autothermal reformers demonstrated in the literature. The higher heating value efficiency[36] of the process is 75%, the hydrogen content of the reformate is 40% on a wet basis and 47% on a dry basis, and the air and steam stoichiometries are similar to those evidenced in practical systems from Nuevera, Argonne National Laboratories and Shell. Conversion of the residual carbon monoxide to hydrogen via the water-gas shift reaction would bring the values even closer to those claimed in the literature.

If it is assumed that high temperature water-gas shift can reduce the carbon monoxide concentration in either case to 1% on a wet basis, and subsequent low temperature shift can reduce that value to 0.1%, which is also attainable, then the product concentrations and molar balances shown in Table 2.1 would result. In the autothermal reforming case (ATR), twice the stoichiometric water flowrate is assumed, while in the steam reforming case (SMR) four times the stoichiometric rate is assumed. These steam-to-carbon ratios more closely match industrial practice than the stoichiometric ideal. The simplified results of Table 2.1 show that at every stage of the process, the hydrogen concentration in the reformate gas is higher for steam reforming than for ATR. This is especially true when the dry reformate composition is considered. Thus, while both processes can theoretically have similar thermal efficiencies, as they are both based on the same reactions, autothermal reforming will always yield a lower hydrogen concentration. This is the motivation behind the use of air separation plants in the industrial partial oxidation and ATR plants described previously. For a small-scale hydrogen generator, the cost and complexity of an air separation plant is considered prohibitive, so these dilute hydrogen concentrations must be assumed. These high dilutions critically impact the performance of the hydrogen purification processes discussed below.

Beyond the basic thermodynamics of the processes, which are similar, there are many systems-level implications of selecting steam reforming versus autothermal reforming. In the area of ancillary cost and complexity, the steam reformer has substantial advantages because it requires only a water pump and a natural gas compressor. The autothermal reformer must also use a separate air compressor. This increases cost and complexity, and because the air flowrate

[36] HHV efficiencies are typically quoted in the literature, and are used where natural gas costs are estimated as costs are quoted on a HHV basis. In Chapter 4, LHV efficiencies are used to facilitate understanding the overall climate change emissions and well-to-wheels efficiency, as vehicle efficiencies are usually reported on a LHV basis.

Table 2.1: Simplified molar balances for steam reforming and autothermal reforming

	After primary reformer				After high-temperature shift				After low temperature shift				Dry gas basis			
Constituent	ATR, volume %	SMR, vol %	ATR, moles	SMR, moles	ATR, volume %	SMR, vol %	ATR, moles	SMR, moles	ATR, volume %	SMR, vol %	ATR, moles	SMR, moles	ATR, volume %	SMR, vol %	ATR, moles	SMR, moles
hydrogen	35%	43%	2.34	3	46%	56%	3.05	3.93	46.7%	57.0%	3.11	3.993	53.9%	79.9%	3.11	3.99
carbon monoxide	12%	14%	0.78	1	1%	1%	0.07	0.07	0.1%	0.1%	0.01	0.007	0.1%	0.1%	0.01	0.01
carbon dioxide	3%		0.22		14%	13%	0.93	0.93	14.9%	14.2%	0.99	0.993	17.2%	19.9%	0.99	0.99
water	25%	43%	1.66	3	14%	30%	0.95	2.07	13.3%	28.7%	0.89	2.007				
nitrogen	25%		1.66		25%		1.66		24.9%		1.66		28.8%		1.66	

is more than twice the natural gas flowrate, will increase compressor power requirements by over 200%. The autothermal reformer has several features in its favor though. It has a greater tolerance for fuel impurities because of the higher temperature employed and it has a less expensive reactor because the reactor structure need not conduct the heat required to support the reaction, while the steam reformer must have a structural temperature hotter than the process conditions to provide heat transfer between the hot combustor gas and the endothermic reforming zone. We see that qualitatively both processes have advantages. Steam reforming offers high product purity and low ancillary cost and energy penalty, while autothermal reforming offers a less expensive and more impurity-tolerant chemical reactor. It is, thus, difficult to choose between the technologies until their interaction with the hydrogen purification technologies is considered.

Three types of hydrogen purification techniques can be considered for small scale hydrogen generators. These include PSA as well as metallic membranes and polymer membranes. The latter techniques have only found limited application in industrial process trains, but may offer advantages in small systems which are not realized at the larger scale. Table 2.2 compares the three techniques qualitatively using a red-yellow-green chart to compare the system attributes with the customer requirements discussed in Section 2.3.1. In this format, red indicates a serious problem which could eliminate the technology from consideration, yellow indicates a potential drawback which must be considered, and green indicates an area where requirements are met completely.

Table 2.2: Comparison of hydrogen purification techniques

Product requirements	PSA	Metal membranes	Polymer membranes
product purity			
hydrogen recovery			
tolerance to impurities			
reliability			
cost			

Table 2.2 shows that both metal membranes and polymer membranes fail to meet at least one product requirement. These shortcomings are described below.

Polymer membranes are exemplified by Monsanto's Permea membranes, which are asymmetric, hollow-fibers of polysulfone. These membranes are permselective, i.e. they permeate many or all substances at a finite rate, but the permeance of certain molecules is much higher than that of others. This difference in permeation rate allows the more permeable constituent of a mixture to be separated from the less permeable ones by simple diffusion. Unfortunately, this means that limiting product purity is inversely proportional to hydrogen recovery, as the relative driving force for impurity permeation increases as the hydrogen is withdrawn, and that the limiting purities at useful recovery levels are less than 97% using typical

feed conditions[37]. This is unfortunate, because the polymer membranes are highly satisfactory in other respects such as ruggedness, simplicity and cost.

Metallic membranes are another promising technology which does not meet the application requirements. Metallic membranes based on the permeation of hydrogen through palladium and its alloys have been commercialized by Oremet Wah-Chang and Johnson-Mathey. The former employs 25 µm films of Pd-40Cu alloy[38], while the latter employs 5 µm films of palladium on a ceramic support or 125 µm wall thickness tubes of Pd-23Ag. When new, these membranes are capable of producing extremely pure hydrogen, matching or exceeding the performance of PSA. However, all Palladium membrane systems are subject to mechanical degradation, and the thin-film systems in particular are subject to the formation of pinhole defects which reduce product purity. Thicker, tubular membranes are quite rugged though, and have been employed commercially in reformate cleanup applications. The biggest problem with

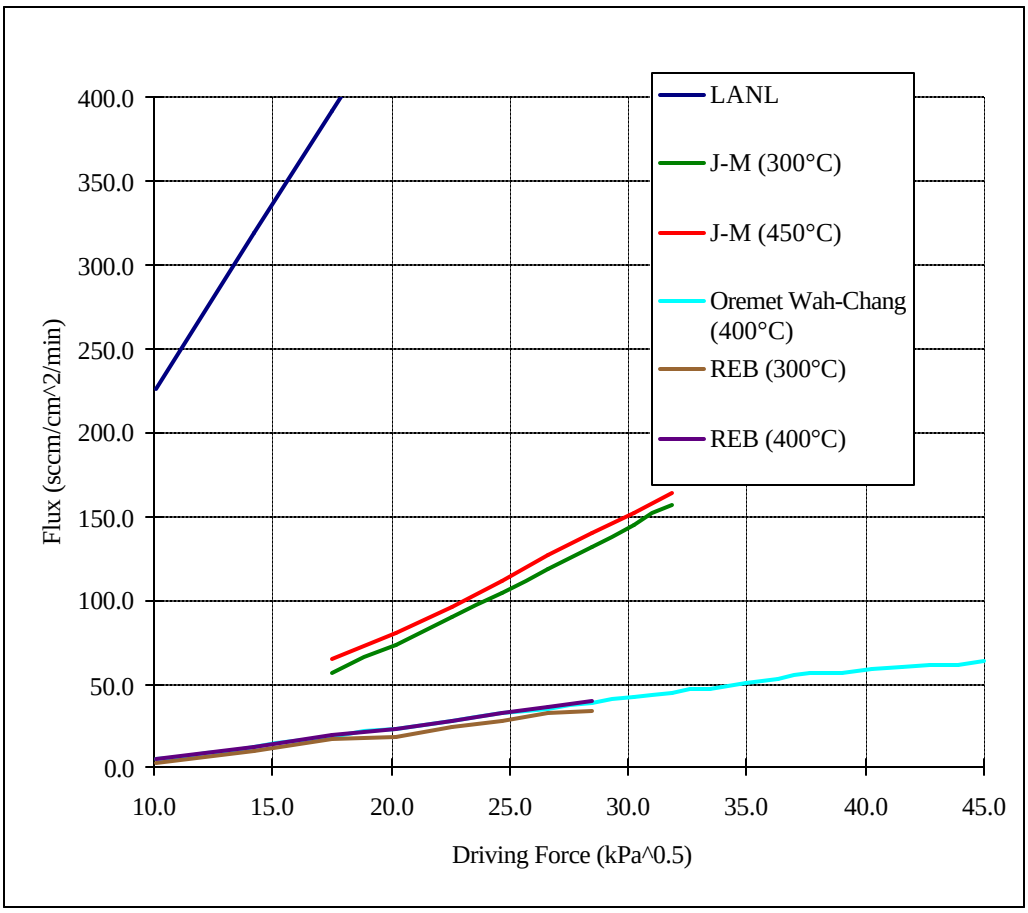

Figure 2.4: Metal membrane performance

[37] "Hydrogen," 1989, p. 384-385.

[38] "Composite-metal membranes for high-temperature hydrogen separations," Oremet Wah-Chang, Albany, OR, 1998.

the metal membranes is simply the cost of the palladium itself. At $200 to $600 per troy ounce depending upon market conditions[39], palladium metal structures are very expensive. This motivates the construction of very thin membranes and systems which do not achieve high recoveries. This is because the permeation through the metal membrane at a differential element is given by the following equation, widely referred to as Sievert's law:

$$\frac{\dot{n}_{H_2}}{A} = \frac{J}{t}\left[\sqrt{p_{H_2 raffinate}} - \sqrt{p_{H_2 permeate}}\right]$$

Where

J = permeability in $\text{gmol}/\text{cm}\sqrt{\text{atm}}$

t = membrane thickness in cm

This equation shows that molar hydrogen flux through the films is determined by the hydrogen permeability, J, which is a function of alloy composition and temperature, and is inversely proportional to the membrane thicknessFigure 2.4 illustrates this effect and compares the hydrogen permeabilities of the aforementioned Oremet Wah-Chang and Johnson-Mathey supported film membranes. Also included in Figure 2.4 are membranes from Robert E. Buxbaum[40] (REB) and Los Alamos National Laboratories[41] (LANL). Both of these high-performance membranes are based on composite construction, and have shown poor reliability in laboratory experiments. The pressures of interest are the hydrogen partial pressures on the high and low pressure sides of the membrane differential element respectively. It must be noted that real membrane separator recovery is limited by the permeate hydrogen pressure, as the high-pressure raffinate hydrogen partial pressure asymptotically approaches this value. The limiting hydrogen recovery is given below:

$$\frac{\dot{n}_{H_2 recovered}}{\dot{n}_{H_2 total}} = \frac{p_{H_2 raffinate-inlet} - p_{H_2 permeate}}{p_{H_2 raffinate-inlet}}$$

The innately high cost of the palladium alloys, and the relatively poor permeability of the more rugged commercially-available membranes makes the cost situation for such membranes bleak in anything but very small scale applications where the cost of the valves used in a PSA system is prohibitive. An example of such an application is the application of Pd-40Cu membranes by Northwest Power to reformers in the 5kWe class. They claim that their technology yielded a membrane cost of $30 to $50 per kWe capacity at the 1998 price for palladium[42]. Since palladium has increased in price 3-fold since then, we can impute a cost of

---

[39] Prices in late 2000 and 1st Q 2001 were as high as $600 per troy oz. Historically, prices were much lower, as shown in Platinum 1996: Interim Review, November 1996.

[40] Buxbaum, R.E., "Hydrogen transport through non-porous membranes of palladium-coated niobium, tantalum and vanadium," Journal of Membrane Sciences, vol 85, 1993, pp. 29-38.

[41] Moss, T.S., Peachey, N.M., Snow, R.C., Dye, R.C., "Multilayer Metal Membranes for Hydrogen Separation," International Journal of Hydrogen Energy, Vol 23, No 2, 1998, pp. 99-106.

[42] Edlund, D.J., Pledger, W.A., "An integrated Fuel Processor for PEM fuel cells," Northwest Power Systems, LLC, Bend, OR, 1998.

$90 to $150 for the palladium alone in the membranes. For the capacity of the proposed reformer of about 80 kWe, this would account for $7,200 to $12,000, exclusive of the costs of manufacturing the membrane, and building an appropriate mechanical structure for it. Further, these costs will be increased when the real effects of reformate operation are considered. Many reformate constituents adsorb strongly on the palladium alloy surface, thus reducing performance compared to neat hydrogen predictions. In the author's experience with metal membrane separators, the real reformate effects reduce hydrogen permeation by about 50% compared to neat hydrogen predictions when sulfur-free reformate is employed. Hydrogen sulfide causes irreversible poisoning of the membranes at concentrations as low as a few ppm.

The problems with the preceding purification options leaves PSA as the only viable alternative. However, industrial PSA systems are not particularly low cost. Luckily, QuestAir Gases of Vancouver, Canada manufactures a line of standardized hydrogen separation PSA systems under the HyQuestor trade name. Although a single system is estimated to cost $50,000, small quantity production should lower prices to the $15,000 level. DTI is working with QuestAir to evaluate these PSA systems for the small scale hydrogen appliance described in this study. The performance of the PSA system is the real factor which determines the choice between autothermal reforming and steam reforming. The weak adsorption of nitrogen on commercially-available adsorbents limits hydrogen recovery with nitrogen to less than 70% when very high purity gas is desired[43]. Conversely, recoveries of 75% or more are possible with nitrogen free gas over the same adsorbents, and higher recoveries may be possible with conventional adsorbents used in industrial steam reforming plants. This represents a 7% higher recovery with steam reforming than with ATR.

When these values are applied to the model feedstreams from Table 2.1, the ATR process yields only 2.2 moles of hydrogen per mole of methane while the steam reforming process could yield almost 3 moles. This results in a higher heating value efficiency limit[44] of about 96% for steam reforming and 70% for ATR. It will be shown in Chapter 4 that the value for steam reforming is reduced when real effects are considered, as the value for the ATR process would be. However, it is clear that the combination of steam reforming and PSA offers a much higher potential for high thermal efficiency than the ATR process does, even before the greater compression power requirements for the ATR process are considered. This leads to the selection of steam reforming with PSA cleanup as the overall process architecture for the proposed hydrogen appliance being developed in this dissertation.

2.3.1 The DTI steam reforming process

To implement a hydrogen appliance product which meets the product requirements set forth previously, several steps have been recognized. First, the steam reforming process with PSA cleanup is selected to maximize thermal efficiency to minimize operating costs. Second, the general goals of process and mechanical simplification are shown to be important for meeting capital cost, operating cost, reliability and safety goals. Previous research conducted by the

---

[43] McClean, C.R., Keefer, B.G., Rowat, D.W., "Pressure Swing Adsorption for Small-Scale On-Site Hydrogen Supply," 1997.

[44] The upper attainable limit of efficiency based on HHV of hydrogen produced versus HHV of fuel added to the process. This limit is unattainable in practice.

author with Directed Technologies Inc. funding has shown that these goals can be met through a combination of a simplified chemical process and an integrated reactor design which combines the functions of many of the process elements found in the industrial system.

Sections 2.1 and 2.2 show that the industrial technology for steam reforming natural gas is highly evolved, and that every process element has its place. For a small-scale process, the following components are required.

1) feed pressurization
2) fuel partial oxidation to remove di-oxygen
3) hydrogen recycle
4) feed hydrodesulfurization (HDS)
5) hydrogen sulfide absorption using zinc oxide
6) steam generation
7) primary reforming
8) product cooling
9) high-temperature shift
10) product cooling
11) low temperature shift
12) product cooling
13) pressure swing adsorption (PSA)
14) tailgas/fuel burner to heat the steam reformer

Of these unit operations, many are required to protect the main process catalysts from feed impurities. Partial oxidation protects the catalysts from oxidation. Hydrogen recycle, HDS and the zinc oxide absorber are all required to protect the primary reformer and the low temperature water-gas shift from sulfur poisoning. If these steps could be eliminated, the process would be reduced to the following:

1) feed pressurization
2) steam generation
3) primary reforming
4) product cooling
5) high-temperature shift
6) product cooling
7) low temperature shift
8) product cooling
9) PSA
10) Tailgas/fuel burner to heat the steam reformer

This simplification, brought about by identifying components which could be combined or eliminated, would afford a 29% reduction in complexity (as evidenced by the number of unit operations) compared to the baseline system. To achieve this goal, the need for feed pretreatment would have to be eliminated. This is impossible using industrial catalysts, and thus most developers have had to abandon this system simplification. However, it could be feasible if new catalysts which required little or no fuel pretreatment could be prepared. Thus, application

of DFMA principles from the concurrent engineering discipline forces consideration of the development of entirely new catalyst technology to afford a mechanical simplification. In a traditional, linear development process, it is unlikely that this route would be considered.

If a catalyst could be designed to simplify the system and to reduce costs, it would have to have the following attributes:

- redox stability to up to 6% oxygen in the natural gas feed
- resistance to up to 10 ppm sulfur in the natural gas feed
- high activity, equivalent to a 10,000 gaseous hourly space velocity (GHSV) on a dry feed basis
- long lifetime, preferably 100,000 hours

The first two requirements are based on limiting concentrations of di-oxygen and sulfur in line natural gas in developed countries. The activity requirement is derived from the desire to produce a compact, inexpensive reactor. The lifetime requirement is derived from a desire to reduce O&M costs, and is not unreasonable, as some industrial reforming catalysts already exhibit this sort of lifetime. Chapter 3 describes the design and test of catalysts which may fulfill these requirements, although it will be shown that the ability to design a low temperature water-gas shift catalyst with acceptable activity and sulfur tolerance may be limited.

This brings us to the question of the low temperature shift reactor. It provides only 1.6% of the theoretical hydrogen yield calculated in Table 2.1, yet has the most stringent sulfur concentration restrictions and presents the greatest hazard due to pyrophorric oxidation. Further, the low temperature shift reactor requires a separate reaction vessel, a heat exchanger and a temperature control loop. If these components were eliminated, the overall system would have the following elements:

1) feed pressurization
2) steam generation
3) primary reforming
4) product cooling
5) high-temperature shift
6) product cooling
7) PSA
8) Tailgas/fuel burner to heat the steam reformer

This system reduces complexity of 20% relative to the system with the low temperature shift reactor, and represents a total reduction in complexity of 43% relative to the industrial system. Both of these figures are again based on complexity as represented by the number of unit operations. This second simplification is an even clearer application of concurrent engineering, as the entire function of a component in the traditional system is called into question. By "thinking out of the box," it becomes clear that the added value attributed to the low temperature water-gas shift reactor is small, while it requires several distinct unit operations to be added to the process.

This system is probably the least complex which will have adequate thermodynamic efficiency to meet the product goals from a unit process standpoint. It is, however, possible to further streamline the system by mechanically integrating separate parts. In the simplified steam reformer system patent application in the Appendix, an integrated reactor is proposed which combines several of the functions remaining in the system into a single mechanical assembly. The primary reformer, product cooler, high-temperature shift reactor and tailgas/fuel burner assembly are all integrated into a single mechanical structure. This simplifies the overall product design into the following subsystems:

1) feed pressurization
2) steam generation
3) reactor assembly
4) product cooling
5) PSA

This simplification is the clearest application of the DFMA principles elucidated earlier, as the simplification is largely mechanical, and requires a revolution in mechanical design only, rather than a comprehensive revolution in the chemical technology of the system. It is obvious from the drastic reduction in the number of unit operations that this mechanical integration yields impressive benefits. However, this integration alone accounts for the elimination of only three unit operations. Overall, the improvements posited above eliminate nine unit operations. Thus, only a third of the proposed reduction in complexity can be attributed to simple mechanical integration, while the rest relies on parallel developments of improved process and catalyst technology.

The reactor assembly design and optimization is the subject of the concurrent engineering exercise described in this dissertation. The design of the burner, which is assumed to be a catalytic burner at this point, was conducted by other personnel at DTI and is thus not described in detail here. The main topics which are addressed are the catalyst design, synthesis and testing, the thermodynamic simulation, the integrated steam reforming and water-gas shift reactor design, and the impact of these three activities on the overall product economics. Each of these is described in a separate chapter of this study. Because product requirements were considered in the selection of the basic process elements selected in the design, the resulting design space is constrained and the scope for optimization is limited somewhat. However, it will be shown that application of a single cycle of concurrent engineering has yielded a new steam reforming process which is fundamentally more simple and more amenable to implementation in small-scale hydrogen generators. Further, a novel integrated reactor concept is demonstrated which offers low cost both for its manufacture and operation.

Chapter 3 Catalyst development and testing

The goal of the current development program is the elimination of as many separate processes and components from the industrial system as possible. This can be achieved through the provision of new catalysts which reduce or eliminate the need for some of the presently required steps. The most important examples of the potential for reducing complexity through catalyst innovation are as follows:

- Primary reformer miniaturization through the use of high activity catalysts with good long-term stability
- Elimination of nitrogen purge, partial oxidation pretreatment and hydrogen reduction systems through the use of a redox stable catalyst (this also reduces safety concerns regarding pyrophoric reactor meltdown)
- Combination of the water-gas shift reactors into a single, non-isothermal heat-exchange reactor using thermally-stable, selective and active catalysts
- Replacement of the expensive and complicated HDS system through the provision of sulfur-tolerant catalysts for steam reforming and water-gas shift

Achieving these goals would allow the entire reformer to be integrated into a single unit with much lower cost and complexity than demonstrated in previous devices. Further, the improved system would likely be less complex, more fault tolerant, and easier to control than existing systems.

The catalyst design process to achieve these goals is iterative, and includes catalyst design, synthesis and testing. To date, one cycle of this iterative process has been completed, and encouraging results are in hand. The theoretical aspects of the design process are outlined first, then the practical aspects of the catalyst manufacture and testing are described. Although the current results are encouraging, it will be shown that drastic improvements in the catalyst performance may still be achieved through the application of advanced synthesis techniques.

3.1 Catalyst design

The catalyst design associated with meeting the goals outlined above comprises several parts: identification of alternative catalysts and supports with acceptable activity, selectivity and redox stability, identification of catalysts with the best potential for aging resistance, and identification of the catalysts with the best sulfur tolerance. These issues must be addressed for both the steam reforming and water-gas shift reactions. This is accomplished in the following sections by way of literature review and theoretical calculations. In the absence of complete experimental data and considering the often conflicting information available, the conclusions drawn must be considered both preliminary and qualitative. However, it will be shown that a significant body of evidence is available which suggests a clear pathway to the synthesis of catalysts which will meet the required performance criteria established previously.

3.1.1 Metal and support effects on activity

A wide variety of noble and base metals have been tested as steam reforming and water-gas shift catalysts. Because the operating conditions and detailed reaction mechanisms of steam reforming and water-gas shift are sufficiently dissimilar, they will be addressed separately here. Further, the performance of alternative base metal catalysts will not be extensively treated because such catalysts lack the desired redox stability. Thus, the candidate catalysts are restricted mainly to the noble metals of group VIIIB, with the exception of rhenium (VIIB) and silver (IB). These later two are considered as water-gas shift catalysts, where some tendency towards oxidation may be tolerated as the feed to these reactors always contains significant quantities of hydrogen which may be expected to reduce any oxides present *in situ.*

The goal of the steam-reforming catalyst design is the identification of candidate catalysts which deliver equivalent or superior activity to the nickel catalysts currently used while providing high redox stability to obviate hydrogen recirculation and safety concerns associated with pyrophoricity. Further, these catalysts should possess stable activity over a period of any years of continuous operation, preferably 100,000 hours, and must thus be highly resistant to sintering, coking and other degradation mechanisms over a temperature range of 450 C to 800 C. Finally, the catalysts should be capable of continuous operation in environments with less than 10 ppm of total sulfur. Only activity will be addressed in this section, with the questions of aging and sulfur tolerance addressed later.

The catalytic activity of the noble metals for steam reforming has been reported by several authors for both industrial and automotive exhaust applications. Their findings regarding the relative activities of the noble metals are fairly consistent although the operating conditions and catalyst types vary substantially. Some of the more numerically explicit findings are represented as constant temperature turnover frequencies[45] in Table 3.1[46]. It is important to note two factors regarding these data. First, the test conditions are at relatively low temperatures. Second, the operating pressures are also much lower than those employed in practical reactors. This is a common feature of all of the literature data available, suggesting that more complete kinetic studies will be required to select the most active catalysts. Another interesting point is that the data on ethane and toluene reforming are based upon γ–alumina supported catalysts while the methane data are derived from silica supported metals. Support interactions are significant in steam reforming, and may also impact the observed results.

Other researchers who have studied steam reforming of hydrocarbons in automotive exhaust conditions have shown similar trends in activity. Whittington, *et al* [47]showed that the relative steam reforming activity of γ–alumina supported noble metals was Pd>Rh>Pt for the reforming of propane. They also showed that promotion of the alumina with ceria reduced the lightoff temperature for the reaction 20 C to 50 C, and changed the order of activity to

---

[45] Turnover frequency is defined as the imputed number of individual reactions per metallic site per unit time.

[46] Rostrup-Nielsen, 1984, p.99.

[47] Whittington, B.I., et al,"Vehicle exhaust catalysis: I. The relative importance of catalytic oxidation, steam reforming and water-gas shift reactions," Catalysis Today, vol 26, pp. 41-45, 1995.

Rh>Pd>Pt. This promotion by ceria has also been noted by, Suzuki, *et al*,[48]. A most interesting relative comparison of steam reforming activities is reported by Barbier and Duprez[49], who have condensed the data of Gandhi, et al. They reported that for propene/propane mixtures at 723K the relative activities of the metals in steam reforming is Rh~Ir>Pt>Co>Ru>Ni~Re. This result is clearly less favorable for ruthenium than those reported by Rostrup-Nielsen, a result which is potentially explained by the stability of ruthenium. Duprez[50] notes that in toluene steam dealkylation (SDA) Pt, Pd, Ru and Os all deactivate much more quickly than Rh and Ir. This is particularly interesting as the SDA reaction runs at very low steam-to-carbon ratios, which would promote coking of the catalyst. It can thus be stated that rhodium, ruthenium, and palladium have uniformly exhibited fairly good activity for the steam reforming of hydrocarbons, with rhodium generally showing the best activity. Notable activity has also been exhibited by platinum and iridium. The relative activities of the metals has been shown to differ under different operating conditions, and the total variation in activity has been shown to be less than one order of magnitude. This last fact is remarkable, and suggests that the reaction is a) highly structure insensitive[51] (i.e. is not affected by differences in metal crystal structure and active site size/configuration) and b) that other factors should be used to select the most desirable metal from an overall standpoint.

Table 3.1: Relative activity of noble metals for steam reforming hydrocarbons

Feed	S:C ratio	Temp	P	Turnover frequencies relative to nickel						
				Rh	Ru	Pd	Pt	Ir	Ni	Re
ethane	4	773K	1 bar	13	9.5	1	0.9		**1**	0.2
toluene	~1	713K	0.34 bar	11	5.8	3.8	2.3	1.6	**1**	
methane	3	773K	1 bar	1.6	1.4	0.6	0.5	0.7	**1**	

The choice of supports for the steam-reforming reaction is a complex one, as the support has been shown to play a significant role in the observed catalyst activity as discussed previously. Industrial catalyst supports for steam reforming include α-alumina, magnesium aluminate spinels and calcium aluminate. These somewhat acidic supports have been shown to possess better activity for steam activation than alternative supports such as titania and magnesia[52]. All of these support materials have low surface areas (< 10 m^2/g), making extensive dispersion of the catalyst metal difficult. However, the need for great mechanical strength in the industrial catalysts, which may be required to support columns of pellets up to 12 m in height, makes the use of these ceramics imperative.

The use of a higher area support would obviously allow for greater catalyst dispersion. Silica and aluminasilicates (synthetic zeolites) are ill-suited for the reforming reaction because they volatilize under the high steam activity in the reacting stream. Carbon supports have not been widely used, which may be due to their weak interaction with steam or their susceptibility

---

48 Suzuki, T., Iwanami, H., Yoshinari, T., "Steam re forming of kerosene on Ru/Al_2O_3 catalyst to yield hydrogen," International Journal of Hydrogen Energy, vol 25, 2000, pp. 119-126.

49 Barbier, J., Duprez, D., "Steam effects in three-way catalysis," Applied Catalysis B, vol 4, p. 116, 1994.

50 Duprez, D., "Selective steam reforming of aromatic compounds on metal catalysts," Applied catalysis A, 1992, p. 116.

51 Duprez, 1992, p. 117.

52 Rostrup-Nielsen, 1984, p.60.

to gasification under the reaction conditions. The high defect structure spinel-type alumina, γ-alumina, is stable in air or vacuum to about 1000 C and has a surface area in excess of 100 m^2/g. Exposure to high steam and hydrogen activity lowers this phase transition temperature[53], but stabilization by rare earth oxides such as baria or ceria may effectively extend the operating range[54]. γ-alumina has been shown by many authors to possess excellent activity for steam activation[55], a crucial step in providing hydroxyl radicals to the metal surface. Thus, γ-alumina is potentially the best candidate support for steam reforming, especially if promotion by baria or ceria proves effective. If not, zirconia has been shown to provide acceptable activity, and has excellent stability to very high temperatures as well as fair surface area (~25 m^2/g). The question of rare-earth metal promotion is an important one which will be addressed further in the section on aging. Steam-reforming catalysts using γ-alumina as well as proprietary refractory supports were prepared and tested. The results and implications of this testing are discussed later in this chapter.

The water-gas shift reaction has been studied for many years[56], and has been brought to a state of relative maturity in the industrial market wherein three major types of active catalysts are available[57]. A chromia-promoted iron catalyst similar to the Fischer-Tropsch catalyst is available and employed for high temperature reactions (400 C – 500 C). This catalyst is not considered very active, but is mechanically robust and very inexpensive, as well as possessing low sensitivity to sulfur poisoning. For low temperature operation, the copper mixed oxide catalysts are used for desulfurized feeds. These were for many years the most active industrial catalysts, whose only drawbacks are low sintering temperature and high sensitivity to sulfur. The final commercial catalysts are sulfided cobalt-molybdenum alloys. These are the most recent development, and are employed wherever a sulfur-bearing reactant stream is to be processed. They require 100's of ppm of sulfur to maintain their sulfided state depending upon feedstock composition and temperature, limiting their applicability to the processing of heavy feedstocks or coal gasification products. All of these catalysts are operated in the reduced state, all are more or less pyrophoric, and none save the venerable iron catalyst are operable under the desired concentrations of feedstream sulfur.

Several basic criteria defining a successful water-gas shift catalyst bear elucidation. First, the catalyst must be very active as the reaction is carried out at fairly low temperatures. Second, the catalyst must prove stable in the desired operating conditions. Both of these points are obvious catalyst design criteria, and have been discussed previously in this work. Finally, the catalyst must show an appreciable selectivity towards the water-gas shift reaction over the methanation reaction. This is because cooled reformate contains a super-equilibrial amount of hydrogen and carbon oxides as compared to the low amount of methane present after the primary reforming process. Thus, the rate of water-gas shift on the catalyst must be much greater than the rate of the methanation reaction or substantial methane formation may be expected. None of

---

53 Rostrup-Nielsen, 1984, p. 32.

54 Harrison, B., et al, "Promoting Platinum Metals by Ceria: Metal Support Interractions in Autocatalysts," Platinum Metals Review, vol 32, no 2, 1988, p. 74.

55 Grenoble, *et al*, 1981, p. 94.

56 Satterfield, C.N., Heterogeneous Catalysis in Industrial Practice, 1996, pp. 442-444.

57 Newsome, D.S., "The Water-Gas Shift Reaction," Catalysis Review – Science and Engineering, vol 21, no 2, 1980, pp. 275-318.

the commercial catalysts show any tendency towards methanation. However, when alternative active metals are considered, it is important to compare relative methanation activities as well as relative water-gas shift activities in order to identify potentially selective catalysts.

The seminal study comparing the activity of supported metal catalysts for the water-gas shift reaction was conducted by Grenoble, *et al*. This study investigated a wide variety of metals on several different supports and produced experimental data pertaining to both metal and support effects. They further postulated two separate reaction mechanisms to explain the differing behavior of noble metal and base metal catalysts. Significant additional work has been conducted in conjunction with exhaust catalyst development, and may prove important in the catalyst design. Unfortunately, as was the case with steam reforming, none of the studies available to date was conducted under appropriate pressures, making quantitative extrapolations to the desired operating conditions (> 5 bar) difficult. Figure 3.1 summarizes the data of Grenoble, *et al* for γ-alumina supported metals in water-gas shift[58]. It is clear from the figure that none of the metals evaluated exhibited activity as high as copper, the most active metal for water-gas shift. However, ruthenium and rhenium show a fairly high activity, with platinum not far behind. All of these alternative metals are more active than the iron catalyst tested by Grenoble, *et al*, although comparison with a commercially-prepared iron catalyst was not conducted. These data suggest that ruthenium and rhenium, along with platinum, comprise the best alternative water-gas shift catalyst candidates. Grenoble, *et al* showed via a volcano-type plot of CO adsorption energies that the lower activities of the alternative metals compared to copper was due to their higher adsorption energy for CO (25+ kcal/mol vs. ~17 kcal/mol for copper)[59]. The adsorption energy of carbon monoxide on silver should be intermediate between those on copper and gold, it's fellow group IB metals. This suggests that silver might prove to have useful activity for the water-gas shift reaction (the activity for gold was slightly less than that for Ir in the Grenoble, *et al* study, with a very low activation energy corresponding to the low CO adsorption energy on gold.) No studies of the water-gas shift reaction on silver are available in the literature, so no firm conclusions can be drawn without testing.

The relative metal activities reported by Grenoble, *et al*, have been confirmed by extensive work in the exhaust catalysis field which is summarized by Barbier, *et al*.[60] In research by Grenoble, *et al* and others the role of a γ-alumina support in improving the activity of supported water-gas shift catalysts has been demonstrated. Increases in activity of up to three orders of magnitude have been reported when similar catalysts prepared on alumina, silica, zeolites and activated carbon are compared. An interesting contribution from the field of exhaust catalysis is the fact that ceria promotion of the support greatly improves the activity of water-gas shift catalysts. This has been demonstrated by a number of workers[61] and is also reviewed by Barbier, *et al*.[62] These considerations suggest that highly active, water-gas shift catalysts may be prepared by supporting ruthenium, rhenium, platinum or silver on ceria-promoted or unpromoted γ-alumina supports.

---

58 Grenoble, *et al*, 1981.

59 Grenoble, *et al*, 1981, p. 95.

60 Barbier, et al, 1994, pp. 111-113.

61 Whittington, et al, 1995 and Harrison, et al, 1988.

62 Barbier, et al, 1994, p. 113-114.

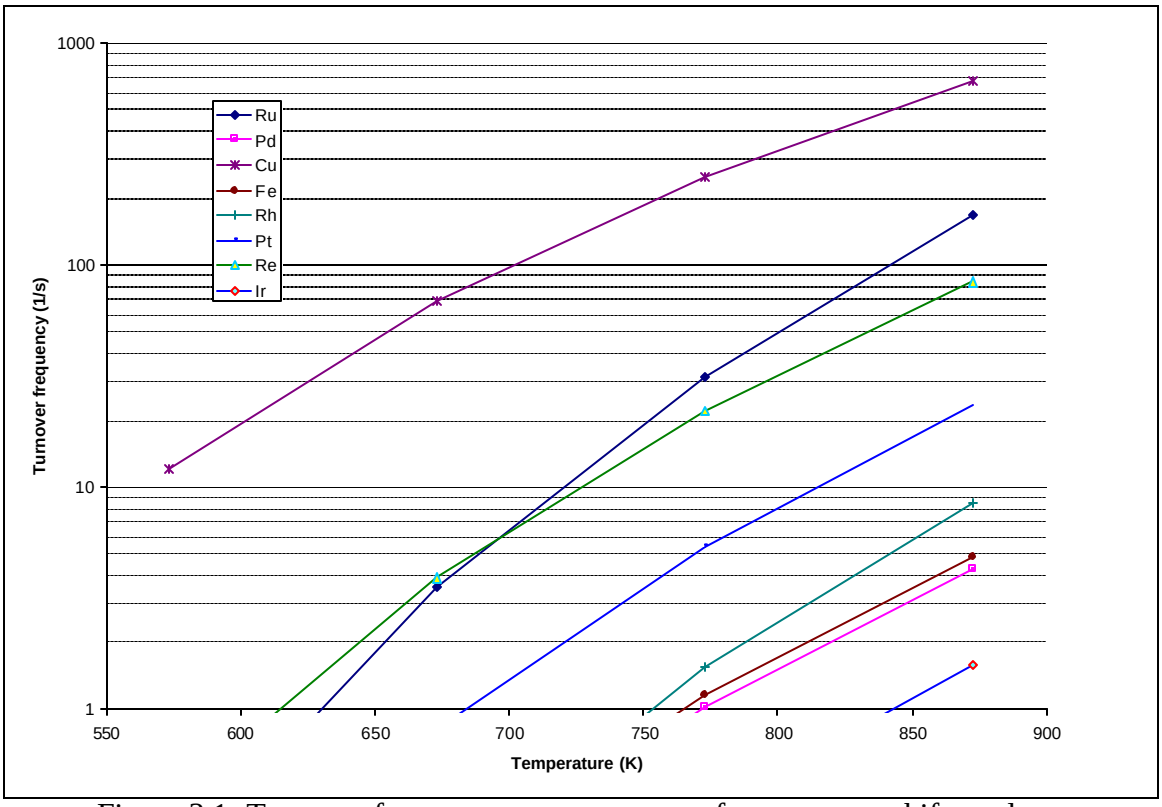

Figure 3.1: Turnover frequency vs. temperature for water-gas shift catalysts

The selectivity of these potential candidate catalysts against methanation is an important question. Extensive research conducted by the U.S. Bureau of Mines[63] in the 1970's showed that the relative activities of supported noble metals for methanation is Ru>>Rh>>Re>Pt. Thus, it is probably wise to rule out ruthenium as a candidate catalyst as the methanation side reaction may reduce hydrogen yield more than the desired water-gas shift reaction will increase it. However, it would appear that both rhenium and platinum persist as good candidates based upon relative selectivity against methanation. No data are available for methanation over silver, making a judgement of selectivity difficult. However, the volcano plot for methanation activity is centered at higher CO adsorption energies than that for the water-gas shift reaction[64] (thus the high methanation activities of ruthenium, nickel and rhodium), suggesting that weakly adsorbing silver would prove relatively inactive for methanation, and thus highly selective. The volcano plots for methanation and the water-gas shift reaction are represented on a single plot from the data of Grenoble and Vannice in Figure 3.2, which shows the relative shift in the optimal adsorption energy. It is important to note that these data were developed on catalysts with different supports (alumina for WGS and silica for methanation) and at different temperatures, but they do show the qualitative shift in peak activity vs. adsorption energy.

[63] Shultz, J.F., Karn, F.S., Anderson, R.B., Noble Metals, Molybdenum, and Tungsten in Hydrocarbon Synthesis, 1967.

[64] Vannice, M.A., "Catalytic activation of carbon Monoxide on Metal Surfaces," p. 167.

It has been shown that noble metal catalysts with higher activity than the existing nickel catalysts are available for steam reforming, while noble metal and new transition metal catalysts for water-gas shift will likely have less activity than their copper-based industrial analogs. In the case of the steam-reforming reaction, the activity alone is a poor criterion in advanced catalyst design. In the water-gas shift reaction activity and selectivity are deciding factors identifying a number of candidate materials. In both reactions, the new catalysts will likely be supported on γ-alumina, with ceria promotion being desirable for the water-gas shift reaction. A final note regarding these materials pertains to their potential cost. The market prices of platinum, rhodium, and palladium are all high, with values historically varying between $300 and $500 per troy ounce, with a dramatic recent increase evidenced in the 3rd and 4th quarters of 2000. The prices of ruthenium and iridium have traditionally been much lower, generally between $30 and $70 per troy ounce[65]. Because total demand for these last two is quite low, their prices are also very sensitive to fluctuations in demand. Recent iridium prices have soared above $400 per troy ounce. The prices for silver and rhenium are both very small in relation to those of the other

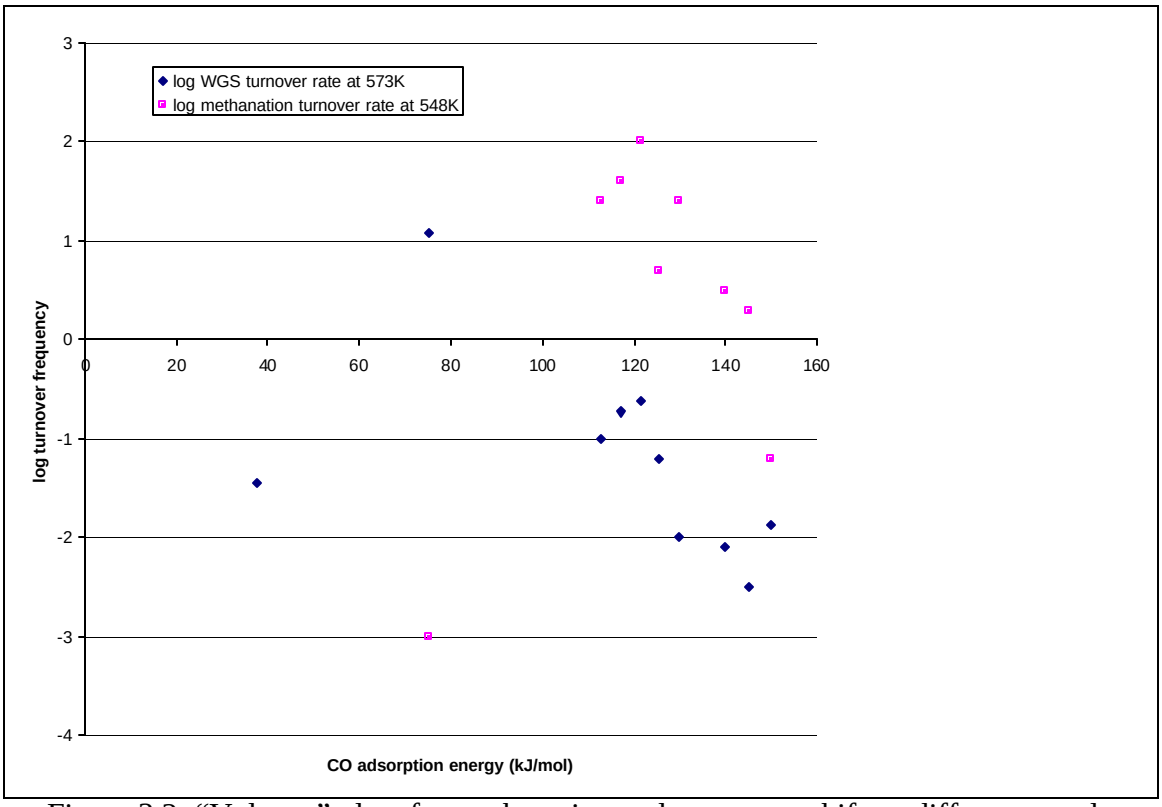

Figure 3.2: "Volcano" plots for methanation and water-gas shift on different metals

metals considered here, generally less than $5 per troy ounce. Catalyst costs are strongly dependent upon preparation technique, metal loading, support cost, promoter cost, annual production volume and other factors, making strict correlations based upon metal cost difficult. However, it is clear that the high cost of the noble metals makes them much more sensitive to factors such as lifetime and metal loading than the less costly compositions. For water-gas shift

65 Platinum 1996: Interim Review, 1996, pp. 20-23.

catalysis in particular, the very high cost of platinum relative to rhenium and silver makes it likely that any acceptable catalyst from a cost standpoint would have to exhibit very low metal loading when compared to a rhenium or silver alternative.

3.1.2 Catalyst aging

Catalyst aging refers to a loss of activity or selectivity after a period of operation. Ideally, the catalysts would continue to operate indefinitely without any change in performance, but in practice, a variety of factors may act to reduce the catalyst performance over extended periods of operation. These include sintering of the active metal, sintering/phase change of the support, coking of the active metal, and chemical interactions between the active metal and the support. Because the active metals of interest are quite expensive, loss of catalyst performance must be minimized in order to allow for an acceptable overall catalyst system life-cycle cost. Thus, each of these important aging mechanisms will be discussed separately below.

As-prepared catalysts have their active, metallic components widely dispersed on the ceramic support material. This maximum state of dispersion usually provides maximum total activity, especially if the reactions are not structure sensitive. However, the high surface energy of the many small, dispersed metallic clusters makes them highly susceptible to agglomeration to yield a system with lower total free energy. The growth of the metal particles occurs through two principal mechanisms, Ostwald ripening and particle coalescence. In the former, individual atoms move about the support surface, eventually enlarging larger particles and leading to the disappearance of smaller ones. In the latter mechanism, the particles themselves may be in motion, coalescing with other particles as they move. Independent of the mechanism of sintering, the onset of sintering is typically correlated with the metal melting temperature. The Tammann temperature, which is 50% of the melting temperature is usually associated with the onset of sintering. Also employed is the Huttig temperature, which is 33% of the melting temperature, and is associated with the onset of surface mobility of the metal atoms[66]. Table 3.2 lists the approximate ranges for the onset of sintering for various metals. Both hydrogen and steam have variously been reported to affect the onset of sintering of metals, so that these temperature ranges may be affected significantly by the operating conditions employed. The steam effect is particularly insidious on alumina and silica supports[67]. It is also important to note that alloying a low melting point material with a higher melting point one usually reduces sintering, but may have unpredictable affects on catalyst activity.

Based upon these sintering temperatures, iridium and ruthenium are likely to be much more resistant to activity loss due to sintering than platinum, palladium and rhodium. Of these latter three, rhodium should offer the best sintering resistance. All of these metals, except palladium, should exhibit better sintering resistance for steam reforming than the industrially-favored nickel compositions. For the milder conditions of the water-gas shift reaction, rhenium and platinum should both be highly stable, whereas silver, like copper, would only be serviceable at low temperatures.

---

[66] Rostrup-Nielsen, 1984, pp.45-46.

[67] Trimm, D.L., "Poisoning of Metal Catalysts," Deactivation and Poisoning of Catalysts, Oudar and Wise, eds., 1985, p. 174.

Table 3.2: Temperature ranges for the onset of sintering[68]

Metal	Melt point (C)	Sintering range (C)
Cu	1083	360-540
Ir	2410	800-1200
Fe	1535	500-750
Ni	1453	500-725
Pd	1552	500-750
Pt	1772	570-880
Re	3180	1000-1500
Rh	1966	600-1000
Ru	2310	730-1200
Ag	962	330-480

The stability of the support against sintering and phase change is of paramount importance in γ-alumina supported catalysts, as this phase is never thermodynamically stable under operating conditions. The transition between this defect spinel phase and the stable α phase is via δ and θ alumina[69]. These transitions occur in the range between 700 C and 1000 C. Each of these transitions is accompanied by a drastic loss in total surface area, as well as probable inclusion of many of the active metal atoms into the ceramic lattice. It has been shown that in humid, oxidizing conditions, the phase change of alumina is accelerated by the water partial pressure to the ½ power. It has also been shown that doping with barium and lanthanum retard sintering under the conditions of exhaust catalysis[70], but the efficacy of these techniques in highly reducing environments with very high steam activities is unknown. Ceria has also been shown to stabilize γ-alumina under some conditions[71], and under reducing conditions, has been shown to yield a variety of interesting spinels[72]. In general, the sintering of γ-alumina is expected to be relatively rapid under operating conditions for steam reforming, and slow under operating conditions for the water-gas shift reaction. If the stability under steam reforming conditions proves inadequate, then more refractory ceramics will have to be substituted. Possible candidates include α-alumina, zirconia, magnesia aluminate spinel, barium hexa-aluminate spinel, calcium aluminates and various nickel spinels. Normally, these refractory supports have very low surface area, which makes metal dispersion difficult. In order to achieve high surface area with any of these supports, special synthesis techniques will be required to generate nano-particles. Such synthesis would represent a significant development hurdle, and would not be undertaken unless the otherwise attractive γ-alumina approach fails.

---

68 Trimm, 1985, p.175.
69 Satterfield, 1996, p. 117.
70 Barbier, et al, 1994, p. 124-125.
71 Harrison, et al, 1988, p.74.
72 Barbier, et al, 1994, p. 130.

The coking of the catalyst can proceed via carbon formation on the support or on the metal itself. The steam-rich operating conditions in the reformer make coke formation highly unfavorable, although it must always be considered as a possible failure mechanism, especially as steam-to-carbon ratios closer to the stoichiometric values are considered. Perhaps the best indicator of limiting coking performance under steam reforming conditions is the deactivation by coking of catalysts for toluene steam dealkylation (SDA). As discussed previously, catalysts based upon rhodium and iridium seem to show the least propensity for coking under these reaction conditions, while catalysts based on the other noble metals are more susceptible. Because the operating conditions in SDA are far more likely to form coke deposits than any foreseeable conditions in steam reforming natural gas or even LPG, the coking issue can be considered relatively unimportant for catalyst design purposes if noble metal catalysts are used. This contrasts strongly with industrial nickel catalysts, which are highly susceptible to coking failure.

A final area for concern is the chemical interactions between the catalyst and the support. Of especial importance in this area is the demonstrated tendency for rhodium to migrate into the alumina structure to form a "dispersed oxide" or a psuedo-spinel. This effect is observed at the required operating conditions for steam reforming, and can drastically reduce exposed rhodium surface area. However, some evidence exists which suggests that ceria promotion may retard this process[73]. Once again, no aging due to support reactions is expected at the low temperatures of the water-gas shift reaction, although at the higher temperature operating conditions it is possible that a volatile rhenium oxide could be formed which would result in eventual catalyst deactivation. It is also possible that interactions between the dispersed metal and the supporting oxide may lead to incorporation of the metal and a very high sensitivity to oxidative potential in the reformer environment. This effect is observed with α-alumina and magnesium aluminate spinel materials when nickel is the active metal, and leads to the industrial use of a hydrogen co-feed with these catalysts. Industrially, calcium aluminates are used as an alternative support which interacts less strongly with nickel and allows startup in flowing steam.

In summary, aging of the candidate water-gas shift catalysts on ceria promoted or unpromoted γ-alumina supports is not anicipated due to the low operating temperatures envisioned. The only exception is the silver catalyst, which will likley age due to metal sintering at temperatures above 300 C, thus restricting its use to lower temperatures. Under the far more aggressive conditions of the steam-reforming reaction, many of the candidate catalyst metals will likely experience excessive aging due to metal sintering. The tendency towards sintering is qualitatively represented in descending order Pd>Pt>Rh>>Ru>Ir. This effectively eliminates platinum and palladium as candidate steam-reforming catalysts. Rhodium may also be eliminated for high temperature use, as it interacts strongly with the alumina support to form pseudo-spinels which are not catalytically active. This reaction can significantly reduce the available rhodium area under reaction conditions. Of the more promising catalysts, ruthenium is generally considered more active than iridium, while iridium will potentially have greater resistance to sintering and coking. Another possible route for catalyst aging in the steam-reforming reaction is the phase transformation of the γ-alumina support to a lower-area phase. This effect may be too slow to be of importance, and may possibly be retarded by the addition of

[73] Barbier, et al, 1994, pp. 126-130 and Harrison, et al, 1988, pp. 78-79.

stabilizers such as baria, lathana or through ceria promotion. If it is not, more refractory supports must be pursued.

3.1.3 Sulfur tolerance of candidate catalysts

Both the steam reforming and water-gas shift reactions have been shown to be catalyzed by a variety of noble metals. For steam reforming, rhodium, ruthenium, osmium, iridium, palladium and platinum all exhibit activity equal to or better than nickel itself. For the water-gas shift reaction, ruthenium, rhenium and platinum have demonstrated good activity and carbon monoxide heat of adsorption suggest that silver is also an excellent candidate. Toxicity concerns eliminate osmium from the possible choices for new steam-reforming catalysts. Poor selectivity against methanation likewise eliminates ruthenium for water-gas shift applications. As previously mentioned, aging problems may also eliminate the more expensive noble metals from consideration as steam-reforming catalysts. However, this still leaves a large array of candidate materials for evaluation. Sulfur tolerance in the catalysts would eliminate the requirement for desufurization of the feedstock (natural gas contains trace amounts of hydrogen sulfide as well as intentionally added mercaptan odorant). Thus, sulfur tolerance of the candidate materials can significantly reduce the possible experimental matrix for new catalyst development.

Sulfur poisoning of catalysts is due to the surface adsorption of hydrogen sulfide, often, but not always, followed by desorption of a di-hydrogen molecule. Thus, the chemisorbed layer may be considered a two-dimensional sulfide. In systems where no stable sulfide is known, it may be inferred that the sulfur remains as hydrogen sulfide. In either case, sulfur poisoning is clearly a chemisorption phenomenon which is limited to monolayer coverage. The presence or absence of additional, physisorbed hydrogen sulfide is of no technical importance, because it is the strong blocking of active catalytic sites by the adsorbed monolayer which reduces catalytic activity. If catalyst surfaces were totally uniform, and the heat of adsorption identical for every site, and thus independent of surface coverage, then a simple Langmuir isotherm could be applied. The Langmuir form relates surface coverage to a limiting partial pressure (p_{sat}) at which the surface is entirely covered by a monolayer of adsorbed molecules.

$$\theta = \frac{s\left(p/p_{sat}\right)}{1 + s\left(p/p_{sat}\right)}$$

where θ is surface coverage and s is an empirically-determined constant

p_{sat} could then be related to the heat of adsorption, which would have to be experimentally determined for each material in question.

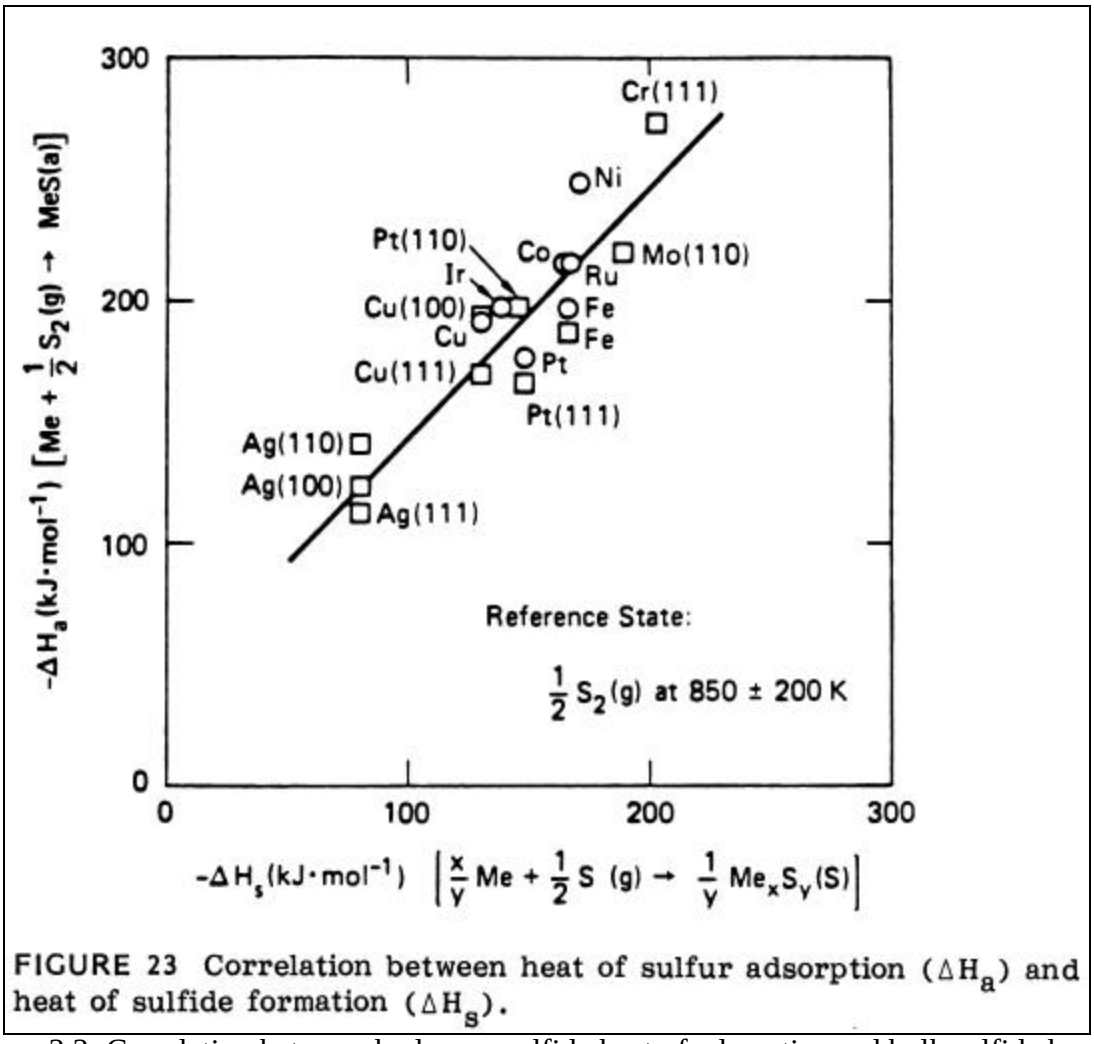

FIGURE 23 Correlation between heat of sulfur adsorption (ΔH_a) and heat of sulfide formation (ΔH_s).

Figure 3.3: Correlation between hydrogen sulfide heat of adsorption and bulk sulfide heat of adsorption (from Wise, *et al*, 1985, p. 45)

$$\frac{p_{H_2S}}{p_{H_2}} = \theta \exp\left[\frac{\Delta H^o(1+B\theta)}{R_u T + B\theta} - \frac{\Delta S^o(1+A\theta)}{R_u}\right]$$

Where

θ = fractional surface coverage

B and A are empirically - derived constants

temperature and partial pressure conditions are at the catalyst surface

Unfortunately, hydrogen sulfide chemisorption is more complicated, as the heat of adsorption decreases with increasing surface coverage[74]. The experimental data available suggest that a modified Temkin isotherm more closely represents sulfur adsorption and poisoning. This form once again can be correlated with experimental data to determine the standard heats and entropies of adsorption (ΔH^o and ΔS^o respectively) and the curve-fitting parameters A and B. Unfortunately, these are not available for all of the candidate materials. Nor is it clear that the data available allow extension to temperatures much different than those used in the original testing. What is shown in Figure 3.3 is that for 50% coverage, there exists a strong correlation between the heat of adsorption (ΔH_a) of hydrogen sulfide and the heat of formation for the most stable bulk metal sulfide (ΔH_s) at that temperature. This suggests that bulk metal sulfide equilibria can be used as a general guide for the selection of sulfur-tolerant catalysts at a given operating temperature.

Metal sulfide equilibria may be calculated for all of the metals of interest without any experimental investigation from readily available reference data. The sole exception being rhodium, for which no stable sulfide thermodynamic data was found[75]. The general metal sulfiding reaction may be represented as follows:

$$nMe_{(s)} + mH_2S_{(g)} \xleftrightarrow{K} Me_nS_{m(s)} + mH_{2(g)}$$

$$\prod (a_i)^{\nu_i} = K = \frac{a_{Me_nS_m} a_{H_2}^m}{a_{Me}^n a_{H_2S}^m}$$

If we assume unity activity (a_i) for the solid phases, and consider that at the high temperatures of interest the gas behavior is likely ideal, the equilibrium constant (K) reduces to

$$K \cong \frac{\left(\frac{y_{H_2} P_{tot}}{P^o}\right)^m}{\left(\frac{y_{H_2S} P_{tot}}{P^o}\right)^m} = \left(\frac{y_{H_2}}{y_{H_2S}}\right)^m$$

$$\frac{y_{H_2}}{y_{H_2S}} = K^{1/m}$$

Thus, by calculating the equilibrium constant across a range of temperatures, we can predict limiting ratios of hydrogen to hydrogen sulfide to prevent bulk sulfiding. Materials showing a much lower affinity for sulfur adsorption would then be characterized by lower limiting ratios. These materials would then be candidates for sulfur-resistant catalysts. The equilibrium constant

---

[74] H. Wise, J. McCarty, J. Oudar, "Sulfur and Carbon Interactions with Metal Surfaces," Deactivation and Poisoning of Catalysts, 1985, p. 43.

[75] This conclusion is drawn after consulting several comprehensive thermodynamic references and chemical encyclopedia. It should be noted that though rhodium is considered in the literature to exhibit very good sulfur tolerance, it does adsorb hydrogen sulfide.

is calculated at a variety of temperatures from tabulated values of the Gibb's energy of formation $\left(G^{o}_{i_T}\right)$ for each of the molecules involved in the sulfide reaction.

$$-R_u T \ln K = \sum_i \nu_i G^{o}_{i_T}$$

$$-R_u T \ln K = mG^{o}_{H_{2T}} + G^{o}_{Me_nS_{mT}} - mG^{o}_{H_2S_T} - nG^{o}_{Me_T}$$

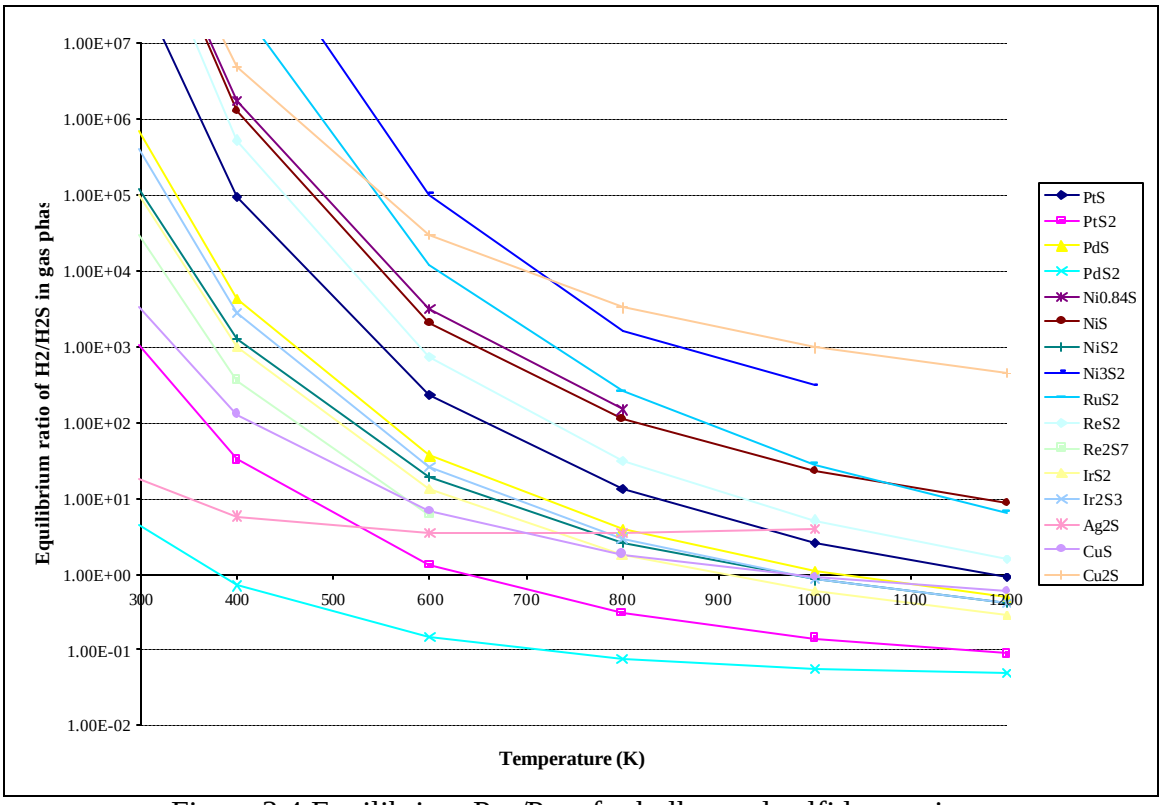

Figure 3.4:Equilibrium P_{H2}/P_{H2S} for bulk metal sulfide reactions

These calculations were conducted for a variety of important metal sulfides for the temperature range between 298 K and 1200 K. The resulting values are plotted in Figure 3.4. Figure 3.4 shows that of the many sulfides formed for each metal, one is typically the most stable at all temperatures. Recalling from Figure 3.3 that adsorption correlates with the formation of the most stable sulfide form, much of the confusing detail can be eliminated from Figure 3.4. Further, a more detailed picture is obtained by considering only the traditional catalyst materials and new candidate materials for each operating temperature range in question.

For the steam-reforming reaction, the temperature range between 800 K and 1200 K is of special interest. Nickel is the traditional industrial catalyst, and noble metals such as ruthenium, platinum, rhodium, and iridium are potential sulfur-tolerant species. No activity is reported for rhenium; silver and copper will sinter well below 800 K, and are thus not practical candidates. Choosing the most stable forms of these candidates and the nickel baseline yields Figure 3.5. The data suggest that all of the candidates will show much higher sulfur tolerance than nickel,

with iridium and platinum potentially exhibiting substantially better performance than ruthenium. Once again, it is interesting to note that no thermodynamic data for any stable sulfides of rhodium were located, suggesting that rhodium may have an even higher tolerance to sulfur poisoning than the metals investigated here. However, literature details on rhodium-sulfur interactions under reducing conditions do not universally support this point[76], and the conflicts suggest that only testing under the desired operating conditions will allow complete understanding of the situation.

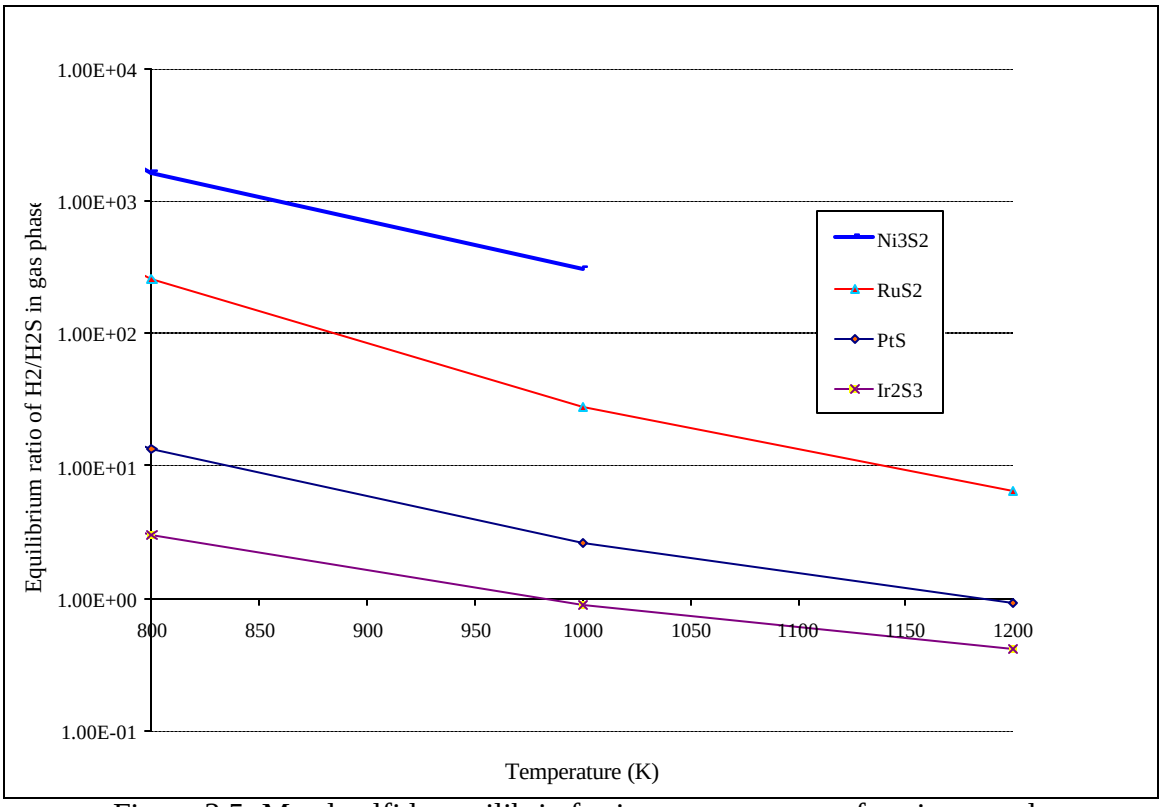

Figure 3.5: Metal sulfide equilibria for important steam reforming metals

Figure 3.6 investigates candidate materials across the anticipated water-gas shift operating temperature range of 450 K to 800 K. Dicopper sulfide formation is plotted as a reference curve as copper-based catalysts are the current best technology for water-gas shift at temperatures below 600 K. Once again, it is clear that most of the candidate materials offer at least moderate advantage over copper in stability against bulk sulfide formation. Platinum catalysts have been shown to exhibit excellent activity and selectivity for the water-gas shift reaction, and will have very good sintering resistance between 600 K and 800 K (platinum

[76] In their review paper on three-way catalysis, Barbier, *et al*, (1992) suggest that sulfur effects are important in steam reforming by rhodium, whereas in Duprez' paper (1994) on SDA, he asserts that sulfur deactivation of rhodium based catalysts is catastrophic. The conditions of sulfur concentration required to achieve this sulfided condition are not discussed in the paper, which asserts that platinum and palladium are much less strongly deactivated than rhodium.

begins to sinter above 900 K)[77]. However, the moderate advantage of platinum over copper in sulfide formation at lower temperatures raises doubts regarding the potential performance of a platinum catalyst in realistic feed gases with several ppm of hydrogen sulfide. Much more encouraging on this count is silver, which exhibits little affinity for sulfide formation. Thus, silver-based catalysis of water-gas shift offers a significant opportunity to create a sulfur-tolerant, low temperature catalyst (silver begins sintering below 600 K).

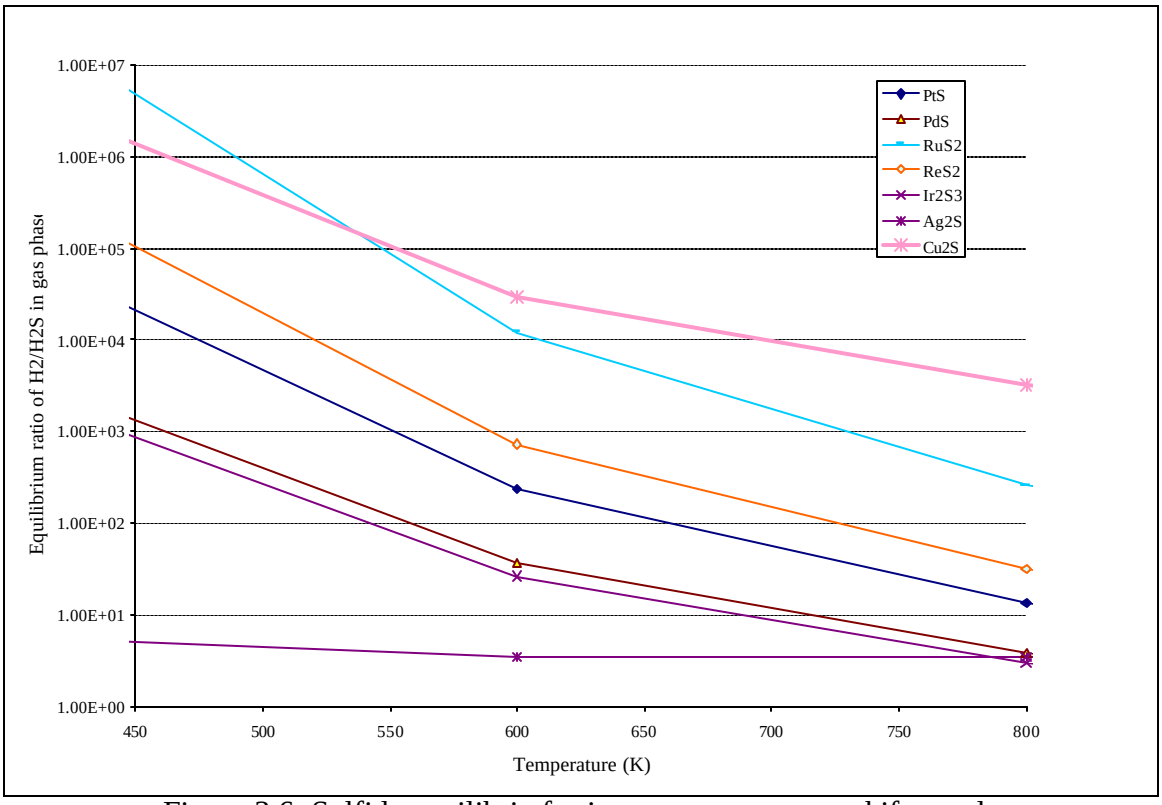

Figure 3.6: Sulfide equilibria for important water-gas shift metals

Although all of the candidate steam-reforming catalysts should exhibit significantly better sulfur tolerance than nickel catalysts used currently, the operability of alternative water-gas shift catalysts in the presence of high sulfur concentrations is less certain. An exception to this statement is the exploratory silver-based catalyst, which should be very sulfur-tolerant. Several mitigating factors may act to make the new catalysts less susceptible to sulfur poisoning than suggested by the thermodynamic predictions for bulk sulfides. In the case of platinum in particular, it is well-known that the adsorption energy for sulfur is a strong function of surface coverage. If the same sites which are high energy sites for sulfur adsorption prove to be high energy sites for carbon monoxide adsorption, the overall performance of the catalyst may be little affected by sulfur coverage, as such strong sites are the chief cause for the low activity of platinum for water-gas shift. In the case of rhenium and platinum, both catalysts may be operated at much higher temperatures without sintering than the more active copper catalyst as well, suggesting that the higher temperature reaction may proceed unpoisoned at the requisite

[77] Dr. Debbie Meyers at Argonne National laboratory has led an effort over the past two years which has developed a highly active Pt-based wgs catalyst. This was reviewed at the 1998 and 1999 DOE/OTT National Laboratory review meeting.

levels of sulfur contamination in the feed. These issues will be best resolved through experimental evaluation, but the thermodynamic situation suggests a reasonable chance for success.

3.1.4 Conclusions on Catalyst Design

The analysis of a number of factors has led to a significant narrowing of the potential field of alternate catalysts for steam reforming and water-gas shift that are active, stable, and sulfur-tolerant while being non-pyrophorric. For the steam-reforming reaction, which is catalyzed by a wide variety of noble metals, ruthenium and iridium and alloys thereof may prove to be the best overall catalysts due to good activity, sintering resistance, and sulfur tolerance. Ruthenium potentially has a slight edge in activity, while iridium may have greater resistance to coking, sintering and sulfur poisoning. The preferred support material for the catalyst is γ-alumina, potentially stabilized by baria, lanthana or ceria. This support is superior to industrial supports because of its much greater surface area and demonstrated ability to activate water. The historically low cost of ruthenium and iridium when compared to the other candidate noble metals argues further in their favor, especially when their lower tendency towards sintering is considered.

For the water-gas shift reaction, the range of alternative catalysts is limited by several factors. The activities of all of the metals tested to date save ruthenium, rhenium and platinum are fairly low, as much as an order of magnitude less than these metals. Of these three candidates, ruthenium is less promising because it is very active for methanation, and thus may not provide adequate selectivity in operation. Another possible candidate is silver, which may have a fairly high activity based predominately on periodic trends in adsorption energy for carbon monoxide. Of these catalysts, only silver has the clear potential to be sulfur tolerant at low temperatures, while the rhenium and platinum catalysts may have to rely on higher temperature operation to attain acceptable performance in the presence of sulfur. The silver and rhenium catalysts will require more study to assess their redox stability and pyrophoricity, as no data are available in the literature to indicate whether they will perform adequately in this regard. All of these catalysts should be supported on γ-alumina, which has demonstrated excellent activity enhancement for the water-gas shift reaction. Ceria promotion of the alumina is also potentially useful, as extensive research for automotive catalysts has shown. It is, however, unclear whether the promoting effects of ceria will continue to be realized at the more aggressive conditions characteristic of the pressurized water-gas shift reaction. Luckily, the existing ferrochrome water-gas shift catalyst is adequately sulfur tolerant, even if redox sensitive and of low activity. Further, this venerable catalyst is inexpensive and has no methanation activity whatsoever. Thus, the imperative to develop a sulfur-tolerant water-gas shift catalyst is not as great as that to demonstrate the predicted attributes of the designed reforming catalysts. Thus, the experimental program to date has focused on reforming, with the advances in water-gas shift chemistry saved for the future.

3.2 Catalyst testing

To date, six different steam reforming compositions have been tested. Catalyst synthesis will not be described in detail as the catalysts tested were synthesized by suppliers according to our sole or joint specifications. These included several noble metals supported on γ-alumina and proprietary refractory supports. The total duration of the testing to date exceeds 1400 hours total time on stream. We have also tested ferrochrome water-gas shift catalyst to confirm its predicted low/zero level of methanation activity and stability in the high temperature heat transfer/catalyst role required in the novel integrated reactor described in the Appendix. The catalyst test effort was preceded by the building and testing of a micro-reactor test apparatus and the development of catalyst test procedures. This latter activity continued in parallel with the early screening tests, and deserves careful review. Thus, the test activities will be covered in two sections, the first describes the test apparatus and the test protocols developed, while the second describes the test results and interprets them in light of the design methodology presented in Sections 3.1.1 through 3.1.4. The results presented here represent only the first cycle in the catalyst development process described previously. Further improvements anticipated in the future will interact with the thermodynamic, kinetic and mechanical modeling and testing described elsewhere in this study to continue to improve the final product. This is an important example of the concurrent development process at work, and will be shown to yield obvious dividends in the course of this dissertation.

3.2.1 Test apparatus and methodology

The test apparatus and methodology evolved between the Fall of 1999 and the Fall of 2000, to the point where catalysts could be subjected to accelerated aging, screened for activity, then if activity warranted, be subjected to a detailed test protocol to empirically derive the impacts of sulfur and oxygen impurities on observed activity. The evolution between the initial hardware and test procedures, which were somewhat crude, and the finalized state of affairs is somewhat tedious and many details will be omitted here. Instead, the final point of evolution of this system as of January 1, 2001 will be documented, and recommended improvements will be outlined.

To understand the test protocols, it is important to understand the capabilities and limitations of the evolved micro-reactor test apparatus. A flow schematic of the evolved system is shown in Figure 3.7. While Figure 3.7 demonstrates the flow architecture, Table 3.3 gives a detailed list of the measurements recorded, the means of measurement, and the approximate accuracy of the measurements.

Figure 3.7 shows that the reactant and purge gases are provided at regulated pressure from conventional gas cylinders. These cylinders are arranged so that different reagent gases can be switched online without an interruption to the test sequence. This feature was added to allow characterization of catalyst response to specific impurities which are added from certified gas mixtures. Water is metered from a gas-pressurized reservoir using a manual metering valve and a rotameter flowmeter. This arrangement requires constant attention due to backpressure regulator "drift," and invariably is subject to large flow variations in unattended operation.

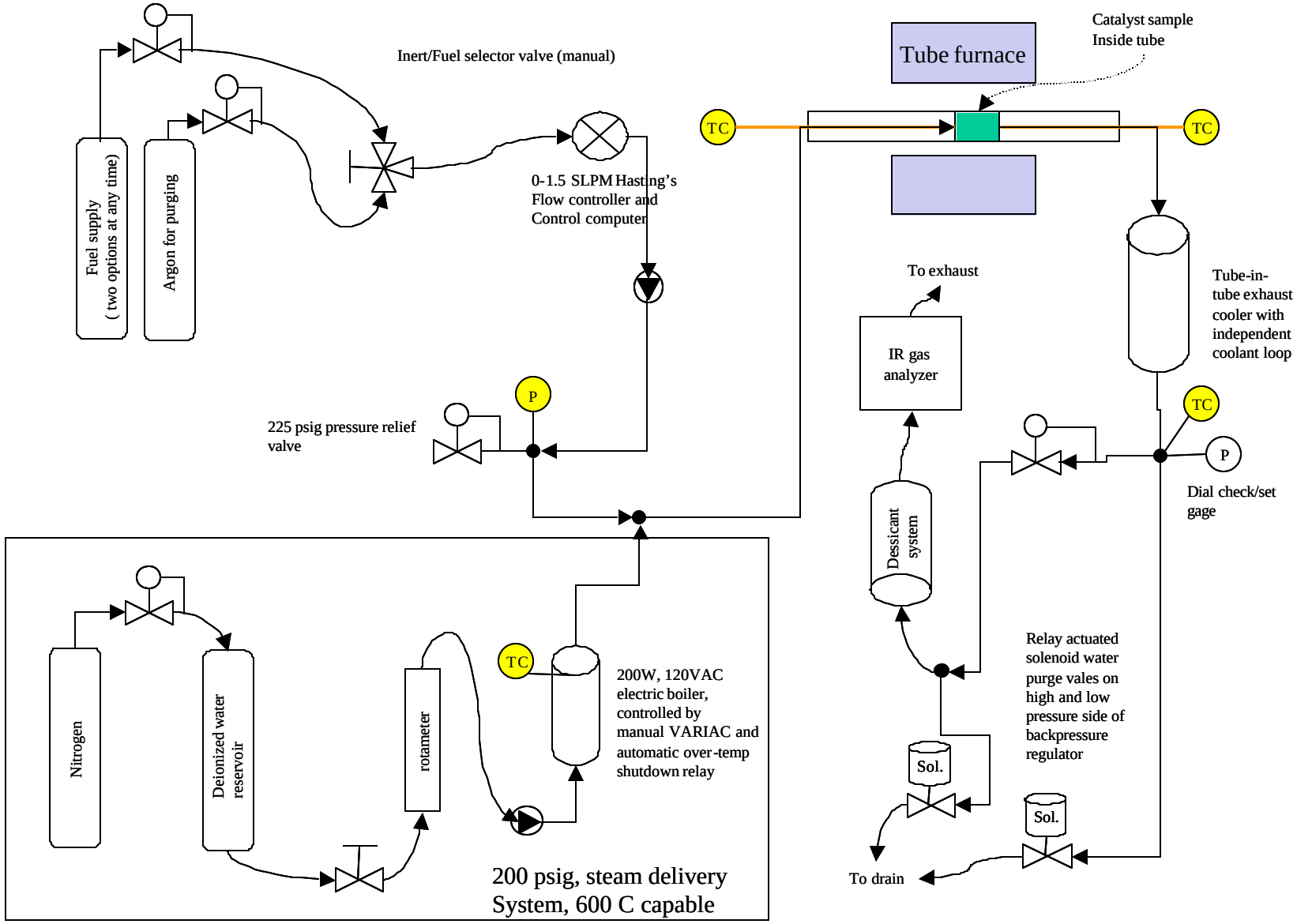

Figure 3.7: Flow schematic for laboratory micro-reactor catalyst test stand

Future systems should employ a high-accuracy plunger metering pump to ensure positive flow control for catalyst endurance testing. This approach is to be preferred over diaphragm pumps and liquid-flow controllers, both of which proved prone to catastrophic failure in our laboratory testing.

Table 3.3: Data recorded in catalyst tests

Measurement	Device	Accuracy (+/-)	Notes
steam temperature	k-type thermocouple	2C to 5C	used for VARIAC control
catalyst inlet temperature	k-type thermocouple	2C to 5C	
catalyst outlet temperature	k-type thermocouple	2C to 5C	
cooled gas temperature	k-type thermocouple	2C to 5C	used to protect backpressure regulator
gas flow	Hasting's 200 series mass flow controller	15 sccm	used as normally-closed shut-off valve for safety purposes
water flowrate	rotameter	2% of value	depends on operator diligence and backpressure regulator drift
pressure	Ashcroft 300 psig transducer	< 3 psig	checked against manual gage
CH4 concentration	Nova Analytic fixed IR	1%	calibrated each run
CO concentration	Nova Analytic fixed IR	1%	calibrated each run
CO2 concentration	Nova Analytic fixed IR	1%	calibrated each run
H2 concentration	Nova Analytic TCD	?	qualitative value, can be fooled by inert gas impurities

The thermocouple, pressure, composition and flowrate data which are logged allow calculation of a reaction rate constant at the mean temperature within the catalyst sample. Depending upon the length of the bed employed, the furnace temperature and the catalyst activity, the difference between the inlet and outlet temperatures can be as little as a few degrees or over 50 degrees. In the latter case, which often occurs with inactive catalysts at low furnace temperatures, the gradients in temperature often set up cyclic behavior in the catalyst, especially when feeds containing di-oxygen are employed. This situation proved difficult to avoid, and generally fell in regimes where activity was so low that measurement accuracy suffers in any event,

compounding the problem. Luckily, such low activity regimes are not important for design, and the problem is not critical.

Initially, it was felt that the steam could be generated in the primary tube furnace, however, testing revealed that this method is unreliable, and leads to periodic quenching of the catalysts, which causes spalling of coated catalysts and attrition of homogeneous ones. The manually-controlled steam generator which was implemented was custom designed using a common 120 VAC cartridge heater, and fabricated by GTAW (gas tungsten arc welding) by Stephen Waide of Directed Technologies Inc.. Experimental experience has shown that the 316L components of the system form surface coke when the mixed gas temperature in the reformer inlet exceeds 400 C while exposed to natural gas, even with a 4:1 steam-to-carbon ratio. Thus, the VARIAC controlling the boiler power and the metering valve must be diligently observed to prevent steam temperature exceeding 400 C. In future systems, it is felt that the combination of a controllable water supply and a PID controller for the boiler will alleviate this coking problem.

The reactant dessicant system also requires constant "care and feeding" . This system employs "drierite" brand ceramic dessicant to remove water vapor prior to the Nova Analytic gas analyzer. Unfortunately, the performance of this dessicant can be stymied by failure of one or both of the solenoid purge valves used to evacuate condensate from the system. The high-pressure valve, in particular, is subject to rapid failure due to the high-pressure and corrosive nature of the condensate, which contains both carbonic and sulfuric acid. Aluminum and brass valves commonly employed for air service are not adequate, and stainless steel valves with corrosion-resistant seats and seals are needed. It has also been determined that independent control of these valves using a timing relay is to be preferred to computer control, as interruptions to the computer power interrupt valve functioning, but do not necessarily stop system operation.

The data acquisition system is based on LabView software from National Instruments and a Pentium PC. The data acquisition software was programmed by Steve Gurski, and can be adjusted to record data points as often as 1hz. The software also controls the solenoid purge valves and a relay to cut power to the boiler if a maximum temperature is exceeded. The data output is in a tab-delimited form, which is then transferred into a spreadsheet environment for interpretation and analysis using standard techniques which will be described below.

In total, the test system described above is perfectly adequate to test 2g to 5g samples of catalyst having a peak space velocity between 2,000 GHSV and 10,000 GHSV over a temperature range of 500 C to 800 C and at pressures to 180 psig. Through the course of the testing, several types of tests were developed. These tests act as filters, and promising materials identified in the first round of tests are subsequently exposed to the later tests. The progression of tests developed is the following:

1) Accelerated aging test with natural gas followed by isobaric screening
2) Detailed kinetic investigation with natural gas
3) Comparitive kinetic tests with neat methane and sulfur-doped methanes
4) Catalyst long-term accelerated life testing with natural gas

Table 3.4: Composition of the catalyst feedstreams

	natural gas	methane	methane w/ ~10ppm H2S	methane w/ ~100ppm H2S
methane	balance	>99.7%	>99.7%	>99.7%
ethane	1.100%	< 2800ppm	< 2800ppm	< 2800ppm
propane	0.202%	< 30ppm	< 30ppm	< 30ppm
n-butane	500ppm	-	-	-
pentane	-	-	-	-
ethylene	-	-	-	-
propylene	-	-	-	-
isobutane	440ppm	-	-	-
C6 and higher	500ppm	-	-	-
carbon dioxide	0.668%	-	-	-
moisture	103ppm	< 4ppm	< 4ppm	< 4ppm
oxygen	1.268%	< 20ppm	< 20ppm	< 20ppm
nitrogen	1.534%	< 300ppm	< 300ppm	< 300ppm
butyl mercaptan	2ppm	-	-	-
hydrogen sulfide	?	-	8.75ppm	98.3ppm

The accelerated aging test exposes the catalyst to 100 hours of operation at about 90 psig and 700 C. The use of 90 psig (7.1 atm) is a legacy of early tests where the microreactor apparatus was only rated to 100 psig. The choice of pressure should probably be moved closer to 13 atm, where the other tests are conducted and where the product system will likely be operated, but it was kept low to maintain a common baseline in this first iteration of catalyst development. After 100 hours of testing, the catalyst kinetics are measured at various temperatures in order to derive an Arhennius plot for the catalyst being screened. The screening procedure has been refined, and should be noted, as proper changes to the test variables are required to obtain data which are not equilibrium limited.

1) Begin tests at a low temperature, adjust flowrates and wait for steady state in temperature and composition
2) Increase flowrates about 50% and adjust furnace temperature to maintain temperature
3) If the compositions change, the data are not equilibrium limited, change the temperature and repeat the process starting at step 1, but at a higher temperature, if compositions do not change, repeat step 2
4) Once the maximum temperature is achieved, reduce temperature in several steps, varying flowrate only to maintain temperature difference across the bed < 50 C

This procedure allows identification of equilibrium-limited conditions where reactant space velocity is insufficient to ensure partial conversion. In the data analysis, regression of activity against space velocity at constant temperature allows "culling" of equilibrium-limited data from the analysis.

A note regarding the catalyst feedstocks is in order, as variations in the feedstocks are a primary tool used in this experimental regimen to establish the effects of impurities. The catalyst screening is conducted with a single lot of pipeline natural gas provided by Matheson. The analysis of this gas is shown in Table 3.4. Because the cause of the poisoning effects seen in the catalyst screening could have been oxygen adsorption or sulfur adsorption, tests employing oxygen- and sulfur-free gas were required. For this purpose, a neat methane gas was used. Finally, the impact of sulfur poisoning was isolated using two levels of sulfur-doped methane. The analysis of these gases, supplied by Air Products, is also shown in Table 3.4.

The detailed kinetic investigation with natural gas involves the collection of temperature-dependent rate data at a variety of pressures in order to determine the overall reaction order with respect to pressure. Because steam-to-carbon ratio control is fraught with inaccuracy in the test apparatus, independent analysis of the rate order with respect to steam and methane was not deemed feasible. Because steam is present is such abundance, and because variations in steam-to-carbon ratio did not seem to produce a measurable result, the reaction is assumed to be zero order in steam.

Repeating the process above with methane and the sulfur-doped methane mixtures is a simple task. When this is done, Arhennius plots for each composition can be produced, and the surface coverage due to sulfur adsorption may be empirically derived. Further, qualitative and quantitative assessments of the rate and degree of sulfur uptake and desorption can be made. All of these representations of the data rely on its reduction to common units for comparison purposes. The calculations performed on the raw data are described briefly below.

The input water (mL/min) and methane (SLPM) flowrates are first transformed into molar flowrates. These values are then combined with the output of the gas analyzer to estimate the output molar flowrate from the catalyst bed on a dry basis.

$$\sum \dot{n}_{out,dry} = \dot{n}_{CH_4 in}\left(1 + y_{H_2}\right)$$

This value is then used to calculate the outlet molar flowrates of the other measured gas species. The total molar flowrate (wet basis) exiting the catalyst is used in determining the catalyst activity, and is determined as follows:

$$\sum \dot{n}_{out,wet} = \dot{n}_{CH_4 in} + \dot{n}_{H_2 Oin} + 2\left(\dot{n}_{H_2 Oin} - \dot{n}_{CH_4 out}\right)$$

The catalyst activity is calculated assuming a first-order overall reaction in methane, and plug-flow through the catalyst bed. The velocity through the bed is evaluated at the inlet conditions, and the superficial velocity[78] is employed to calculate the residence time (r_t).

$$k_{CH_4} = \frac{1}{r_t}\left[\ln\left(\frac{\dot{n}_{CH_4 in}}{\sum \dot{n}_{in}}\right) - \ln\left(\frac{\dot{n}_{CH_4 out}}{\sum \dot{n}_{out,wet}}\right)\right]$$

The calculation procedure above can result in erroneous negative values of the methane reaction rate coefficient (k_{CH4}) in cases of very low conversion with natural gas. This is because the infrared methane detector records a methane concentration in excess of unity with natural gas feed due to the higher hydrocarbon presence. The calculations are conducted on a methane basis, and activities below unity are rejected.

The data are sorted and culled based on transients in temperature and concentration. Generally, large blocks of data after each change in conditions are discarded to account for the long residence time of the cooling coil, dessicant bed and transfer lines. This is especially true under low-flow conditions where as much as five minutes are required to establish a new steady state.

3.2.2 Catalyst test results

The apparatus and methods described above were used to conduct a large variety of catalyst tests. This section shows that these tests demonstrate the feasibility of operating a designed catalyst on line natural gas without any pretreatment. Out of the five catalysts tested, one has shown exceptional performance over the course of several tests. A second derivative of this composition was prepared with half the mass loading of noble metal in order to compare the effect of metal loading on catalyst activity and sulfur and oxygen poisoning resistance. Finally, a catalyst of the preferred composition was subjected to an endurance test in excess of 460 hours in length. The results of the testing will be described below. Because of the proprietary nature of the catalyst compositions, they are not revealed. This limits discussion of the realization of the design goals somewhat, but general links will be sought and established where possible.

The first test conducted sought to determine the stability of a baseline catalyst of the designed type in the steam reforming environment. A standard 0.5 wt% ruthenium on γ-alumina catalyst was obtained and tested using the accelerated aging test described above. The results of this testing are shown in Figure 3.8, which is an Arhennius plot. This style of plot compares the natural logarithm of the activity (k_{CH4}) to the inverse of the mean sample temperature. This allows determination of the activation energy of the reaction from the slope of the resulting line and allows identification of trends at low total activity which might go unnoticed on a linear plot. Figure 3.8 shows that although the initial activity of the catalyst was quite high, the aging was unacceptably rapid. The huge drop in activity at a given inverse temperature occurs within about twelve hours of the initiation of the experiment. This aging, which is far more rapid than that

[78] The superficial velocity (U) through a packed bed is defined as the velocity through the bed in the absence of the packing material.

exhibited in testing with other supports, is attributed to the collapse of the support surface area during the phase change from γ-alumina to the thermodynamically-stable α-alumina. The catalyst went from a peak activity of over 24.5 inverse seconds to a value of about 2.7 inverse seconds in about twelve hours on stream at 725C. This clearly indicates that γ-alumina is an unsuitable support for the high temperature zones of the reformer.

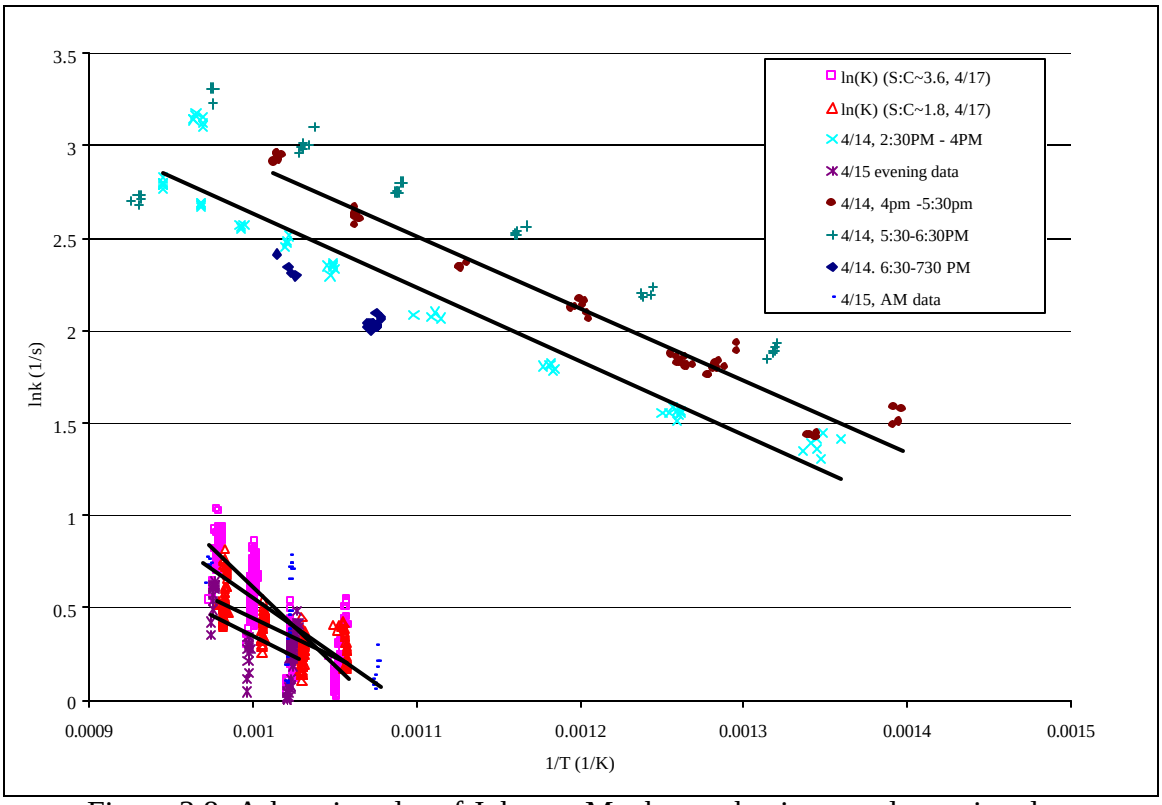

Figure 3.8: Arhennius plot of Johnson-Matthey ruthenium catalyst aging data

Subsequent to this finding, a variety of proprietary refractory supports were evaluated with noble metal active species. Curve fits to their activity are represented as a linear activity plot in Figure 3.9. The data show a broad range of stabilized activities for the various catalysts. Another catalyst not included in the figure was FCR-4, which showed highly unstable activity due to redox cycling, which will be discussed later. The range in stabilized activities is greater than an order of magnitude, and the data clearly suggest that the FCR-10 composition has an inherently superior activity to the other catalysts tested.

This variation in activity is, in fact, largely attributable to the active metal species. FCR-10 employed a different active metal than was used in the other catalysts screened. Because of the high activity of FCR-10, more detailed studies were warranted to determine its suitability as a catalyst in a reactor of the type being pursued. Especially interesting is the behavior noted when the data is plotted in the Arhennius format. This is shown in Figure 3.10, which shows results for the FCR-5 and FCR-10 catalysts. In both cases, at temperatures below 600C the catalysts showed behavior ranging between a low, or poisoned activity state with a high activation energy and a high, or clean catalyst activity state with a much lower activation energy. As can be seen

from the data for the FCR-10 catalyst, this was actually accompanied by cyclic variations in activity and temperature (the interconnected points in the lower right corner of the figure). These cycles had a period on the order of minutes, and were actually observed to some extent with all the catalysts screened using natural gas feed. Because the test apparatus contained no feature to force these oscillations, it was deduced that an actual cycling in catalyst states was being observed. It was further noted that the stable "high" state was observed at low mean temperatures when a large temperature gradient existed across the catalyst bed and the "low" state was associated with near isothermal operation. Cycles between the states inevitably involved associated temperature cycling, which is likely due to the changes in the rate of the endothermic steam-reforming reaction.

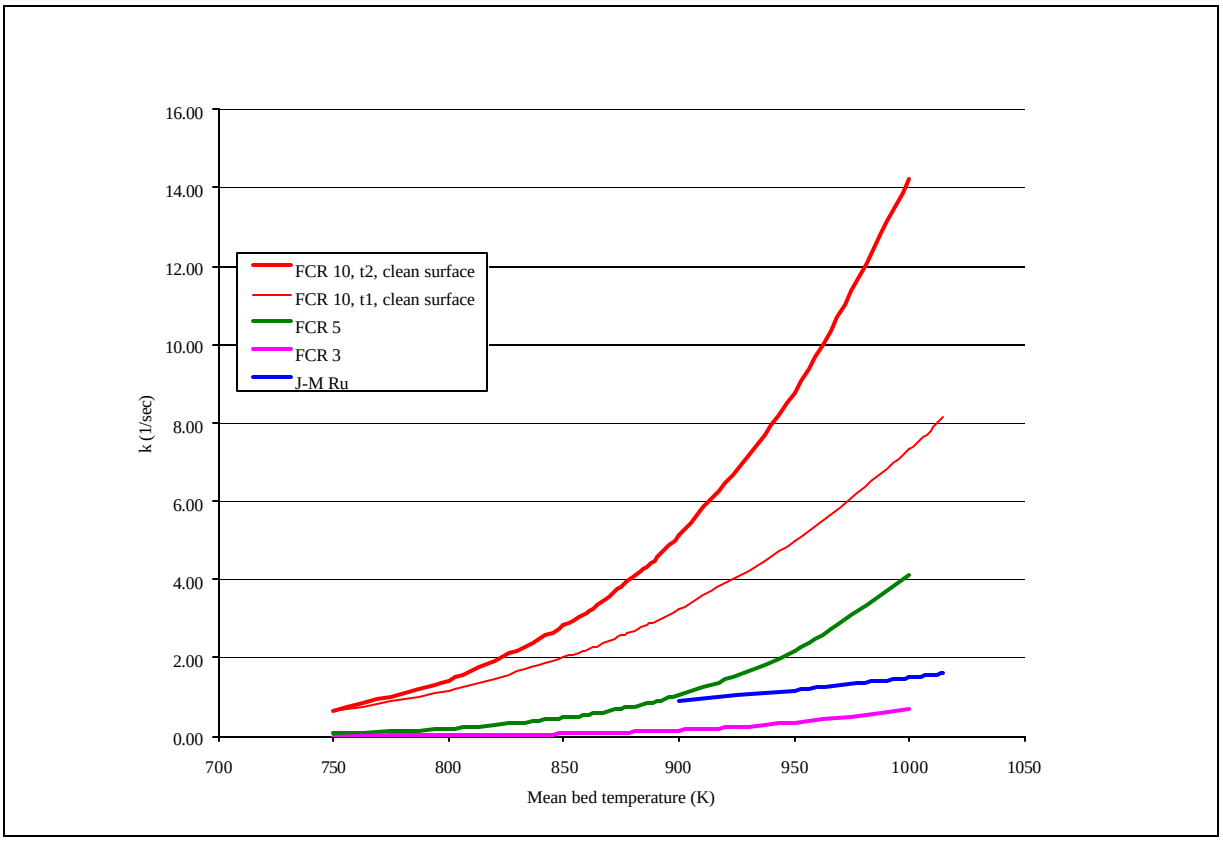

Figure 3.9: Curve fits to activity (k_{CH4}) data for screened catalysts

Sulfur-poisoning was believed responsible for the observed behavior, but discussions with Sud-Chemie and review of the data suggested an alternative hypothesis; the cycles were due to redox instability of the catalyst in the di-oxygen bearing natural gas feed. This position was bolstered by previous observations by Sud Chemie that the metal/support combination used in FCR-5, as well as several of the other candidates, is subject to incorporation of the active metal into the supporting oxide. This thesis is supported by the dependence of the cycling on the temperature gradient, as in a high-gradient situation hydrogen produced in the hot section of the bed could diffuse to the low temperature section to reduce the catalyst.

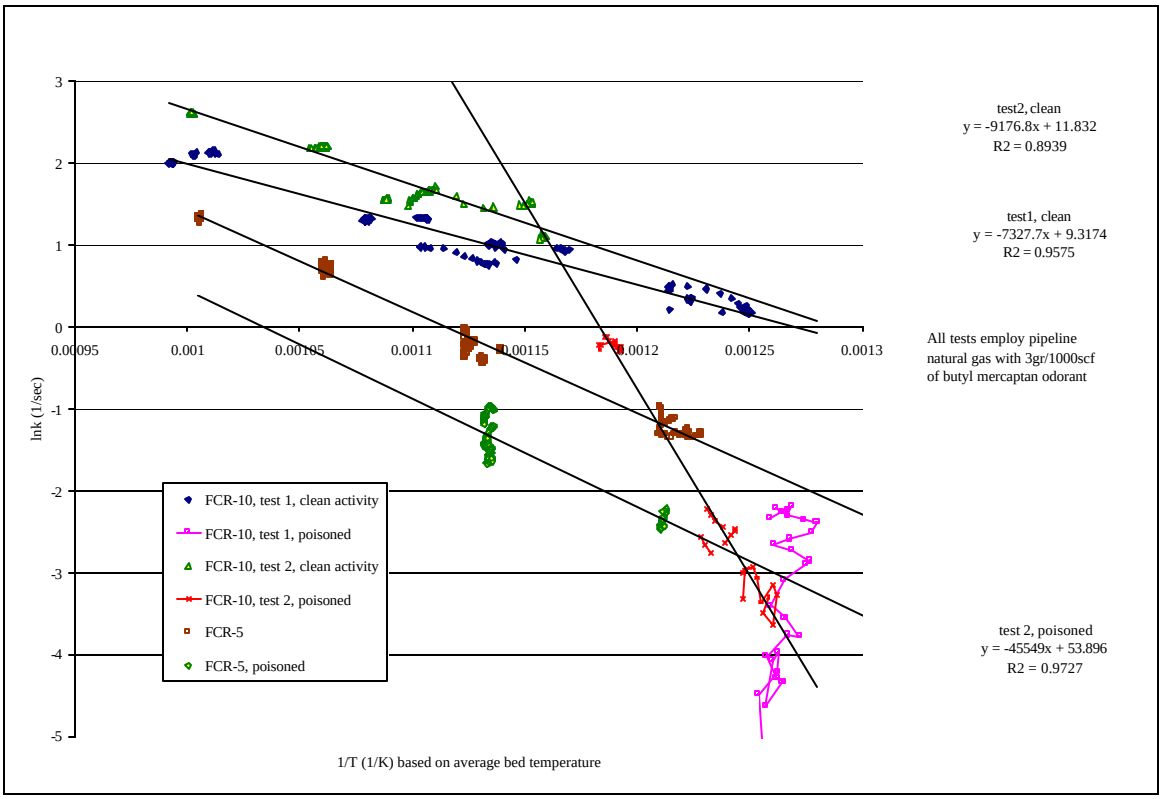

Figure 3.10: Arhennius plot of screening test data

To test this hypothesis, the mixed-gas screening tests described previously were conceived and implemented. For the reactor design calculations presented in Chapter 5, the activity of FCR-10 shown in test series 1 was employed, with a transition from the "low" state to the "high" state at 587 C. If the poisoning is due to di-oxygen, as the evidence amassed later suggests, then the catalyst activity employed in the low-temperature sections of the reactor will be very conservative, as the di-oxygen will be consumed in the first few differential elements of the reactor.

The mixed gas screening of FCR-10 yielded confirmation that oxygen poisoning was reducing the activity measured previously. Figure 3.11 shows an Arhennius plot comparing the activity of FCR-10 on the various gas compositions. Though this is a separate sample of FCR-10, and operated at twice the pressure, the same general activity curve for natural gas may be discerned, supporting the first-order assumptions in the data analysis, with the distinct bimodal behavior evidenced in previous tests. As before, the catalyst was aged for 100 hours before testing occurred, then screening was conducted with natural gas. The next test was with neat methane, which showed a monotonic activation energy, and much higher activity at low temperature than was observed with natural gas. It is very comforting to note that the activities for both feeds are essentially the same at higher temperatures, where oxygen adsorption should be much reduced.

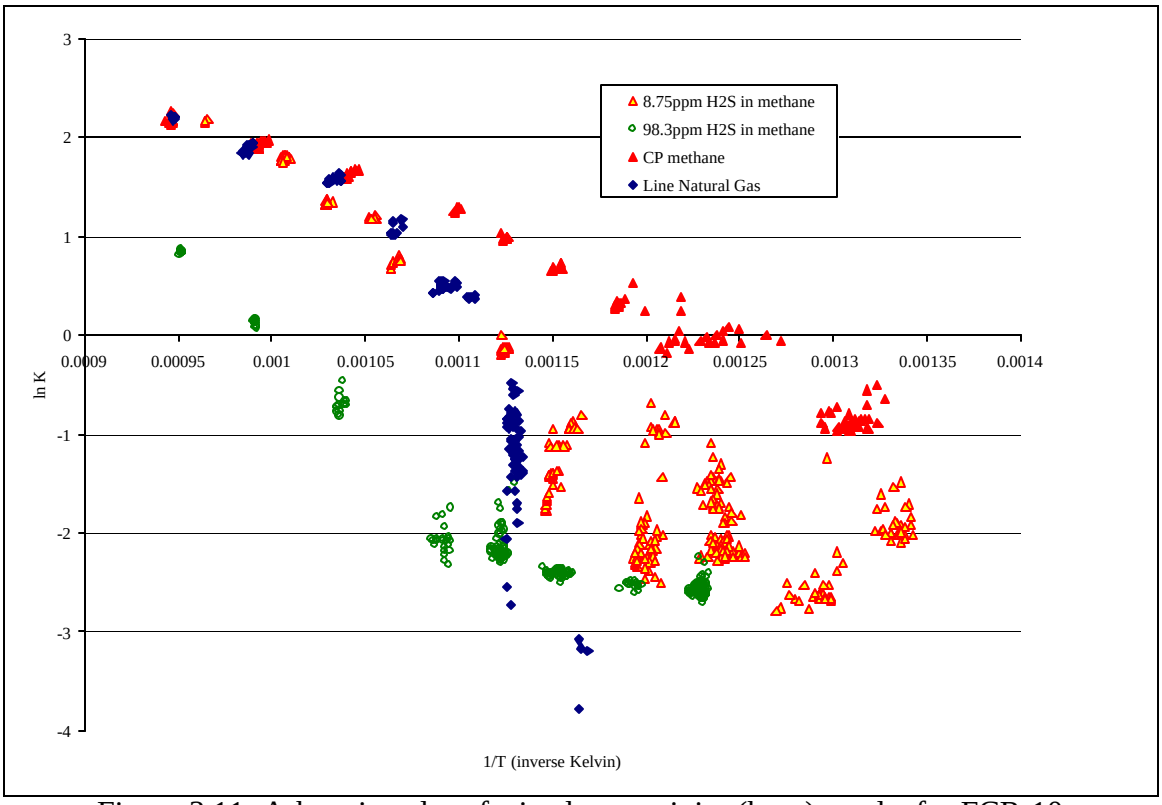

Figure 3.11: Arhennius plot of mixed gas activity (k_{CH4}) results for FCR-10

The most significant point revealed by these data is that the 8.75 ppm hydrogen sulfide doped methane shows better low-temperature activity than natural gas, which has only 2 ppm of total sulfur. This lends credence to the hypothesis that di-oxygen is the agent responsible for the activity loss in the natural gas tests. Further, these test data confirm that the FCR-10 catalyst composition is operable on total sulfur levels at the upper end of those expected from line natural gas. Another observation from the tests supports this point. The activity changes due to sulfur take tens of minutes to over an hour to take place, whereas the activity cycling with natural gas is observed to be periodic with a frequency of about one minute. This means that the kinetics of the mechanism behind the cycling with natural gas is fundamentally faster than the poisoning kinetics of hydrogen sulfide, di-oxygen again emerges as the clear culprit. It is possible to eliminate the possibility that the furnace temperature was forcing the variation in temperature and activity inside the tube, as the furnace temperature was observed to remain stable during these cycles. Less encouraging from an operational standpoint is the poor catalyst activity in the face of 98.3 ppm hydrogen sulfide doped methane. This feed, which is supposed to respresent a "spike" in line sulfur content, leads to a strong suppression of catalyst activity, which only returns to meaningful levels at the higher temperatures tested. The poisoning was observed to be at least partially reversible, but would certainly cripple the reactor in operation. Thus, a zinc oxide sulfur guardbed of the type anticipated in the patent application of The Appendix may still be advisable to prevent catastrophic reductions in performance and operability should a sulfur spike be encountered.

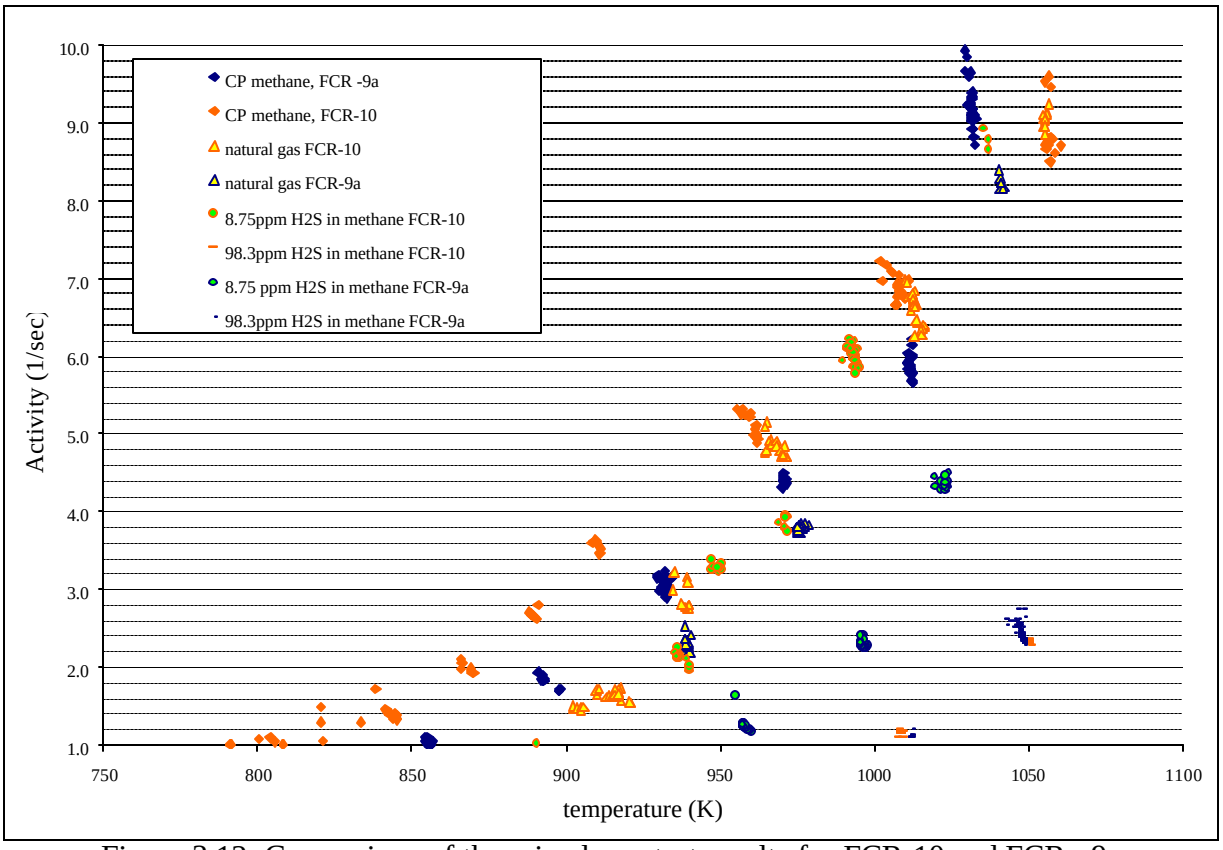

Figure 3.12: Comparison of the mixed-gas test results for FCR-10 and FCR –9a

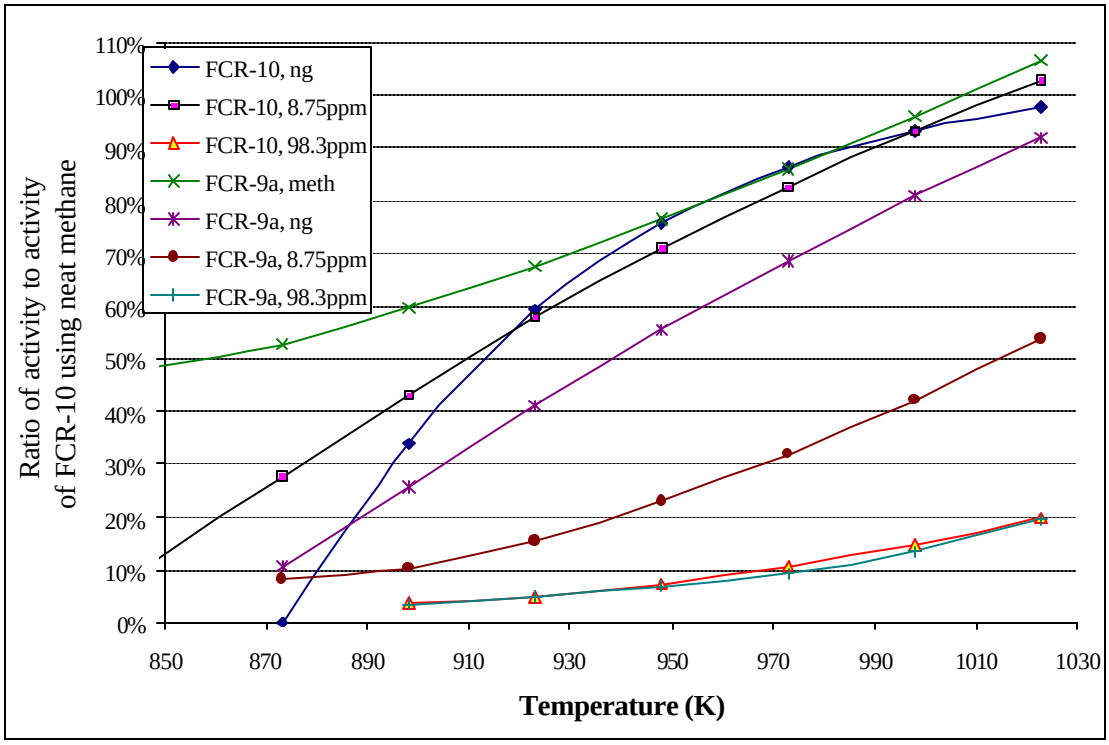

Figure 3.13: Ratio of test case activity to activity of FCR-10 on neat methane

As will be discussed in Chapter 5, the noble metal-based FCR-10 catalyst is projected to be quite expensive, and to represent a large fraction of the total cost of the finished chemical reactor. Thus, experiments were conducted with a catalyst with the same composition as FCR-10 but with one half the noble metal loading. This catalyst, FCR-9a, was subjected to the same series of tests as FCR-10. A thermocouple malfunctioned during the tests, forcing reliance on bed exit temperature rather than average temperature, which makes the comparisons in activity shown tentative, but the results suggest a variety of interesting questions about the catalyst and the reactor design. The data are shown on a linear activity plot with the activities below unity excerpted for clarity in Figure 3.12. This truncation enhances understanding, as the accuracy of the measurements below this level may be called into question.

The same pattern of high activity on neat methane at low temperatures which is approached by the natural gas activity at high temperatures is observed. The only strong differences with FCR-9a seem at first glance to be in its performance on the 8.75 ppm hydrogen sulfide doped methane, where the activity is notably lower than that evidenced by FCR-10. The differences in activity are more clearly observed when a nonlinear regression of the data is performed and the resulting functions are compared over the operating temperature range. This was done, and the comparison between the activity of each test case and the activity of FCR-10 on neat methane is plotted in Figure 3.13.

These curves show several interesting points about the catalysts and test conditions that are not readily apparent from the linear activity or Arhennius plots.

1. Activity reductions at low temperature with mixed feeds often exceed 50%
2. The FCR-9a catalyst activity monotonically-approaches that of FCR-10 as temperature increases, suggesting mass transport limitations
3. The activity of both catalysts with 98.3 ppm hydrogen sulfide is the same, and is less than 20% as high as FCR-10 at all conditions

This first point may have important implication for reactor sizing, cost and catalyst design. Although di-oxygen will be eliminated early in the reactor, the lingering results of sulfur poisoning would reduce the activity of FCR-10 to about 10% of it's value on neat methane in the low-temperature zones of the reactor. This suggests that the zinc oxide pretreatment discussed above may be economically attractive if sulfur concentration could be limited to that represented by odorant, which is typically only 2 ppm to 3 ppm. Further, it may mean that changes to the catalyst composition may be warranted to improve activity at these lower temperatures, including modifications to the noble metal composition and perhaps a switch back to a less stable, but higher area support in low-temperature zones of the reactor. These points will have to await resolution until after the reactor model of Chapter 5 is fully vetted and represent the next cycle in the concurrent design process.

The second point is interesting, as it implies that under lower absolute activity conditions, the FCR-10 catalyst, which has more metal loading and, thus, more surface area, is substantially more active than the lower-loaded FCR-9. The fact that the activities collapse to a common value at the higher temperatures where the intrinsic rates are much higher suggests that another

factor is limiting surface area. In the lower-area, high-temperature supports employed in the FCR-10 and 9a compositions, it is likely that mass transfer inside the catalyst particles provides this limitation. This means that a support with a greater porosity, and perhaps a higher total area, should be preferred to provide enhanced activity at these higher temperature conditions. Thus, the chemistry and perhaps the preparation route of the support material may need to be altered to provide a more porous structure than that realized here.

This result is confirmed by the test data for the 8.75 ppm hydrogen-sulfide loaded methane. Whereas the higher surface area FCR-10 catalyst shows activity very close to its own performance on neat methane, the FCR-9a catalyst with undisputably lower metal area shows poor performance relative to its own performance on methane and relative to FCR-10. This can be easily explained by reference to the issue of mass transport limitation. If we assume that the fractional, equilibrium surface coverage on both catalysts is the same, then if the entire surface was being utilized in both catalysts they would exhibit similar responses to the same sulfur concentrations. Yet, we actually observe a much more severe response from FCR-9a. This implies that under normal conditions, a much smaller fraction of the metal area in the FCR-10 catalyst is being productively used. This poor utilization is referred to as a low effectiveness factor in the chemical engineering literature, and is represented by the ratio of the observed activity to the activity of the catalyst if all of the area was at the surface conditions of the pellet. If we assume that the effectiveness of both FCR-9a and FCR-10 is unity at 850 K, then we can state that the effectiveness factor of FCR-10 is 0.5 at 1030 K. Since the activity of the sulfur-poisoned FCR-9a is about half that of the neat methane values for FCR-10 while the sulfur-poisoned values for FCR-10 are the same as the neat values, we can impute an effectiveness factor for the poisoned FCR-10 catalyst of about unity.

Since we have shown above that the metal area of the FCR-9a is about one half of that for the FCR-10 material, it is surprising that their activities are so similar with the highly sulfur-doped methane. This suggests that the observed activity with a sulfur-poisoned surface may not be due to the metal at all, but may be a result of instrinsic activity of the sulfided support material. The role of the support in catalyzing steam reforming was discussed in Section 3.1, so this result is not completely surprising.

The limitations of the high-temperature support discussed above were anticipated in the catalyst design section. Its selection was motivated by the desire to improve high-temperature stability relative to the miserable results observed with γ-alumina and shown in Figure 3.8. In order to verify long-term stability, it is necessary to conduct long-duration tests. As described previously, this was difficult in our microreactor apparatus due to problems with water flowrate

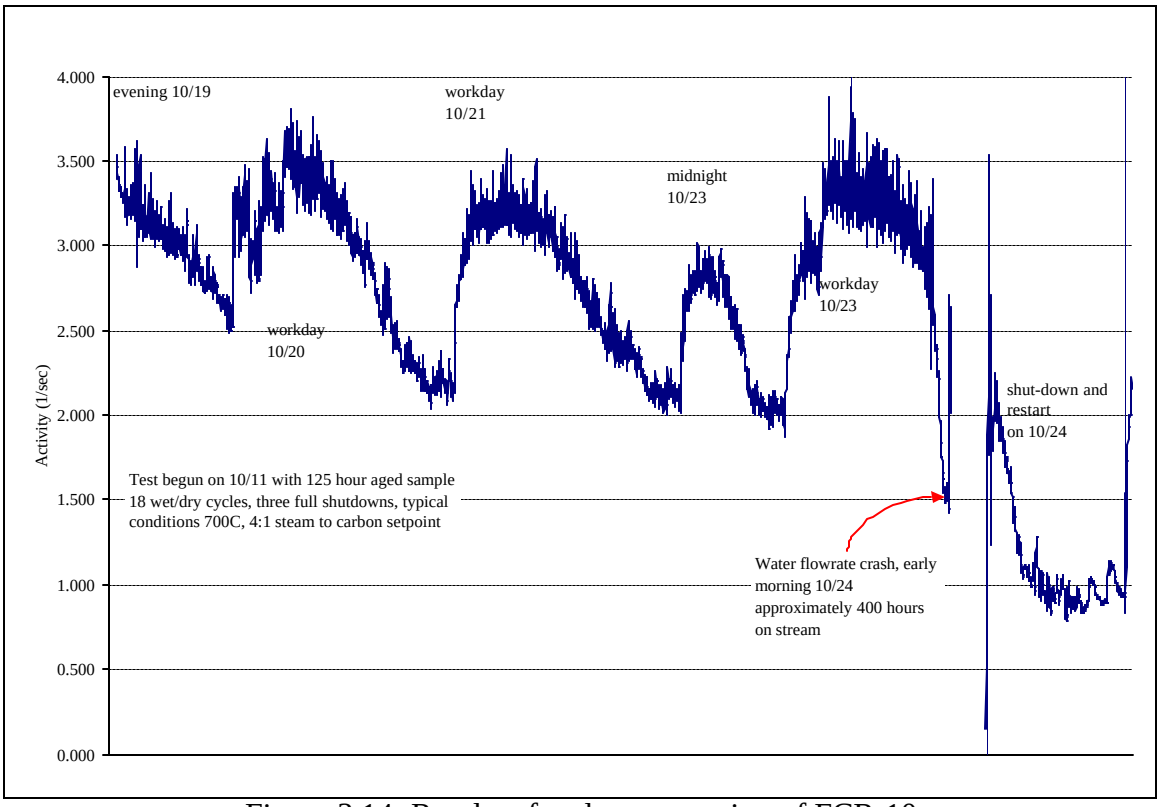

Figure 3.14: Results of endurance testing of FCR-10

control. Despite these difficulties, a 460 hour endurance test at 13 atmospheres and 700C was conducted using the FCR-10 catalyst. The results of the test are shown in Figure 3.14, which shows diurnal cycling of the measured "activity" during the test leading up to the final failure of the system due to catastrophic coking. The reason that these values do not reflect true activity is that they reflect equilibrium-limited, low-flow conditions employed to save reagent. Under these conditions, when water flowrate decays under unattended operation, the observed conversion is further constrained by equilibrium, and a lower "activity" is calculated. What is interesting in this case is that the peak activity observed remained constant over 18 cycles into steam to carbon regimes that would shortly deactivate a standard reforming catalyst.

This suggests two conclusions. First, the FCR-10 formulation is extremely resistant to coking. In fact, sectioning the test reactor tube used in the experiment above revealed carbon growth from the tube wall encapsulating the catalyst, rather than a coking of the catalyst surface. This behavior is more consistent with metal carburization of the stainless steel tube than catalyst coking. Secondly, the catalyst does not age significantly during an admittedly brief endurance test. Even the heavily coked catalyst exhibited about 50% of the activity which typifies FCR-10 when tested after the crash of October 24, 2000. This is incredible, as the catalyst was literally encased by carbon.

To conduct more conclusive endurance tests, a more reliable means of metering water must be employed. Further, reactor tubes must be fabricated from materials less susceptible to carburization than the alloy 316L austenitic stainless employed in these tests.

3.3 Catalyst conclusions

As discussed above, a series of candidate catalysts were developed using basic chemical principals, and were synthesized and tested. This process yielded mixed results, which are summarized below:

1. γ-alumina is not suitably stable to serve as a support in the high temperature zone of the steam reformer
2. noble metal catalysts with appropriate high temperature supports can demonstrate stable activity in the presence of both sulfur and oxygen
3. the stable activity of the FCR-10 catalyst failed to meet the original activity goals
4. support selection and development are critical factors limiting high temperature performance
5. metal selection and the degree of sulfur removal in the guardbed are important variables in the performance of the catalyst at low temperature
6. the stability of the noble metal catalyst against coking is superlative
7. initial performance of the catalyst in long-term testing is encouraging

These results are an encouraging product of linking the catalyst development and testing to the eventual application requirements. It must be emphasized that these results failed to meet the desired total activity performance, which was only briefly met by the fresh ruthenium catalyst on γ-alumina support. However, because the goals for performance are known, and the mechanisms behind the shortfall are fairly well understood, it is likely that in the next few iterations of the process an exceptional material may be designed, synthesized and demonstrated which meets all of the program goals.

As was discussed in the design section, the current ferrochrome water-gas shift catalysts possess many attributes which are desirable for the water-gas shift application in the integrated reactor. Further, many other developers are demonstrating noble metal catalysts that are similar in manifestation to our designed catalysts specified in Section 3.1. Thus, far less effort has been expended on developing these catalysts than was directed towards the steam reforming application. The tests which were conducted were solely to verify the low methanation activity of the ferrochrome. Since the results were satisfactory, no further evaluation was conducted. In the future iterations of the concurrent design process, the same sort of catalyst testing described above will be applied to the ferrochrome catalyst and to alternative compositions. Whether these tests will suggest an alternative material is yet to be determined.

In all, the conclusions drawn from the catalyst testing must interact with the reactor design modeling, reactor testing, and thermodynamic modeling to suggest the optimum selection of materials and system manifestations to achieve the optimum system with the lowest cost and best reliability. Thus, the catalyst results discussed in this chapter form an integral part of the analysis in Chapters 4 and 5, and help determine the levelized costs of hydrogen calculated in Chapter 6.

Chapter 4: Thermodynamic Modeling

Selection of operating conditions for an integrated chemical process requires a detailed thermodynamic and mass balance around each component and the system as a whole. This activity, often referred to as process design or flowsheeting in the chemical engineering community, proceeds through several logical steps. The first step involves evaluating basic process thermodynamics using simple manual calculations. These calculations are similar to those of Chapter 2, and are conducted to aid basic understanding of the process requirements. The second step involves automation of these calculations, often using spreadsheet software, to quantify the effects of temperature, pressure, etc. on process feasibility. The final step involves transition of the process model into a specialized chemical engineering programming environment, where much more detailed thermodynamic calculations are automated, and where a wide variety of parameters may be readily varied to conduct a discrete or continuous trade-off analysis.

The first two steps of this process were conducted previously for steam reforming systems with metallic membrane hydrogen purification as part of my master's project[79]. Further, Directed Technologies Inc. funded the first steps towards transition of the model to the Hysys[80] programming environment, conducted by Jason P. Barbour. In all of these early analyses, metallic membranes were the means of hydrogen purification studied. As discussed in Chapter 2, metallic membranes have several disadvantages which make them unsuitable for the low-cost hydrogen generation system envisioned here. Thus, the scope of work described here includes the modification of the system model to reflect the use of a Pressure Swing Adsorption (PSA) hydrogen purification system, and the use of this evolved model to conduct a discrete trade-off analysis of the process. During the course of this work, two chief evolutions of the model architecture and assumptions were employed, version 3.1 and version 3.2.

The final working version of the model generated in this study, version 3.4, incorporates lessons learned from the catalyst testing and component selection exercise for the 1/3rd-scale pilot reactor described in Chapter 5 and represents the current vision of the product process train. Although specific detailed assumptions regarding component efficiencies and heat exchanger sizing were modified between the versions, the basic assumptions regarding the architecture and the behavior of the major process elements remained unchanged. Thus, the conclusions reached using version 3.1, while quantitatively altered to a lesser or greater degree in the later models, remain qualitatively correct and informative. Therefore, this chapter will trace the progression between these models, and recount the evolution in the overall design philosophy which occurred as a result of the interaction of the results of the thermodynamic modeling, the detailed catalyst development, reactor design and test activities. This discussion will be preceded by a detailed discussion of the model architecture and assumptions, using the evolved, version 3.4 model as the example case.

---

[79] Lomax, F.D., Investigation of Steam Reformation of Natural Gas for the Very Small Scale Production of Hydrogen Fuel for Light Duty Vehicles in Appliance-type Refueling Systems, May 1997.

[80] HYSYS Plant/Process Version 2.2, Hysys is a product of AEA Technology, Calgary, Canada.

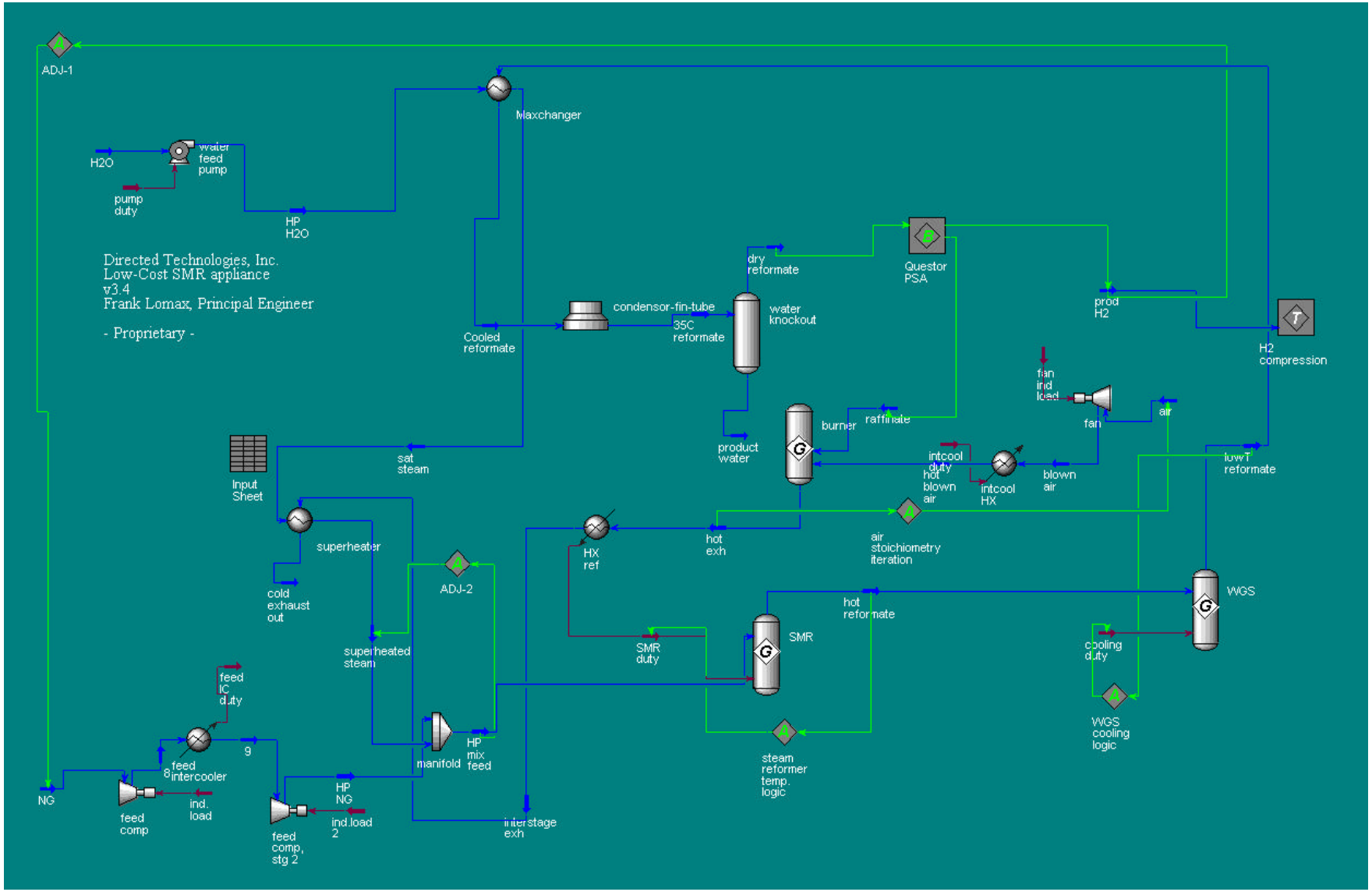

Figure 4.1: Thermodynamic process model flowsheet, version 3.4

4.1 Model architecture and parameters

The HYSYS flowsheet for version 3.4 of the process thermodynamic model is shown in Figure 4.1. The Hysys modeling environment provides standardized unit operations which may be combined in a variety of sequences to yield the finished process. Each unit process may be specified based upon the desired mode of operation, known component parameters, or desired boundary conditions. The overall mass and heat balances are preserved everywhere in the system, and detailed calculations of the thermodynamics are achieved using Peng-Robinson equations of state. The model is obviously somewhat complex, and the parameters governing each unit process are specified in detail. It is first important to understand the top level assumptions of the model, then the detailed parameters may be explored in more detail.

The steam reformer, water-gas shift reactor, combustor and HyQuestor PSA system are the most important chemical engineering elements of the system. Realistic modeling of their operation is crucial if the results of the thermodynamic trade study are to be believed. All three chemical reactors are modeled as equilibrium-limited reactors constrained by minimization of the total Gibbs free energy. This allows consideration of carbon formation, and overall reaction endpoints without any constraint due to reaction pathways.

In the combustor, equilibrium always strongly favors complete conversion. The choice of a Gibb's reactor is simply one of convenience, as essentially the same result would be obtained using a conversion-based or kinetic reactor. The logical operator shown adjusts the air flowrate to maintain a set output temperature from the combustor. The logical operators employed in HYSYS, and denoted in green in Figure 4.1, serve to implement iterative calculations and to provide constraints on the calculations. They are not actually a physical part of the reactor system. Likewise, the input flowsheet is simply a means to simplify changes in process parameters to allow for streamlined sensitivity analyses.

For the steam reformer, the use of equilibrium constraints closely mimics the performance of reactors in the field[81], and is important in the thermodynamic study as conversion is linked to pressure, temperature and steam-to-carbon ratio. The steam reformer is linked to the "HX ref," a cooler function which simply calculates the effects of removing a certain quantity of sensible heat from the combustor product gases, referred to in the model as "hot exhaust." The use of this arrangement is required because the HYSYS software does not have the ability to model heat-exchange reactors with counterflow. The much less interesting and computationally simpler case of co-flow reactants is available, but is not applicable here. The logic operator shown in Figure 4.1 adjusts the heat duty into the steam reformer to obtain the desired outlet temperature of the reformate.

The water-gas shift reactor performance is also strongly equilibrium limited, with full conversion favored by low temperatures and high steam-to-carbon ratios. Thus, the heat duty removed from the reactor by the compressed air steam is varied by the logical operator to yield a

[81] Rostrup-Nielsen, J.R., 1984, p. 6.

target outlet temperature from the reactor. This parameter is then varied in the sensitivity analysis to determine its effect on the overall thermodynamic efficiency.

The PSA system is not modeled in detail in our thermodynamic simulation. Instead, the performance of the HyQuestor 600-series PSA system was estimated from performance maps provided by QuestAir Gases, Inc.. Since QuestAir manufactures the unit, their data are considered reliable for design purposes. The hydrogen recovery curves versus feed pressure and composition are shown in Figure 4.2. It is important to note that the maximum allowable product carbon monoxide concentration is an important constraint on the current HyQuestor. This sensitivity is due to the adsorbents employed, which are optimized for the separation of nitrogen from reformate produced by autothermal or partial oxidation reforming. If the adsorbents were changed to a composition which has a greater ability to separate carbon monoxide, then a greater product recovery could be anticipated at all operating pressures[82].

A curve fit to the data provided by QuestAir was employed to set the hydrogen product recovery in the model. By applying a mass balance, the composition and flowrate of the raffinate, or waste gas stream are then calculated. This raffinate is then employed as the fuel to fire the combustor. In the model cases described in this chapter, co-firing with raw natural gas fuel is not contemplated. It will be shown that co-firing may offer an attractive route towards increased efficiency at lower reformer costs, and will be studied in subsequent iteration of the design process.

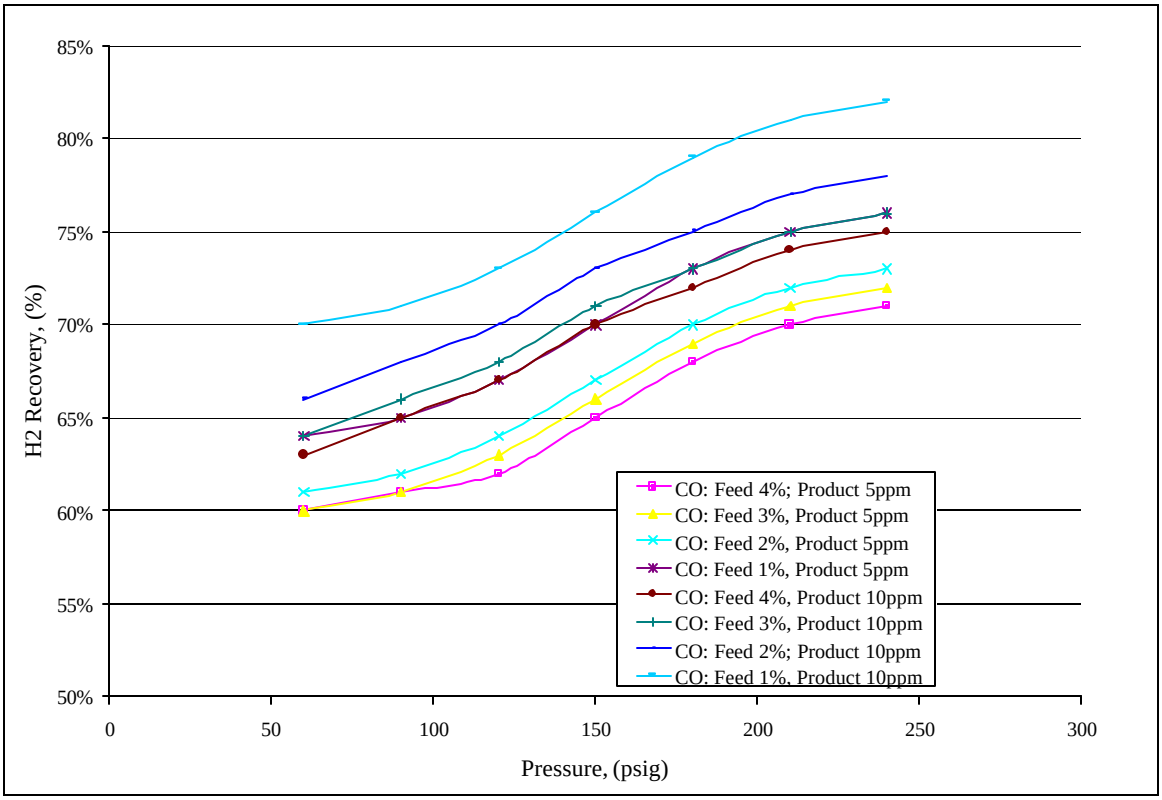

Figure 4.2: HyQuestor 600-series PSA recovery map

82 Personal communication with Bowie Keefer of QuestAir gases, January 2000.

Once the main chemical reaction and separation components of the system are described, the next most significant components in terms of overall energy efficiency are the fluid handling devices. The natural gas and hydrogen compressors, air blower, and water feed pump can all impact thermodynamic efficiency. The last of these, the water feed pump, contributes little to energy demand, and is modeled as having an adiabatic brake efficiency of 25%. Each stage of the natural gas and hydrogen compressors, which are assumed to be low-speed, reciprocating devices, is given an isentropic efficiency of 75%. The natural gas compressor is modeled as a two-stage, intercooled unit, much like the Quincy QRNG25 compressor actually used in the 1/3rd-scale pilot plant. The 75% isentropic efficiency is actually less than the values calculated from Quincy's test data, but are retained for conservatism as the Quincy data have not been verified in the lab, and the 82% values obtained from back-calculation seem somewhat incredible. The hydrogen compressor is modeled as a three-stage, intercooled compressor. This should yield conservative performance estimates, as compressors with as many as six stages are commercially available. All of the intercoolers are modeled with a 50 C outlet temperature.

The air blower adiabatic, isentropic efficiency is set at 72% based upon efficiency curves provided by Vortech Engineering for their V-1S heavy-duty blower[83]. This is a centrifugal, automotive-derivative device with a high efficiency impeller. The attainable efficiency of the blower can vary widely depending upon the impeller and diffuser geometries and the operating conditions, and although the 72% value is used here, detailed comparison of the energy costs and capital costs of any candidate blower system must be evaluated during the selection process.

The final components that must be considered are the three major heat exchangers which are modeled in detail in the thermodynamic model. These include the superheater, reformate cooler, and fin-tube condensor. Each of these heat exchangers has different design constraints, and each is modeled differently.

The superheater, which recovers heat from the cooled combustion products exiting the heat-exchange reformer by raising and superheating steam, is sized by the model to provide a superheated steam temperature consistent with a mixed feed temperature into the steam reformer of 400 C. This value was set as a safe upper limit to avoid coking of the reactor inlet by the natural gas, and was determined experimentally in the catalyst tests described in Chapter 3. The version 3.1 and 3.2 models sized this device by other means, but the total energy extracted from the combustion product gas was comparable in all cases. The HYSYS model predicts a UA for the heat exchanger, and develops temperature profiles through the unit based on the assumption of a tube-and-shell geometry. As will be described in Chapter 5, a cross-flow geometry is anticipated in practice, but the model does not possess the capability to model general cross-flow heat exchangers, as these are not much employed in large chemical plants for process heating.

The reformate cooler, denoted "Maxchanger" in Figure 4.1, exchanges heat between the superheater feedwater and the low temperature reformate stream exiting the water-gas shift reactor. It was found that for the temperature and pressure conditions that exist in the reformer system, the best available heat exchanger technology for this application is the welded-plate heat exchanger sold under the Maxchanger trade name by Tranter. Brazed-plate heat exchangers

---

[83] Performance specifications provided by Dave Austin of Vortech Engineering, July 28, 2000.

were unable to meet the temperature requirements and temperature-gradient requirements, while tube-and-shell units were rejected because of high cost. The Maxchanger heat exchangers are extremely inexpensive per unit capacity, and the smallest unit available exceeds the typical design requirements for the reformate cooler. Therefore, the reformate cooler performance was set based on a pinch-point temperature specification of 5 C. The approach may be closer than this in practice, but the energy difference is so small that it does not impact the validity of the model results.

The fin-tube condensor is a fan-cooled, cross-flow heat exchanger of either the finned-tube or plate-fin type. The sizing calculations used in the model are structured around providing the most challenging design-case performance. This point is provided by the requirement to deliver 45 C reformate to the water knockout trap on days with a 40C ambient inlet temperature. Since the power load for the fan is quite small under normal conditions, the use of these exaggerated design conditions does not alter the model predictions, and allows comparison of the condensor sizing for different process conditions.

Using the model structure described above, it is possible to simulate various combinations of parameters in order to determine thermodynamic efficiency, electrical power draw, heat exchanger sizing and the like. Further, the model output may be used as an aid in the specification of components such as the heat exchangers described above and the reactor assembly described in Chapters 2 and 5 and The Appendix. The use of the model to estimate the thermal efficiency and electricity demand is reviewed below, and the impact of important variables on the realized efficiency is discussed in detail.

4.2 Thermodynamic modeling results and discussion

Three phases of thermodynamic analysis and comparison were conducted as part of the current design cycle. The first stage employed the version 3.1 model to compare operating parameters on the basis of total thermodynamic efficiency of the system on a lower heating value basis. This analysis identified important trade-off variables for consideration in the system design. The second phase employed the version 3.2 model to estimate system parameters for various burner and reformer temperatures in order to facilitate the reactor design of Chapter 5. The final phase employed the more refined version 3.4 model to estimate electricity and primary fuel requirements for the final economic trade study of Chapter 6. Each of these three phases is described separately in this section.

4.2.1 Impact of reactor parameters on system efficiency

Several important reactor parameters were investigated using the version 3.1 model. These included molar steam-to-carbon ratio, reformer outlet temperature, water-gas shift outlet temperature, and pressure. The results were compared on the basis of lower heating value efficiency by resolving all of the shaft input electrical loads back onto a fuel basis. Thus, the efficiency for hydrogen production is given by the following equation.

$$\eta_{LHV} = \frac{\dot{n}_{H_2} LHV_{H_2}}{\dot{n}_{CH_4} LHV_{CH_4} + \left(\frac{\sum P_{shaft}}{\eta_{generation} \eta_{motor}} \right)}$$

where

$\eta_{generation} = 33\%$ LHV and $\eta_{motor} = 90\%$

Since the true purpose of these calculations is to compare greenhouse gas emissions from the various test cases, it is important to realize that this expression assumes electricity derived from fossil fuels. In areas where significant fraction of electricity is derived from renewable or carbon-free sources such as solar, wind, hydro-electric or nuclear, the contribution due to electricity becomes less important. Further, these calculations assume that all of the hydrogen produced is compressed to 409 bar. This reflects the worst-case scenario for drive sizing, not the average energy consumption, as most of the hydrogen is compressed to a pressure below this final storage pressure as the receivers being filled are only partially pressurized under normal conditions. These assumptions, combined with low natural gas compressor efficiencies on the order of 50% of isentropic assumed in version 3.1, combine to yield low estimates of the attainable efficiencies. Further, the use of somewhat low compressor efficiencies tends to make the reduced data of Figure 4.3 favor lower pressures of operation than would otherwise be predicted.

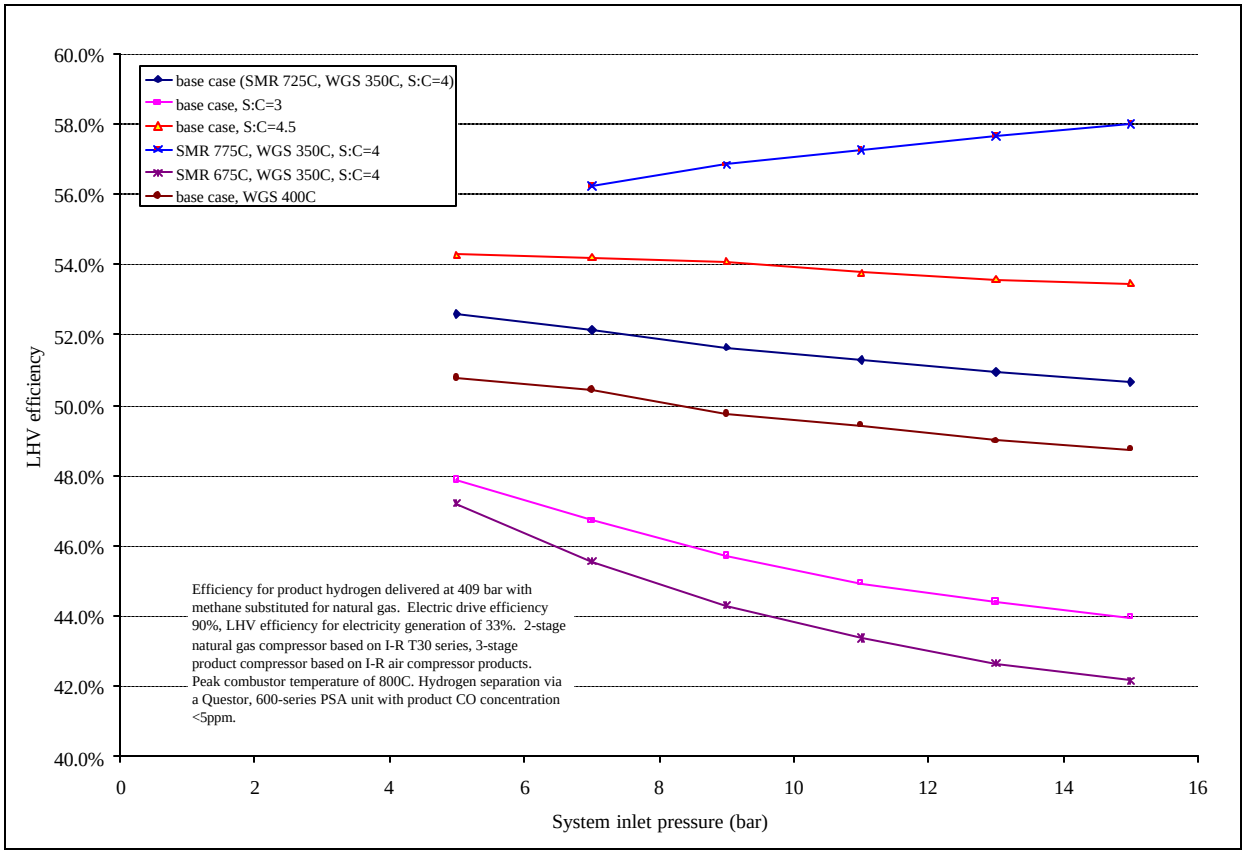

Figure 4.3: Model version 3.1 trade study results

Despite these limitations, the results of the version 3.1 trade study show several important trends. The first of these is the strong impact of reformer outlet temperature on realized thermal efficiency. The best efficiency predicted with a 675 C reformer is about 47%, whereas the peak efficiency at 775 C is 58%. Initially even more puzzling is the fact that the best low temperature performance is realized at the lowest pressure studied, 5 bar, while the high temperature performance is maximized at the highest pressure, 15 bar. The same pattern of changes in efficiency may be noted when steam-to-carbon ratio is varied between 3:1 and 4.5:1, the latter being the maximum attainable with 725 C reformer temperature due to pinch-point concerns in the system heat exchangers. As the steam-to-carbon ratio increases, the efficiency dramatically increases, and the correlation between the efficiency and pressure transitions from a negative slope towards a neutral slope at the highest steam-to-carbon ratio. These results are less puzzling when the form of the equilibrium expression for the steam-reforming reaction is recalled.

$$\frac{K_{eq}}{P_{Total}^2} = \frac{y_{CO} y_{H_2}^3}{y_{CH_4} y_{H_2O}} \qquad \text{where} \qquad K_{eq} \propto e^{T}$$

This expression suggests that the equilibrium conversion of methane input should be inversely proportional to the total pressure squared, linearly correlated with steam concentration, and exponentially related to absolute temperature. When this behavior is coupled with the sigmoidal relationship between hydrogen recovery and total pressure in the PSA shown in Figure 4.2, the form of the efficiency relationships shown in Figure 4.3 becomes more clear.

It may be inferred from the results of the study of steam reforming parameters that below a reformer temperature of about 750 C at a steam to carbon of 4:1, increasing pressure is detrimental, despite the enhanced hydrogen recovery, because of equilibrium limitations to methane conversion. Above this design point, increasing pressure increases efficiency, due to the salutary effects of improved hydrogen recovery in the PSA with increasing pressure. Thus, to maximize efficiency, reformer outlet temperatures above 750 C and/or steam-to-carbon ratios above 4:1 are desirable. The improvement in efficiency with pressure would likely be more marked if the higher compressor efficiencies associated with the Quincy reciprocating natural gas compressor were used, as the increase in reactor pressure directly reduces the required pressure ratio for the compression of the far greater volume of product hydrogen.

Another important conclusion from the data of Figure 4.3 is the limited influence of water-gas shift outlet temperature in the useful design range between 350 C and 400 C. The increase in water-gas shift outlet temperature imposes a relatively constant penalty of about 2% on total efficiency. Chapter 5 shows that providing a large enough catalytic reactor to achieve this 350 C design point is quite inexpensive. Thus, the value of 350 C is used as the target water-gas shift temperature throughout this study.

4.2.2 Impact of burner temperature on system efficiency

The version 3.1 model assumed everywhere that a very low pressure drop through the system limited the air blower power draw to 1.5 kW or less with a burner temperature of 800 C.

Initial reactor modeling exercises suggested that the minimum attainable pressure drop through the reactor core, catalytic combustor and superheater was more likely 15 kPa, bringing the assumptions of the version 3.1 model under closer scrutiny. In order to study the impact of varying burner temperatures on airflow requirements and system efficiency, the model was altered to the version 3.2 standard and cases were run to establish the required flow conditions for a range of burner outlet temperatures between 850 C and 1050 C. The output of these cases was then used in the reactor design calculations of Chapter 5, and in the thermodynamic study discussed below.

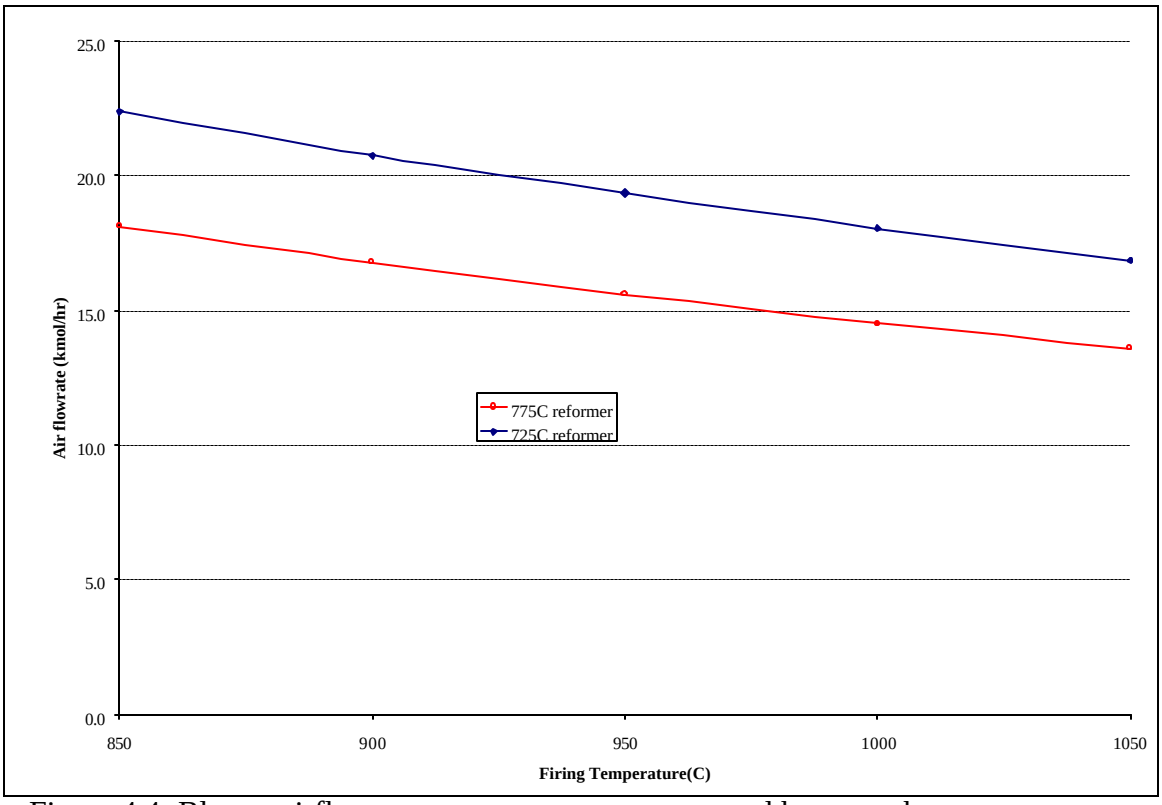

Figure 4.4: Blower airflow versus reactor temperature and burner exhaust temperature

Figure 4.4 shows the relationship between required airflow and reactor and burner temperatures for the case of a 13 bar system with 4:1 steam-to-carbon ratio. The choice of 13 bar for the analysis was dictated by the upper pressure limit of available ancillaries, and the desire to minimize the reactor size, which decreases with increasing pressure. Higher pressures may be feasible, but a great deal more study is required to verify that sufficiently inexpensive components are available at those pressures. The data show that airflow requirement is monotonically reduced with increasing burner temperature, an unsurprising result. The predicted airflow for the case of the 725 reformer is everywhere 4 kmol/hr to 5 kmol/hr greater than that for the 775C reformer, an artifact of the greater energy content of the raffinate stream from the PSA at lower reformer temperatures.

Another consequence of the increased burner temperatures and the decreased flowrates is a variation in the log mean temperature difference (LMTD) across the steam reformer. This effect is shown in Figure 4.5, which demonstrates a nonlinear increase in LMTD with increased

burner temperature. It will be shown in Chapter 5 that this increase in LMTD translates directly to reduced reformer cost at high burner temperatures.

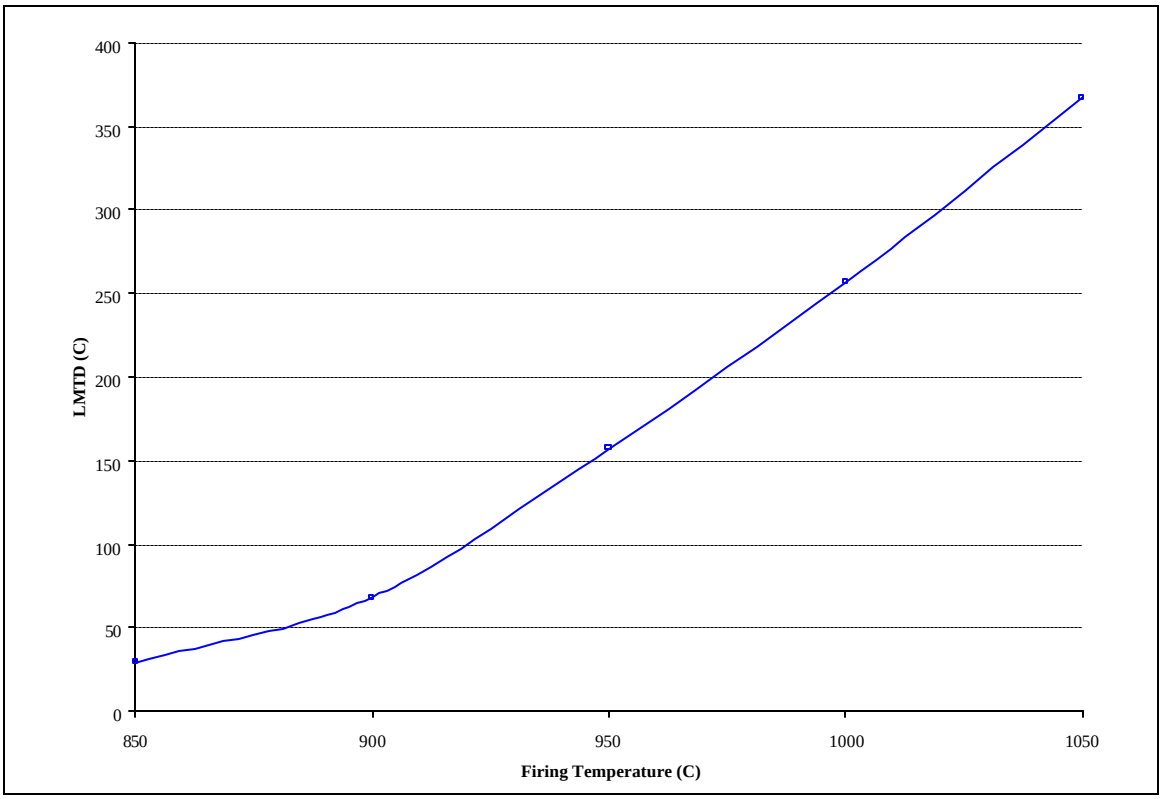

Figure 4.5: Steam reformer LMTD versus burner temperature for a 775C reformer outlet

The air flowrate interacts with the system pressure drop to determine the final impact of the blower on the system efficiency. Figure 4.6 shows the size of the blower power when translated to a fuel basis by the 33% generation efficiency and 90% motor efficiency used previously for the version 3.1 model. In the calculations of Figure 4.6, a brake efficiency of 72% is assumed for the blower, thus resulting in a total efficiency term of 21.4% LHV for drive energy to the blower. The power requirement is calculated as follows:

$$P_{LHV} = \frac{\dot{n}_{Air} T_{ambient} R_u \gamma}{(\gamma - 1)\prod \eta}\left(r_p^{\frac{\gamma-1}{\gamma}} - 1 \right)$$

The power is then compared to the product hydrogen flowrate as follows:

$$\text{blower power ratio} = \frac{P_{LHV}}{\dot{n}_{H_2} LHV_{H_2}}$$

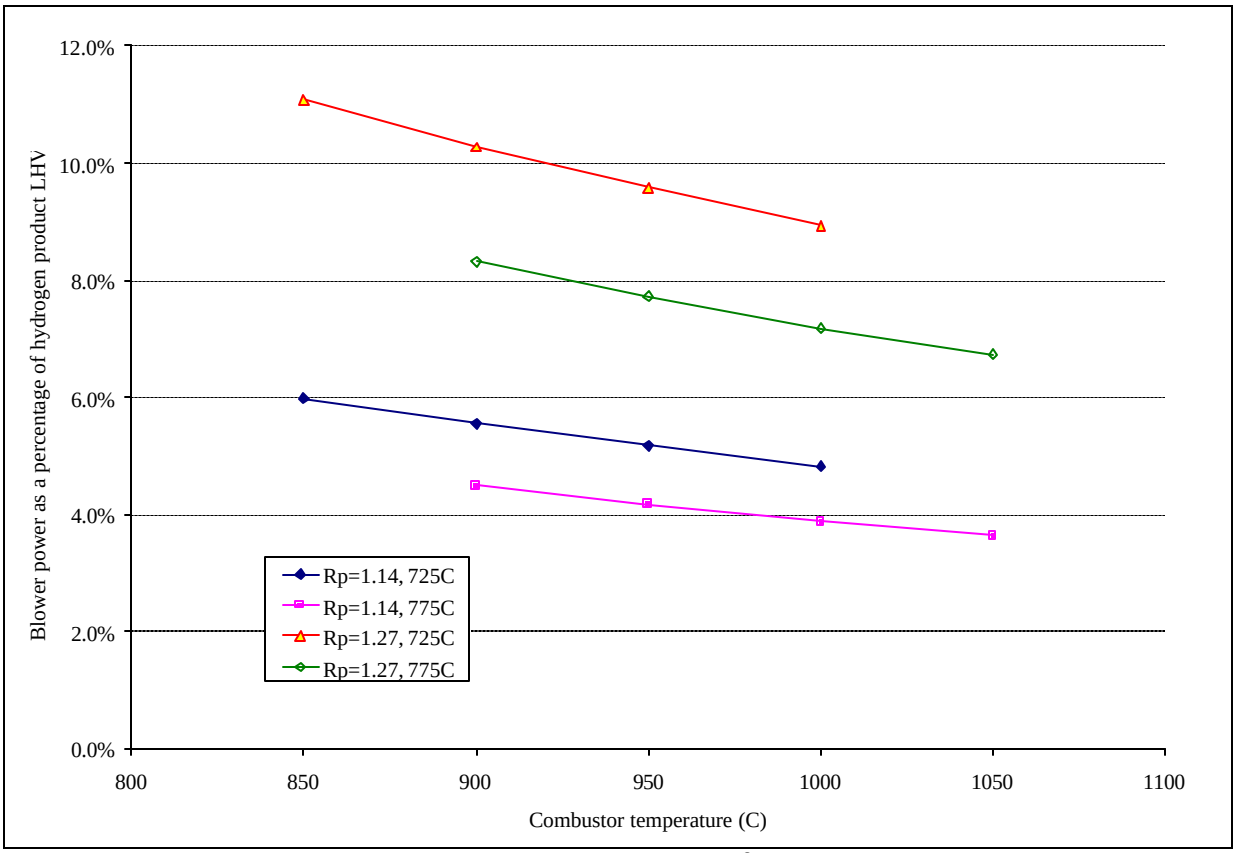

Figure 4.6: Energy consumption of the air blower

The data of Figure 4.6 show that blower power can dominate the efficiency of the system, potentially having a greater impact than changes in the water-gas shift reactor temperature or the reactor pressure. In order to reduce the energy wasted by the blower, several steps are possible.

- Employ an efficient blower, motor and controller
- Minimize the air flowpath pressure drop
- Increase the burner temperature
- Increase the reformer temperature

The first two factors probably have the largest potential influence on the blower power draw, although the proposed design falls in a regime between conventional centrifugal blowers and far less efficient axial and squirrel-cage blowers for low-pressure use. Minimizing the pressure drop of the reactor flowpath is a worthy goal, but initial investigation suggests that a 15 kPa pressure drop may be a realistic lower limit. Finally, both increasing the reformer temperature and increasing the burner temperature can each reduce power consumption by over 20%. This suggests that if possible, a higher-temperature system with lower airflow is to be preferred from a thermodynamic standpoint.

4.2.3 Detailed modeling using version 3.4

Although the thermodynamic comparisons described above are extremely useful as an aid in determining a preferred operational variable space, values which are not reduced to a fuel basis are more useful for calculating the levelized cost of hydrogen from the proposed system studied in this report because of the diversity of fuel and electricity costs which may be encountered in practice. Further, a set of values which separate electrical from fuel inputs might be useful for future trade studies regarding the relative merits of different sorts of compressor drives (natural gas engine versus electric motor) or the impact of siting the units in different jurisdictions on greenhouse gas emissions. Thus, the same cases which are analyzed in Chapter 5 to determine reactor cost, namely 725 C and 775 C reformers with steam to carbon of 4:1, 350 C water-gas shift reactors and a range of combustor temperatures, were also simulated using the version 3.4 model described in section 4.1. The results of these simulations are used in the economic calculations of Chapter 6, and are discussed briefly below.

Table 4.1 includes a detailed summary of the electrical demands and fuel requirement for a variety of simulation cases for the reformer system. These cases are the same ones for which detailed reactor design is conducted in Chapter 5, and are used in the economic analysis of Chapter 6. The chief difference between these values and those discussed previously

Table 4.1: Detailed simulation results from version 3.4

		775C reformer				725C reformer			
	burner temp	900C	950C	1000C	1050C	850C	900C	950C	1000C
Blower motor power - brake	kW	2.0	1.9	1.8	1.6	2.7	2.5	2.3	2.2
H2 compressor power - brake	kW	10.0	10.0	10.0	10.0	10.0	10.0	10.0	10.0
Water pump power - brake	kW	0.065	0.065	0.065	0.065	0.065	0.065	0.065	0.065
NG comp power - brake	kW	2.9	2.9	2.9	2.9	3.3	3.3	3.3	3.3
NG comp. motor eff	%	81%	81%	81%	81%	81%	81%	81%	81%
Water pump motor eff	%	64%	64%	64%	64%	64%	64%	64%	64%
H2 motor eff	%	85%	85%	85%	85%	85%	85%	85%	85%
Blower motor eff	%	80%	80%	80%	80%	80%	80%	80%	80%
Blower electric draw	kWe	2.5	2.4	2.2	2.1	3.4	3.1	2.9	2.7
H2 compressor electric draw - peak	kWe	11.7	11.7	11.7	11.7	11.7	11.7	11.7	11.7
H2 compressor electric draw - average	kWe	8.8	8.8	8.8	8.8	8.8	8.8	8.8	8.8
NG comp electric draw	kWe	3.5	3.5	3.5	3.5	4.1	4.0	4.0	4.1
Pump electric draw	kWe	0.10	0.10	0.10	0.10	0.10	0.10	0.10	0.10
Condensor fan draw	kWe	1	1	1	1	1	1	1	1
Sensors, etc.	kWe	0.4	0.4	0.4	0.4	0.4	0.4	0.4	0.4
Total electric draw	kWe	16.4	16.2	16.0	15.9	17.7	17.5	17.2	17.1
Electricity per unit hydrogen	kWhr/kg	3.4	3.4	3.3	3.3	3.7	3.6	3.6	3.5
w/ premium eff motors	kWhr/kg	3.2	3.2	3.2	3.1	3.5	3.4	3.4	3.4
Natural gas efficiency	%HHV	76%	76%	76%	76%	66%	66%	66%	66%
MMBTU natural gas per unit hydrogen	MBTU/kg	0.15	0.15	0.15	0.15	0.17	0.17	0.17	0.17

is the fact that the different electric drives are addressed individually, rather than being lumped together. Further, the individual drive motor efficiencies were estimated assuming typical 3-phase, 230VAC electric motor efficiencies[84]. This practice highlights the particularly poor

[84] Avallone, E.A., Baumeister, T., Marks' Standard Handbook For Mechanical Engineers: Tenth Edition, 1996, p. 15-39.

efficiency to be expected of low-power electric drives. The use of premium efficiency motors is expected to reduce consumption by about 5%, although the improvement may be greater for the very small motors. Another point is that the average hydrogen compressor power draw is estimated as 75% of the peak draw. Unless the compressor is provided with means for delivering gas from between the stages an improvement beyond this point is unlikely as the compression ratios of the first two stages require over 60% of the power draw for the full compression.

4.3 Thermodynamic modeling conclusions

Extensive thermodynamic analysis of small-scale reformer systems over the past four years has led to the development of a fairly sophisticated system model based in the HYSYS simulation environment. This model has been used to simulate a wide range of process configurations, and the simulation results suggest several general conclusions.

- Efficiency is very sensitive to reformer temperature and steam-to-carbon ratio
- Efficiency varies in a complex fashion with pressure, depending upon the reformer temperature and steam-to-carbon ratio
- Efficiency is not very sensitive to water-gas shift temperature
- Electric drive power draws significantly reduce efficiency

These general conclusions also suggest new directions for study. These include the impact of co-firing the combustor with natural gas, the impact of a higher-recovery PSA system with a greater number of beds, and the possible impact of switching to natural gas engine drive for the hydrogen compressor. Other interesting opportunities for increasing efficiency undoubtedly exist, and should continue to be studied as they are suggested. Although the thermodynamic modeling of the system is arguably further advanced than the catalyst development and reactor design activities, it is important to continually revisit the model to analyze proposed design changes and to understand opportunities to improve the system performance.

Chapter 5 Reactor Design, Costing, Build and Test

Chapter 4 showed that the temperature and pressure conditions within the reactor have an important impact on the efficiency of the hydrogen generation system. This efficiency change translates directly to the operating cost of the system through the natural gas and electricity consumption, and thus the levelized cost of hydrogen produced. This chapter will show that the selection of process conditions can have a profound effect on the capital cost of the chemical reactors employed.

The detailed chemical kinetic modeling of an integrated hydrogen generation reactor of the type initially described in Chapter 2 has been conducted, and will be described in this Chapter. This model was combined with Design For Manufacture and Assembly (DFMA) techniques as described by Boothroyd, *et al* (1994), to yield estimates of the cost to manufacture the reactor in a production environment. The details of this process and the variations in reactor cost with operating conditions will be described. Finally, a 1/3rd-scale reactor capable of generating 19 m^3/hr of product hydrogen was designed, fabricated, and tested. This process and the test results will be discussed and compared with the modeling predictions. The goal of this chapter is to demonstrate a model approach to the problem of designing a chemical reactor wherein the variables in the design are suggested by the thermodynamic analysis and laboratory-scale testing, and are varied such that the overall design may be finalized based upon a discrete global economic trade-off analysis described in Chapter 6. The importance of testing and verification of the model, and the linkage with reactor mechanical design and fabrication will be given particular importance, as these factors exert a strong influence on capital cost, especially in compact chemical equipment of the type being discussed here.

5.1 Chemical reactor modeling

5.1.1 Model formulation and structure

As discussed in Chapter 2, an integrated chemical reactor which combines the functions of primary steam reforming and catalytic, non-isothermal water-gas shift reaction has several exemplary features which combine to reduce the cost and complexity of small-scale hydrogen generation systems relative to those of the prior art. From a chemical engineering design standpoint, the design of the integrated reactor is most readily pursued in two parts: the steam reformer and the water-gas shift reactor. These two parts were treated in two manifestations of a common mathematical architecture, and used much shared computer code and a common approach to the treatment of heat transfer and fluid properties. The overall approach employed was evolved from the initial modeling work conducted by the author for this project[85] and improved upon in subsequent commercial work for the Ford Motor Company and Mobil Oil Company in the design of gasoline fuel reformers. A detailed description of the development of the steam reforming model will allow easy understanding of both models, and only the changes required to produce the water-gas shift model are covered.

[85] Lomax, F.D., May 1997.

The steam-reformer design described in Chapter 2 and in the U.S. patent application of the Appendix couples the endothermic steam-reforming reaction to a counter-flowing hot combustion gas through a compact heat-exchange array. In the case of the detailed model results reported here, that array comprises a multi-pass, cross-flow tubular heat exchanger structure, wherein the steam-reforming catalyst is contained in the tube-side of the structure under 10-15 atmospheres of pressure and the counterflowing hot combustion product is contained at near atmospheric pressure in the shell-side. Thus, from a chemical reactor design standpoint, the steam reformer is a non-isothermal, heterogeneous, catalytic system. These features make simulation of the reacting system somewhat complicated, but are further aggravated by several other features of the system:

- Total pressure on the tube-side drops through the reactor
- Gradients in concentration and temperature may exist radially within each tube, and within each catalyst particle.
- Gradients in tube temperatures must be expected across each baffle pass
- Fluid properties on both the shell and tube-sides vary with temperature and composition
- The counterflow nature of the heat transfer makes a closed solution difficult

The loss of total pressure on the tube-side can be substantial in some reactor geometries, and was explicitly accounted for using the Ergun equation[86]:

$$\frac{dP}{dL} = -\frac{U}{(9.81 m/\sec^2) D_{part}} \frac{1-\phi}{\phi^3} \left[\frac{150(1-\phi)\mu}{D_{part}} + 1.75\rho U \right]$$

which was applied to each differential element in the model.

Gradients across the tube cross-section present a formidable modeling obstacle in full-scale industrial steam reformers with decimeter-scale reactor tube diameters[87]. However, these gradients should be much less important in tubes of 1-2 cm diameter like those contemplated for the compact reactor. Further, the gradients across the tube are captured in the catalyst test data used in the design model, as the tests used 0.95 cm o.d. tubes, which are similar to those modeled here.

Were we extrapolating from a powdered catalyst to a pelletized system of a far different size, traditional chemical engineering techniques would be required to account for intra- and inter-particulate gradients in concentrations and temperature. These gradients were explored in earlier work[88] and shown to be unimportant in small particles of 3 mm o.d., and are captured in this study because the test data collected employed the same catalyst particle size employed in the full scale reactor. This means that the kinetic expressions derived from the data include the effects of mass transport. This significantly simplifies the reactor model, as such gradients usually require an iterative solution of partial differential equations.

---

86 Fogler, H.S., Elements of Chemical Reaction Engineering: 2nd Edition, 1992, p. 128.

87 Rostrup-Nielsen, J.R., 1984, pp 26-28.

88 Lomax, F.D., May 1997, p 50.

Gradients across each baffle pass are a thornier issue. It is certainly the case that the tube nearest the entrance to a given cross-flow pass will contact hotter combustion gas than that tube farthest from the inlet. It is also indisputably true that this will result in a higher heat flux to that inlet tube than is delivered to the outlet tube. However, consideration of the overall geometry suggests that the inlet tube of one pass is also the outlet tube in the preceding pass. Thus, it may be argued that over a few passes, the gradients will tend to cancel out from pass to pass. This may be better understood by imagining that the extreme tube farthest from the centerline along the direction of the airflow will be exposed to the coldest gas in the first pass, and will be exposed to quite similar air temperature in the next pass as it is the inlet to that second pass. The inlet tube to the first pass, however, is exposed to much hotter air from the combustor in the first pass, but is then exposed to colder air at the outlet of the second pass, which is far colder than the inlet of the second pass. Over many cross-flow stages, it can be surmised that the tubes at various locations in the bundle are exposed, on average, to very similar heat transfer conditions. This argument is particularly attractive, as we know that typical convective heat-transfer correlations are only valid within 10% to 20%, and that the variations engendered by the gradients across each pass are likely to be disguised by the poor precision inherent to such design calculations. Thus, gradients across each pass are not explicitly treated and the entire array of tubes is effectively modeled as in the case of a pure counterflow. This approximation should hold as long as the number of cross-flow passes is high. This restriction is not considered problematic, as large thermal gradients also present structural challenges due to thermal expansion loads, and the minimum number of passes in a viable design is, thus, set as between four and five in this research.

The variation in fluid properties along the flow path introduces significant changes in local heat-transfer conditions. Thus, the fluid density, thermal conductivity, Prandtl number and absolute viscosity are calculated at each differential element in the model. The methods employed are discussed below.

The counterflow nature of the overall flow acts to dictate the form of the simulation model employed. Analytic models using differential equation solutions are possible when co-flowing fluids are employed, or when the firing temperature is an independent variable, as in the case of radiantly-heated industrial furnaces[89]. Such solutions do not easily present themselves in the case of complex boundary-value problems involving systems of nonlinear partial differential equations. A solution pursued successfully by the author in past work[90] employs a mathematically-simple, Eulerian solution based on a one dimensional finite difference approach to the system.

The reactor is reduced to a single, heat-transfer-averaged tube, as discussed above. This average tube is treated as a plug flow (PFR), non-isothermal, heterogeneous catalytic reactor. The tube is then subdivided into differential elements, which may be varied in dimension along the tube length to reduce run-time for the code. The fluid within the tube, which is the reacting fluid, is assumed to exchange heat with the counter-flowing combustion product on the shell-side. Once again, this counter-flowing fluid is treated as an average of the conditions on the

[89] Rostrup-Nielsen, 1984, p. 25.

[90] Lomax, F.D., May 1997, Appendix B.

shell-side, and the effects of gradients due to the baffled construction of the reactor are ignored. The thermodynamic conditions at the inlet of the model are known from the thermodynamic simulation conducted previously and described in Chapter 4. Each differential element is then treated as a Continuous Stirred-Tank Reactor (CSTR). It is well-known that many CSTR's in series may be used to approximate a PFR[91], in the model described here, more than 1,000 differential elements are generally employed for stability, which should very closely approximate a PFR. The advantage of using a CSTR is that the expression for the change in concentration in the differential element becomes a simple algebraic expression for our first-order reaction rate.

$$\frac{dC_{CH_4}}{dt} = \left(C_{CH_4} - C_{eq_{CH_4}}\right)k_{CH_4}$$

The reaction rate constant k was derived from the experimental data for the FCR 10 catalyst, and included the impact of oxidative poisoning everywhere in the reactor, although it may be argued that the di-oxygen in the feed will be consumed in the first few differential elements of the reactor. The expression employed used two different rate expressions which converged at 857K. These correspond to the most conservative rate data measured for FCR 10, as reported in Chapter 3. Both correlations yield the rate constant in units of inverse seconds.

$$k_{poisoned} = 2.55x10^{23} e^{-\frac{45549}{T}}$$

$$k_{clean} = 11100e^{-\frac{7327.7}{T}}$$

The energy balance between the counterflowing fluids is explicitly considered. The two streams are considered adiabatic with respect to the surroundings, and their energy balance is expressed as follows:

$$dH_{tube} = \frac{dC_{CH_4}}{dt} V_{d.e.} \Delta H_{r_{steamreformin\,g}} + \frac{dC_{CO}}{dt} V_{d.e.} \Delta H_{r_{watergasshift}} + U_{oa} A_{d.e.} + \left(c_{pinlet} \dot{m} \Delta T_{d.e.}\right)_{tube} = 0$$

$$dH_{shell} = -U_{oa} A_{d.e.} + \left(c_{pinlet} \dot{m} \Delta T_{d.e.}\right)_{shell} = 0$$

The water-gas shift reaction is assumed to proceed to equilibrium in each differential element. This simplification is suggested in the literature[92] and conforms with the experimental results obtained with the noble metal catalysts tested to date. In the physically important design cases, the combustion product has a higher temperature than the reacting gas, and heat flows from the combustion product to the reacting gas. The amount of heat removed from the gas is then added back into the counterflowing stream, which increases in temperature as the model "marches" forward. The reacting gas may increase or decrease in temperature, depending upon the rate of reaction. The new temperatures at the end of the differential element, which are the outlet temperature of the reacting gas and the inlet temperature of the combustion gas (remember that only the outlet temperature of this stream was known at the boundary!), are used as the basis for

91 Fogler, H.S., 1992, pp. 38-48.

92 Rostrup-Nielsen, J.R., 1984, p. 58.

the calculation of the gas properties in the next differential element. The Eulerian mathematics and the use of only one temperature to characterize the fluid properties, reaction rates, etc. make the model strongly susceptible to the step-size. Experiments have been conducted with the model, and the stability of the model against step size variation has been established. In general, when graphical representation of the model results exhibits discontinuities (i.e. a jagged or "sawtooth" curve), then step-size reduction is called for.

The overall heat-transfer coefficient U_{oa}, is determined using the empirical correlations of Grimson, Kays, and Zaukauskas on the shell-side of the heat exchanger[93] and the tube-side correlation of Li and Finlayson. The former have been employed by the author in the past to design heat exchangers and boilers and have demonstrated an error less than 15%. The latter have demonstrated poor predictive performance in laboratory tests, and the calculated values are halved for conservatism. This factor of 1/2 is based upon experimental tests using granulated media of the type employed in the reactor in 3/8" outer diameter tubes in the microreactor apparatus described in Chapter 3.

To calculate the heat-transfer coefficients, the local flow conditions on both the shell and tube-sides must be calculated. In order to do so, the geometry of the individual tubes as well as that of the tube bundle must be specified. This includes the parameters of tube outer diameter, wall thickness, tube spacing, shell diameter, and baffle spacing along the reactor length. Each of these then represents an independent variable which may be altered in the optimization of the reactor.

The final calculation for the overall heat-transfer correlation includes the resistance due to conduction through the tube wall, and takes the form.

$$U_{oa} = \frac{1}{R_{bed} + R_{wall} + R_{shell}}$$

$$R_{bed} = \left(\frac{d_{tube}}{d_{tube} - 2t_{wall}} \right) \frac{1}{h_{bed}}$$

$$R_{wall} = \frac{d_{tube}}{k_{tube}} \ln \left(\frac{d_{tube}}{d_{tube} - 2t_{wall}} \right)$$

$$R_{shell} = 1 / h_{shell}$$

The calculation of the fluid properties, as mentioned previously, is of critical importance to the accuracy of the reaction model. The density of the fluid was obtained assuming the ideal gas law with a compressibility of unity. These assumptions are valid at the low-pressure, high-temperature conditions in the reactor. The thermal conductivities of the individual gases were estimated using temperature-dependent correlations[94]. They were combined according to the following formula to yield a mixture heat capacity.

---

93 Holman, J.P., Heat Transfer: 7th Edition, 1990, pp. 309-312.

94 Black, W.Z., Hartley, J.G., Thermodynamics: 2nd Edition, 1991, p. A-51.

$$c_{pmix} = \left(\sum_i c_{pi} y_i MW_i \right) \Big/ MW_{mix}$$

For both the dynamic viscosity and the thermal conductivity of the tube-side gas mixture, the method of Wilke was employed[95]. The Wilke equations are shown below for the example of dynamic viscosity, but the equations for conductivity are structurally the same. The input species viscosity and thermal conductivity values were curve-fit from the literature, as Chapman-Enskog derived values were observed to deviate substantially from published values. Thus,

$$\mu_{mix} = \sum_{i=1}^{n} \frac{y_i \mu_i}{\sum y_j \varphi_{ij}}$$

$$\varphi_{ij} = \frac{1}{\sqrt{8}} \left(1 + \frac{MW_i}{MW_j} \right)^{-0.5} \left[1 + \left(\frac{\mu_i}{\mu_j} \right)^{0.5} \left(\frac{MW_j}{MW_i} \right)^{0.25} \right]^2$$

The water-gas shift model is structurally-identical to the reforming model described above. Naturally, the tube geometry, and tube spacing of the reforming section must be retained between the two sections of a given reactor, but the baffle spacing may be changed separately. Several important changes were made to reflect the different chemistry of the ferrochrome water-gas shift catalyst. These changes include the following:

- Ferrochrome catalyst has zero methanation activity, thus, there are no changes in methane molar flowrate through the reactor
- Ferrochrome catalyst activity from the literature used to model water-gas shift activity

The first of these points has been demonstrated in laboratory experiments described in Chapter 3. Further, this view has been held by others in the field[96]. The choice of literature catalyst activity relations, instead of experimentally derived ones measured in the laboratory apparatus, is motivated by the excellent quality of the research of Hans Bohlbro of Haldor Topsoe. Bohlbro published results[97] of an extensive study of ferrochrome activity which suggested the form for the rate expression shown below. The work of Bohlbro included the effects of variations of multiple feed constituents in an experimental program which would be impractical to reproduce. Although the theoretical underpinnings of Bohlbro's model have been challenged, the practicality of the model has been confirmed[98].

---

95 Welty, J.R., Wicks, C.E., Wilson, R.E., Fundamentals of Momentum, Heat and Mass Transfer: 3rd Edition, 1984, p. 102.

96 Personal communication with Dr. Debbie Myers, Argonne National Laboratory. Personal communication, Dr. Aaron Wagner, Sud-Chemie, Inc.

97 Bohlbro, H., "The kinetics of water gas shift conversion IV: Influence of Alkali on the rate equation," Journal of Catalysis, vol 3, pp. 207–215, 1964.

98 Podolksi, W., Kim, Y.G., "Modeling the water gas shift reaction," Industrial and Engineering Chemistry: Process Design and Development, vol 13, No 4, 1974, p. 419.

$$v_{CO} = k(T)P^{(l+m+n)} \frac{p_{CO}^{l} p_{H_2O}^{m}}{p_{CO_2}^{n}} (1-\beta)$$

$$v_{CO} = 3.87\times10^{7} e^{\frac{-13789}{T}} P^{0.55} \frac{p_{CO}^{0.9} p_{H_2O}^{0.25}}{p_{CO_2}^{0.6}} (1-\beta) \quad gmol_{CO} / g_{cat}\, hr$$

where $\beta = \dfrac{p_{CO_2} p_{H_2}}{K_{eq} p_{CO} p_{H_2O}}$ and pressures are in atm's

Naturally, the inlet conditions for the water-gas shift reactor are chosen as the thermodynamically-determined outlet conditions of the reformer section from the model of Chapter 4. The model 'marches" forward until the thermodynamic outlet conditions of the water-gas shift reactor are achieved. As will be discussed below, the approach to equilibrium in the water-gas shift reactor is not assured at all exit temperatures, and care must be exercised to ensure that the desired CO conversion is achieved.

The structure of the chemical reactor models required for the primary steam reforming and water-gas shift sections of the integrated reformer concept described in chapter 2 has been described. These models employ an Eulerian, finite-difference approach to calculate the required reactor length for a user-input combination of inlet conditions and tube-array geometry. The effects of fluid-property variation and tube-side pressure drop are explicitly addressed. Inter and intra-particular mass-transport gradients are indirectly captured in the catalyst rate data derived from the microreactor tests described in Chapter 3. These models have been exercised to size reactors under a variety of thermodynamic boundary conditions and tube-array geometries. These results are discussed at length below.

Several checks on the model have been performed in addition to the internal checks such as redundant molar and mass balances. The first check is the comparison of endpoint gas temperatures to the values predicted by HYSYS, a commercial process simulator. This check confirms that the thermodynamics and fluid thermal capacities written into the model agree with the predictions of HYSYS at the boundary values for the same flow conditions. This test also verifies that the heat transfer and chemical reaction calculations are implemented in a fashion that does not adversely impact the overall heat balance of the reactor. A second check is that the overall activity of the reactor at its average temperature is compared to the experimentally-derived activities at the same temperature. This shows that the overall kinetic parameters of the reactors being modeled are similar to those measured in the more nearly isothermal microreactor experiments. These successful tests mean that no gross errors have been introduced in the implementation of the kinetic expression in the model. Finally, the behavior of the model in response to changes in input parameters has been observed, and the results have been analyzed based on engineering fundamentals, microreactor testing experience and literature results. The behavior of the model appears qualitatively correct. All of these checks are important to verify that the model is functional. The next step is the actual calibration of the model against test data for large-scale reactor test articles. This activity has begun, and will be continued in future work.

5.1.2 Reactor modeling results

The reactor model was exercised over a wide parameter space in order to establish an understanding of the relationships between the various design parameters and the resulting reactor size. The sizing data were then combined with an understanding of the reactor metallurgy and the required mechanical design considerations to yield manufacturing cost estimates for the various reactor configurations.

The models described in section 5.1.1 output data for fluid temperatures and compositions along the reactor length. It is generally observed that in the steam-reforming reactor, the approach to equilibrium is essentially complete at the outlet temperature, a result confirmed in the literature[99]. This means that the required size of a steam-reforming reactor for a given set of design conditions may be equated with the length of tube required to achieve the desired tube-side reactant temperature. The typical temperature profiles along the axis of the steam reforming section is shown in Figure 5.1, which shows the reduction in shell-side temperature towards the reactor inlet (reactor length of zero) and the increase in tube-side temperature from inlet to outlet. In the case of the data of Figure 5.1, a reactor length of about 0.95 m is required to reach a 775 C outlet temperature from the reformer.

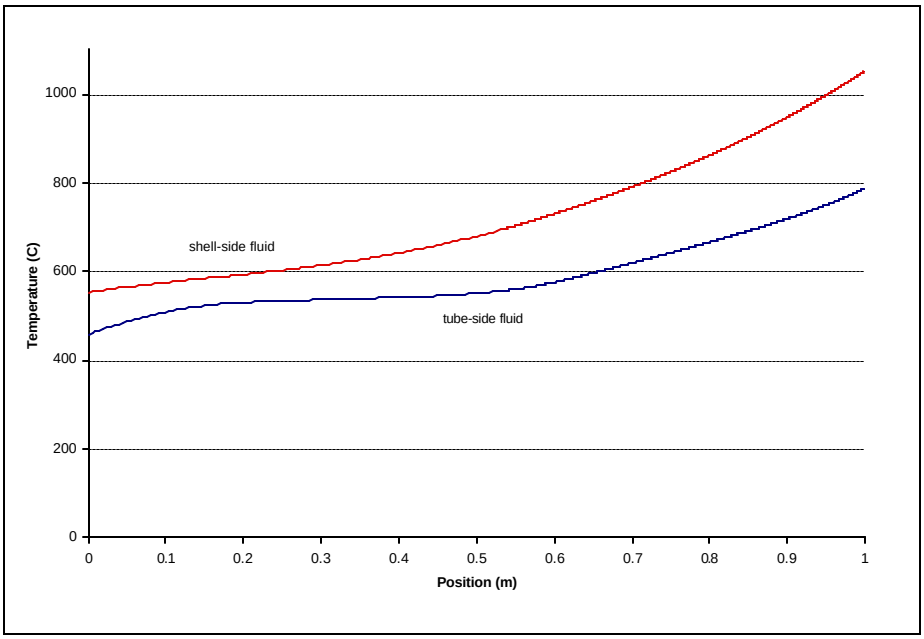

Figure 5.1: Typical temperature profiles generated by the steam reforming model

The parameters investigated in the trade-off study conducted here include the reformer outlet temperature, combustor firing temperature, tube outer diameter, tube spacing, baffle spacing and shell diameter. The parameter values studied are shown in Table 5.1. It should be noted that not all parameter combinations yield feasible configurations, as temperature cross within the heat exchanger causes the model to fail to reach the desired outlet conditions. Thus, results are only reported here for feasible combinations of parameters. Some viable design

[99] Rostrup-Nielsen, J.R., 1984, p. 6.

conditions have not been studied. It is, thus, probable that a more extensive discrete trade-off study is warranted once the model has been fully vetted against experimental results for the 1/3rd scale reactor described later in this chapter. The results of the admittedly incomplete trade study conducted to date are shown in Table 5.2. Several tentative conclusions may be drawn from this initial trade study, and these are discussed below.

Table 5.1: Parameter space for reactor design optimization

Parameter	Values Investigated
Tube outer diameter	12.7 mm, 15.9 mm, 19.1 mm
Tube diametrical spacing ratio	1.25, 1.5
Combustor temperature	850C, 900C, 950C, 1000C, 1050C
Reformate outlet temperature	725C, 775C
Baffle spacing	101-228 mm

Figure 5.2 shows the results for a segment of the variable space investigated with fixed reactor outer shell diameters similar to 12" schedule 40 pipe. The impact of variations in baffle spacing and tube diameter on shell-side pressure drop, catalyst volume, and total tube length are shown by these data. Surprisingly, tube diameter has no significant impact on shell-side pressure drop, which seems to be determined almost

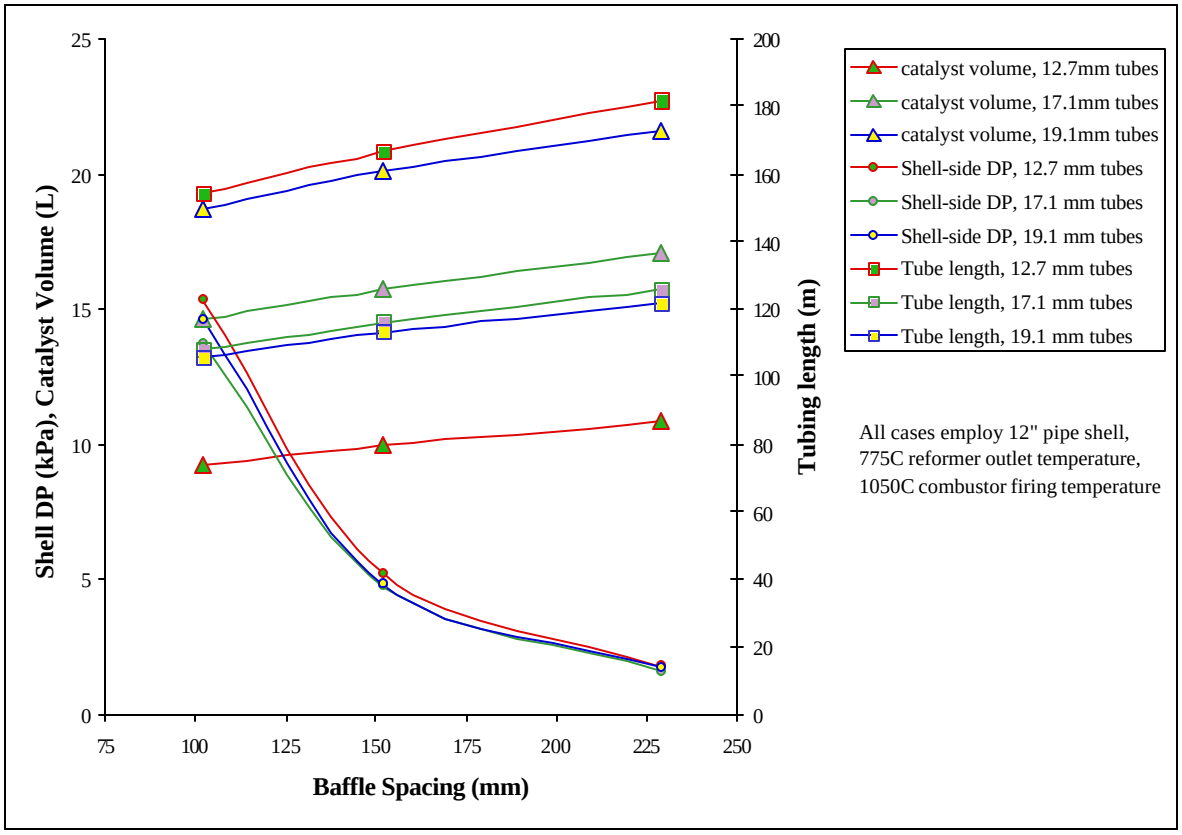

Figure 5.2: Impact of tube diameter and baffle spacing on reactor performance

Table 5.2: Preliminary steam reformer trade study results

Tube od (mm)	Matrix /od ratio	baffle interv. (mm)	Pipe id (mm)	max tube count	Max-min flow area (sqm)	tubes in Pipe	friction factor	Delta Pout (kPa/pass)	V per pass (L)	HX area per unit length (sqm/m)	Length for Tref (m)	Tref	Tcomb	DP down bore (kPa)	Passes	total shellside DP (kPa)	total volume (L)	catalyst volume (L)	total tube length (ft)	reactor length (ft)
12.7	1.5	127	247.65	13.0	0.01048	153	0.063	1.32	6.12	6.11	0.85	775	1050	55.7	6.7	11.7	40.9	7.7	427	2.79
12.7	1.5	152	247.65	13.0	0.01258	153	0.065	0.95	7.34	6.11	0.884	775	1050	57.7	5.8	7.3	42.6	8.1	445	2.90
12.7	1.5	76	247.65	13.0	0.00629	153	0.057	3.34	3.67	6.11	0.77	775	1050	49.6	10.1	44.7	37.1	7.0	387	2.53
12.7	1.5	229	247.65	13.0	0.01887	153	0.070	0.45	11.01	6.11	0.974	775	1050	63.8	4.3	2.6	46.9	8.9	490	3.20
12.7	1.5	229	298.45	15.7	0.02274	223	0.072	0.39	15.99	8.88	0.816	775	1050	27.4	3.6	1.8	57.1	10.8	596	2.68
12.7	1.5	152	298.45	15.7	0.01516	223	0.067	0.81	10.66	8.88	0.747	775	1050	24.3	4.9	5.2	52.3	9.9	546	2.45
12.7	1.5	102	298.45	15.7	0.01011	223	0.062	1.70	7.11	8.88	0.693	775	1050	22.3	6.8	15.3	48.5	9.2	506	2.27
12.7	1.5	102	196.85	10.3	0.00667	97	0.058	2.39	3.09	3.86	1	775	1050	155.0	9.8	31.2	30.4	5.8	318	3.28
12.7	1.5	152	196.85	10.3	0.01000	97	0.062	1.14	4.64	3.86	1.102	775	1050	172.2	7.2	11.0	33.5	6.3	350	3.62
12.7	1.25	152	196.85	12.4	0.00600	139	0.034	4.22	4.64	5.56	0.785	775	1050	60.8	5.2	28.7	23.9	6.5	359	2.58
12.7	1.25	203	196.85	12.4	0.00800	139	0.036	2.50	6.18	5.56	0.827	775	1050	63.8	4.1	13.7	25.2	6.9	378	2.71
12.7	1.25	203	196.85	12.4	0.00800	139	0.036	2.79	6.18	5.56	0.867	775	1000	67.9	4.3	15.5	26.4	7.2	397	2.84
12.7	1.25	203	196.85	12.4	0.00800	139	0.035	2.97	6.18	5.56	1.284	775	950	98.3	6.3	24.5	39.1	10.6	587	4.21
12.7	1.25	203	196.85	12.4	0.00800	139	0.035	3.14	6.18	5.56	2.291	775	900	173.2	11.3	47.2	69.7	19.0	1048	7.52
12.7	1.5	229	247.65	13.0	0.01887	153	0.068	0.54	11.01	6.11	1.489	775	950	97.2	6.5	4.6	71.7	13.6	749	4.89
12.7	1.5	229	247.65	13.0	0.01887	153	0.066	0.57	11.01	6.11	2.592	775	900	166.1	11.3	8.6	124.9	23.6	1303	8.50
12.7	1.5	229	247.65	13.0	0.01887	153	0.069	0.51	11.01	6.11	1.029	775	1000	67.9	4.5	3.0	49.6	9.4	517	3.38
17.1	1.5	229	298.45	11.6	0.02274	122	0.068	0.27	15.99	6.58	1.0313	775	1050		4.5	1.6	72.1	17.1	413	3.38
17.1	1.5	152	247.65	9.6	0.01258	84	0.061	0.66	7.34	4.53	1.112	775	1050	46.6	7.3	6.4	53.6	12.7	307	3.65
17.1	1.25	152	247.65	11.6	0.00755	121	0.034	2.46	7.34	6.52	0.8296	775	1050	18.2	5.4	17.7	40.0	8.9	330	2.72
17.1	1.5	152	298.45	11.6	0.01516	122	0.063	0.57	10.66	6.58	0.9488	775	1050	20.3	6.2	4.7	66.4	15.7	380	3.11
17.1	1.5	229	247.65	9.6	0.01887	84	0.066	0.32	11.01	4.53	1.2	775	1050	51.7	5.3	2.2	58.8	13.9	337	4.01
17.1	1.5	102	247.65	9.6	0.00839	84	0	1	4.894	4.53	1.0250	775	1050	42.5	10.1	18.6	49.4	11.7	283	3.36
17.1	1.5	102	298.45	11.6	0.01011	122	0	1	7.107	6.58	0.8835	775	1050	18.2	8.7	13.7	61.8	14.6	354	2.90
19.1	1.5	152	298.45	10.4	0.01516	99	0.062	0.50	10.66	5.92	1.14	775	1050	21.3	7.5	4.8	79.7	20.1	370	3.74
19.1	1.5	229	298.45	10.4	0.02274	99	0.067	0.24	15.99	5.92	1.23	775	1050	23.3	5.4	1.7	86.0	21.6	399	4.04
19.1	1.25	229	298.45	12.5	0.01365	142	0.037	0.89	15.99	8.53	0.9281	775	1050	9.1	4.1	4.8	64.9	23.5	434	3.04
19.1	1.25	152	298.45	12.5	0.00910	142	0.034	1.86	10.66	8.53	0.8824	775	1050	8.1	5.8	14.3	61.7	22.4	412	2.90
19.05	1.5	101.6	298.5	10	0.01	98.93	0.1	1.1	7.1	5.92	1.065	775	1050	20.3	10.5	14.6	74.5	18.7	346	3.49
12.7	1.5	152.4	197	10.33	0.01	97	0.061	1.96	4.64	3.86	0.472	725	1050	143	3.1	7.2	14.4	1.9	150	1.55
12.7	1.5	101.6	197	10.33	0.00667	97	0.057	4.11	3.09	3.86	0.423	725	1050	164	4.2	20.6	12.9	1.7	134	1.39
12.7	1.5	152.4	197	10.33	0.01	97	0.06	2.13	4.64	3.86	0.592	725	1000	95	3.9	10.0	18.0	2.4	188	1.94
12.7	1.5	152.4	197	10.33	0.01	97	0.059	2.29	4.64	3.86	0.778	725	950	79	5.1	14.1	23.7	3.2	247	2.55
12.7	1.5	152.4	197	10.33	0.01	97	0.058	2.47	4.64	3.86	1.036	725	900	81	6.8	20.1	31.5	9.6	329	3.40
12.7	1.5	152.4	248	13	0.01258	153	0.061	2.04	7.34	6.11	0.851	725	900	28	5.6	13.7	41.0	12.4	428	2.79
12.7	1.5	152.4	248	13	0.01258	153	0.06	2.22	7.34	6.11	1.216	725	850	34	8.0	21.2	58.6	19.5	611	3.99

Note: green shading corresponds to 5/8” o.d. tubes, blue shading corresponds to ¾” o.d. tubes

entirely by baffle spacing, with an essentially parabolic relationship between the two being evidenced. Conversely, baffle spacing exhibits only a weak positive, nearly-linear correlation with tube and catalyst requirements, which seem to be dictated almost entirely by tube diameter. The weak dependence of reactor size on baffle spacing and the strong role this spacing plays in pressure drop suggest using the largest practical baffle spacings for a given set of flow conditions. The value of this spacing would depend upon the combination of allowable shell-side pressure drop and the need to maintain a minimum number of baffle passes to reduce thermal gradients. The analysis to date suggests baffle spacings of 75% to 100% of the shell diameter may be most appropriate as the shell-side pressure drop is low and the resultant tube length and catalyst volume increases over closer baffle spacings are modest as shown in Figure 5.2. The choice of tube diameter depends upon the balance between the cost of the tube and the catalyst, and will be addressed in detail later in this chapter. At this point, it suffices to note that catalyst volume increases markedly and monotonically with tube diameter, while total tube length decreases in a nonlinear fashion with increased tube diameter.

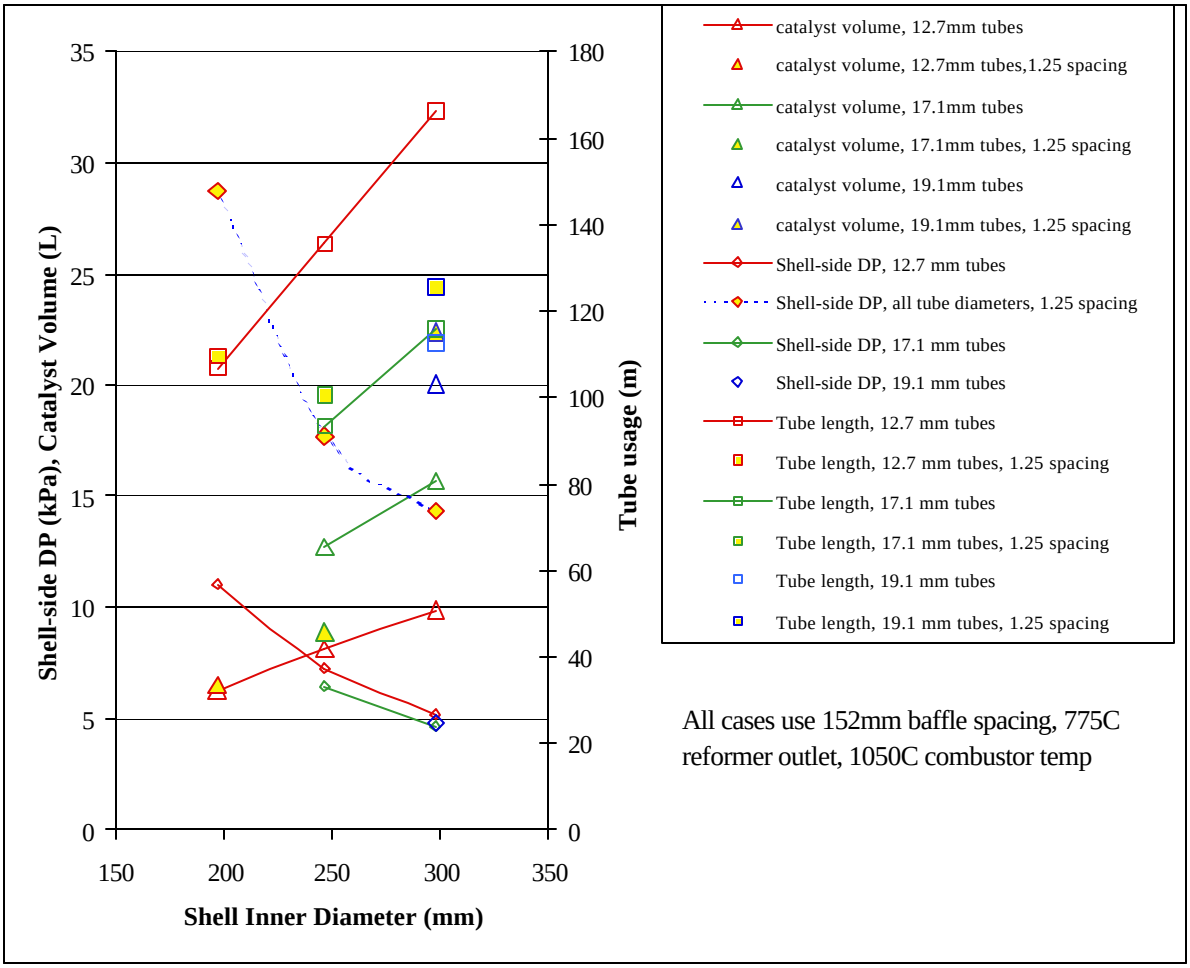

Figure 5.3: Impact of shell diameter and tube spacing on reactor performance

Two other important variables in the reactor design are the shell diameter and the tube diametrical spacing. In all cases in this study, the common equilateral triangular array of tubes is employed, and spacings of 1.5:1 and 1.25:1 on a tube-diameter basis were employed. Larger

spacings of 2:1 and inline tube arrays are sometimes specified in extremely pressure-drop-sensitive designs, but generally require larger reactors, which negatively impacts parasitic heat loss, materials cost and packaging. The impact of these parameters is quantitatively shown in Figure 5.3. Figure 5.3 largely confirms the independence of shell-side pressure drop on tube diameter, and similarly confirms the trends between tube diameter and catalyst volume and tube length shown in Figure 5.2. Several interesting new conclusions may be drawn from the data of Figure 5.3 though.

First, changes in shell diameter have a strong, positive correlation with both tube and catalyst usage. This effect appears nearly uniform for all tube diameters investigated. Second, the relationship between increased shell diameter and shell-side pressure drop appears weaker than that between baffle spacing and pressure drop. All of this suggests that a less expensive reactor may be fabricated by using a smaller diameter shell and greater baffle spacing, if the shell-side pressure drop constraints are equal, as they must be to achieve acceptable thermal efficiency, as discussed in Chapter 4. Perusal of Table 5.2 shows that tube-side pressure drop increases strongly with reduced shell diameter, an effect which may become important under some situations. The total economic tradeoff between these parameters will be investigated later in this chapter, but it certainly appears that longer-aspect-ratio reactors may be less expensive to manufacture.

Another surprising result of the data of Figure 5.3 is the poor performance afforded by tightly-packed tube arrays. First, the switch to tightly-packed arrays markedly increases shell-side pressure drop. In fact, the increase in pressure drop always exceeds 100% for the cases presented here. For most cases investigated, tube and catalyst usage increase slightly as well, although one anomalous point for catalyst usage casts some doubt on the generality of this result. Suffice it to say, were the shell diameter or baffle spacing increased sufficiently to reduce the shell-side pressure drop to competitive levels, the tube and catalyst usage would be economically unacceptable. Perusal of the results in Table 5.2 shows that total volume is markedly decreased by tighter packing, and this suggests that tight-packed arrays would only find applicability in volume-constrained applications.

As discussed in Chapter 4, several thermodynamically-feasible design states are possible for the reformer system at any given reformer outlet temperature. The major determinant between the cases on a thermodynamic basis is theoretical energy recovery from the combustion gas, which may leave the combustor at a variety of temperatures depending upon the stoichiometry of the combustor. In a traditional chemical engineering design process, the exact state would be specified by the process engineers and the reactor designers would be "stuck" with it. Preliminary analysis in the trade study suggests that combustor temperature and reformer temperature are the most important determinants of reactor cost and geometry. This result is shown in Figure 5.4, which shows the impact of different reformer and combustor temperatures on the reactor size.

Figure 5.4 shows that the increased blower airflows associated with lower combustor temperatures and lower reformer temperatures both act to dramatically increase reactor pressure drop for a given overall geometry. This suggests that low-temperature combustors will require some combination of increased shell diameter and baffle spacing in the reactor to achieve

acceptable pressure drops. In extremity, higher tube spacing may be needed in low-temperature systems to reduce the shell-side pressure drops to lower values. At a fixed reformer outlet temperature, reducing combustor temperature below a certain value leads to dramatic increases in tubing and catalyst requirement. This temperature is about 1000 C for the 775 C reformer cases and 950 C for the 725 C reformer cases.

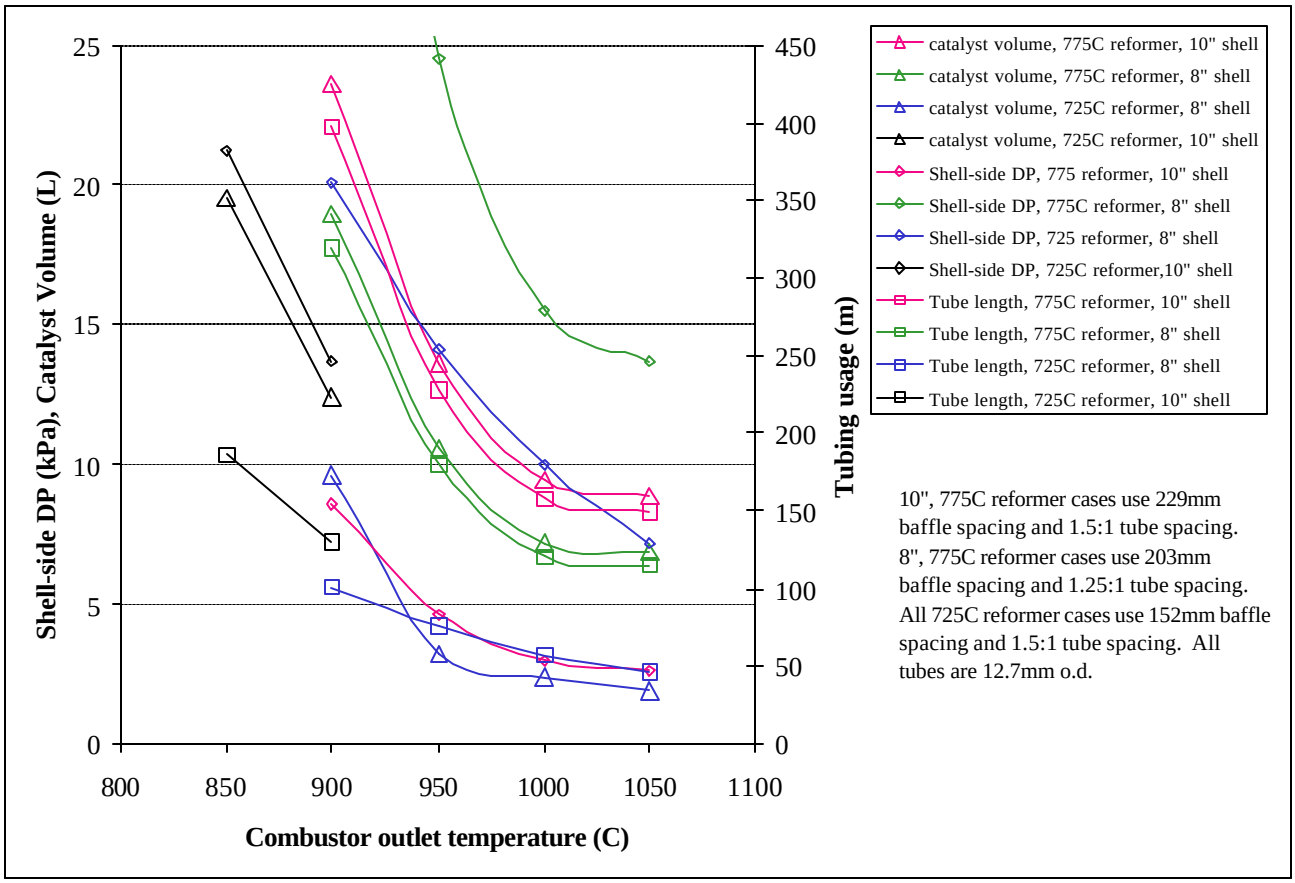

Figure 5.4: Impact of burner and reformer temperature on reactor performance

If a limit of about 6.9 kPa is set for the shell-side pressure drop, then a much constrained "world" of possible configurations is obtained. This limit is set for two reasons. It allows high themal efficiencies to be attained. Second, many low-cost blowers can overcome this pressure head, whereas blower cost increases precipitously for higher pressure heads. This set of configurations does not include any of the 725 C reformer cases shown in Figure 5.4, and eliminates the 900 C firing temperature case with the 775 C reformer. This is unfortunate, as the reduction in reformer temperature to 725 C does seem to afford marked reductions in catalyst and tube requirements. For the economic analysis of the various cases, this means that lower pressure-drop configurations for 725 C reformer temperatures are needed.

These were run, and are shown, along with the pressure-drop constrained cases from Table 5.2, in Table 5.3. Water-gas shift reactor sizing is only conducted for steam reformer cases that exhibit less than 6.9 kPa shell-side pressure drop and at least four shell-side passes to limit thermal stresses. It is interesting to note that the open, 2:1 tube spacing is required in the

Table 5.3: Final steam reformer cases for cost estimation

Tube od (mm)	Matrix/ od ratio	baffle interv. (mm)	Pipe id (mm)	max tube count	Max-min flow area (sqm)	tubes in Pipe	friction factor	Delta Pout (kPa/pass)	V per pass (L)	Inner volume per length (cubm/m)	HX area per unit length (sqm/m)	Length for Tref (m)	Tref	Tcomb	DP down bore (kPa)	Passes	total shellside DP (kPa)	total volume (L)	catalyst volume (L)	total tube length (ft)	reactor length (ft)
12.7	1.5	229	247.65	13.0	0.01887	153	0.070	0.45	11.01	0.0091	6.11	0.974	775	1050	63.8	4.3	2.6	46.9	8.9	490	3.20
12.7	1.5	152	298.45	15.7	0.01516	223	0.067	0.81	10.66	0.0132	8.88	0.747	775	1050	24.3	4.9	5.2	52.3	9.9	546	2.45
12.7	1.5	203	247.65	13.0	0.01677	153	0.066	0.67	9.79	0.0121	6.11	1.536	775	950	64.8	7.6	6.6	74.0	18.5	772	5.04
12.7	1.5	254	247.65	13.0	0.02097	153	0.068	0.47	12.23	0.0141	6.11	2.4	775	900	81.0	9.4	6.0	115.1	33.7	1202	7.84
12.7	1.5	203	247.65	13.0	0.01677	153	0.067	0.63	9.79	0.0093	6.11	1.007	775	1000	62.8	5.0	4.1	48.5	9.4	506	3.30
17.1	1.5	229	298.45	11.6	0.02274	122	0.068	0.27	15.99	0.0166	6.58	1.0313	775	1050		4.5	1.6	72.1	17.1	413	3.38
17.1	1.5	152	247.65	9.6	0.01258	84	0.061	0.66	7.34	0.0114	4.53	1.112	775	1050	46.6	7.3	6.4	53.6	12.7	307	3.65
17.1	1.5	152	298.45	11.6	0.01516	122	0.063	0.57	10.66	0.0166	6.58	0.9488	775	1050	20.3	6.2	4.7	66.4	15.7	380	3.11
17.1	1.5	229	247.65	9.6	0.01887	84	0.066	0.32	11.01	0.0114	4.53	1.2	775	1050	51.7	5.3	2.2	58.8	13.9	337	4.01
19.1	1.5	152	298.45	10.4	0.01516	99	0.062	0.50	10.66	0.0176	5.92	1.14	775	1050	21.3	7.5	4.8	79.7	20.1	370	3.74
19.1	1.5	229	298.45	10.4	0.02274	99	0.067	0.24	15.99	0.0176	5.92	1.23	775	1050	23.3	5.4	1.7	86.0	21.6	399	4.04
19.1	1.25	229	298.45	12.5	0.01365	142	0.037	0.89	15.99	0.0253	8.53	0.9281	775	1050	9.1	4.1	4.8	64.9	23.5	434	3.04
12.7	2	101.6	248	9.75	0.01258	86	0.03798	0.40	4.89	0.005661	3.44	0.683	725	1000	139	6.7	3.2	32.9	3.9	193	2.24
12.7	2	101.6	248	9.75	0.01258	86	0.03739	0.43	4.89	0.007201	3.44	0.888	725	950	112	8.7	4.5	42.8	6.4	251	2.91
12.7	2	101.6	248	9.75	0.01258	86	0.03681	0.47	4.89	0.008228	3.44	1.18	725	900	115	11.6	6.5	56.8	9.7	334	3.87
12.7	2	127	248	9.75	0.01573	86	0.03769	0.34	6.12	0.009004	3.44	1.761	725	850	148	13.9	5.6	84.8	15.9	498	5.78

Table 5.4: Final water-gas shift cases for cost estimation

Tref	Tcomb	Tube od (mm)	Matrix/ od ratio	baffle interv. (mm)	Pipe id (mm)	max tube count	Max-min flow area (sqm)	tubes in Pipe	friction factor	Delta Pout (kPa/pass)	Inner volume per length (cubm/m)	HX area per unit length (sqm/m)	Length for 350C (m)	DP down bore (kPa)	Passes	total shellside DP (kPa)	total volume (L)	catalyst volume (L)	total tube length (ft)	reactor length (ft)	nCO (gmol/sec)	ndry (gmol/sec)	%CO dry
725	850	12.7	2	127	247.65	9.8	0.01573	86	0.038	0.34	0.0090	3.44	0.224	9.117	1.8	0.4	10.8	2.0	63	0.7	0.0221	1.255	1.76%
725	900	12.7	2	101.6	247.65	9.8	0.01258	86	0.038	0.34	0.0082	3.44	0.214	10.13	2.1	0.5	10.3	1.8	60	0.7	0.0229	1.255	1.82%
725	950	12.7	2	101.6	247.65	9.8	0.01258	86	0.038	0.34	0.0072	3.44	0.217	14.182	2.1	0.5	10.5	1.6	61	0.7	0.0236	1.255	1.88%
725	1000	12.7	2	101.6	247.65	9.8	0.01258	86	0.038	0.34	0.0057	3.44	0.224	23.299	2.2	0.5	10.8	1.3	63	0.7	0.0249	1.254	1.99%
775	900	12.7	1.5	101.6	247.65	13.0	0.00839	153	0.067	0.71	0.0101	6.11	0.140	4.052	1.4	1.1	6.7	1.4	70	0.5	0.0272	1.213	2.24%
775	950	12.7	1.5	101.6	247.65	13.0	0.00839	153	0.067	0.71	0.0121	6.11	0.142	3.039	1.4	1.1	6.8	1.7	71	0.5	0.0282	1.212	2.33%
775	1000	12.7	1.5	101.6	247.65	13.0	0.00839	153	0.067	0.71	0.0093	6.11	0.146	5.065	1.4	1.0	7.0	1.4	73	0.5	0.0298	1.210	2.46%
775	1050	12.7	1.5	101.6	247.65	13.0	0.00839	153	0.067	0.71	0.0091	6.11	0.152	5.065	1.5	1.0	7.3	1.4	76	0.5	0.0297	1.210	2.45%
775	1050	12.7	1.5	101.6	298.45	15.7	0.01011	223	0.067	0.85	0.0132	8.88	0.126	2.026	1.2	0.9	8.8	1.7	92	0.4	0.0285	1.212	2.35%
775	1050	17.1	1.5	101.6	298.45	11.6	0.01011	122	0.067	0.63	0.0166	6.58	0.190	2.026	1.9	1.0	13.3	3.1	76	0.6	0.0245	1.216	2.01%
775	1050	17.1	1.5	101.6	247.65	9.6	0.00839	84	0.067	0.52	0.0114	4.53	0.228	4.052	2.2	1.1	11.0	2.6	63	0.7	0.0256	1.215	2.11%
775	1050	19.1	1.5	101.6	298.45	10.4	0.01011	98	0.067	0.57	0.0176	5.91	0.222	2.026	2.2	1.0	15.5	3.9	72	0.7	0.0233	1.217	1.91%
775	1050	19.1	1.25	101.6	298.45	12.5	0.00606	142	0.040	0.82	0.0254	8.50	0.156	-	1.5	1.6	10.9	4.0	73	0.5	0.0234	1.217	1.92%

very high flow regime of the 725C reformer cases. Even with the configurations shown, tube-side pressure drop is questionably high. This suggests that an intermediate spacing of about 1.75:1 might be best. Unfortunately, the literature correlations available to us do not provide heat transfer or pressure drop data for that case, which will have to be left to later experimentation if the low-temperature reformer seems the best way to go.

As mentioned previously, the water-gas shift model is only run for cases in which the steam-reformer section meets the performance requirements set forth above. This provides a constrained matrix of cases which is shown in Table 5.4. Several interesting points are evident from the data of Table 5.4. The first is that the water-gas shift sections are exceedingly short. This is because of the very high LMTD of the water-gas shift reactor relative to the reformer section. This is shown qualitatively in the temperature profile plot of Figure 5.5. The brevity of these stages means that a meaningful number of baffle passes is not possible, and that the desired conditions of pure counterflow are not met. Several possible solutions to this problem exist, including the redesign of the water-gas shift section as a laminar flow, pure counterflow zone. It has been the author's experience that such laminar-flow, tubular exchangers are quite large for the heat transferred, which will incur a cost penalty.

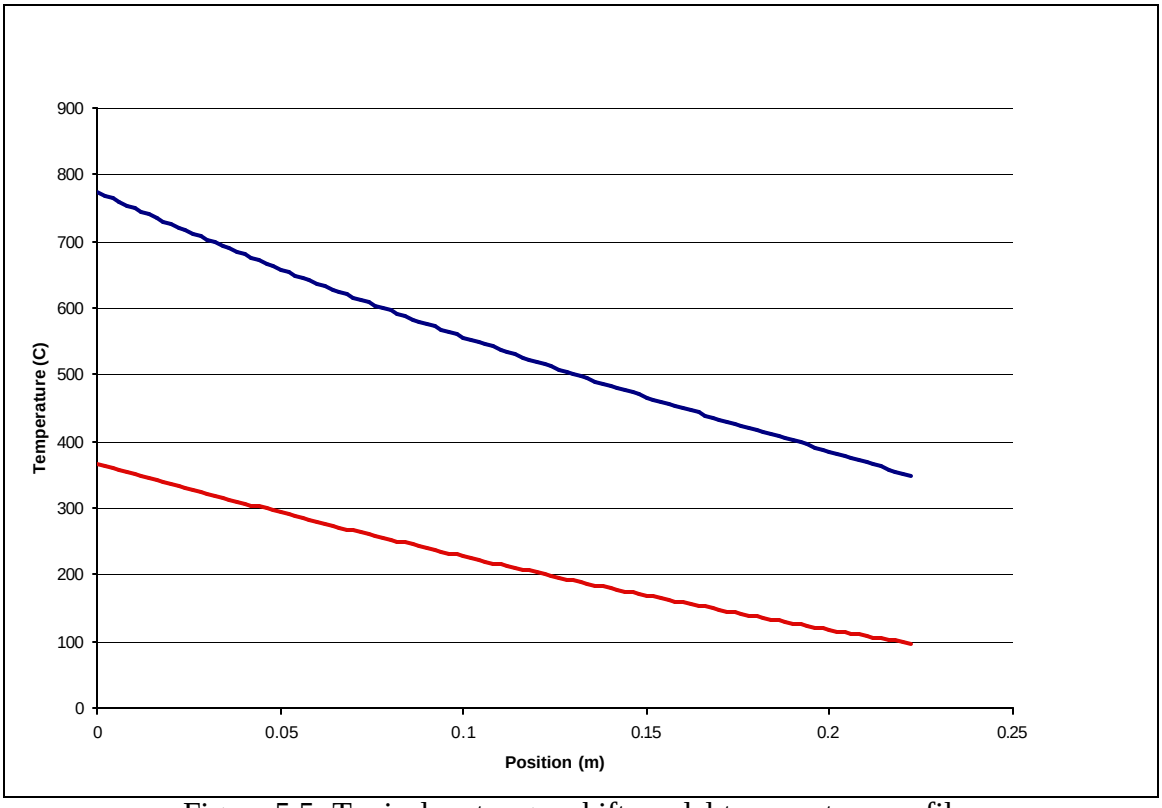

Figure 5.5: Typical water-gas shift model temperature profiles

Another possible solution, which is discussed at length in the patent application of The Appendix, is suggested by the data of Figure 5.6. These data show that the exit carbon monoxide concentration from the water-gas shift zone does not meet equilibrium at the 350 C outlet temperature identified in the thermodynamic study of Chapter 4. This situation may be

remedied at a low cost by appending a traditional, adiabatic packed bed to the exit of the water-gas shift zone. This only requires a short length of pipe and some relatively inexpensive ferrochrome catalyst. It can be seen from Table 5.4 that all of the water-gas shift reactors modeled in this study would require an appended bed to reduce their outlet CO concentration to the approximately 1% value on a dry basis which represents the thermodynamic limit.

Detailed sizing of the appended bed is not conducted for this study. Instead, a bed size consistent with about 2,000 GHSV is selected. This space velocity is widely cited as the appropriate one for ferrochrome catalysts, and yields a volume of 12.6 L for the appended bed. This corresponds to a 0.18 cm long bed in a 12" pipe shell. The use of such a large bed of ferrochrome catalyst is doubly justified to cover any losses due to deactivation of the catalyst with thermal or oxidative cycling. If a more expensive noble metal, water-gas shift catalyst is adopted in the future, the use of the appended bed may be discontinued altogether as unnecessary because of the improved activity of the noble metal water-gas shift catalysts.

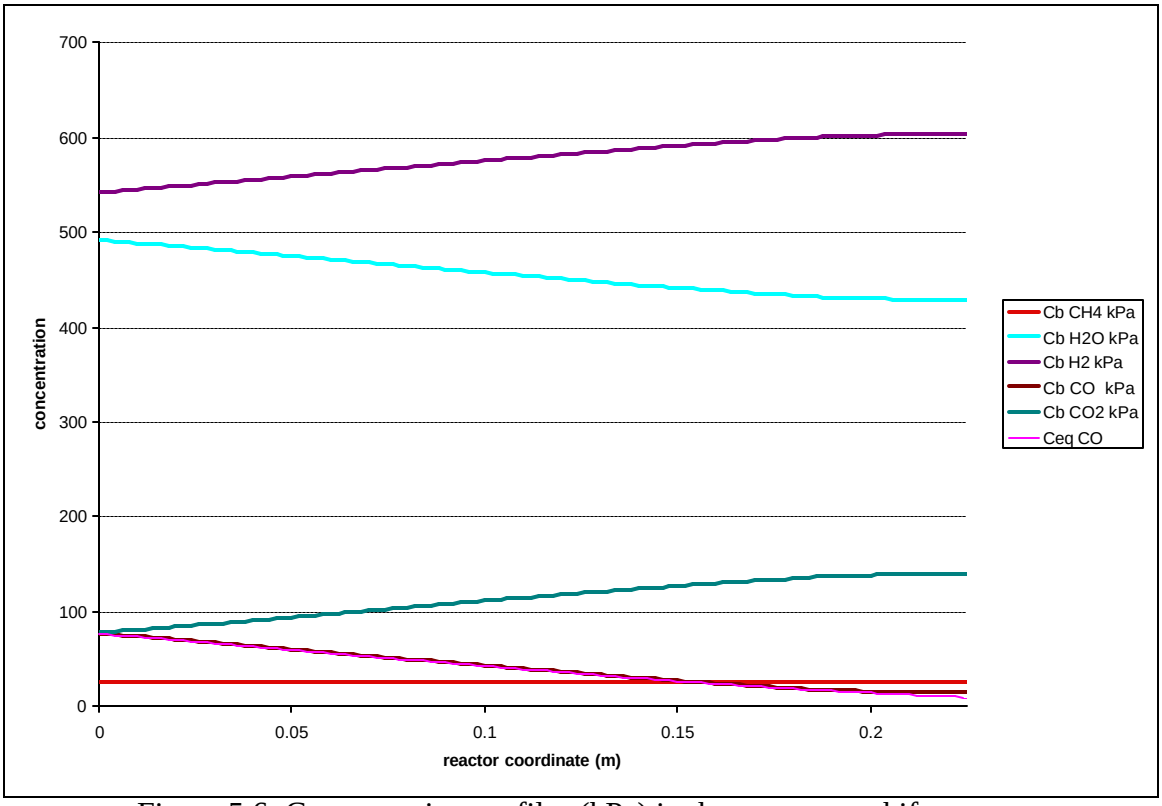

Figure 5.6: Concentration profiles (kPa) in the water-gas shift reactor

It is clear from the foregoing discussion that the results of the reactor simulations conducted to date suggest that the design conditions of the primary steam reformer exert a significant influence on the size and preferred geometry of the reactor assembly. Most importantly, the temperature of the combustor outlet and the reformer outlet strongly influence the size of the reactor. For a given set of design conditions, the reactor layout may be varied to achieve certain design goals, such as shell-side pressure drop, by altering the shell diameter or

baffle spacing. Tube spacing and tube diameter seem to serve less useful purpose in the design regime investigated in this study, though they might prove important in other regimes of catalyst activity. The net result of the modeling is a set of reactor configurations which meet the system design specifications and may be compared on a cost basis after consideration of mechanical design issues and manufacturability.

5.2 Mechanical design and manufacturing cost

The mechanical design of the reactor assembly, which is formally a pressure vessel subject to the provisions of the ASME boiler and pressure vessel code, can be separated into two major activities. The first is the selection of the alloy for the reactor tubes and the sizing of those tubes, the critical pressure-bearing members of the design which are subjected to the highest design temperatures in the unit. The second is the selection and sizing of the other components according to the provision of the ASME and TEMA[100] codes. This activity is associated with the preparation of engineering drawings, the solicitation of quotations, etc. John P. Reardon of Directed Technologies Inc. assisted in this effort, and this joint work will, thus, be discussed only briefly here. Finally, the mechanical manifestations selected for the various reactor cases can be subjected to an analysis based on the principles of Design For Manufacture and Assembly[101] (DFMA), a system of techniques for the estimation of the cost of manufactured articles which has gained wide acceptance in the design community since its inception in the 1980's. Each of these three activities will be discussed separately, with an emphasis on the first and last.

5.2.1 Selection and sizing of the reformer tubes

The reformer tubes form continuous pathways for the flow of the pressurized reformate in the integrated reactor assembly being considered in this study. The tubes are subjected to very high temperature in the first stage of the primary reformer contacted by the hot combustion product. For conventional tubes with a constant cross-section, the wall thickness is determined by the resistance of the tube alloy to the conditions in that hottest zone of the reactor. The following important considerations involved in the tube-alloy selection and the tube-wall thickness:

- Mean temperature at the hottest point in the reactor
- Internal pressure of the reactor
- Creep strength of the alloy at the design temperature
- Corrosion rate of the alloy at the design temperature

The first two elements are best addressed within the scope of the ASME boiler and pressure vessel code, which is one of the most widely accepted set of design guidelines for pressure equipment. The wall thickness required under the code is given in the following equation:

---

[100] Standards of the Tubular Exchanger Manufacturers Association: Eighth Edition, 1999.

[101] Boothroyd, *et al*, 1994.

$$t_w = \frac{PD}{2S + P} + 0.005D + e$$

In this formula, P is the maximum allowable working pressure, D is the outer diameter of the tubing, S is the allowable stress, and e is a factor associated with the means of attachment of the tube to the header, which is zero for the welded joints anticipated here[102]. The allowable stress value is generally taken from tabulated values provided by the ASME at a temperature corresponding to the mean metal temperature in the tube. It is important to note that the code is silent on the issue of corrosion, and simply specifies that the designer should specify an "adequate" corrosion allowance. It will be shown below that at elevated temperatures with small diameter tubes, the corrosion allowance may exceed the mechanical stress wall thickness for reformer tubes.

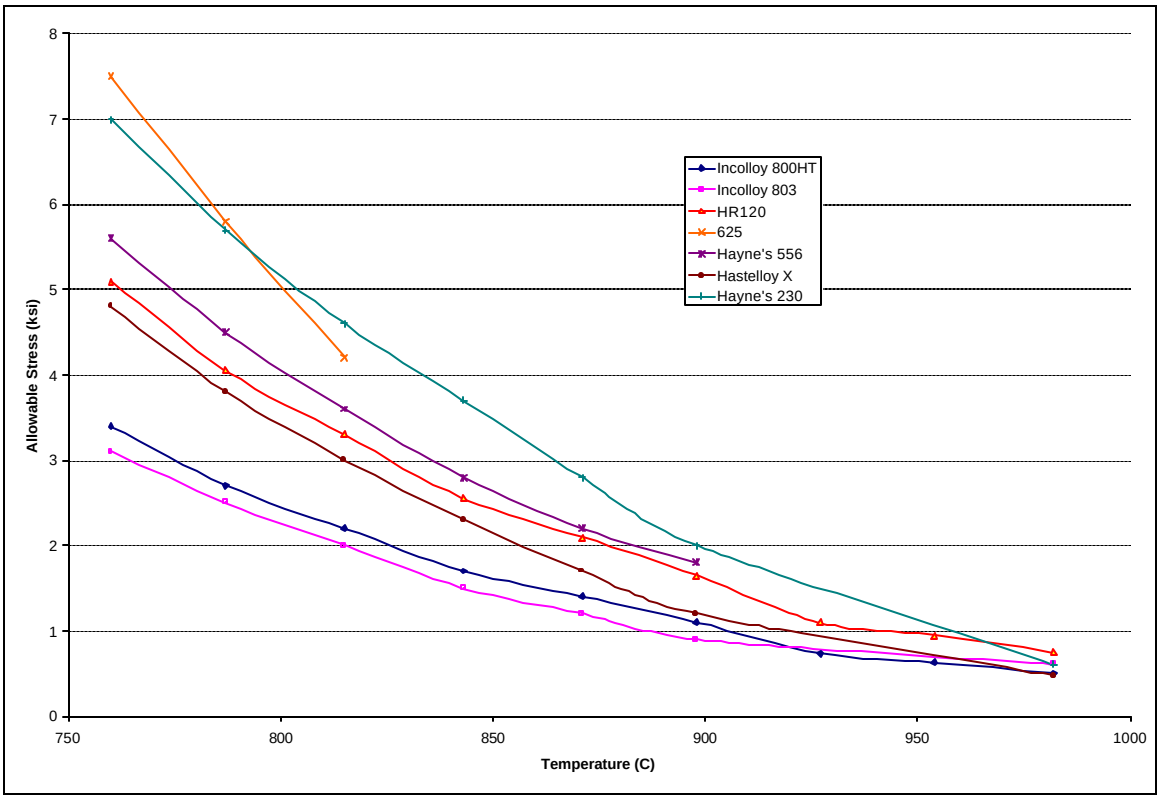

Figure 5.7: Allowable stress versus temperature for candidate alloys

The ASME allowable stresses are tabulated in section II, part D of the boiler code. The allowable stresses often do not reach the expected average temperatures of service for the tubes in the reformer. In these cases, the designer is referred to the Division I, subsection NH code for components in elevated temperature service. This code, as well as Section 2, specify that under creep loading conditions, the stress intensity must not exceed 2/3 of the 100,000 hour rupture stress at the temperature of interest. Alloy manufacturers supply these data for their high-

[102] 1998 ASME Boiler and Pressure Vessel Code: Rules For Construction of Power Boilers: Section I, American Society of Mechanical Engineers, NY, July 1, 1998, PG-27.

temperature alloys, and these values are used where actual ASME allowable stresses cease to exist. The resulting allowable stresses for a variety of candidate high-temperature alloys are shown in Figure 5.7. It is apparent from the data presented in Figure 5.7 that although there is a great diversity in allowable stress at fairly low metal temperatures, as the temperatures increase the differences in the allowable stresses become smaller.

Wall thicknesses required to meet the code requirements were calculated using the allowable stresses shown in Figure 5.7, and the wall thickness equation presented previously. The calculated values for the case of a 775 C, 13 bar reformer are shown in Figure 5.8 for tubes of 12.7 mm outer diameter. For some common superalloy materials, only low temperature operation is feasible because of poor elevated-temperature creep strength. For most of the materials investigated, standard 0.035" wall-thickness tubing would be adequate to meet the code requirements. It will be shown below that this picture changes dramatically when corrosion is considered.

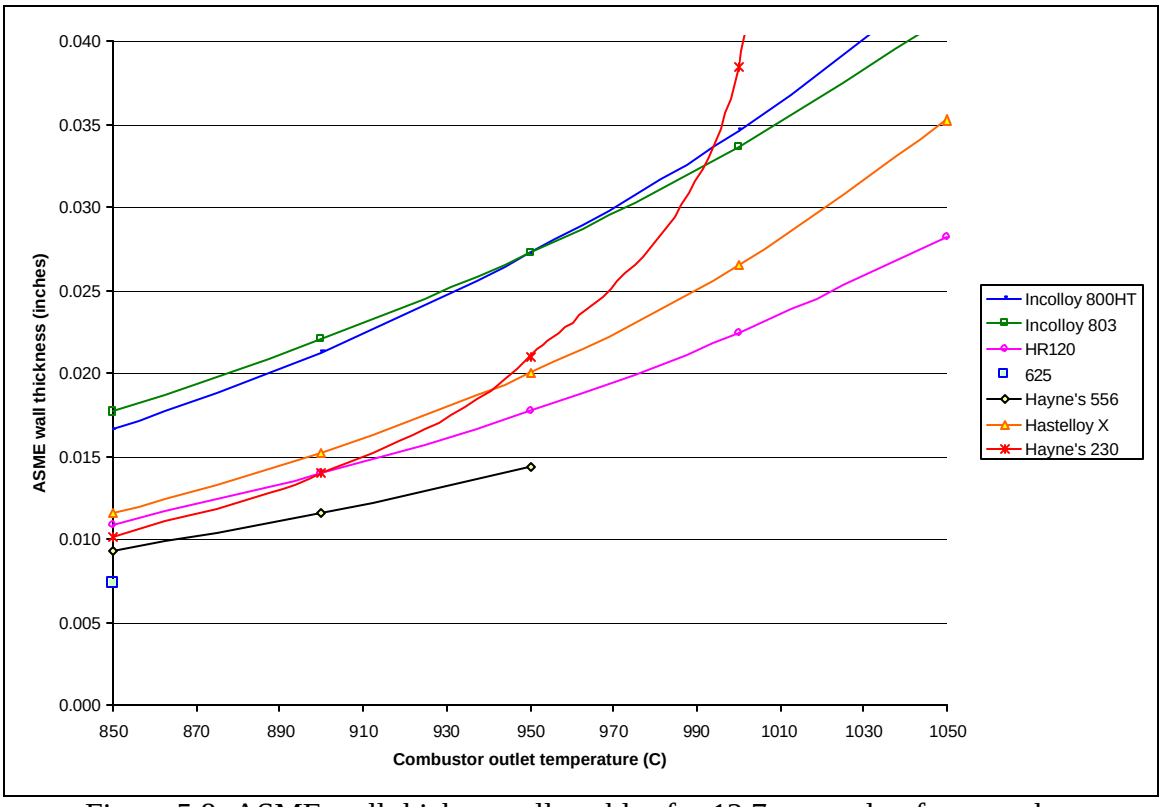

Figure 5.8: ASME wall thickness allowables for 12.7 mm o.d. reformer tubes

High-temperature corrosion can take many forms depending upon the chemical environment to which the material is exposed. Steam-reformer tubes are exposed to a hot, oxidizing gas on their outer surface, and a hot reducing gas on their inner surface. The chemical differences between these environments lead to different forms of corrosive attack. In the oxidizing environment, oxidation and metal wastage occur. Inside the tubes, carburization and metal dusting are generally observed. These latter forms are discussed first here, because their impact is less well understood, and because data on their rates are not generally available.

Carburization of high-temperature alloys can proceed through many pathways, but generally results in some combination of bulk and grain-boundary carbon absorption. The absorbed carbon forms hard carbides with several alloying elements, notably chromium. These carbides initially act to stiffen the structure of the metal, and may not lead to deleterious effects beyond some degree of embrittlement of the alloy tubes. However, an insidious element of this carbon absorption may appear depending upon the rate of uptake and the chromium concentration of the alloy. Because chromium forms a C_6Cr_{23} carbide, the chromium concentration in the bulk alloy decreases on carburization, and may drop to a value below which the protective chromia surface of the alloys is damaged. When this occurs, catastrophic carburization, or metal dusting, can occur[103].

Metal dusting is difficult to predict, although some proprietary methods are available to industrial organizations involved in high-temperature design. The problem is generally prevented in alloys which are either aluminized externally as a coating, or contain sufficient aluminum to form a coherent alumina scale. Alumina surface layers are generally perceived to be resistant to metal dusting and carburization in general, and have been shown to provide improved performance in carburizing environments[104]. What was clear from the literature is that alloy 800H is highly susceptible to metal dusting, as are typical austenitic stainless steels. Thus, the use of these materials must be approached cautiously in the high-temperature sections of the reformer. Because solid data are not available for all of the alloys considered here, and because carburization may have no deleterious effects, no direct allowance for carburization was made in this study. Review of the proposed process by Air Products and Chemicals using their proprietary software suggested that metal dusting may prove problematic, and future efforts on the design will include their input on suggested methods for avoiding carburization attack.

Oxidative attack on the candidate alloys is a better understood issue which has clear implications for component lifetime. While oxidative attack in flowing, heated air may be mild, attack in a combustion product stream is always accelerated and is made worse by temperature cycling[105]. Data are available from the alloy manufacturer's for their products and those of their competitors. These data are summarized for the alloys of interest in Figure 5.9. The data are all from tests employing direct impingement of burner gases from #2 fuel oil burners and are, thus, impacted heavily by the high fuel sulfur content, which accelerates corrosion. It is clear from the data that cyclic tests which consist of rapid cycles between contact with burner air and ambient air, show much higher corrosion rates, likely due to spalling of the protective oxide surfaces. As with carburization, corrosion resistance may be enhanced by pack aluminizing or the use of alumina-forming alloys, an avenue which will be pursued in the future.

The raw data of Figure 5.9 were fit to exponential rate equations and used to predict corrosion wall-thickness allowances for the reformer tubes, assuming essentially steady exposure conditions rather than the accelerated cyclic conditions. The assumption of steady conditions, though less conservative, seems reasonable because the rapid thermal cycling conditions of the cyclic tests are not realized in the proposed hydrogen generation system. These corrosion

---

[103] Davis, J.R., Heat resistant materials, 1997, pp. 315-316.

[104] Agarwal, D.C., Brill, U., "High-temperature-strength Nickel Alloy," Advanced Materials and Processes, October 2000, pp. 32-34.

[105] Davis, J.R., 1997, pp. 313-314.

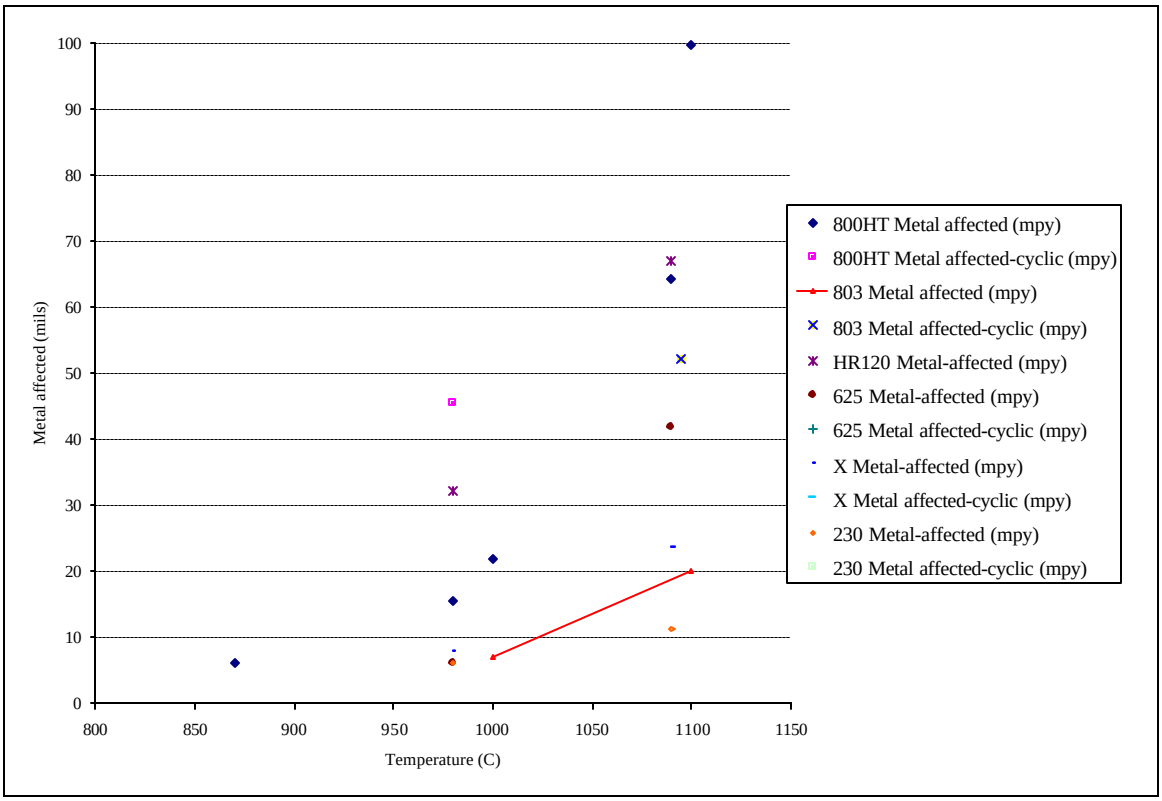

Figure 5.9: Raw oxidation data for candidate superalloys

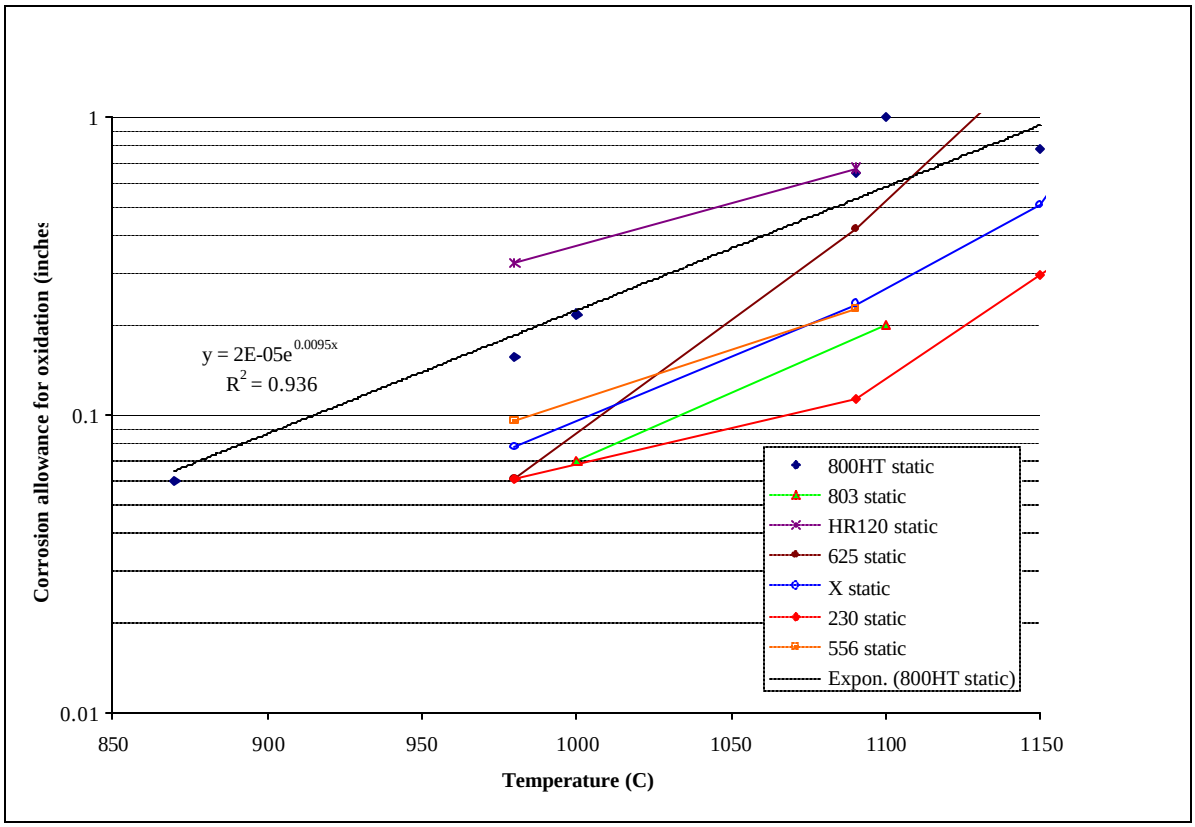

Figure 5.10: Estimated corrosion allowances for 10-year continuous operation

allowances are shown in Figure 5.10. It is important to note that as burner temperature increases, the corrosion allowances begin to show important variations between the different alloys, and the required thicknesses generally exceed the code-required wall thickness. This means that for high temperature operation, corrosion resistance plays a deciding role in the tube wall thickness requirement and cost.

The total estimated wall thicknesses for the case of 12.7 mm outer diameter tubing versus combustor temperature are shown in Figure 5.11. Were the alloys ranked solely on wall thickness, Hayne's alloy 230 and Hastelloy X would be the preferred materials below 1000 C, whereas Incolloy 803 is to be preferred at 1050 C. However, there are significant differences in material cost between the alloys which must be considered. Alloy billet cost for alloys 625, 800H and 803 were obtained from Special Metals, the manufacturer of these alloys. Cost ratios published by Hayne's[106] were then used to estimate the billet cost of the other alloys. When these costs are combined with the wall thicknesses for the candidate alloys, tube cost can be directly estimated per unit length. This has been done, and the resulting material cost estimates are shown in Figure 5.12. It should be noted that the tube-fabrication cost is not estimated here, and will be discussed in some detail later in this chapter.

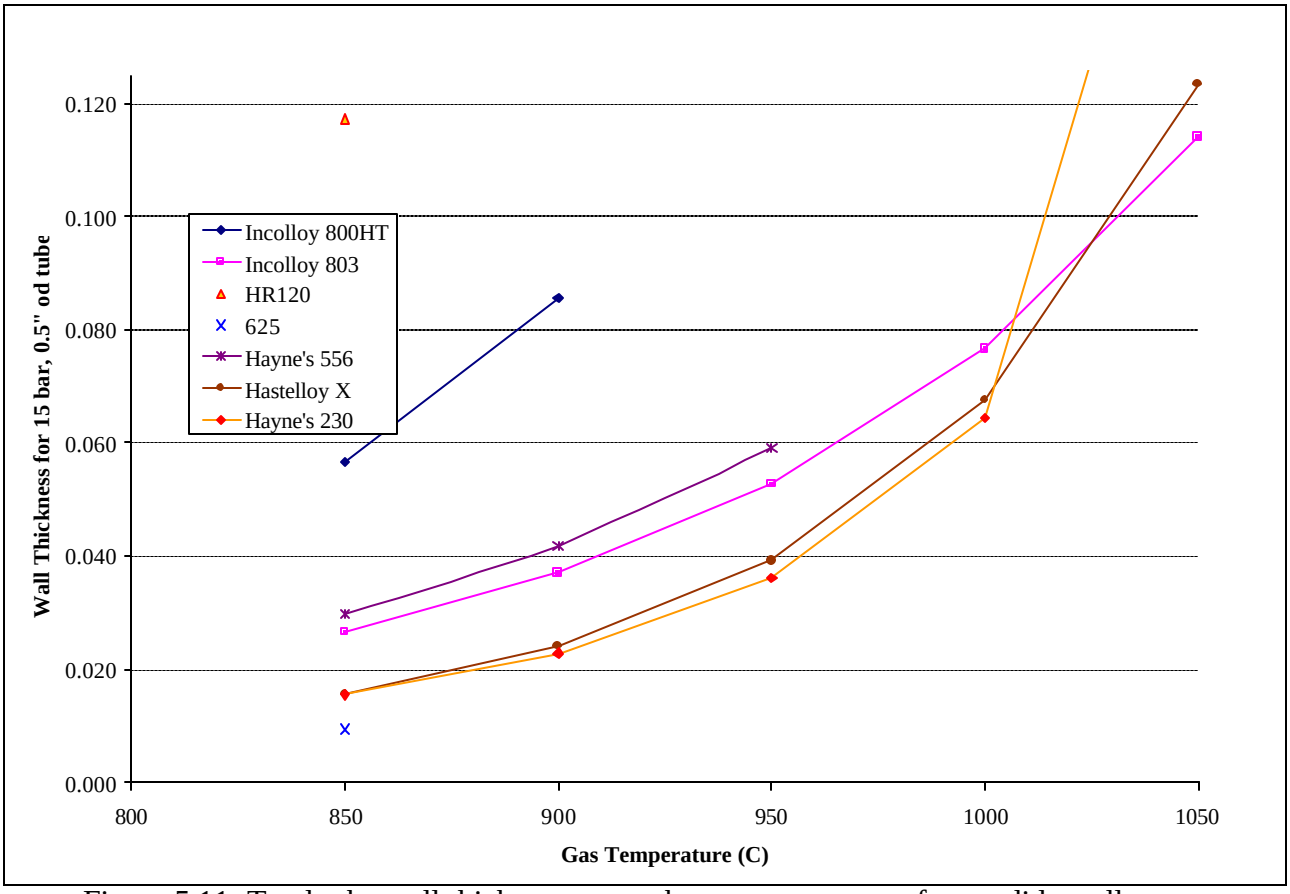

Figure 5.11: Total tube wall thickness versus burner temperature for candidate alloys

106 Haynes HR-120 alloy, Haynes International, Inc., USA, p. 26.

Once material cost is considered, the expensive quaternary alloy, Haynes 230, becomes uncompetitive. Only alloy X, a nickel-based alloy, and Incolloy 803, an iron-based alloy are competitive. Incolloy 803 in particular offers particular materials cost advantages in high temperature applications. It can be seen from the data of Figures 5.11 and 5.12 that there are severe cost penalties for increasing burner temperature when only the direct tube cost per unit length is considered. This factor must be weighed against the reduced reactor volume and total tube length afforded by higher firing temperatures to determine the economically-best operating point. This exercise will be conducted later in this chapter. Another conclusion which may be drawn from this analysis is that closer scrutiny of aluminizing coatings and their impact on cost and corrosion performance is warranted. In the future, collaboration with the alloy suppliers and with Air Products should allow a firmer set of conclusions to be reached. Specifically promising are new low-cost alloys with very high carburization and oxidation resistance which have been developed by Special Metals and Krupp. These materials may offer dramatic improvements in cost performance over Incolloy 803.

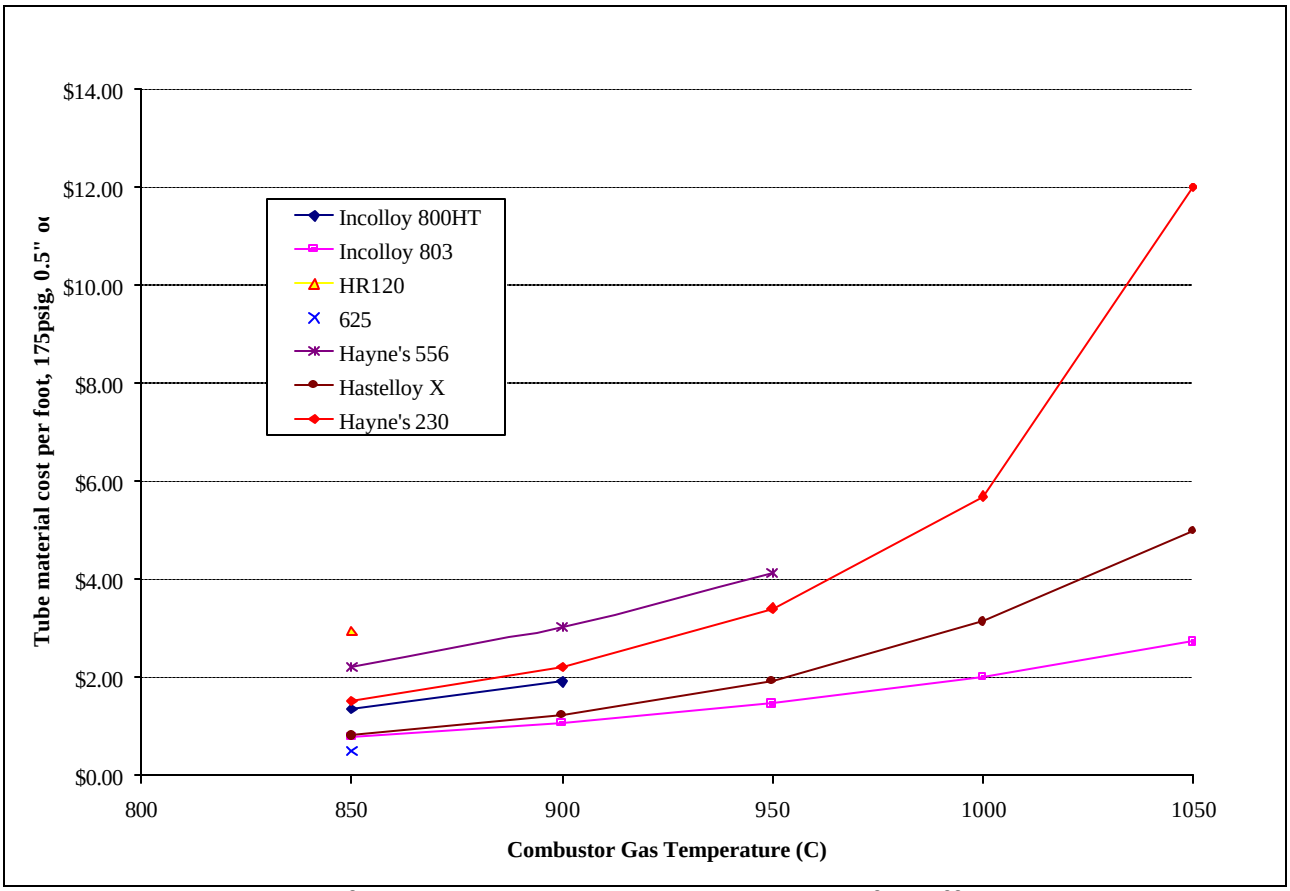

Figure 5.12: Reformer tube material cost per unit length for different alloys

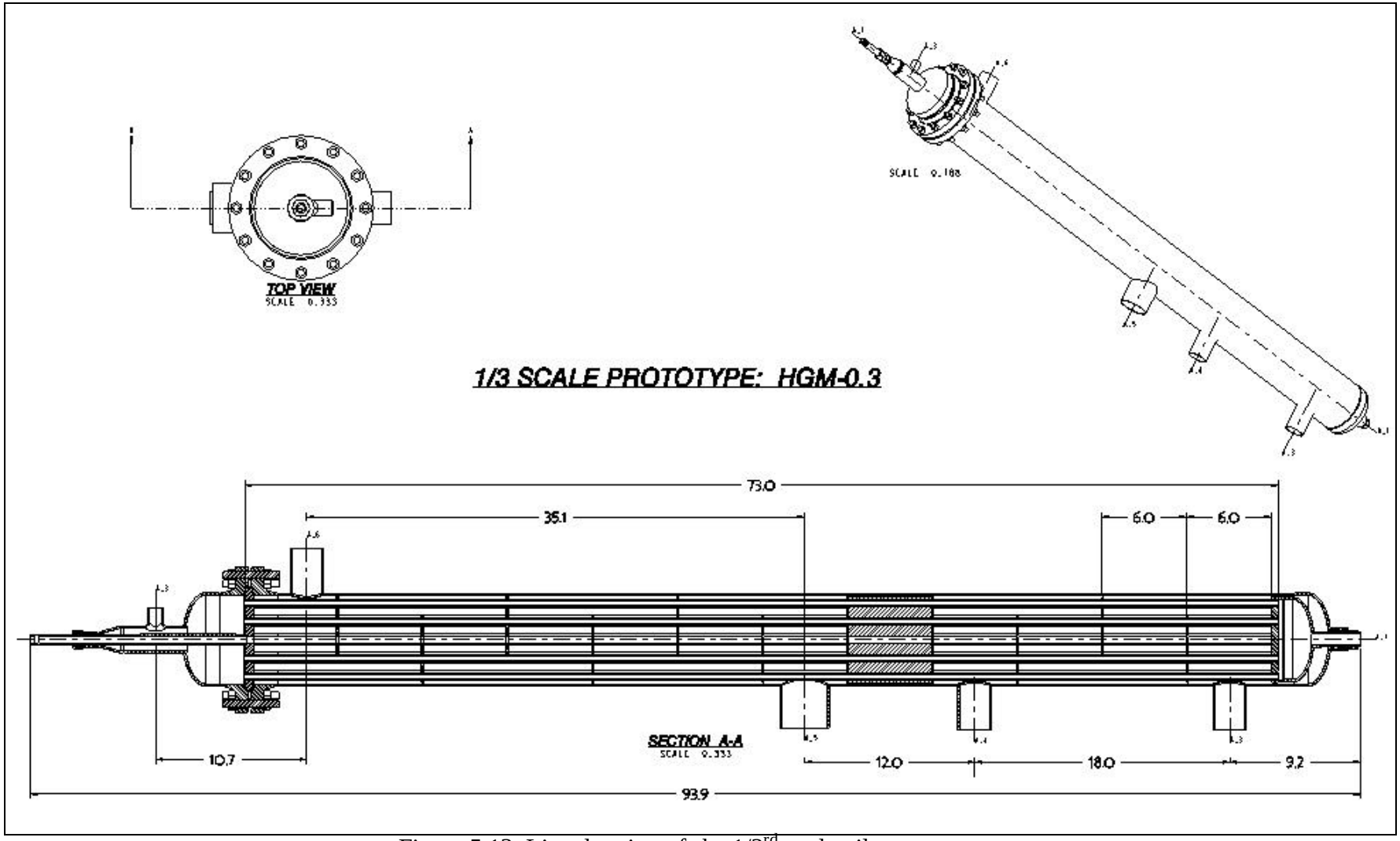

Figure 5.13: Line drawing of the 1/3rd-scale pilot reactor

5.2.2 1/3rd-scale pilot reactor design and fabrication

For proof of concept of the proposed integrated reformer design, Directed Technologies Inc. funded the design and construction of a 1/3rd-scale pilot-plant reactor. The flow layout of the reactor was chosen using the same design models described previously, and the mechanical design was conducted in accordance with the provisions of the ASME and TEMA codes. These codes specifically address the design of the tube headers, baffle, shell, and flanges and sealing surfaces. The TEMA code in particular is structured to provide proper corrosion allowances and manufacturing tolerances for the finished article. The design was conducted to the TEMA R standard for petrochemical applications, and was largely constructed from alloy 800H and 310 stainless steel to minimize component cost and leadtime. In particular, alloy 800H tubing was used as Incoloy 803 tubing would have required a minimum billet order of one ton, which was inconsistent with the state of our selection of the final product tube alloy. Thus, corrosion concerns will likely limit the useful life of the pilot reactor to 10,000 hours or less, which was deemed sufficient for the purpose of demonstrating the technology.

The detailed design and layout of the pilot reactor was largely conducted by John Reardon of Directed Technologies Inc. The resulting layout is shown in Figure 5.13. Several unique facets of the pilot reactor were included specifically to facilitate experimental testing and are not anticipated to be desirable in the final product.

- Removable top head to facilitate replacement of catalyst
- Provision of a central thermowell assembly to measure axial temperature profile
- Use of small diameter (2" pipe) air inlets and outlets

In the final product, it is projected that an all welded construction devoid of flanges and bolts may be employed, thus significantly reducing the thermal mass and cost of the unit, while guaranteeing a leak-tight final assembly. The thermowell was eventually discarded in favor of distributed thermocouples in the pilot reactor, but it is anticipated that temperature profiles will not be needed in the final product. This change will also eliminate leak paths and reduce parts count and complexity. Finally, it is anticipated that full-shell-diameter combustor outlet and cooled combustor gas exhausts will be provided in the final product. The former to provide a better radiant view factor between the combustor monolith and the inlet tubes, and the latter to allow the low pressure drop fairing in of the superheater core.

Several notable features of the pilot reactor will be carried into the final design. The first of these is the provision of a "dead" stage to reduce thermal gradients between the water-gas shift zone and the reforming zone. This zone is packed with granulated refractory in the pilot reactor, but may be filled with die-cut refractory felt in the product units, as some leakage of granulated refractory has been noted in testing. This dead zone also seals the shell-side to prevent air leakage which would effectively short-circuit the combustor. This allows more precise control of the reactor firing temperature. Finally, a small but novel feature is the provision of thermal expansion capability between the shell and tube bundle through the use of a small-diameter packed fitting at the reactor base. This feature, which is hard to discern in Figure

5.13, reduces the cost of thermal expansion relief relative to a full-diameter seal or a bellows-type expansion joint.

Much of the fabrication work was subcontracted to outside vendors, including the tube drawing, machining of the tube headers, forging the flanges, and spinning of the pipe caps. The final assembly and weld fabrication of the unit was completed at Directed Technologies Inc. by Stephen Waide. The fabrication process pointed out several interesting potential design changes which may be incorporated into the product design, and substantiated many of the fabrication cost estimates included in Section 5.2.3.

5.2.3 Manufacturing cost estimates for the integrated reformer

The groundwork for the estimation of the manufacturing cost of the integrated reformer was laid in the previous sections, which detailed the estimation of the amount of material required to construct the various design manifestations. However, total cost of a manufactured product does not always depend only on material cost, and issues of costs due to manufacturing the component parts must be addressed. Further, appropriate markups must be applied to reflect the costs of scrap, profit, general and administrative costs and research costs. The decision to purchase component parts or build them in house must also be resolved. Luckily, formal methods exist to aid the process of estimating these costs. These methods have become broadly known as Design For Manufacture and Assembly (DFMA), and have evolved from the drive to improve the cost-competitiveness of domestic manufactured goods in the 1980's in the face of intensifying competition from abroad. The leaders in this field, Boothroyd, Dewhurst, and Knight, of the University of Rhode Island, have published texts and produce software to aid in the DFMA process. The author has previously written DFMA studies based on a "naïve" fuel reformer architecture of the conventional style[107] and of gasoline fuel reformers of the type developed by Arthur D. Little[108]. These studies may be the first applications of DFMA techniques to chemical process apparatus.

Several steps are involved in the estimation of the manufactured cost of the integrated reformer. The first is the promulgation of a detailed design which allows formulation of a bill of materials. This process has been conducted and was described earlier in this chapter. The second step is the estimation of the total cost of purchased materials and components based either on fundamental DFMA analyses or upon quotations from suppliers. Finally, the cost of manufactured parts and the cost of final assembly must be estimated. These costs must then be combined and a mark-up applied to reflect the recovery of costs associated with the manufacturing process. The final figure obtained is then the variable cost to manufacture each reformer assembly. Each of these steps will be covered separately below, beginning with the formulation of an example bill of materials.

The bill of materials for a reactor with a 10" shell, using a 775C reformer outlet and 1050C combustor outlet is shown in Table 5.5. This bill of materials includes the specific

---

[107] Thomas, C.E., James, B.D., Lomax, F.D., Kuhn, I.F., "Integrated Analysis of Hydrogen Vehicle Transportation Pathways," prepared for the National Renewable Energy Laboratory, March 1998.

[108] James, B.D, *et al*, 1997.

components of the reactor, the number of each component required, whether the component is manufactured by an outside vendor or processed in house from raw material, and the material of construction. These data will be combined with the materials costs per unit to yield total material costs for the reactor assembly.

Table 5.5: Example bill of materials for the reactor assembly

Subassembly	Component	Usage	Make/Buy	Material
Tube bundle				
	tubes - 4'	153	Buy	803
	Baffles-chorded	5	Make	800H
	Baffles-full	2	Make	800H
	tube header	2	Make	310
	tie rods	4	Make	310
	end domes	2	Buy	310
	inlet fitting	1	Make	310
	Outlet fitting	1	Make	310
	Outlet bed pipe	1	Buy	310
	Reforming catalyst	8.9L	Buy	
	WGS catalyst - sized	2.6L	Buy	
	WGS catalyst -pelleted	12.6L	Buy	
	sealing gasket	6	buy	refractory
Shell				
	Top pipe	1	Buy	800H
	Middle Tee	1	Buy	800H
	Bottom Pipe	1	Buy	310
	Inlet pipe	1	Buy	310
	bottom outlet pipe	1	Buy	310
	Top outlet fairing	1	Buy	800H
	shell cap	1	Buy	310

The cost of 310 stainless steel as processed billet is approximately the same as 316L, at $2.40 per kg in late 1998[109]. The price for billet 800H purchased for the pilot reactor in 2000 was as low as $16.90 per kg[110]. If materials are sourced through a single supplier and bought in substantial lots, their cost can be reduced to approximately the billet price for the raw starting material. The subsequent processing cost to form finished pieces must be added to the billet prices. For small lots of specialty components such as pipe caps, which are generally required to be ASME code stamped and certified, the final price may bear little semblance to the initial billet price. For non pressure-bearing parts, the exorbitant markups are not needed and direct cost estimation is possible. For the pipe caps required to complete the tube bundle, the markup for manufacture is high, reaching about $150 in 2000 for the custom caps employed in the pilot

[109] Personal communication with Michael Frankland, marketing manager, Armco specialty flat rolled steels, September 29, 1998.

[110] Cost of 1/8th inch plate, Mach II metals, 10/27/2000.

reactor, this cost can likely be reduced to $50 apiece if standard caps are employed. This value is added to the billet mass in the cost estimates here. Because the hydraulic forming of the shell tee is not easily modeled, its fabrication cost is conservatively estimated at $150, as the component would almost certainly be custom fabricated.

The reformer tubes themselves are also custom drawn for this application, but in their case a fairly good volume is required, and cost quotes are available for the estimation of the fabrication costs. Table 5.6 shows the estimated costs for lots of custom-drawn tubing from several suppliers, and imputes an overall manufacturing markup based upon subtraction of the market price of the billet material from the price quotes. All of the quotations secured were for seamless, drawn over mandrel tubing. What is readily apparent from the data is that the drawing cost for iron-based superalloy tubing is about $1/4^{th}$ of that for nickel-based superalloy tubing. Thus, iron-based superalloys such as Incolloy 800, 800H, 803, and 890 and Haynes HR-120 should have a drawing cost of about $1 per foot while nickel-based alloys such as alloy 625, alloy X, Haynes 230, and 602CA should be closer to $4 per foot. This drastically swings the cost analysis for the tubing in favor of high performance, iron-base superalloys such as Incolloy 803 which is considered here. It is interesting to note that the existing data show no strong dependence of drawing cost on tube diameter or wall thickness, although the scope of wall thickness data is limited, so no strong conclusions may be drawn.

Table 5.6: Calculation of tube manufacturing costs from supplier quotations

Supplier	volume quoted	material	billet price ($/kg)	outer diameter (inches)	wall thickness (inches)	cost per foot	weight per foot (kg)	Manufacturing cost ($/foot)
Salem Tube	1,000'	800H	$ 16.87	0.500	0.080	$ 4.61	0.196	$ 1.30
Greenville Tube Corporation	55,000'	800	$ 15.18	0.375	0.035	$ 1.96	0.064	$ 0.98
Greenville Tube Corporation	55,000'	800	$ 13.66	0.3125	0.035	$ 1.77	0.054	$ 1.04
Superior Tube Company	1,500'	625	$ 27.94	0.375	0.035	$ 8.18	0.068	$ 6.27
Superior Tube Company	50,000'	625	$ 27.94	0.375	0.035	$ 6.40	0.068	$ 4.49
Handy & Harman Tube Co.	5,000'	625	$ 27.94	0.375	0.035	$ 5.98	0.068	$ 4.07
Handy & Harman Tube Co.	5,000'	625	$ 27.94	0.3125	0.035	$ 6.40	0.057	$ 4.81

Note: Customary units in the tubing industry are imperial, (2000US$).

The cost of Incolloy 803 tubing versus combustor and reformer temperature may be estimated using the calculated manufacturing cost for iron-based superalloy tubing derived from Table 5.6. The results of this process are shown in Figure 5.14. It is apparent from the data that increasing combustor temperature from 850C to 1050C increases the tube cost per linear foot by a factor of about 2:1.

The manufactured cost of tubing, endcaps and the tee-shaped pipe section of the shell have all been estimated. The only other components with significant manufacturing cost inputs are the tube headers and baffles, both of which require an array of precision holes to be created in planar superalloy parts. Because the number of holes is so large, and the precision in locating the holes is high (x-y tolerances on placement of about 25μm), numerically-controlled processes are to be preferred for finish machining of the holes. For the baffles, which are 3.18 mm in thickness as specified by the TEMA code, two options exist, the first is simple CNC machining of the baffles as was done in the pilot reactor. The second involves CNC laser cutting of the baffles. For the headers, which must be about 12.7 mm thick, the holes may be machined from a billet, or rough castings or forgings may be prepared which may then be finish-machined to impart appropriate conformance to the tolerances specified.

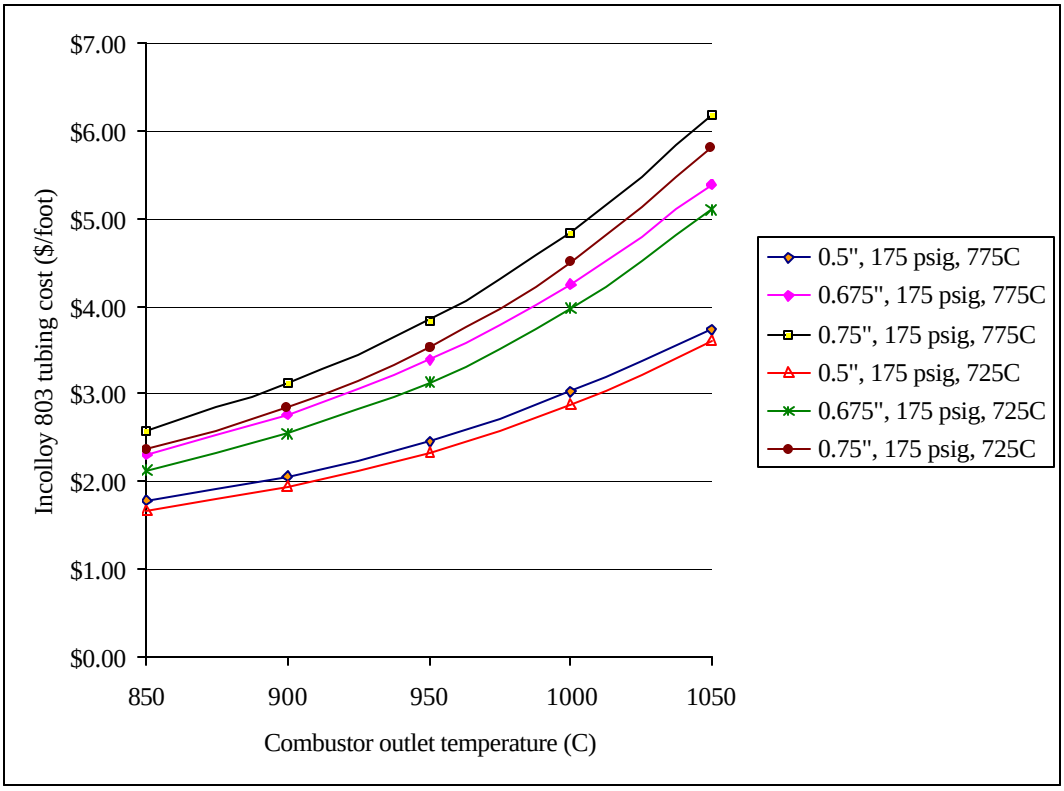

Figure 5.14: Estimated reformer tube cost per linear foot vs. reformer and combustor peak temperatures (2000US$)

Design For Manufacture (DFM) software[111] was employed to analyze production of 500 203 mm header assemblies over a four year period, with monthly batches of 10 assemblies being machined from yearly batches of 125 castings. This was projected as an appropriate baseline volume over which to amortize the tooling costs, etc. The processes analyzed were machining from wrought plate, sand casting, semi-automatic sand casting, and investment casting. It is comforting to note that the expert-system features in the software agreed with the previous analysis that suggested these processes as the most feasible.

[111] Concurrent Costing, v1, Boothroyd Dewhurst Inc., released May, 1999.

A summary of the results for the production of 500 parts is shown in Table 5.7. The data suggest several points. The first is that machining from plate may be the most economical approach for low volume production. However, this assumes that plate is available at fairly low costs typical of high-volume production, which may be a poor assumption at low volumes. Additionally, the setup costs obtained in the machining-only case are strangely low, suggesting that the machining-only software, which is about three years old, may have slightly lower setup rates than the machining module of the more recent concurrent costing package. Simple sand casting also appears cost competitive at low volumes, with the lowest projected cost. Because casting houses typically buy alloy in large quantities, it is perhaps more realistic to expect that the sand-casting cost is representative. Both semi-automatic sand casting and investment casting suffer from high tooling cost. However, it is apparent that the investment casting approach offers much lower machining and casting costs per part than the other processes. This result begs an inquiry into the effect of life volume on the best choice of process.

This analysis assumed austenitic stainless steel as the material of construction, and a total of 95 tubes and tie-rods in the tube bundle. For the purposes of a top-level estimate of processing costs for the headers, it could be assumed that the machining costs are apportioned evenly between each header perforation. This would result in a machining cost of $0.70 for each hole plus a setup charge of about $5 per header. In the analysis in this study, it will be assumed that the headers are machined from plate using the assumptions above. These assumptions are the most conservative, and do not take advantage of the process economies and low scrap rates of casting processes. This is largely because complicated inspection procedures are required for cast pressure-vessel components, while wrought ones (i.e. wrought plate) can be used with minimal inspection and post-processing.

Table 5.7: Estimated manufacturing cost at a life volume of 500 units (2000US$)

Process	Material Cost ($/part)	Casting cost ($/part)	Machining Costs ($/part)	Set-up costs ($/part)	Tooling Cost ($/part)	Total part cost ($/part)
Machining from plate	45.15		66.28	4.83		116.26
Sand casting	15.05	16.58	65.56	10.82	5.16	113.17
Semi-automatic sand casting	14.6	7.12	65.56	15.1	29.29	131.67
Investment casting	28.11	7.3	40.72	10.26	45.06	131.45

If the baffles are machined from plate, their processing costs will be similar to those for the headers, because much of the machining time is consumed indexing the machining head and changing cutting tools. However, economies may be achieved by CNC laser cutting. For the case of a 95-perforation baffle with 12.7mm outer diameter tubes, the total perimeter cut is about 4.4m. The cutting head must also index at least 96 times, at a time per index of about one second. If a conservative cutting rate of 0.5m/minute is assumed, and a machine cost of $1/minute is likewise assumed for a CNC laser cutting machine, then a representative total cutting cost would be $10.30. If a similar $5 setup fee is charged, then the laser cutting could be about $15 per baffle versus about $70 for a machined baffle. Even if a conservative $5 per baffle is added for post-cutting bright annealing for stress relief, the total cost is still modest. Thus,

CNC laser cutting is assumed for the baffle fabrication, with costs estimated according to the method outlined here.

The cost of the FCR-10 catalyst has been derived based upon discussions between Directed Technologies Inc. and Sud-Chemie, Inc. The cost in batches larger than 100kg was projected to be $289/L. This cost is comprised of 52% for the noble metal, 15% for the ceramic substrate, 11% for the catalyst application, and 21% for markups. These costs are based on quotations for the cost of the metal salts used in the catalyst synthesis, which significantly exceed the cost of metal at these small quantities. For reference, the cost of the ferrochrome catalyst is $9.88/L in the industrial tabletted form, and about $50/L for the crushed and sieved form for use in the reformer tubes. In general, the catalyst cost could be dramatically reduced if the noble concentration was reduced, as in the FCR-9a catalyst, or if the cost of noble metals drop to their historic values. Current costs are very high due to supply control being exercised by Russian noble metal producers.

When these costs are applied to the bill of materials shown in Table 5.5, and appropriate markup factors are applied, the total cost summary of Table 5.8 results. These figures include markups derived by Directed Technologies Inc. in our commercial and government work in estimating low-production-volume manufacturing costs[112] and have been vetted by comparison with quotations from numerous vendors over the years. These markup factors assume that our production occupies less than 30% of the capacity of the machinery that is required to conduct the operations. This is caused by the low rate of production which we are projecting for the reactor assembly. Components manufactured in house are marked up 50% to account for operating expenses and profit. Those components simply purchased and assembled are marked up only 21%, as G&A costs are much lower. Components for which we have estimated the costs from scratch, like the baffles, and which are bought from a specialty supplier, are subject to the suppliers 50% markup and our 21% markup, for a total of 81%. It can be seen from Table 5.8 that markups can significantly increase the estimated manufacturing cost but are crucial to accurately reflect the cost of doing business in a manufacturing environment.

The costs shown in Table 5.8 do not include the in-house assembly of the components into a complete reactor assembly. Due to the experience of constructing the pilot-scale reactor, we have a fairly accurate idea of the time required to assemble the components into the subassemblies in a low-rate production environment. We also have ideas as to the order of operations in the assembly process. Generally, the assembly process cost would be estimated based upon formalized Design For Assembly techniques. Because of the very low production rate being studied, it is likely more accurate to estimate the time for each process based upon the pilot-scale fabrication process. Where possible, that is done here, and the resulting assembly cost is, thus, conservative when compared to the economies which might be achieved in a more automated assembly scheme. The proposed assembly process is diagrammed in Figure 5.15. This somewhat simplified process has 25 independent operations, many of which require repetitive tasks, such as obtaining and placing parts and welding individual welds. Some salient

[112] James, B.D., Lomax, F.D., Thomas, C.E., "Manufacturing Cost of Stationary Polymer Electrolyte Membrane (PEM) Fuel Cells," prepared for the National Renewable Energy Laboratory, November, 1999, pp. 13-15.

Table 5.8: Representative reactor bill of materials (of Table 5.5) with materials and manufacturing costs and markup (2000US$)

Subassembly	Component	Usage	Make/Buy	Material	Material mass per part (kg)	Billet cost ($/kg)	Finished material cost/part	Manufacturing cost	Finished part cost w/o markup	Markup	Total cost per part	Total cost
Tube bundle												
	tubes - 4'	153	Buy	803			$ 15		$ 15	1.21	$ 18	$ 2,770
	Baffles-chorded	5	Buy	800H	0.13	$ 16.90	$ 2.23	$ 23	$ 25	1.81	$ 45	$ 224
	Baffles-full	2	Buy	800H	0.20	$ 16.90	$ 3.38	$ 27	$ 30	1.81	$ 55	$ 109
	tube header	2	Make	310	8.01	$ 2.40	$ 19.21	$ 115	$ 134	1.5	$ 201	$ 402
	tie rods	4	Make	800H	0.11	$ 16.90	$ 1.80	$ 0	$ 2	1.5	$ 3	$ 11
	end domes	2	Buy	310	0.40	$ 2.40	$ 0.96	$ 50	$ 51	1.21	$ 62	$ 123
	inlet fitting	1	Buy	310					$ 20	1.21	$ 24	$ 24
	Outlet fitting	1	Buy	310					$ 20	1.21	$ 24	$ 24
	Outlet bed pipe	1	Buy	310	5.02	$ 2.40	$ 12.04	$ 1	$ 13	1.21	$ 16	$ 16
	Reforming catalyst	8.9L	Buy			$289/L			$ 2,572	1.21	$ 3,112	$ 3,112
	WGS catalyst - sized	2.6L	Buy			$50/L			$ 130	1.21	$ 157	$ 157
	WGS catalyst -pelleted	12.6L	Buy			$9.88/L			$ 124	1.21	$ 151	$ 151
	sealing gasket	6	buy	refractory					$ 10	1.21	$ 12	$ 73
Shell												$ -
	Top pipe	1	Buy	800H	9.15	$ 16.90	$ 154.64	$ 1	$ 155	1.21	$ 188	$ 188
	Middle Tee	1	Buy	800H	12.20	$ 16.90	$ 206.19	$ 150	$ 356	1.21	$ 431	$ 431
	Bottom Pipe	1	Buy	310	3.05	$ 2.40	$ 7.32	$ 1	$ 8	1.21	$ 9	$ 9
	Inlet pipe	1	Buy	310					$ 20	1.21	$ 24	$ 24
	bottom outlet pipe	1	Buy	310					$ 20	1.21	$ 24	$ 24
	Top outlet fairing	1	Buy	800H					$ 20	1.21	$ 24	$ 24
	shell cap	1	Buy	310	0.40	$ 2.40	$ 0.96	$ 50	$ 51	1.21	$ 62	$ 62
											Total cost =	$ 7,959

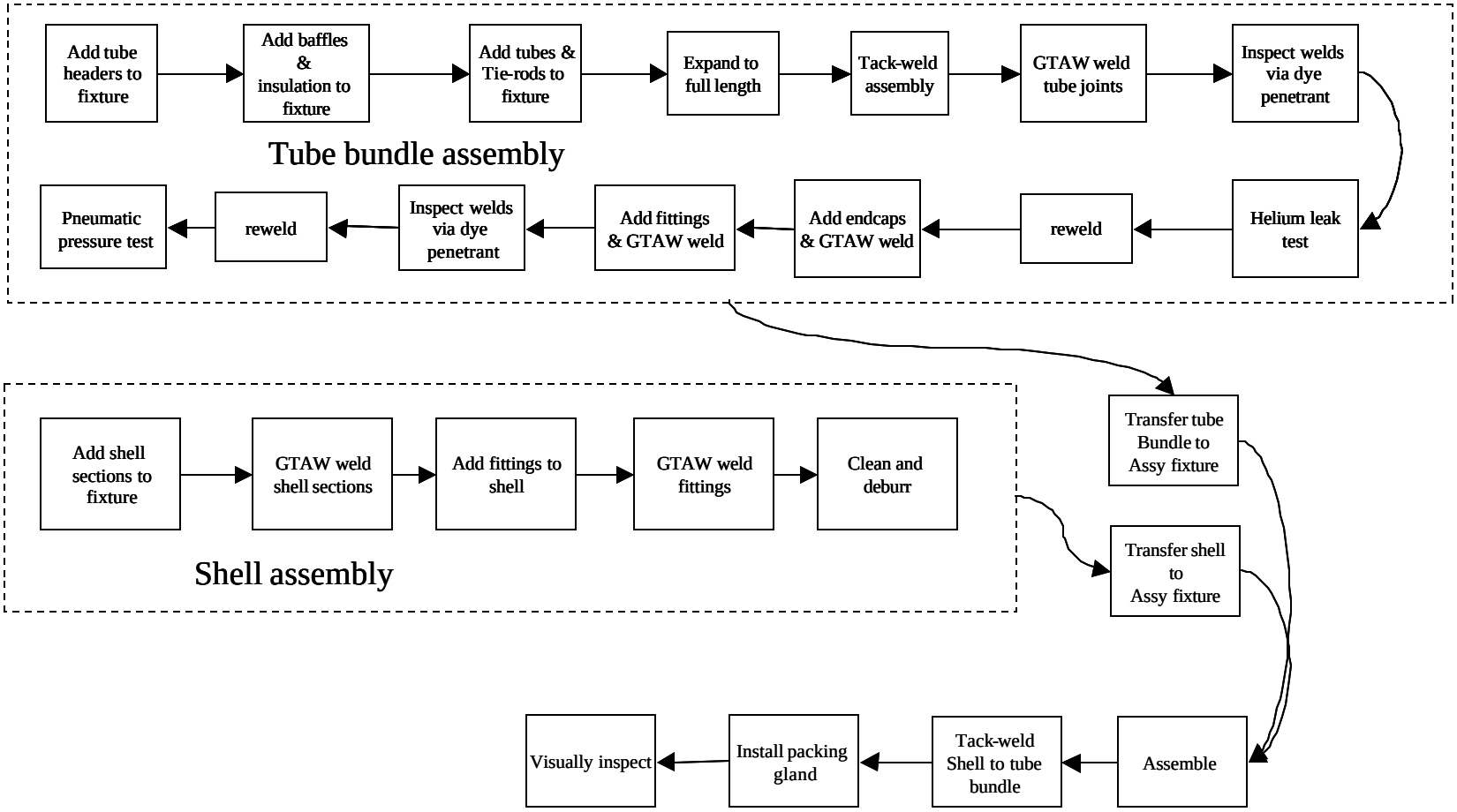

Figure 5.15: Reactor assembly process flow diagram

features of the proposed process are described below, including the provision of appropriate special fixtures to aid assembly of the device.

Because of the multitude of parts, the tight tolerances, and the need for multiple welding operations, the tube bundle assembly presents the biggest challenge for reducing assembly costs. In a very-high-production-volume environment, a complete assembly line approach might be taken to separate the assembly operations and facilitate rapid and inexpensive construction. In a low-volume environment such as that described here, a single tube-bundle assembly is fabricated every other working day. In this environment, it is likely that a single welder might be responsible for fabricating the entire tube assembly from start to finish. This approach can be slow and labor-intensive, as repetitive operations are not "learned" to allow very rapid assembly as described in Boothroyd, *et al*[113]. Further, the assembly is extremely heavy and unwieldy once all the components are in place and presents extreme handling difficulties. For these reasons, it is desirable to provide a fixture which would allow assembly of several tube bundles simultaneously, with the production worker first assembling several parts "kits" into the reusable fixtures, then either passing the assembly on to a dedicated welder who completes the expensive, slow, and skill-intensive joining process. Alternatively, the same worker then moves on to weld the assemblies. This approach complements a continued increase in manufacturing rate, as additional workers may be hired to use the same tools to produce more units more quickly as demand dictates.

Assembly operations are most efficient when assembly is downward[114] and when the work piece is held in a comfortable position. This would imply that the axis of symmetry of the reformer tubes be vertical, and that a means for raising and lowering the assembly fixture be provided. It was observed in the fabrication of the pilot-scale unit that assembly of the tubes into the headers and baffles was difficult because of the tight clearances of the components. More generous tolerances might increase the ease with which assembly can be achieved. In the assembly of the pilot unit, the headers, baffles, and insulation components were indexed and stacked, and the tubes were slid into the compressed stack of components. The baffles and headers were subsequently slid into position, a task which required two persons and several minutes. The assembly fixture could either a) seek to copy this approach, but automate the spacing of the baffles etc using mechanical or hydraulic actuators or b) place the baffles and other components in their final positions then lace the tubes through each component in sequence. Both of these approaches presents drawbacks and potential difficulties, and each would be improved immeasurably by the loosening of the baffle-tube tolerances from their current value of 25 μm to 125 μm to perhaps two to three time these values. One can envision a scaffold-like, metallic fixture which would locate and index the baffles and headers and still allow welding of the tubes while the assembly is securely held by the fixture. The assembly worker could then load several of these fixtures with components at a comfortable workstation with a hydraulic floor lift, and the fixtured assemblies could then be transferred by crane or hoist to the welding area.

For the example reactor considered in the bill of materials, the DFA (Design For Assembly) process would individually address the placement of each component in the fixture.

---

113 Boothroyd, *et al*, 1994, p. 73-75.

114 Boothroyd, et al, 1994, p. 65.

For instance, each tube header would require 3 seconds to obtain and 4 seconds to place in the fixture. The baffles and insulation, due to their lower weight, would require 2 seconds to obtain and 4 seconds to place. This would then theoretically require 92 seconds to obtain and place all fifteen components into the fixture. Even allowing for the worker wearing gloves and an imperfect fixture would only add 30 seconds to this time. These high rates of assembly may at first seem impossible, yet they are based on a wide diversity of time-motion studies across many industries. The most important difference being that the estimates are based upon workers who are skilled and experienced in assembling a single item. Thus, the worker learns the repetitive task and can execute it with a speed and precision that actually is usually better than that shown by robots. In the case of our low production volumes, it is unlikely that an empty fixture could be placed and filled with headers and baffles in less than 10 minutes, even with well-built fixtures.

The placement of the tubes provides another interesting comparison point, as so many tubes must be placed to assemble even one tube bundle assembly. If the tube is obtained from a rack in two seconds wearing gloves, then laced through all fifteen baffles, insulation layers and headers, at 3.5 seconds per layer, then each tube would require 54.5 seconds to insert into the fixture. This estimate seems reasonable based upon the pilot plant assembly, as it is easy to imagine a well-placed rack of pre-cut tubes being repeatedly grasped and inserted into the fixture in about a minute each.

Once the fixtured assembly is in place, welding begins via GTAW (Gas Tungsten Arc Welding). It was observed that each tube weld takes about two minutes to accomplish by a skilled welder. If two additional minutes are allowed for each tack weld (three per chorded baffle and four per full baffle or 29 total in this example), then a total of 335 welds is required for the example tube bundle, or 670 minutes. If the welder costs about $1 per minute, and the weldor (the welding apparatus) costs $0.50 per minute, then this welding process costs $1005 for the example tube bundle. It is predicted that the dye penetrant inspection takes about 20 minutes, or another $20. If all of the remaining steps are allowed 10 minutes each, then the tube bundle assembly can be charged $7 per tube for assembly and welding plus about $150 to $200, depending upon the number of tack welds and the extent of reweld required. For the purposes of this study, a value of $200 plus $7 per tube will be assessed for the tube-bundle assembly. It is clear that if production volume warranted, an assembly-line process might be implemented which could slash the $200 component of this cost. Further, the cost of tube welding could be reduced by robotic welding or furnace brazing the assembly.

If the same $10 per station cost is assessed to the shell assembly, then it would add $50 to the assembly cost. Similarly, the balance of the process would require another $60. Normally, these generous estimates would be imprudent, but the low production rate of the assembly coupled with the skilled nature of the operations involved make conservatism necessary. If these values are uniformly applied, then assembly would require $310 of fixed cost and $7 additional per tube. If the low-rate markup values of 50% are applied to this internal added value, then the assembly cost would tally $465 fixed plus $10.50 per tube. This is a considerable cost, and can easily amount to a large fraction of the finished reactor cost. Figure 5.16 shows the cost breakout of the example reactor divided into tube cost, catalyst cost, other materials, and assembly. It is customary to add a 10% contingency to all values to cover unexpected

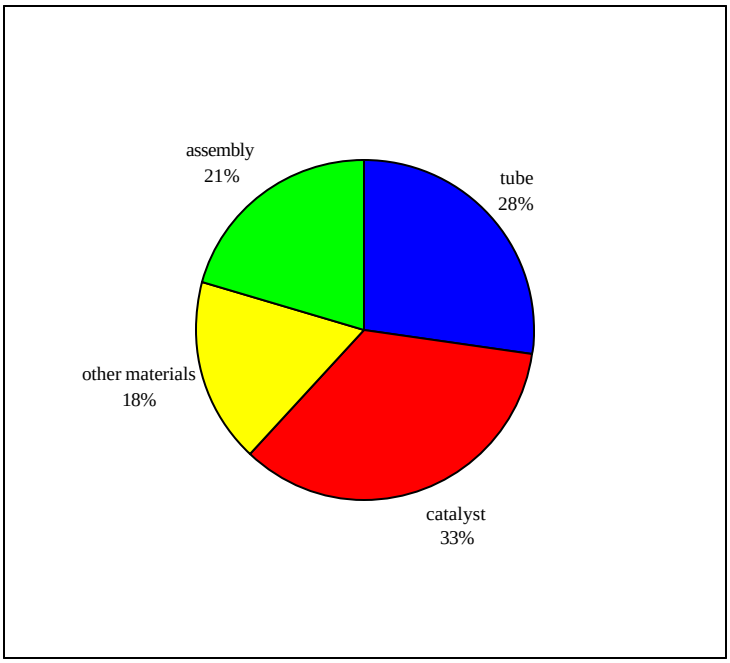

Figure 5.16: Relative cost contribution to example reformer cost

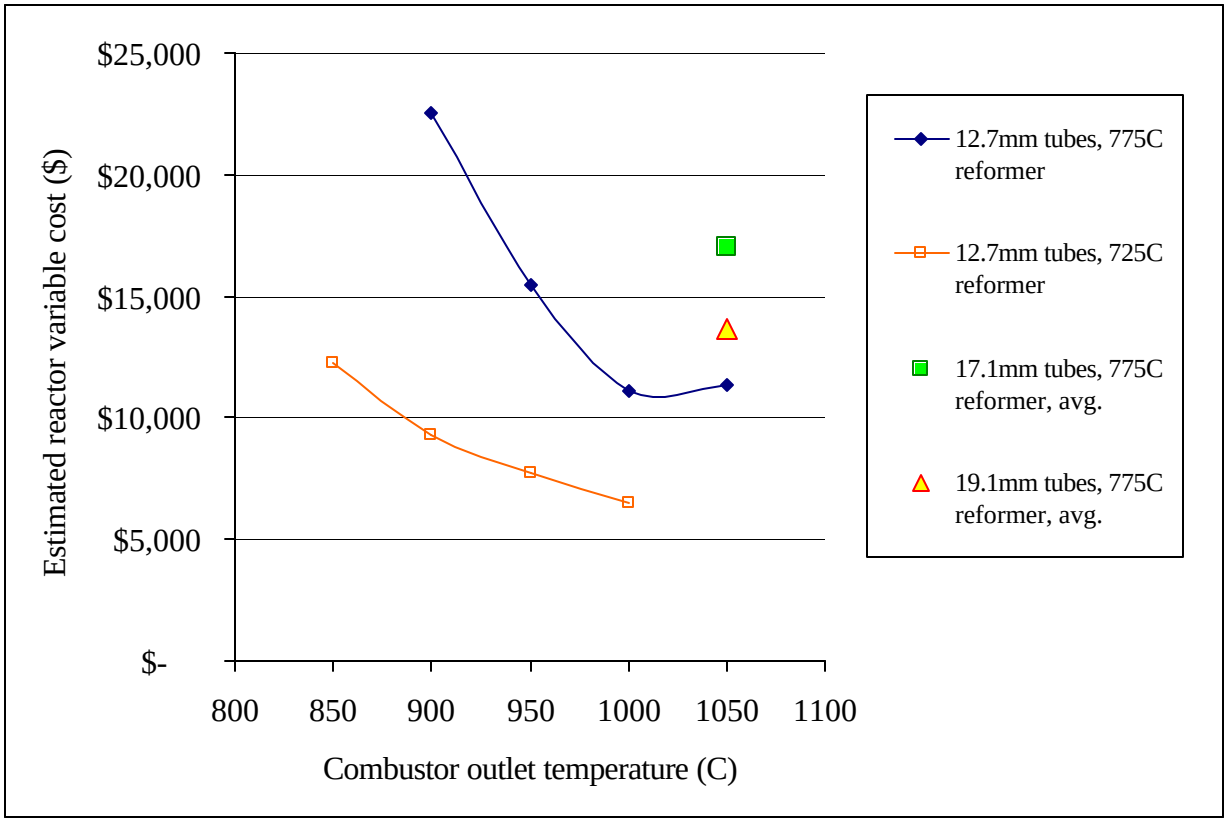

Figure 5.17: Reactor cost versus combustor temperature, reformer temperature and tube diameter (2000US$)

Table 5.9: Reactor cost estimates (2000US$)

Tube od (mm)	Matrix/ od ratio	baffle interv. (mm)	Pipe id (mm)	tubes in Pipe	Tref	Tcomb	SMR catalyst volume (L)	WGS catalyst volume (L)	Length (m)	Total tube usage (ft)	Other materials cost	Catalyst cost	Tube cost	Assembly cost	Total cost
12.7	1.5	152	298	223	775	1050	9.9	1.7	1.0	712	$ 2,344	$ 3,816	$3,221	$ 2,802	$ 13,401
12.7	1.5	229	248	153	775	1050	8.9	1.4	1.2	617	$ 2,024	$ 3,434	$2,793	$ 2,074	$ 11,358
12.7	1.5	203	248	153	775	1000	9.4	1.4	1.3	631	$ 2,068	$ 3,609	$2,305	$ 2,074	$ 11,061
12.7	1.5	203	248	153	775	950	18.5	1.7	1.8	895	$ 2,364	$ 6,931	$2,674	$ 2,074	$ 15,448
12.7	1.5	254	248	153	775	900	33.7	1.4	2.6	1323	$ 2,712	$12,381	$3,314	$ 2,074	$ 22,530
17.1	1.5	229	298	122	775	1050	17.1	3.1	1.3	530	$ 2,223	$ 6,504	$3,457	$ 1,747	$ 15,325
17.1	1.5	152	298	122	775	1050	15.7	3.1	1.2	497	$ 2,312	$ 6,011	$3,242	$ 1,747	$ 14,644
17.1	1.5	152	248	84	775	1050	12.7	2.6	1.4	398	$ 2,111	$ 4,884	$2,594	$ 1,348	$ 12,031
17.1	1.5	229	248	84	775	1050	13.9	2.6	1.6	428	$ 2,037	$ 5,332	$2,790	$ 1,348	$ 12,658
19.1	1.5	152	298	99	775	1050	20.1	3.9	1.5	475	$ 2,431	$ 7,621	$3,555	$ 1,504	$ 16,623
19.1	1.5	229	298	99	775	1050	21.6	3.9	1.6	504	$ 2,321	$ 8,193	$3,774	$ 1,504	$ 17,370
19.1	1.25	229	298	142	775	1050	23.5	4.0	1.2	554	$ 2,186	$ 8,871	$4,148	$ 1,961	$ 18,883
12.7	2	102	248	86	725	1000	3.9	1.3	1.0	285	$ 1,946	$ 1,622	$ 994	$ 1,370	$ 6,525
12.7	2	102	248	86	725	950	6.4	1.6	1.2	341	$ 2,104	$ 2,551	$ 966	$ 1,370	$ 7,691
12.7	2	102	248	86	725	900	9.7	1.8	1.5	423	$ 2,335	$ 3,758	$ 998	$ 1,370	$ 9,307
12.7	2	127	248	86	725	850	15.9	2.0	2.1	590	$ 2,603	$ 5,990	$1,200	$ 1,370	$ 12,279

developments and difficulties in transitioning to practice; and when that is included, the example reactor variable cost allowance is $11,033.

The real power of detailed DFMA cost estimation does not lie in the estimation of the cost of a single design, but in the comparison of several design options to identify overall cost drivers and to determine a cost-optimized design pathway. When this is done, the simplifications inherent to the process detract equally from every estimate; and the designs may be considered on a fairly consistent basis. The resulting cost estimates are shown in Table 5.9, which shows a marked sensitivity of reactor cost to combustor temperature, reformer temperature, and tube diameter. For the case of Incolloy 803 tubing and FCR-10 catalyst, the sensitivity of the cost to these factors is better seen in Figure 5.17. These data show that reactor cost may be halved by reducing the reformer temperature from 775 C to 725 C. They also show that reformer cost is approximately doubled by reducing the firing temperature by 150 C for either reformer temperature. Finally, it can be seen that no advantage is gained by increasing the tube diameter from the minimum value of 12.7 mm. This suggests that the design is fundamentally heat-transfer-limited, as the reduction in tube size affords dramatic increases in heat-transfer area per volume of catalyst employed.

These findings suggest other questions which should be addressed in the future development of this technology. Can reductions in catalyst cost shift the cost balance in favor of lower firing temperatures? If expensive coatings or different and more expensive tube alloys are required, are lower firing temperatures to be preferred? Can the thermodynamic conditions of the process be altered to achieve high thermal efficiency at lower reformer temperatures by increasing steam-to-carbon ratio? All of these questions must wait until the accuracy of the model is established by complete correlation with experimental results. However, it is clear that the combination of detailed reactor modeling and DFMA cost estimation can serve as a powerful economic trade-off analysis tool. The first steps have been taken to test the veracity of the model using a 1/3rd-scale pilot apparatus designed, fabricated and under test at Directed Technologies Inc.'s northern Virginia laboratory facility. The test apparatus and system will be described below, limitations of the current test apparatus will be discussed, and the first true test data will be compared to the predictions of the reactor model described in Section 5.1.

5.3 1/3rd-scale pilot reactor test system, results and observations

Fabrication and test of a chemical reactor capable of generating about 60 kW of lower heating value hydrogen flow is a complex endeavor fraught with a myriad of serious technical and safety complications not involved in microreactor tests in the laboratory. The flow rates of reagents involved necessitate the provision of actual pipeline natural gas and tap water, as K-cylinders and purchased dewars would be exhausted every few minutes. Full-scale systems for the provision of burner air, full-size combustors, heat exchangers, and an extensive safety and control system are called for.

Directed Technologies Inc. has extensive experience in testing power systems, hydrogen storage devices and chemical processors, and DTI's team was crucial in the implementation of the pilot reactor. Jonathan Ho and Stephen Waide in particular committed many hours to the

pilot reactor work, which has been ongoing for three months. Thus, this section will not dwell on the details of the pilot-plant implementation, but will only address the general architecture of the system and important lessons learned for future designs.

The test apparatus eventually limited early pilot-scale testing to slightly less than 50% of the design point for the apparatus, and continued testing is necessary to fully validate the design model. However, the 50% test data are an informative starting point, and are compared to the design model predictions in this section as well.

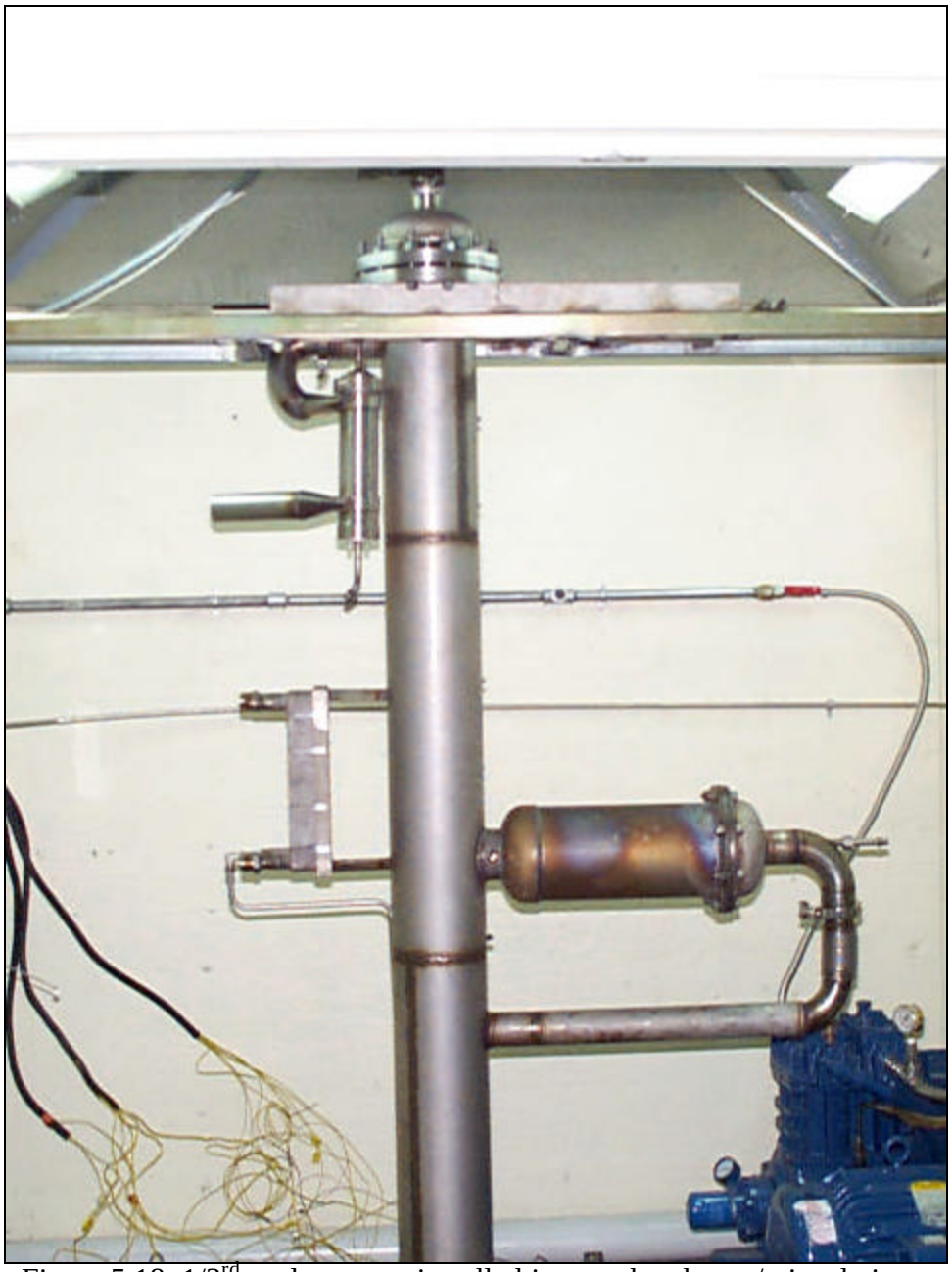

Figure 5.18: 1/3rd-scale reactor installed in test chamber w/o insulation

The pilot reactor was mounted inside a fire-resistant enclosure, with dedicated exhaust fans, IR flame detector, and hydrogen sensor. Non-hazardous operations such as water metering were accomplished outside the enclosure while the pilot reactor was sequestered inside the enclosure. The maximum design flowrate of hydrogen into the room is less than 25% of the lower flammability limit at the rated exhaust rate. The enclosure and the instrumented but un-insulated pilot reactor are shown in Figure 5.18.

The laboratory pilot system supplied natural gas to the reformer and to the catalytic combustor, which was run on natural gas to simplify control of the pilot reactor. This was accomplished by providing a Quincy, QR25NG natural gas compressor. This compressor was connected to the low-pressure natural gas line in the laboratory and was used to pressurize a surge tank held near 300 psig. This reservoir was connected to flow controllers to supply the combustor and reactor. Naturally, this system required safety relief valves, inert purging, and automatic shutoff valves, which were linked to both the control computer and to the enclosure flame and hydrogen detectors. Emergency shut-down was provided by cutting power to the system. This supply strategy was found to have several drawbacks. First, the natural gas compressor was observed to draw down the low-pressure gas circuit for the building, causing the heating furnace to cease operation. Since initial shakedown testing was conducted on a Sunday, it is likely that natural gas supply pressure problems would be worse on a weekday. Thus, a large-diameter, 2-psig natural gas line was set as a solution for this supply problem. Another serious problem encountered was an interaction between the control logic of the flow control valves and the inlet and back-pressure regulators for the system. This caused periodic variations in the system pressure and natural gas flow, which are undesirable. This suggests that the final system should use a variable speed drive to meter gas directly into the reactor using the Quincy compressor. Not only does this approach substantially reduce complexity and cost, it should also substantially enhance reliability.

City water was deionized in a multi-bed de-ionization apparatus and subsequently pressurized using a Teel, vane-style pump. The variable-speed controller delivered to operate this pump was inoperable, so for the initial testing a manual metering valve and a rotameter were employed, with the Teel pump operating at 1725 rpm and relieving through the internal relief valve. This allowed flow control within about +/- 10%. For subsequent tests, a much more elegant variable-speed drive has been implemented to control water flowrate from the positive displacement pump.

Table 5.10: Laboratory flow capabilities relative to design values on January 7, 2001

Process stream	Design capability	Minimum in pilot on Jan 7, 2001	Maximum in pilot on Jan 7, 2001	Set point % of design
Water	0.107 gpm	0.06 gpm	0.7 gpm	56%
Natural gas to reformer	138 SLPM	50 SLPM	1500 SLPM	49%
Combustor gas to reactor	2054 SLPM	400 SLPM	949 SLPM	46%
Steam temperature	~500 C	-	~200 C	61%

Air delivery was the most significant challenge in the initial tests of the system. Due to unexpectedly high pressure drop in a steam boiler which was re-used from a previous project, the available flowrate of air to the system was well below the design requirement. The Ametek blowers originally intended to provide the airflow had to be mounted in series to improve head capability, and even then the flowrate obtained was very low. In fact, the low airflow conspired to significantly limit the initial testing of the reactor. Table 5.10 compares the attainable flowrates for the important process streams to their design values. The water flowrate could not be controlled below 56% of the design value, while the air delivery limited combustor gas flow to about 48% of the design value. When the flow mismatch is coupled with the very low temperature of the steam delivered, 61% of the absolute temperature specified, the energy deficit in the incoming streams was extremely high. The shortfall was reflected in the observed performance, which included a high methane outlet concentration (39.5% dry basis) consistent with a reformer outlet condition between 550 C and 575 C.

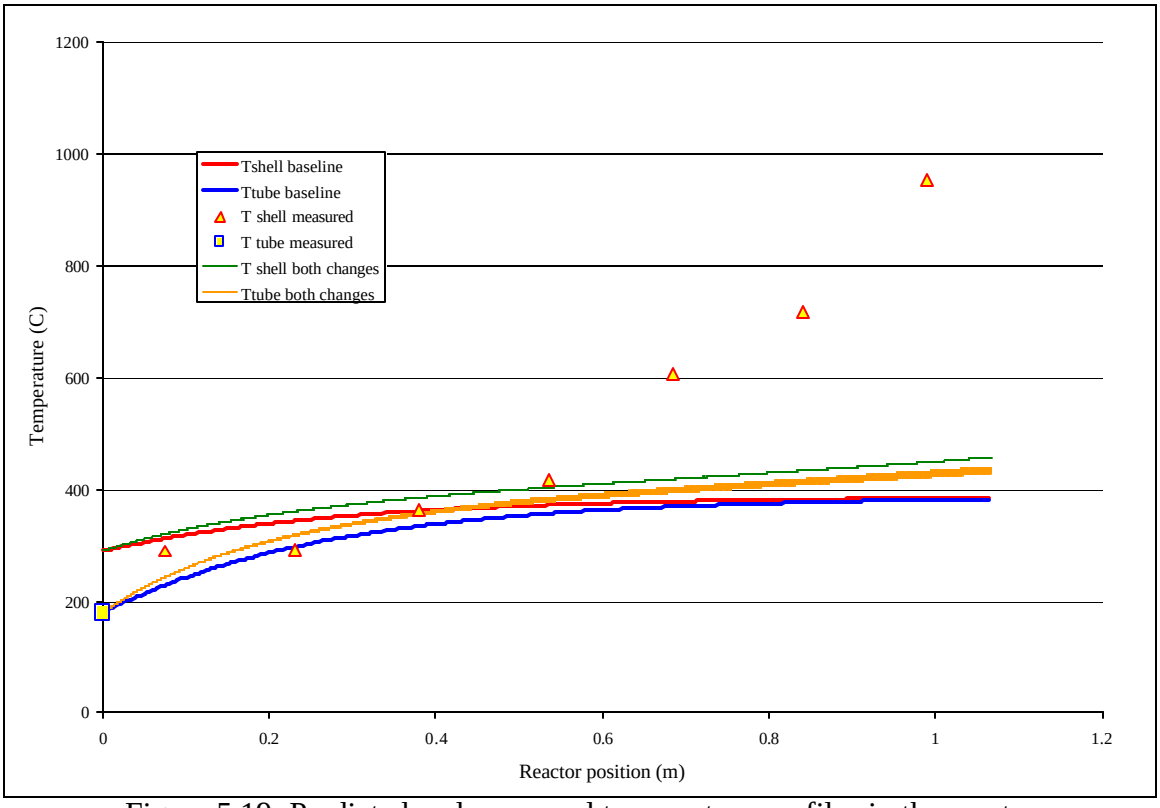

Figure 5.19: Predicted and measured temperature profiles in the reactor

An attempt was made to compare the test condition to the predictions of the steam-reformer design model. The results of this comparison are shown in Figure 5.19, which shows the predicted and measured temperature profiles in the steam reforming zone of the reactor. It can be seen from the data that the baseline reformer model described previously predicts that the measured case is impossible due to temperature cross. This is not surprising, given the general conservatism of the baseline model. The model assumptions were changed to reduce conservatism in order to see if this improved the predictive power. The assumption that oxygen poisoning exists at all points in the reactor below 857 K was removed, and the halving of the bed

heat-transfer coefficients were removed. With these changes, the predictions improve, but are still very conservative compared to the test results.

Several interpretations of the difference between the model predictions and the results are possible. The data collected were at a point which is thermodynamically incapable of performing correctly. This makes the model, which is designed to conservatively estimate sizing for thermodynamically feasible boundary conditions, incapable of rendering a design prediction. The model was specifically designed to weed out design conditions such as this test point where the parameter combinations were not certain to produce success. This suggests that a predicted temperature cross may occur where all low energy data sets are input, whereas data points collected with excess input energy should result in a prediction, albeit a conservative one. At a more pragmatic level, the testing revealed several shortcomings in the data collected. The first is that the measured temperature in the shell-side is taken at the center of each baffle stage. While an inlet combustor gas temperature was known, the outlet mixed gas temperature was not recorded. Further, the paucity of datapoints on the tube-side makes data analysis difficult. The inlet temperature recorded here is actually outside the reactor head where the steam and natural gas mix and the temperature at the inlet to the tube bundle was unknown. Further, no good measurement of the tube outlet temperatures was available. In an ideal world, temperatures inside the tube would be measured. It was deemed infeasible to insert thermocouples into the reformer tubes themselves, a point which makes analysis of the phenomena at play in the first test difficult.

Despite these setbacks, the initial test of the pilot-scale reactor succeeded in generating hydrogen from untreated natural gas. Improvements to the test apparatus are required to allow testing at a full design level and verification of the design models. This activity is crucial to the eventual successful implementation of the overall design process described in this chapter.

Chapter 6 Economic analysis

As discussed previously, the fuel and electricity consumption values and the detailed manufacturing cost estimates developed in Chapters 4 and 5 cannot be evaluated independently. This coupling becomes especially evident when it is considered that the least expensive reactor design points from Chapter 5 are also the least fuel efficient, and will thus have the highest fuel costs. The impact of the design choices contemplated must be based on an integrated economic analysis which includes the impact of all of these factors, as well as the cost of the balance of plant, capital recovery and operations and maintenance costs (O&M). These factors are discussed here, and a cost analysis is conducted. The results of this analysis are discussed, and their implications for the next design cycle are discussed in detail here and then further in Chapter 7.

To estimate the levelized cost of hydrogen produced by the reformer system, estimates for the cost of the balance of plant (BOP) required to deliver the product hydrogen are needed. The cost of appropriate ancillaries has been estimated previously by Directed Technologies Inc. as part of the business plan for the continued development of the reformer technology described in this study[115]. These estimates have been updated here to reflect the costs for ancillaries during the development of the 1/3rd scale pilot plant, and are shown in Table 6.1. These figures reflect the estimated costs at approximately 100 units per year, and are based upon supplier quotations where feasible. Because the lion's share of these costs are based upon actual price quotations or bill's of lading for delivered components used in our commercial product, the sources for the cost figures are not revealed here.

The data of Table 6.1 do not show the cost for hydrogen storage, compression, or dispensing. These costs were estimated at $31,200 for the compressor[116], $10,000 for the storage[117] and $20,000 for the dispensor based on previous work by Directed Technologies Inc. as well as additional supplier quotations. It is important to note that these estimates in particular, are quite sensitive to the volume of components ordered and the supplier. Quotations received for all three components have varied over a factor of two between manufacturers.

When these costs are added to the reactor costs estimated in Chapter 5, a total capital cost for the refueling system is obtained. The impact that this cost has on the levelized cost of hydrogen produced in constant dollars depends critically on the economic assumptions used to derive the capital recovery factor (CRF). The economic assumptions used here are intended to reflect realistic assumptions for the cost of doing business in the United States, and are shown in Table 6.2. The 15-year lifetime is slightly longer than the design lifetime of the reformer if it is operated at a capacity factor above 76%. However, prior work has determined that the average annual capacity factor for refueling stations is 69%, and this value is used here in this study. Obviously, for industrial applications with a steady demand for hydrogen, this capacity factor is

---

115 Venture prospectus for the development of a hydrogen fueling appliance, Directed Technologies Inc., August, 2000.

116 Based on data from five hydrogen compressor supplier quotations during the 2nd quarter of 2000.

117 Based upon volume quotations from steel gas cylinder manufacturer in the 2nd quarter of 2000 for volumes of 1,000 cylinders.

conservative. Indeed, in such applications, the hydrogen compression, storage and dispensing modules are likewise superfluous, and a separate analysis could be conducted to optimize the system for the purely industrial market. It is anticipated that the greatest demand for the product is in refueling applications, thus the full system is analyzed here.

Table 6.1: Projected balance of plant costs for the steam reformer system (2000US$)

Assembly	Sub-assembly	Quantity	Component Cost	Cost w/o markup	Total cost w/ markup
Reactor insulation and mounting		1		$ 1,000	$ 1,500
Superheater		1		$ 2,000	$ 2,420
Maxchanger		1		$ 760	$ 920
Condensor		1		$ 1,500	$ 1,815
Compressor, Quincy QRNG25		1		$ 1,000	$ 1,210
Water system				$ 1,845	$ 2,232
	pump	1	$ 120		
	pump motor	1	$ 200		
	variable speed drive	1	$ 500		
	check valve	1	$ 25		
	deionizer	1	$ 1,000		
NG compressor drive system				$ 1,507	$ 1,823
	5 hp, 3ph motor	1	$ 363		
	variable speed drive	1	$ 744		
	mounting	1	$ 400		
PSA system				$ 15,000	$ 18,150
Ancillaries				$ 3,744	$ 4,530
	fan, variable speed	1	$ 1,000		
	Blower	1	$ 800		
	blower motor	1	$ 1,200		
	variable speed drive	1	$ 744		
Catalytic combustor				$ 1,350	$ 1,634
	catalyst		$ 1,000		
	housing		$ 100		
	pilot burner		$ 200		
	fiitings		$ 50		
Housing				$ 1,080	$ 1,620
	frame		$ 600		
	panels		$ 400		
	assembly		$ 80		
Controls				$ 5,200	$ 6,292
	controller		$ 1,600		
	TC's		$ 1,600		
	sensors		$ 1,000		
	NEMA housing		$ 1,000		
Piping, misc, assy				$ 3,299	$ 4,948
contingency					$ 4,517
Total				$38,284	$52,111

The O&M costs were estimated based upon a fixed percentage of the capital cost for each element of the system. Values were again taken from prior work on the subject[118] and are listed in Table 6.3. The economic parameters were established based upon a broad consensus among four major North American industrial gas supply companies, Air Products and Chemicals, Praxair British Oxygen Corporation and Stuart Energy. The values have also been peer reviewed by the project sponsors at the Ford Motor Company and the U.S. Department of Energy. These values are very dependent upon the component technology in question, and are thus only approximate. Indeed, in some cases, such as the storage tanks, it is difficult to envision how O&M costs could contribute the 2.5% of capital cost on a yearly basis.

The correct real after tax rate of return for a project is a subject of lively debate. Although the 10% value used here was seen as a threshold in the industrial gas industry, other companies in other industries may choose a higher or lower rate of return for planning purposes. It is interesting to note that in the United States, the historical (1956-1996) average real after tax rate of return to capital investments in the non-financial corporate sector has been roughly 5%[119]. Thus, the assumption of 10% rate of return implies performance at twice the national average. Higher profitability floors must be interpreted as an attempt to capture financial risk in the analysis, and are thus subject to accepted practice in a given market sector. Notably, the profit allowance included in cost estimation figures employed in high rate manufacture by the Ford Motor Co. are also 10%[120], lending credence to the acceptability of this level in general commercial practice.

Table 6.2: Economic parameters employed[121]

Insurance rate	0.002	
Property tax rate	0.012	
Inflation rate	0.02	
Marginal corporate income tax rate	0.26	
After-tax real rate of return	0.1	
Lifetime (years)	10	15
Capital Recovery Factor (CRF)	0.206	0.177

The fuel costs assumed for the calculations are subject to the greatest variation of all the parameters investigated. Both electricity and natural gas prices are subject to geographic and temporal variations. Dramatic recent price increases may or may not persist in time, and seasonal as well as daily variations in price may be severe. Thus, although a natural gas price of $6/MBTU and an electricity price of $0.10/kWhr are assumed, it should be kept in mind that these values are subject to the vagaries of the marketplace, and may change dramatically. The sensitivity of the predictions here to variations in energy price will be analyzed in detail below.

---

[118] Thomas, C.E., Barbour, J.P., James, B.D., Lomax, F.D., Cost Analysis of Stationary Fuel Cell Systems Including Hydrogen Co-Generation, ACG-8-18012-01, December, 1999, p.25.

[119] Poterba, J.M., "The rate of return to corporate capital and factor shares: new estimates using revised national income accounts and capital stock data," NBER working paper 6263, November, 1997.

[120] Values communicated by Robert P. Mooradian, noted cost consultant within the Ford Motor Company, and used by the author in several published studies conducted for the Ford Motor Company.

[121] Thomas, C.E., *et al*, 1999, p.25.

Table 6.3: Example economic calculation results using the baseline assumptions (2000US$)

		775C reformer outlet, 12.7mm tubes				725C reformer outlet, 12.7mm tubes				775C ref, 1050C combustor	
	O&M rate	900C	950C	1000C	1050C	850C	900C	950C	1000C	17.1mm tubes	19.1mm tubes
reactor cost	0.035	$ 22,530	$ 15,448	$ 11,061	$ 11,358	$ 12,279	$ 9,307	$ 7,691	$ 6,525	$ 16,997	$ 13,664
ancillary cost	0.035	$ 52,111	$ 52,111	$ 52,111	$ 52,111	$ 52,111	$ 52,111	$ 52,111	$ 52,111	$ 52,111	$ 52,111
hydrogen compressor	0.045	$ 31,200	$ 31,200	$ 31,200	$ 31,200	$ 31,200	$ 31,200	$ 31,200	$ 31,200	$ 31,200	$ 31,200
hydrogen storage system	0.025	$ 10,000	$ 10,000	$ 10,000	$ 10,000	$ 10,000	$ 10,000	$ 10,000	$ 10,000	$ 10,000	$ 10,000
hydrogen dispensor	0.05	$ 20,000	$ 20,000	$ 20,000	$ 20,000	$ 20,000	$ 20,000	$ 20,000	$ 20,000	$ 20,000	$ 20,000
Annual capital cost, 10 year life		$ 27,983	$ 26,524	$ 25,621	$ 25,682	$ 25,872	$ 25,259	$ 24,926	$ 24,686	$ 26,843	$ 26,157
Annual capital cost, 15 year life		$ 24,044	$ 22,790	$ 22,014	$ 22,066	$ 22,230	$ 21,703	$ 21,417	$ 21,211	$ 23,064	$ 22,475
O&M cost		$ 5,266	$ 5,019	$ 4,865	$ 4,875	$ 4,908	$ 4,804	$ 4,747	$ 4,706	$ 5,073	$ 4,956
MMBTU natural gas/kg hydrogen		0.15	0.15	0.15	0.15	0.17	0.17	0.17	0.17	0.15	0.15
kWhr/kg hydrogen		3.22	3.19	3.16	3.13	3.49	3.44	3.40	3.36	3.13	3.13
Annual hydrogen production at 69% capacity factor, 365 operating days (kg)		29160	29160	29160	29160	29160	29160	29160	29160	29160	29160
10 year levelized capital cost ($/kg)		$ 0.96	$ 0.91	$ 0.88	$ 0.88	$ 0.89	$ 0.87	$ 0.85	$ 0.85	$ 0.92	$ 0.90
15 year levelized capital cost ($/kg)		$ 0.82	$ 0.78	$ 0.75	$ 0.76	$ 0.76	$ 0.74	$ 0.73	$ 0.73	$ 0.79	$ 0.77
Levelized O&M cost ($/kg)		$ 0.18	$ 0.17	$ 0.17	$ 0.17	$ 0.17	$ 0.16	$ 0.16	$ 0.16	$ 0.17	$ 0.17
Fuel Cost @ $6/MMBTU ($/kg)		$ 0.90	$ 0.90	$ 0.90	$ 0.90	$ 1.04	$ 1.04	$ 1.03	$ 1.03	$ 0.90	$ 0.90
Electricity cost @ $0.1/kWhr ($/kg)		$ 0.32	$ 0.32	$ 0.32	$ 0.31	$ 0.35	$ 0.34	$ 0.34	$ 0.34	$ 0.31	$ 0.31
10 year hydrogen cost ($/kg)		$ 2.36	$ 2.30	$ 2.26	$ 2.26	$ 2.44	$ 2.41	$ 2.39	$ 2.38	$ 2.31	$ 2.28
15 year hydrogen cost ($/kg)		$ 2.23	$ 2.18	$ 2.14	$ 2.14	$ 2.32	$ 2.29	$ 2.27	$ 2.26	$ 2.18	$ 2.16

Table 6.4: Alternate energy case assumptions

case #	baseline	1	2	3
natural gas price ($/MMBTU)	$ 6.00	$ 6.00	$8.00	$3.00
electricity price ($/kWhr)	$ 0.10	$ 0.04	$0.133	$ 0.10

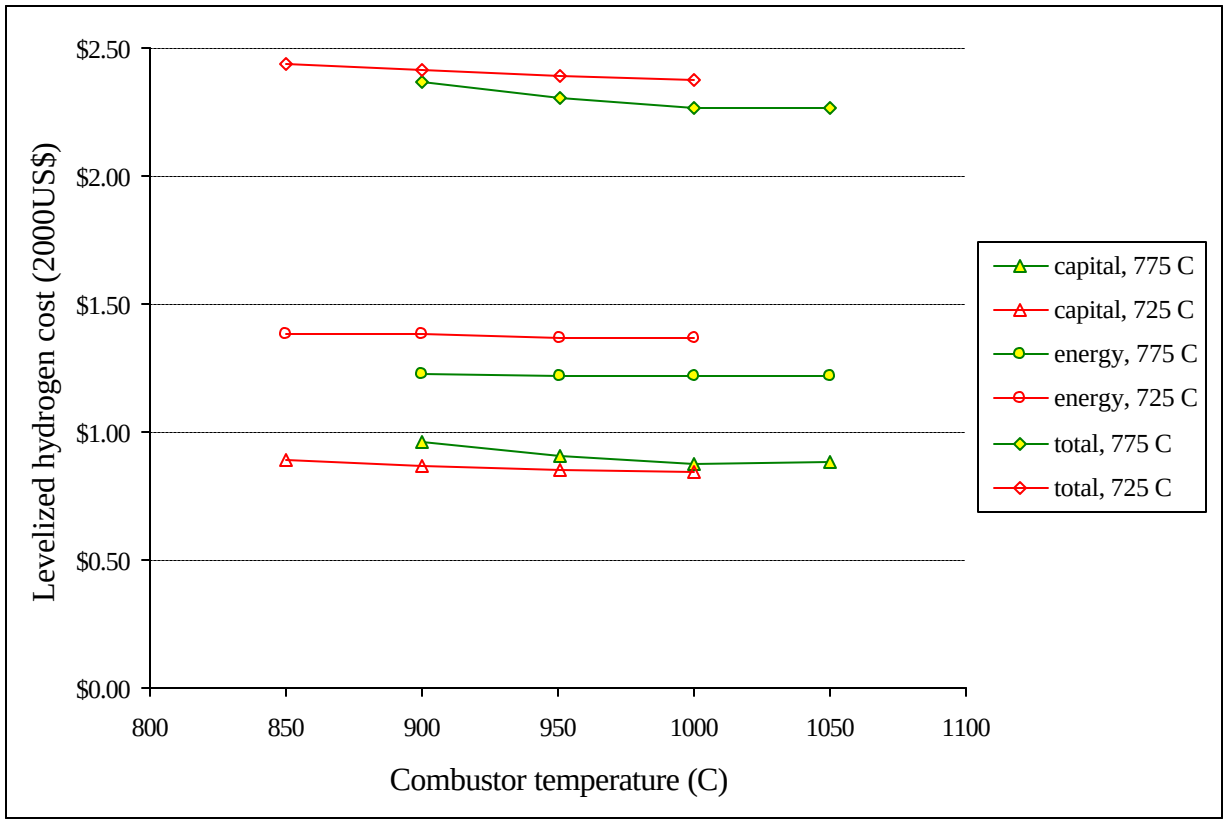

Figure 6.1: Results of the baseline economic trade study at 10-year lifetime for various reformer and combustor peak temperatures

An example of the detailed economic predictions resulting from the process above is shown in Table 6.3. It can be seen from the data that under the assumptions described above, capital recovery constitutes a fraction of the product hydrogen cost similar to that due to fuel costs. Further, the large changes in reactor cost have a relatively small impact in the overall price of hydrogen produced, amounting to perhaps a 6% total range in the levelized hydrogen price. This point is emphasized in Figure 6.1, which reveals that under the baseline assumptions, the improved fuel efficiency of the high-temperature reformers outweighs their high capital cost. This result has important implications for higher-volume production, as increased production will afford economies in the purchasing of ancillary components unattainable at low volume. This will result in an even lower capital-cost component, and will magnify the contribution of fuel costs.

To investigate the contribution of energy costs to the current optimization, three alternate cases are considered. These cases are meant to reflect realistic regional conditions which might effect the trade study and/or possible changes to the overall price of energy. The first alternative case, denoted case 1, retains the baseline natural gas price but substitutes a low electricity price of $0.04/kWhr. This is roughly representative of rates for hydroelectric power in the Canada or the Pacific Northwest. The second case represents a general increase in energy prices, and comprises a general increase of 33% in both fuel and electricity prices. The third case presents the scenario where natural gas prices are low, and electricity prices are average, such as areas

near significant natural gas production fields. These cases were analyzed, and the resulting data is shown in Figure 6.2.

Figure 6.2 shows that under all of the cases investigated, the more fuel efficient, but more capital-intensive designs for the reformer system are to be preferred. This is especially true under case 2 assumptions, where energy costs in general are shown to increase, but is also true in both cases 1 and 3 where the total energy costs decrease. Case 3 provides the only instance where some design cases for the 725C reformer prove more attractive than the more efficient 775C reformer, although when the most efficient and cost-effective 775C designs are considered there is still a healthy margin in their favor.

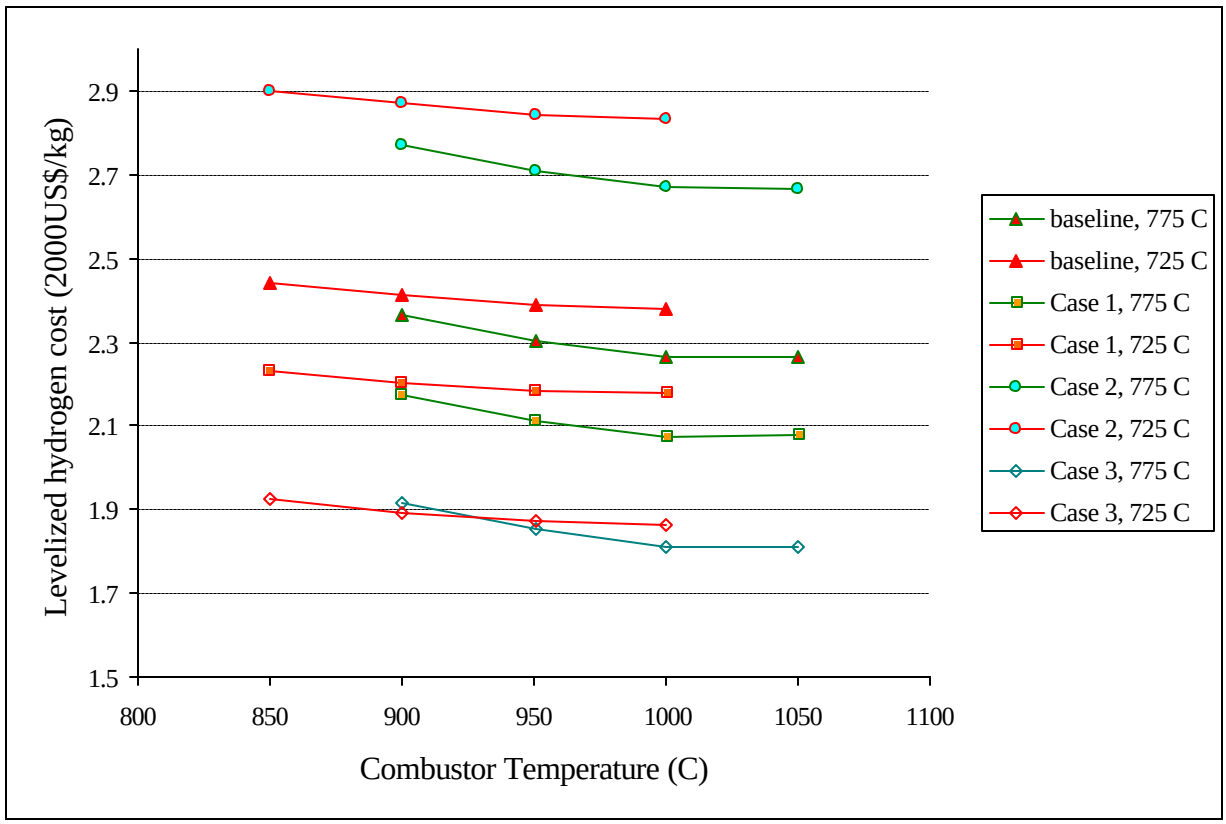

Figure 6.2: Results of the energy price trade study at 10-year system lifetime

All of these results form the basis for making some general observations regarding preferred paths forward in the next design iteration of the reformer system.

1. Increased fuel economy in hydrogen production can successfully offset fairly large changes in component costs
2. For any reformer temperature, there is a burner temperature beyond which no further reductions in system cost may be realized
3. Both capital and energy costs must be reduced to provide hydrogen at costs below $2/kg, especially if energy prices are expected to rise.

In Chapter 7 these general economic conclusions will be discussed in the context of the technology development programs described in Chapters 3, 4 & 5. It will be shown that when all of the aspects are considered together, clear routes forward are evident. It is also worth observing here that the rather minor difference in hydrogen cost evident between the study cases is a direct result of the concurrent design process, which eliminated operating conditions, materials of construction, catalyst compositions and the like that were clearly uneconomic. This resulted in a constrained matrix of technical manifestations for analysis. The method also allowed us to develop projections that are clearly internally consistent and comparable, even if they may be shown in later analyses to be quantitatively incorrect.

Chapter 7 Conclusions and Recommendations

7.1 Conclusions

The goal of the current research was the application of well-known concurrent engineering practices to the development of a chemical engineering system, a small-scale hydrogen generation system for PEM fuel cell vehicle refueling. During this process, product requirements were established, a top-level analysis was conducted to determine the most favorable system architecture to meet the requirements, and three separate areas for parallel research and development were identified. These three areas, catalyst design and testing, thermodynamic modeling and optimization of the system, and detailed chemical, mechanical, metallurgical and manufacturing design of the reactor assembly were studied in detail, and the results of each activity were used to influence the other two. After the analysis, design, fabrication and testing in each area were completed, the results were synthesized into an overall economic comparison to determine the best path forward in the next development cycle.

Several exciting advances were achieved in the current research. First, by applying concurrent development practices, a new type of reforming system was conceptually developed which requires little or no feed pretreatment, and has dramatically reduced cost and complexity when compared to previous designs. Second, a designed catalyst approach was used to develop a class of new heterogeneous catalysts for the steam reforming reaction. These catalysts facilitate the novel system design, and exhibit performance which exceeds that of all previously-demonstrated materials in several important areas: sulfur tolerance, redox stability, coking resistance, and sintering resistance. Finally, the economic trade study conducted at the end of this first cycle of development suggests that the application of concurrent-engineering practices at the early development stages provided a means to eliminate many economically-unfavorable system manifestations.

To objectively assess the merit of applying concurrent engineering practices to the hydrogen generator design problem, it is first necessary to review the product goals established in Chapter 2. The progress in the first round of development can then be compared to these goals, and qualitative assessments regarding the efficacy of the approach can be made.

- Logistic fuel/infrastructure
- Safety
- Reliability
- Low capital cost
- Low operating cost
- Maximum of 5 ppm carbon monoxide in hydrogen product
- 340 bar delivery pressure
- ~ 3 min refueling of light duty vehicle with compressed hydrogen product

The first step towards realizing these product requirements was a top-level system analysis to determine the most favorable system architecture for further development. In order to conduct this analysis, the author's experience in over five years of work in the fuel cell and reformer

industry was leveraged. A summary of important considerations is shown in the literature review section of Chapter 2.

The top-level system analysis suggested that a catalytic steam reformer system capable of reforming natural gas or LPG was the best primary chemical reformer technology. This reformer, when coupled with a Pressure Swing Adsorption (PSA) cleanup system, can yield product hydrogen of the required purity, and do so more reliably than other available technologies. To meet the high pressure requirement a hydrogen compressor unit is required, and gas storage is needed to meet the fast-fill criteria. Thus, the top-level systems analysis resulted in a system which fulfills several of the product goals. Such a hydrogen generator would employ a logistic fuel, would deliver hydrogen at an adequate product purity, and could do so at an adequate pressure and with the needed rapidity. However, this simple analysis did not solve the other problems of safety, reliability, and low cost to purchase and operate.

Basic design for manufacture and assembly tenets were applied to the reformer system in order to determine which components, if any, could be eliminated from the traditional industrial system which is employed by competing producers of small hydrogen generators. The analysis showed that a vastly simplified, and potentially far safer and more reliable system could be realized if several technical goals were met.

1. Design a new catalyst for steam reforming which is redox-stable, sulfur-tolerant, active and has a long life
2. The system could be configured to have an acceptable thermodynamic efficiency, despite drastic reductions in the quantity and complexity of process equipment required
3. A novel, integrated reactor assembly could be developed which minimizes parts count, fittings, valving, heat loss and other deficiencies of traditional systems

These three technical areas are detailed in this study in Chapters 3, 4 and 5 respectively. The proposed new system can conceivably reduce the complexity by 64% when compared to a traditional system. This advance was made possible by the application of concurrent engineering techniques to the development of the product over the course of an 18 month design cycle, despite the fact that competing products have been in development since the late 1960's.

The catalyst research and development program identified several candidate catalyst materials, and culminated in their synthesis and testing. Of the materials designed, the proprietary FCR-10 composition developed under a joint program by Directed Technologies, Inc. and Sud-Chemie, Inc. evidenced the best performance. This catalyst demonstrated several of the desired technical properties. FCR-10 demonstrates superior resistance not only to sulfur and technically-important levels of di-oxygen, but is also extremely resistant to deactivation by carbon deposition. The catalyst is active, although the activity level is less than half of the goal level set in the development program. Good lifetime has been demonstrated to date in accelerated testing, although the duration of testing to date precludes any firm conclusions. The only concern regarding the catalyst is its cost, which has become an issue because of the recent precipitous increase in noble metal market prices. Several steps may be taken to improve the cost picture for the catalyst, and these are described later in the recommendations section.

Despite the scope for improvement, this FCR-10 catalyst composition represents a major advance in the catalysis of the steam-reforming reaction, especially for small-scale applications.

The thermodynamic modeling conducted during this research helped establish preferred operating conditions for obtaining optimum fuel efficiency. These included steam reformer outlet temperatures above 750 C, steam-to-carbon ratios of 4:1 or greater, and water-gas shift outlet temperatures around 350 C. The preferred pressure of operation depended upon the other operating conditions, but when a higher steam-reformer temperature was employed, higher pressures were to be preferred. Other interesting conclusions centered on the fact that low reactor shell-side pressure drop is needed to obtain low electricity consumption in the blower providing the combustor air stream. In fact, total pressure drops through all of the airside flowpath of less than 15 kPa are desirable. Further, increasing the burner outlet temperature reduces the blower parasitic load further, because it reduces the required airflow to burn the fixed quantity of tailgas. Unfortunately, the increase in burner temperature and reactor temperature, both of which reduce fuel consumption, increases the reactor material cost dramatically, an issue which requires careful study and simulation to assess.

The conditions of operation suggested by the thermodynamic trade study are significantly different than those employed industrially. This is because the parallel consideration of mechanical feasibility issues pointed out limitations in commercially-available ancillary technology for feed compression and delivery. Further, the peak reformer temperatures and combustor temperatures are far below those employed industrially. This choice is influenced by the adverse safety, cost and feasibility implications of higher operating temperatures in compact, small-scale reformers.

Thus, the tradeoff between reformer temperature, burner temperature, reactor configuration and cost were driving factors in the reactor assembly design study conducted in Chapter 5. The research resulted in a model which can be used to evaluate the required reactor configurations for different thermodynamic boundary conditions generated in the thermodynamic model described in Chapter 4. The configuration data from the model, are combined with metallurgical considerations, and a manufacturing cost-estimation framework to yield estimates for the manufactured cost of the reactor assembly as a function of the thermodynamic boundary conditions assuming the FCR-10 catalyst performance from Chapter 3. This procedure actually yields estimates of the reactor assembly cost which vary over a factor of four, suggesting that the detailed thermodynamic conditions critically impact the cost of hydrogen produced. To the author's knowledge, this research represents the first instance where commercial DFMA techniques have been seamlessly-integrated with the reactor design modeling process and the reactor mechanical engineering design to yield a basis for internally-consistent trade-off between design configurations of a mass-produced petrochemical reactor system.

All of the results above were synthesized into an economic analysis is Chapter 6 to establish a direct linkage between the thermodynamic modeling, reactor design, reactor manufacture and the resulting levelized hydrogen cost. The results of the analysis show that because of other factors, the large swings in reactor cost do not drastically affect the cost of the hydrogen produced by the hydrogen appliance. Optimal economic conditions are slanted towards higher efficiency, with high steam reformer temperatures always being favored despite

the penalty in reactor capital cost. The optimal combustor temperature is usually towards the high end of the values studied, but not usually the highest temperature. This is due to the tradeoff between the reactor size and the tube wall thickness discovered in the analysis of Chapter 5. Without the integration of the thermodynamic optimization, reactor chemical and mechanical design and manufacturing cost, it would be infeasible to reach conclusions regarding this linkage. This modeling tool can also be used to evaluate other materials of design, operating conditions, heat transfer matrices, and system manifestations while maintaining a high level of confidence in the results of the comparisons. Clearly, this is a powerful trade-off technique, which may even lend itself to formal optimization approaches in the future.

When these results are analyzed at a high level, it is clear that conducting each activity in parallel offered surprising benefits. The reactor model was used to study cases suggested by the thermodynamic model, and the results of the two were combined to indicate paths forward for enhanced product efficiency and lowest cost. Further, the results of the reactor sizing suggest that catalyst cost is the primary driver behind the reactor cost, motivating catalyst-based solutions to address the cost to activity ratio of the catalyst. At an even higher level, it is clear that establishing the product goals early in the process, and using these goals to drive every aspect of the engineering process, led to big savings in development time because only important problems were addressed. When it is considered that no other reformer development company has stumbled upon the design solutions described here, despite more than 30 years of development in some cases, it is clear that the concurrent development process yielded substantial dividends.

The one factor missing from the development to this point is the team aspect. In this effort, the roles of the team members which would comprise a normal industrial team for concurrent chemical engineering were all embodied in the author. The real challenge is how effectively the process can be pursued when other team members are involved. This application is obviously beyond the scope of an academic environment. Fortunately, the commercialization of the hydrogen generator product described in this report is being carried forward by the author within the framework of a new private company, H2Gen Innovations, Inc.. Thus, the recommendations described in the following paragraphs will comprise the early development goals of the new company, where an actual team will be assembled to carry out the next iteration in the concurrent development of this concept.

7.2 Recommendations

The recommendations for future work here are limited to the specific areas covered in this study. Obviously, a lot of work remains in areas such as system control, integration with the PSA system, safety code compliance, etc. but since these areas are commercially sensitive, and not directly related to the subject of this study, they will not be covered here.

On a global level, the conclusions derived from the economic study of Chapter 6 suggest that the fuel costs and capital costs have similar impacts of the delivered hydrogen cost. Improvements in the system efficiency to reduce costs seem cost-effective, although they may change the cost of a given component substantially. Thus, means of improving efficiency are

likely worthwhile pathways to reduce the cost of the hydrogen product. Another general observation is that the hydrogen compression, storage, and dispensing costs dominate the capital cost. Thus, reduction in the cost of these elements may be the best way to reduce cost for the total system.

To improve efficiency and reduce fuel costs, the thermodynamic analysis suggests some avenues which should be investigated. The main options would require co-firing the burner with raw fuel, as is done in industrial plants. This would allow either an increase in steam-to-carbon ratio or an increase in pressure, and, thus, recovery of hydrogen in the PSA. The latter would yield modest benefits with the HyQuestor 600 evaluated in this research but could dramatically change matters if a more complex system with more beds was pursued. Improvements to the PSA system are being discussed with QuestAir Gases.

On the reactor design front, greater efficiency at lower cost means either improved catalysts or cheaper materials of construction. The latter could be achieved through the use of aluminizing of the alloys of construction to yield lower rates of corrosion. Another option is the pursuit of inherently more corrosion-resistant alloys such as Krupp's 602CA or Special Metal's Incoloy 890. Also, the cost impact of adding a sulfur-adsorbent guardbed to the reactor needs to be assessed based on the results of the catalyst testing with FCR-9A and FCR-10. Such a guardbed could reduce sulfur levels slightly to ensure no sulfur spikes reach the catalysts, which are easily deactivated by such spikes. This might afford a slightly greater overall activity, especially at the low temperatures near the reformer inlet.

These considerations bring us to the catalyst itself. The test program definitely needs to be expanded to include long-duration tests to ensure adequate commercial catalyst lifetime. Further, the issue of catalyst activity at both the low and high temperature ranges need to be addressed. For the high temperature range, the FCR-10 catalyst appears to be diffusion-limited. The situation could be altered by providing a support with higher porosity and greater surface area. Different support chemistries and different preparation modes for the current chemistry are options for achieving this goal. A higher area support might also improve low-temperature activity, which seems to be significantly impaired by sulfur. If a greater proportion of the catalyst metal were exposed by higher dispersion of the metal into smaller crystallites, then the sulfur poisoning would be less important. Another option is the use of a different noble metal species as the active metal or of a combination of active metals with better sulfur tolerance.

It can be seen that these issues will once again interact in the next design cycle. This is especially true in the area of providing a sulfur guardbed, which is largely a reactor issue, and the changes in the catalyst design and cost, which are more fundamental chemistry/materials science areas. These factors will interact to determine the most economical design point, which may actually evolve over time as the technology for the catalysts is improved. In the next design iteration, these issues will also begin to interact with issues of safety and control which are not yet evident, and will have to be considered as they arise. Undoubtedly, the fact that the design team will consider all of the factors in parallel, and will advance on all the fronts simultaneously will yield dividends in lower final product cost and more rapid development.

References

Agarwal, D.C., Brill, U., "High-Temperature-Strength Nickel Alloy," Advanced Materials and Processes, Materials Park, OH, October 2000.

Avallone, E.A., Baumeister, T., Marks' Standard Handbook For Mechanical Engineers: Tenth Edition, McGraw-Hill, New York, NY, 1996.

1998 ASME Boiler and Pressure Vessel Code: Rules For Construction of Power Boilers: Section I, American Society of Mechanical Engineers, New York, NY, July 1, 1998.

Black, W.Z., Hartley, J.G., Thermodynamics: 2nd Edition, Harper Collins, New York, NY, 1991.

Barbier, J., Duprez, D., "Steam effects in three-way catalysis," Applied Catalysis B, Elsevier Science Publishers, Amsterdam, 1994.

Bloomfield, D.P., US 4,004,947, January 25, 1977.

Bohlbro, H., An Investigation of the Kinetics of the Conversion of Carbon Monoxide with Water Vapour over Iron Oxide Based Catalysts, Haldor-Topsoe, Vedbaek, Denmark, 1966.

Bohlbro, H., "The kinetics of water-gas shift conversion IV: Influence of Alkali on the rate equation," Journal of Catalysis, Academic Press, New York, NY, vol 3, 1964.

Boothroyd, G., Dewhurst, P., Knight, W., Product Design for Manufacture and Assembly, Marcel Dekker, New York, NY, 1994.

Bonk, S.P., Morganthaler, G.F., Miura, Y. , US 4,921,680, May 1, 1990.

Buswell, R.F., Sederquist, R.A., Setzer, H.J., Snopkowski, D.J., US 3,446,594, May 27, 1969.

Buswell, R.F., Clausi, J.V., Cohen, R., Louie, C., Watkins, D.S., US 5,360,679, November 1, 1994.

Buswell, R.F., Clausi, J.V., Louie, C., US 5,464,606, November 7, 1995.

Buswell, R.F., Cohen, R., Clausi, J.V., Leavitt, S.L., Watkins, D.S., US 5,484,577, January 16, 1996.

Buxbaum, R.E., "Hydrogen transport through non-porous membranes of palladium-coated niobium, tantalum and vanadium," Journal of Membrane Sciences, Elsevier Science Publishers, Amsterdam, vol 85, 1993.

"Composite-metal membranes for high-temperature hydrogen separations," Oremet Wah-Chang, Albany, OR, 1998.

Corrigan, T.J., US 3,909,299, September 30, 1975.

Corrigan, T.J., US 5,516,344, May 14, 1996.

Dantowitz, P., US 3,541,729, November 24, 1970.

Davis, J.R., Heat resistant materials, American Society of Materials International, Materials Park, OH, USA, 1997.

DeJong, K.P., Lednor, P.W., Oud, A.E.M., Schoonebeek, R.J., Vonkeman, K.A., VanDerZwet, G.P., US 5,486,313, January 23, 1996.

Duprez, D., "Selective steam reforming of aromatic compounds on metal catalysts," Applied Catalysis A, Elsevier, Amsterdam, vol 82, 1992.

Edlund, D.J., Pledger, W.A., "An integrated Fuel Processor for PEM fuel cells," Northwest Power Systems, LLC, Bend, OR, 1998.

Fogler, H.S., Elements of Chemical Reaction Engineering: 2nd Edition, Prentice Hall, NJ, 1992.

G-72D Sulfur Removal Catalyst Product Bulletin, United Catalysts, Inc., Louisville, KY.

Greiner, L., Moard, D.M. , US 5,207,185, May 4, 1993.

Greiner, L., Moard, D.M. , US 5,299,536 April 5, 1994.

Grenoble, D.C., Estadt, M.M., Ollis, D.F., "The chemistry and catalysis of the water-gas shift reaction," Journal of Catalysis, Academic Press, New York, NY, vol 67, 1981.

Harrison, B., Diwell, A.F., Hallett, C., "Promoting Platinum Metals by Ceria: Metal-support Interactions in Autocatalysts," Platinum Metals Review, London, UK, vol 32, no 2, 1988.

Haynes HR-120 alloy, Haynes International, Inc., Kokomo, IN.

Hedgedus, L.L., McCabe, R.W., Catalyst Poisoning, Marcel Dekker, New York, NY, 1984.

Heydorn, B., Zuanich, J., Market Assessment: Small Scale Hydrogen Generators, SRI consulting for Gas Research Institute, Chicago, IL, #5096-930-3902, January, 1998.

Hitachi, Kondo, Y., Amamo, Y., Kimura, S., Horiuchi, S., US 5,110,559, May 5,1992.

Holman, J.P., Heat Transfer: 7th Edition, McGraw-Hill, Inc., New York, NY, 1990.

"Hydrogen," Encyclopedia of Chemical Technology: 4th edition, John Wiley and Sons, New York, NY 1995, pp. 878-884.

"Hydrogen," Ullmann's Encyclopedia of Industrial Chemistry: 5th edition, VCH Verlagsgesellschaft mbH, FRG, 1989, pp. 297-442.

"Hydrogen Production: Krupp Uhde technology with top-class performance," ThyssenKrupp Engineering, Dortmund, Germany, 9/99.

Iwaki, T., Eqashira, S., Okagami, A., US 3,551,124, December 29, 1970.

Jacobs, L.L.G., Lednor, P.W.,Limahelu, A.G.G., Schoonebeek, R.J., Vonkeman, K.A., US 5,510,056, April 23, 1996.

James, B.D., Lomax, F.D., Thomas, C.E., Colella, W.G., PEM Fuel Cell Power System Cost Estimates: Sulfur-Free Gasoline Partial Oxidation and Compressed Direct Hydrogen, report to the PNGV fuel cell technical team for Ford Motor Company, Washington, DC, 10/17/97.

James, B.D., Lomax, F.D., Thomas, C.E., "Manufacturing Cost of Stationary Polymer Electrolyte Membrane (PEM) Fuel Cells," prepared for the National Renewable Energy Laboratory, Golden, CO, November, 1999.

Kumar, K.N.P., Lange, J.P., Searcy_Roberts, K., Van der Zwet, G.P., Van Leon, P.J.M., Oosterveld, M., Senden, M.M.G., Jacobs, L.L.G., Lednor, P.W., Limahelu, A.G.G., Schoonebeek, R.J., Vonkeman, K.A., US 5,628,931, May 13, 1997.

Kumar, K.N.P., Lange, J.P., Searcy_Roberts, K., Van der Zwet, G.P., Van Leon, P.J.M., Oosterveld, M., Senden, M.M.G., Jacobs, L.L.G., Lednor, P.W., Limahelu, A.G.G., Schoonebeek, R.J., Vonkeman, K.A., US 5,639,401, June 17, 199.

Kumar, K.N.P., Lange, J.P., Searcy_Roberts, K., Van der Zwet, G.P., Van Leon, P.J.M., Oosterveld, M., Senden, M.M.G., Jacobs, L.L.G., Lednor, P.W., Limahelu, A.G.G., Schoonebeek, R.J., Vonkeman, K.A., US 5,658,497, August 19, 199.

Kumar, K.N.P., Lange, J.P., Searcy_Roberts, K., Van der Zwet, G.P., Van Leon, P.J.M., Oosterveld, M., Senden, M.M.G., Jacobs, L.L.G., Lednor, P.W., Limahelu, A.G.G., Schoonebeek, R.J., Vonkeman, K.A., US 5,720,901, February 24, 1998.

Lesieur, R.R., US 5, 733,347, March 31, 1998.

Lomax, F.D., Investigation of Steam Reformation of Natural Gas for the Very Small Scale Production of Hydrogen Fuel for Light Duty Vehicles in Appliance-type Refueling Systems, VPI&SU, Blacksburg, VA, MSE Project and Report, May 1997.

Luntz, A.C., Harris, J., "CH4 dissociation on metals: a quantum dynamics model," Surface Science, Elsevier, Amsterdam, vol 258, 1991.

Mayland, B.J., Trimarke, C.R., Harvin, R.L., Brandon, C.S., US 3,477,832, Nov 11, 1969.

McClean, C.R., Keefer, B.G., Rowat, D.W., "Pressure Swing Adsorption for Small-Scale On-Site Hydrogen Supply," Questor Industries, Inc., Burnaby, BC, Canada, 1997.

Mills, G.A., Steffgen, F.W., "Catalytic Methanation," Catalysis Reviews, Marcel Dekker, New York, vol 8, no 2, 1973.

Misage, R., Scheffler, G.W., Setzer, H.J., Margiott, P.R., Parenti, E.K., US 4,781,241, November 1, 1988.

Newsome, D.S., "The Water-gas shift Reaction," Catalysis Review – Science and Engineering, Marcel Dekker, New York, 1980.

Moss, T.S., Peachey, N.M., Snow, R.C., Dye, R.C., "Multilayer Metal Membranes for Hydrogen Separation," International Journal of Hydrogen Energy, Pergamon, Coral Gables, FL, Vol 23, No 2, 1998, pp. 99-106.

Oudar, J., Wise, H., Deactivation and Poisoning of Catalysts, Marcel Dekker, New York, NY, 1985.

Platinum 1996: Interim Review, Johnson Matthey, London, England, November 1996.

Podolksi, W., Kim, Y.G., "Modeling the water-gas shift reaction," Industrial and Engineering Chemistry: Process Design and Development, vol 13, No 4, 1974.

Poterba, J.M., "The rate of return to corporate capital and factor shares: new estimates using revised national income accounts and capital stock data," National Bureau of Economic Research, Cambridge, MA, working paper 6263, November, 1997.

"Presentation of Topsoe Technologies for the Refining Industry," Haldor-Topsoe, Inc., Hyatt Hill Country Resort, San Antonio, TX, September 17-19, 1997.

Rostrup-Nielsen, J.R., Catalytic Steam Reforming, Reprint from Catalysis-Science and technology, Springer-Verlag, New York, NY 1984.

Satterfield, C.N., Heterogeneous Catalysis in Industrial Practice, Krieger Publishing Co., Malabar, FL, 1996.

Schey, J.A., Introduction to Manufacturing Processes: Third Edition, McGraw Hill, New York, NY, 2000.

Schlatter, J.C., "Water-Gas Shift and Steam-reforming reactions Over a Rhodium Three-way Catalyst," 1978 SAE congress at Cobo Hall, Detroit, MI

Sedequist, R.A., US 5,470,360, November 28, 1995.

Setzer, H.J.,Whiting, R.W., US 3,485,746, December 23, 1969.

Setzer, H.J. , US 3,655,448, April 11, 1972.

Shultz, J.F., Karn, F.S., Anderson, R.B., Noble Metals, Molybdenum, and Tungsten in Hydrocarbon Synthesis, U.S. Department of Interior, Bureau of Mines, Washington, DC, 1967.

Sie, S.T., US 5,186,859, Feb 16, 1993.

Standards of the Tubular Exchanger Manufacturers Association: Eighth Edition, Tubular Exchanger Manufacturers Association, Inc., Tarrytown, NY, 1999.

Suzuki, T., Iwanami, H., Yoshinari, T., "Steam reforming of kerosene on Ru/Al_2O_3 catalyst to yield hydrogen," International Journal of Hydrogen Energy, Elsevier Science Lmtd., Oxford, UK, vol 25, 2000, pp. 119-126.

Szydlowski, D.F., Lesiur, R.R., US 4,976,747, December 11, 1990.

Thomas, C.E., James, B.D., Kuhn, I.F., Lomax, F.D., Baum, G.N., Hydrogen Infrastructure Report, U.S. Department of Energy, Washington, DC, Report # DOE/CE/50389-504, July 1997.

Thomas, C.E., James, B.D., Lomax, F.D., Kuhn, I.F., "Integrated Analysis of Hydrogen Passenger Vehicle Transportation Pathways," prepared for the National Renewable Energy Laboratory, Golden, CO, March 1998.

Thomas, C.E., Barbour, J.P., James, B.D., Lomax, F.D., Cost Analysis of Stationary Fuel Cell Systems Including Hydrogen Co-Generation, National Renewable Energy Laboratory, Golden, CO, ACG-8-18012-01, December, 1999.

Trimm, D.L., "Poisoning of Metal Catalysts," Deactivation and Poisoning of Catalysts, Oudar and Wise, eds., Marcel Dekker, Inc., New York, NY 1985.

Vannice, M.A., "Catalytic Activation of Carbon Monoxide on Metal Surfaces," source unknown.

Venture prospectus for the development of a hydrogen fueling appliance, Directed Technologies Inc., Arlington, VA, August, 2000.

Voecks, G.E., US 4,909,808, Mar 20, 1990.

Welty, J.R., Wicks, C.E., Wilson, R.E., Fundamentals of Momentum, Heat and Mass Transfer: 3rd Edition, John Wiley & Sons, New York, NY, 1984.

Wise, H., McCarty, J.,Oudar, J., "Sulfur and Carbon Interactions with Metal Surfaces," Deactivation and Poisoning of Catalysts, Marcel Dekker, Inc., New York, NY, 1985.

Whittington, B.I., Jiang, C.J., Trimm, D.L., "Vehicle exhaust catalysis: I. The relative importance of catalytic oxidation, steam reforming and water-gas shift reactions," Catalysis Today, Elsevier, Amsterdam, vol 26, 1995.

Yamase, O.,Miura, T., Kubota, H., US 5,284,717, February 8, 1994.

Yang, R.T., Gas Separation by Adsorption Processes, Imperial College Press, Singapore, 1987.

Yokoyama, E., Kaneko, T., Amano, Y., Sugimoto, S., US 4,554,223, November 19, 1985.

Appendix

This section contains the complete US patent application pertaining to the novel hydrogen generator and hydrogen generation system filed by the author and John P. Reardon and assigned to Directed Technologies Inc.

193956US23

TITLE OF THE INVENTION

IMPROVED SYSTEM FOR HYDROGEN GENERATION THROUGH STEAM REFORMING OF HYDROCARBONS AND INTEGRATED CHEMICAL REACTOR FOR HYDROGEN PRODUCTION FROM HYDROCARBONS

ABSTRACT OF THE DISCLOSURE

The present invention provides a reactor, which includes:

a unitary shell assembly having an inlet and an outlet;

a flow path extending within the shell assembly from the inlet to the outlet, the flow path having a steam reformer section with a first catalyst and a water-gas shift reactor section with a second catalyst, the steam reformer section being located upstream of the water-gas shift reactor section;

a heating section within the shell assembly and configured to heat the steam reformer section; and

a cooling section within the shell assembly and configured to cool the water-gas shift reactor section. The present invention also provides a simplified hydrogen production system, which includes the catalytic steam reforming and subsequent high temperature water-gas shift of low-sulfur (< 100ppm by mass) hydrocarbon fuels followed by hydrogen purification through the pressure swing adsorption (PSA). The integrated reactor offers significant advantages such as lower heat loss, lower parts count, lower thermal mass, and greater safety than the many separate components employed in conventional and is especially well-suited to applications where less than 15,000 standard cubic feet per hour of hydrogen are required. The improved system also may be started, operated and shut down more simply and quickly than what is currently possible in conventional systems. The improved system preferably employs active temperature control for added safety of operation. The hydrogen product is of high purity, and the system may be optionally operated with a feedback control loop for added purity.

BACKGROUND OF THE INVENTION

Field of the Invention

The present invention relates to an integrated chemical reactor for the production of hydrogen from hydrocarbon fuels such as natural gas, propane, liquefied petroleum gas, alcohols, naphtha and other hydrocarbon fuels and having a unique unitized, multifunctional structure. The integrated reactor offers significant advantages such as lower heat loss, lower parts count, lower thermal mass, and greater safety than the many separate components employed in conventional systems to achieve the same end. The integrated reactor is especially well-suited to applications where less than 15,000 standard cubic feet per hour of hydrogen are required.

The present invention also relates to the generation of hydrogen for use in industrial applications, as a chemical feedstock, or as a fuel for stationary or mobile power plants.

Discussion of the Background:

Hydrogen production from natural gas, propane, liquefied petroleum gas (LPG), alcohols, naphtha and other hydrocarbon fuels is an important industrial activity. Typical industrial applications include feedstock for ammonia synthesis and other chemical processes, in the metals processing industry, for semiconductor manufacture and in other industrial applications, petroleum desulfurization, and hydrogen production for the merchant gas market. The demand for low-cost hydrogen at a smaller scale than produced by traditional industrial hydrogen generators has created a market for small-scale hydrogen production apparatus (< 15,000 standard cubic feet per hour (scfh)). This demand has been augmented by the growing enthusiasm for hydrogen as a fuel for stationary and mobile powerplants, especially those employing electrochemical fuel cells, which require hydrogen as a fuel.

Hydrogen is typically produced from hydrocarbon fuels industrially via chemical reforming using combinations of steam reforming and partial oxidation. This is typically achieved at scales larger than one ton per day using well-known process and catalyst designs. For several reasons, it is difficult to adapt these large-scale technologies to economically produce hydrogen at small scales. Typical industrial applications produce far more than 15,000 standard cubic feet per hour (~1 ton per day), and often employ catalytic steam reforming of light hydrocarbons in radiantly-fired furnaces. Steam reforming of hydrocarbons is illustrated for the simple case of methane below.

$$CH_4 + H_2O \rightarrow CO + 3H_2$$

The above reaction is highly endothermic, and the reacting fluid must have energy transferred to it for the reaction to proceed. Further, the extent of the reaction is low at low temperatures, such that greatly elevated temperatures, often as high as 800°C, are required by conventional systems to convert an acceptable amount of hydrocarbon to hydrogen and carbon monoxide. The catalyst employed in industrial reactors is typically composed of an active nickel metal component supported on a ceramic support.

The radiantly-fired furnaces employed in large-scale industrial reactors have many disadvantages that make them unsuitable for small-scale systems. The most important disadvantage is the very high temperature of the radiant burners and the gas contacting the reactor surfaces, which are usually tubular in form. The temperature of the radiant burners often approaches or exceeds the melting temperature of the alloy from which the tubes are fabricated. Melting of the tubes is prevented by the rapid endothermic catalytic reaction inside the tubes. If, however, the catalyst fails due to carbon formation, sulfur poisoning or other causes, then the tubes form what is referred to in the literature as a "hot spot," which greatly accelerates the failure of the reactor tube in question. In large-scale systems, careful monitoring and control of the furnace and tube temperatures as well as exceptionally rugged construction of the tubes makes the risks of hot spots acceptable. For systems producing below 1 ton per day, however, the complexity and cost of such safety measures can become prohibitive. Nonetheless, small-

scale steam reformers utilizing radiant heat transfer are known and described, for example, in U.S. 5,484,577 to Buswell, *et al*. The extreme measures necessary to control the temperature in arrays of reformer tubes are likewise documented in U.S. 5,470,360 to Sederquist.

A means of transferring the necessary heat to the reacting gases without radiant heat transfer and its attendant risks, which is especially well-suited to small-scale steam reforming, is the use of compact heat exchange surfaces, such as arrays of tubes or finned-plates. The heat transfer mechanism in such devices is dominated by convection and conduction with minimal radiant transfer. An example of this approach is described in U.S. 5,733,347 to Lesuir, wherein finned plates are employed to increase heat transfer. Tubular compact heat exchangers for steam reforming are sold by Haldor Topsoe, Inc. of Houston, TX.

Conventional hydrogen generation systems employing steam reforming of hydrocarbon fuels typically include three main reaction steps for producing hydrogen; steam reforming, high-temperature water-gas shift, and low temperature water-gas shift. The important reactions for methane are as follows:

It is evident from the equation for steam reforming of hydrocarbon fuel that the principal products are hydrogen and carbon monoxide. The carbon monoxide may be converted into additional hydrogen via a catalytic reaction with steam (water-gas shift reaction.

The water-gas shift reaction is mildly exothermic and thus is thermodynamically favored at lower temperatures. However, the kinetics of the reaction are superior at higher temperatures. Thus, it is common practice to first cool the reformate product from the steam reformer in a heat exchanger to a temperature between 350°C and 500°C and conduct the reaction over a catalyst composed of finely divided oxides of iron and chromium formed into tablets. The resulting reformate gas is then cooled once again to a temperature between 200°C and 250°C and reacted over a catalyst based upon mixed oxides of copper and nickel. An example of this approach is given in U.S. 5,360,679 to Buswell, *et al*. In cases where an exceptionally pure hydrogen product is required, the temperature of the low-temperature shift converter is controlled by including a heat exchanger in the reactor itself, and an example of this approach is given in U.S. 5,464,606 to Buswell, et al. In all cases, the low temperature shift converter is quite large because of the poor catalyst activity at low temperatures.

In conventional systems, subsets of the process components are connected to one another via external plumbing; each component of the process being typically referred to as a "unit process," in the chemical engineering literature. This approach is preferred in large, industrial units because standard hardware may be used. Owing to the large size of industrial units, the unit process approach also makes shipping of the components to the site of the installation feasible, as combinations of the components are sometimes too large to be transported by road or rail.

For systems producing less than 1 ton per day, however, the unit process approach has many disadvantages. The first disadvantage is the high proportion of the total system mass dedicated to the hardware and plumbing of the separate components. This high mass increases

startup time, material cost, and system total mass, which is undesirable for mobile applications such as powerplants for vehicles.

Another disadvantage of the unit process approach in small systems is the complexity of the plumbing system to connect the components. The complexity increases the likelihood of leaks in the final system, which presents a safety hazard, and also significantly increases the cost of the assembly process itself. Moreover, the requirement that each component have its own inlet and outlet provisions also adds considerable manufacturing cost to the components themselves.

A third disadvantage is the high surface area of the plumbing relative to the unit process hardware itself, which means that a disproportionately large amount of heat is lost through the connecting plumbing in small scale systems. This can drastically reduce the thermal efficiency of the system and adds cost and complexity associated with adequately insulating the plumbing system.

A fourth disadvantage to the unit process approach in small-scale systems is that this approach requires a large volume to package, as each component and its associated plumbing must be accessible for assembly and maintenance purposes. This is particularly disadvantageous in space-sensitive applications such as building fuel cell power stations, fuel cell vehicle refueling stations, and fuel cell mobile powerplant hydrogen generation.

Hydrogen is typically separated from the other reaction products using pressure swing adsorption (PSA) technology. The design of these PSA systems is largely dictated by the catalyst chemistry employed in the steam reformer and the low-temperature water-gas shift reactor. These catalysts, typically based on nickel metal in the former and copper in the latter case, are extremely sensitive to poisoning and deactivation by sulfur or molecular oxygen. Thus, the incoming feed gas must be carefully treated to remove these materials. Further, the system must protect the catalysts against these agents during startup, shut-down, and during intervals when the system is shut down. Especially in the case of molecular oxygen, exposure of the active catalyst can lead to catalyst damage and even create a safety hazard through pyrophoric oxidation of the finely-divided base metal catalysts.

Several steps are necessary in conventional systems to prevent damage to the reforming and Low Temperature Shift (LTS) catalysts.

(1) During operation, the incoming fuel must be treated to remove both sulfur and molecular oxygen. Sulfur in particular is generally reduced below 1 part per million, and more preferably below 100 parts per billion. This is typically achieved through a combination of a partial oxidation to remove oxygen followed by a hydrodesulfurization (HDS) process. Such systems typically require recycle of high-temperature, hydrogen-rich product gas to the inlet through the use of a gas compressor or a fluid ejector as exemplified by U.S. 3,655,448 to Setzer, U.S. 4,976,747 to Szydlowski and Lesieur, and U.S. 5,360,679 to Buswell, et al. Because accurate temperature control is required for the HDS reaction, several heat exchangers as well as active temperature control logic circuits and flow control valves are also required. Provision of

these reactors, heat exchangers, valves, as well as sensors and controls adds significantly to the complexity of conventional systems.

(2) Startup of conventional system requires bringing all of the components to near operating temperature, usually while blanketed in inert gas, then carefully initiating the reaction. Before the system is at operating conditions, full removal of sulfur and molecular oxygen is not guaranteed, so the process feed gas must be vented to the atmosphere, wasting fuel, generating air pollution, and creating a potential safety hazard while further increasing system complexity. Because the added components for fuel pretreatment add significant mass to the system, they also extend the warmup time required for hydrogen production. In situations with a variable hydrogen demand, this can create a need for extensive onsite hydrogen storage to supply the hydrogen demand while the system reaches operating conditions.

(3) During shutdown and periods when the conventional system is not operating, the reaction system is typically purged with inert gases under pressure. Alternatively, substantially leak-tight valves must be supplied to prevent ingress of atmospheric air to the unit with the resultant catalyst deactivation/damage.

For large-scale applications the added cost/complexity of the conventional systems does not adversely affect the system economics. When this traditional approach is applied to small-scale systems, however, the relative cost of these added components becomes disproportionately large, and the resulting hydrogen cost is dominated by the cost of the system. Accordingly, it is not advantageous to simply scale down large scale systems if a small scale system is desired.

Conventional steam reformer systems for natural gas and other light hydrocarbons fall into two broad classes. In the first, the reactors are operated at or near ambient pressure at low temperatures (typically less than 650 °C). This is typical of conventional systems designed for small-scale applications producing impure hydrogen. For pure hydrogen to be produced, the reformer product must be compressed to high pressure for subsequent cleanup via PSA, metal separation membranes, or other conventional techniques. Because steam reforming creates additional moles of gas, the compression of the product gas is very energy-intensive and requires expensive and complicated compression and intercooling equipment. The second class of reformers is typically used in large-scale applications and is operated at high pressures (often above 20 bar). Because of the thermodynamics of the steam-reforming reaction, these high pressure reactors must be operated at much higher temperatures, often approaching 900°C, to attain adequate conversion of the hydrocarbon fuel to hydrogen. The higher temperatures and pressures require the use of more expensive materials of construction than are employed in the low-pressure systems, but this is more than offset by the reduction in reactor volume obtained due to enhanced chemical reaction rates. Unfortunately, in small-scale systems, the provision of compression and pumping equipment to deliver the reactants into a high-pressure (20 bar or higher) reactor can undesirably increase the cost of such a system.

Conventional pressurized steam reformer systems often are operated with very high temperatures in the combustion products used to heat the endothermic reaction zone. This high temperature allows a reduction in the amount of heat transfer area required to complete the reaction, and thus a reduction in reformer cost. Often, the mode of heat transfer to the wall of the

tubes in the conventional reformers is a combination of radiation and convection, with the combustion carried out in a conventional premixed or diffusion-flame burner. The operation of the primary steam reformer with such high gas temperatures can lead to significant excursions in the reformer tube wall temperature due either to poor control of the distribution of the hot gases or to poisoning of the reforming catalyst. If the catalyst for the endothermic steam-reforming reaction is locally-poisoned, the heat flux from the combustion products to the wall can form a local "hot spot." In either case, the increase in the reformer wall temperature can lead to premature reformer structural failure, presenting both a safety and an operational liability.

Conventional systems for hydrogen generation through steam reforming of hydrocarbons have several inherent deficiencies which make them ill-suited to economical small-scale hydrogen production. The first is the requirement for strict control of sulfur and molecular oxygen concentrations in the steam reforming and LTS reactors. The second concerns the problems with operation in the ambient pressure regime where the large volume of reformate gas must subsequently be compressed prior to purification. The third is associated with operating the reactor in the high-pressure regime typical of large-scale units where appropriate compression and pumping equipment adds considerable cost at small scales. The final shortcoming is the risk of overheating the steam-reforming reactor structure due to the very high gas temperatures employed in the combustors in conventional systems and their reliance on radiant heat transfer, especially in high-pressure systems as employed in large-scale applications.

It has been recognized previously that integrating the elements of the unit process more closely beneficially reduces heat losses and improves compactness. U.S. 5,516,344 to Corrigan describes a steam reforming system wherein the unit process elements are integrated into a common mounting rack having a reduced requirement for insulation and having improved compactness. This approach, however, undesirably retains the multiple connections and extensive plumbing characteristic of the unit process approach. Moreover, because of its complicated packaging, the assembly of the Corrigan system undesirably presents a significant challenge.

Another attempt at improving compactness is described in U.S. 5,733,347 to Lesieur, wherein the primary reforming reactor and the catalytic burner are integrated into a planar reactor with compact heat transfer surfaces. This reactor requires separate heat exchangers to cool the gas after the primary reformer, as well as separate reactors for the water-gas shift. These all require interconnections, as do the array of planar reactors envisioned by Lesieur. These connections once again present the same drawbacks found in unit process reactor systems.

SUMMARY OF THE INVENTION

Accordingly, one object of the present invention is to provide a reactor for hydrogen production that avoids the problems associated with conventional systems.

Another object of the present invention is to provide a reactor for hydrogen production that is suitable for applications where less than 15,000 standard cubic feet per hour of hydrogen are required.

Another object of the present invention is to provide a reactor for hydrogen production that is safer and more cost efficient than conventional systems.

Another object of the present invention is to provide a reactor for hydrogen production that is less complex and is more space-sensitive than conventional systems.

Another object of the present invention is to provide for the production of hydrogen from a hydrocarbon fuel such as natural gas, propane, naphtha, or other hydrocarbons low in sulfur content (< 100 ppm sulfur by mass).

Another object of the present invention is to produce hydrogen which is substantially pure (>99.99%) by separating impurities using a pressure swing adsorption (PSA) system.

Another object of the present invention is the provide for the elimination of the pretreatment of the fuel feed to the steam reformer for the removal of sulfur and molecular oxygen.

Another object of the present invention is the provide for the operation of the system in a mesobaric regime, between 4 and 18 atmospheres, where appropriate fluid compression devices of small capacity, low cost, high efficiency and high reliability are readily available, and the resultant thermal efficiency of the hydrogen production system is very high.

Another object of the present invention is to provide for the feedback control of the delivery of fuel and/or air to a catalytic combustor in proportions such that the peak temperature of the gases entering the primary steam reformer does not exceed a safe maximum temperature determined by the metallurgy of the steam reformer.

Another object of the present invention is to provide for the operation of a steam reforming system without a low temperature water-gas shift reactor.

Another object of the present invention is to provide for the operation of a hydrogen production system with feedback control of product carbon monoxide content.

Another object of the present invention is to provide a process having a simplified system construction, operation, and control resulting in low cost and relatively fast start-up and shut-down.

These and other objects have been achieved by the present invention, the first embodiment of which provides a reactor, which includes:

a unitary shell assembly having an inlet and an outlet;

a flow path extending within the shell assembly from the inlet to the outlet, the flow path having a steam reformer section with a first catalyst and a water-gas shift reactor section with a second catalyst, the steam reformer section being located upstream of the water-gas shift reactor section;

a heating section within the shell assembly and configured to heat the steam reformer section; and

a cooling section within the shell assembly and configured to cool the water-gas shift reactor section.

Another embodiment of the present invention provides a reactor for the production of hydrogen from at least one selected from the group including natural gas, propane, liquefied petroleum gas, alcohols, naphtha, hydrocarbon fuels and mixtures thereof, the reactor including:

a unitary shell assembly having an inlet and an outlet;

a flow path extending within the shell assembly from the inlet to the outlet, the flow path including a convectively-heated catalytic steam reformer and a convectively-cooled water-gas shift reactor.

Another embodiment of the present invention provides a method for producing hydrogen, which includes:

feeding at least one fuel selected from the group including natural gas, propane, liquefied petroleum gas, alcohols, naphtha, hydrocarbon fuels and mixtures thereof, into a reactor which includes a unitary shell assembly having an inlet and an outlet, and a flow path extending within the shell assembly from the inlet to the outlet, the flow path including a convectively-heated catalytic steam reformer and a convectively-cooled water-gas shift reactor, whereby hydrogen is produced.

Another embodiment of the present invention provides a method for producing hydrogen from at least one fuel selected from the group including hydrocarbon fuel, natural gas, propane, naphtha, hydrocarbons with < 100 ppm sulfur by mass, and mixtures thereof, which includes:

producing hydrogen by steam reforming the fuel; and

substantially purifying said hydrogen with a pressure swing adsorption (PSA) system;

wherein prior to the producing, no pretreatment of the fuel to remove at least one impurity selected from the group including sulfur and molecular oxygen and mixtures therof is carried out.

BRIEF DESCRIPTION OF THE FIGURES

Various other objects, features and attendant advantages of the present invention will be more fully appreciated as the same becomes better understood from the following detailed description when considered in connection with the accompanying drawings in which like reference characters designate like or corresponding parts throughout the several views and wherein:

Figures 1a and 1b are schematics of two preferred embodiments of the reactor flow geometry on both the tube-and-shell-sides. Figure 1b differs from Figure 1a in that it has an integral catalytic burner.

Figure 2 shows a preferred embodiment of the reactor of the present invention without an internal catalytic burner and without extended surfaces on the tubes in the tubular array, which is provided with baffles to create a multi-pass cross-flow geometry in the shell-side fluid pathway.

Figure 3 shows a preferred embodiment of the reactor of the present invention with plate fin heat exchange surfaces attached to the tubes on the shell-side and an adiabatic water-gas shift reactor zone placed after the convectively cooled water-gas shift reactor zone. This figure also illustrates the preferred combination of extended tube surfaces and baffles.

Figure 4 shows a preferred embodiment of the reactor of the present invention without baffles, and with shell-side extended surface comprising loose packing material. This figure also shows one manifestation of a catalytic burner included within the reactor shell. Figure 4 also depicts an outer housing and insulation system.

Figure 5 is a schematic of the hydrogen production system of a preferred embodiment of the present invention.

Figure 6 is a logic diagram for a preferred combustor outlet temperature control apparatus of the present invention.

Figure 7 is a logic diagram for a preferred gas purity control apparatus of the present invention.

Figure 8 illustrates a computer system upon which a preferred embodiment of the present invention may be implemented.

DETAILED DESCRIPTION OF THE PREFERRED EMBODIMENTS

Various other objects, features and attendant advantages of the present invention will be more fully appreciated as the same becomes better understood from the following detailed description of the preferred embodiments of the invention.

Preferably, according to one embodiment of the present invention, an integral reactor for the production of hydrogen from natural gas, propane, liquefied petroleum gas, alcohols, naphtha and other hydrocarbon fuels and mixtures thereof is provided where several components of the process system are combined into a single mechanical structure. These components will preferably include a convectively-heated catalytic steam reformer, a cooler for the reformate product from the steam reformer and a convectively-cooled water-gas shift reactor. The reactor may additionally and optionally include a preheat section to heat the inlet feeds. The packing of this preheat section may additionally and optionally serve as a sulfur absorbent bed. The reactor may additionally and optionally include an adiabatic water-gas shift reactor appended to the exit of the convectively cooled water-gas shift reactor.

Preferably, the reactor of present invention includes a tubular array wherein the fuel and water to be reformed flow through the tubes, and the cooling and heating fluids flow outside the tubes, with a single reforming side inlet tube header and a single reforming side outlet tube

header. The interior of these tubes is preferably provided with a catalyst in the form of a coating, a monolith, or as a loose packing of pellets, extrudates or the like. Preferably, the reactor also includes a shell assembly, with a means of thermal expansion relief, one or more inlets for a cooling medium for the water-gas shift reactor, and one or more outlets for the hot combustion product. The reactor shell assembly may additionally and optionally have one or more outlets for heated coolant for the water-gas shift reactor and one or more inlets for the hot combustion product to heat the steam-reforming reactor.

Preferably, the reactor tube array surface area may be enhanced on the shell-side of the tubes for the purposes of aiding heat transfer between the shell-side fluid and the tube walls. The surface augmentation may be accomplished through the use of twisted tubes, finned tubes, rifled tubes, plate fins, by means of a loose packing material, or by other means apparent to one skilled in the art.

Another preferred embodiment of the invention provides that the fluids flowing outside the tubes in the shell-side may be forced to flow across the tubular array, substantially normal to the axis of the tubes, by baffles. These baffles may be employed with or without the surface area enhancements which are another embodiment of the present invention.

Another preferred embodiment of the present invention provides that a catalytic burner may be incorporated in the shell-side of the reactor assembly. This catalytic burner may be provided with one or more inlets for fuel delivery. This burner may also be provided with a means of mixing the fuel and heated air. This burner may also be provided with a means of preheat and/or ignition. This burner may also be provided with one or more temperature sensors.

Preferably, the steam-reforming catalyst is resistant to poisoning by sulfur and molecular oxygen.

Preferably, the water-gas shift catalyst is resistant to poisoning by sulfur.

Preferably, the reactor includes an outer housing and insulation assembly.

Referring to Figure 1a, one embodiment of the overall flow geometry of the reactor of the present invention is provided with an inlet on the tube-side for entry of vaporized, mixed water and fuel, which flow through a first region packed with steam-reforming catalyst, where catalytic steam reforming takes place, and a second region packed with water-gas shift catalyst, where the water-gas shift reaction takes place, after which the reformed gases exit the reactor. A second fluid stream enters the shell-side near the outlet of the tube-side, and flows generally in counterflow to the reformate flowing through the tube-side. This second fluid stream is lower in temperature than the exiting reformate, and it removes heat from the water-gas shift portion of the tube-side of the reactor. In the embodiment of Figure 1a, the heated air then exits the shell-side through an outlet port and is conveyed to an external catalytic combustor, where the heated air is mixed with one or more fuel streams and combusted over a catalyst or in a conventional burner. The hot combustion product is then returned to the shell-side of the reactor, where the hot combustion product convectively heats the lower temperature reformate in the steam reformer section of the tube-side.

Another preferred embodiment of the overall flow geometry of the present invention is shown in Figure 1b, which differs from that of Figure 1a in that the catalytic combustor is located within the shell-side of the reactor. In the embodiment of Figure 1b, the fuel for the combustor is introduced into the shell-side fluid flow, and the fuel-air mixture is combusted on a catalyst, which is located inside the reactor shell and intimately in contact with the reactor tube walls.

Referring to Figure 2, the preferred reactor of the present invention has an inlet for mixed, pre-vaporized fuel and steam 1, which communicates with a plenum 2, which distributes the mixture to the array of reactor tubes 3. These reactor tubes are mounted to the inlet tube header 4 by welding, brazing, swaging or other processes capable of creating a leak-tight joint in the materials of construction. Most preferably, the reactor tubes 3 are joined to the inlet header 4 by brazing or welding. The reactor tubes are provided, as is illustrated in the cut-away view of Figure 2, with a charge of steam-reforming catalyst material 5. This catalyst material 5 may be a loose packing as illustrated, or may be a catalytic coating, or may be a section of monolithically-supported catalyst. Such coated, packed bed, or monolithic catalyst systems are well known to those skilled in the art. The reactor tubes are also provided with a water-gas shift catalyst 50, which is located downstream from the steam-reforming catalyst, 5. The tubes 3 are further joined to a outlet tube header 6 by processes similar to those for attaching the tubes to the inlet header 4. The outlet tube header 6 communicates with an outlet plenum 7, which delivers the reformate product to an outlet port 8. The reactor tubes 3 pass through holes in one or more baffles 9, which share the same geometrical pattern of holes as the inlet and outlet headers 4 and 6. The spacing between these baffles is governed by the allowable pressure drop and required heat transfer rate on the shell-side of the reactor. The baffle spacing may be different in various portions of the reactor. The baffles 9 shown in Figure 2 are chorded to allow fluid to flow around the end of the baffle and along the tube axis through a percentage of the cross-sectional area of the shell. The baffles are chorded between 50% and 10%; more preferably they are chorded between 40% and 15%, most preferably they are chorded between 30% and 20%. The direction of the chorded side alternates by 180 degrees such that fluid is forced to flow substantially perpendicular to the long axis of the tubes 3. Alternative baffle designs are apparent to one skilled in the art and are included within the scope of the present invention. Preferred examples of alternative baffle designs include baffles chorded in more than one location, circular baffles of alternating ring and circle shapes, and wedge-shaped baffles.

The baffles fit with a close tolerance to allow a sliding fit to the shell assembly 10. The shell assembly is secured to either one or both of the inlet and outlet headers by welding, brazing, swaging, or other methods which are apparent to one skilled in the art. The close tolerance fit between the baffles and the shell is chosen such that the baffles will not bind against the shell wall during assembly and operation while still minimizing leakage between the baffles and the shell wall. If the shell 10 is rigidly secured to both headers it is especially preferable to provide a means for relative thermal expansion and contraction between the reactor tubes and the shell to occur without undue restraint. In Figure 2 thermal expansion is provided for by a corrugated tube or bellows 11. If the shell is fixed to only one header, relative expansion may be provided for with a sliding fit and seal system between the shell bore and the outer surface of the other reactor header to minimize leakage while allowing free thermal expansion of the tubular

array. Other means of providing free thermal expansion of the tube array will be apparent to one skilled in the art, and are included within the scope of the present invention.

The reactor of Figure 2 employs the overall flow geometry of Figure 1a, and is thus provided in the shell-side of the water-gas shift section with a cold air inlet 12 as well as a hot air outlet 13. Most of the shell-side air is prevented from bypassing the hot air outlet 13 by an unchorded baffle 14, which fits snugly against the shell assembly 10 inner wall. The reactor is further provided in the shell-side of the steam reforming section with a hot combustion product inlet 15 and a cooled combustion product outlet 16. The inlets and outlets are depicted as single tube sections in Figure 2, but it must be understood that other inlet and outlet types are possible, including ring manifolds and multiple tube fittings. Such alternative embodiments may be advantageously employed to reduce thermal stresses in the tubes, to modify heat transfer characteristics, or for other purposes apparent to one skilled in the art.

The reactor of Figure 2 is provided with an external burner assembly 18. In the embodiment of Figure 2 this burner assembly is a catalytic burner with catalyst zone 22, and it will be understood that alternative burner designs are known in the art which employ premixed or diffusion burning or combinations thereof. Other preferable types of burners are also apparent to one skilled in the art, and it is intended that the choice of external burner shall not limit the reactor of the present invention. The external burner assembly 18 is provided with at least one fuel injection port 19. The air inlet may additionally be provided with at least one air preheater element 23. This preheater element may alternatively be replaced or augmented with a pilot light, a spark ignitor, or an electrically heated catalyst. These and other modifications to the burner assembly are apparent to one skilled in the art.

The tubes 3 are preferably filled with at least two catalyst systems. In the steam reforming zone, a catalyst 5 active for steam reforming is used, while in the water-gas shift zone a catalyst 50 active for water-gas shift but substantially inactive for methanation is employed. These catalyst systems may be in the form of surface coatings, a packed bed of loose particles, or as a monolithically-supported catalyst of the shape of the inside of the tubes. Most preferably the catalyst is either coated or is in the form of a packed bed. In Figure 2, the catalyst is a packed bed of loose particles retained between the inlet and outlet headers by catalyst support screens 17. Prior to the steam reforming zone, a zone of chemically inert packing may be provided as a heat transfer media only. In this configuration, the reactants may be preheated in order to bring their temperature to a level where the catalytic steam-reforming reaction occurs at a meaningful rate. An preferred embodiment of the present invention replaces the inert packing in this preheat zone with a sulfur absorbent such as zinc oxide. This sulfur absorbent can serve as a guardbed to protect the steam-reforming catalyst from poisoning by sulfur.

In a preferred embodiment, the steam-reforming catalyst is capable of operation in the presence of less than 100 ppm of sulfur by mass in the fuel feed and is insensitive to the presence of molecular oxygen in the fuel feed. More preferably, the catalyst is capable of being shut down from operation and restarted without the use of reducing or inert gas. Most preferably, the catalyst active metal is chosen from one or more of those in group VIIIB of the periodic table, incorporated herein by reference. Examples of the preferred metals are ruthenium, rhodium, iridium, platinum and palladium. These metals are preferably supported on a ceramic support of

high surface area. Preferred examples of supports are oxides of aluminum, zirconium and magnesium, as well as mixed oxide spinels such as calcium aluminate, nickel aluminate or magnesium aluminate. Other ceramic supports will be apparent to one skilled in the art and are included in the scope of the present invention.

In a preferred embodiment, the water-gas shift catalyst is capable of operation in the presence of less than 100 ppm of sulfur by mass in the fuel feed and can be started in the presence of partially reacted mixtures of fuel and water, i.e. reformate from the steam-reforming reactor. The catalyst also preferably does not require inert gas for shutdown. An example of a preferred catalyst is a finely divided mixture of oxides of iron and chromium, marketed as high temperature water-gas shift, or "ferrochrome" catalyst. A second example of a preferred catalyst includes platinum supported on aluminum oxide, with or without promotion by oxides of cerium or other metal oxides.

Referring to Figure 3, a preferred embodiment of the reactor of the present invention is depicted which employs both baffles 9 as in Figure 2 as well as extended heat exchange surfaces on the outer walls of the reactor tubes 3. In this case, a plurality of closely-spaced plate fins 20 are provided. These fins may be bonded to the reactor tube by brazing, or more preferably by hydraulically expanding the tubes 3 into close contact with the plate fins 20. The plate fins, like the baffles 9, also have a pattern of holes which is identical to that in the inlet and outlet headers.

Figure 3 also shows an adiabatic water-gas shift reactor 21 appended to the outlet tube header 6. This reactor increases the volume of catalyst accommodated without increasing the usage of the expensive metal alloy reactor tubing. The additional catalyst volume can be used to better approach the equilibrium conversion of the water-gas shift reaction at the outlet temperature conditions. This is typically desired when the outlet temperature of the reformate from the water-gas shift reactor is below 400°C.

Figure 4 shows a preferred embodiment of the reactor of the present invention wherein the overall flow geometry is that of Figure 1b. In this embodiment the shell-side is packed with a loose packing material to provide extended surface area for the tubes 3. It should be understood that other types of extended surfaces are possible, such as finned tubes, rifled tubes, twisted tubes, and combinations thereof. All of these eliminate the possibility of using baffles in conjunction with the extended surface area, whereas plate fins and loose packing do not. It should be noted that in the embodiment of Figure 4 baffles are not employed, and the overall flow is substantially parallel to the axis of the tubes 3. The embodiment of Figure 4 also includes a catalytic burner integrated within the reactor shell. The catalytic burning is accomplished by a zone of packing 29 which is catalyzed with an appropriate combustion catalyst, such as mixtures of palladium and platinum supported on a ceramic support. The size of this catalyzed zone is chosen to meet the requirements of the specific application, and may fill the entire reactor shell above the unchorded baffle 14. Alternatively, the unchorded baffle 14 may be omitted, and the heated air from the water-gas shift zone may proceed directly to the steam reforming zone where catalytic combustion will occur.

Near the shell-side inlet 15 to the catalytic combustion zone there is a fuel distribution assembly 24, which allows fuel to be introduced into the catalytic combustion zone.

Alternatively, and preferably, the combustion zone may be provided with more than one fuel distribution assembly 24, which may be employed to control the temperature profile in the combustion zone. It should be understood that any number of configurations for this fuel distribution assembly are possible and may be employed in the reactor of the present invention. The one or more fuel distribution assemblies 24 are provided with a fuel feed controller 25, and the reactor is provided with at least one temperature sensor 26 to be used in control of the combustion temperature. The temperature sensor 26 is illustrated as located at the shell of the reactor, but may be alternatively located in a thermowell located in a reaction tube or at other locations within the reactor. The intimate contact between the catalyst and the reactor tubes allows very good heat transfer, but makes temperature control more difficult as well. Another preferred embodiment of the present invention replaces the loose, catalyzed packing with a catalyzed monolith provided with a pattern of holes which are larger than the reactor tube outer diameters. This type of monolithic combustion catalyst, because it is aligned by the shell assembly, and does not contact the reactor tubes, will pose less of a danger to overheating the reactor tubes and causing the formation of hot spots. Even if the monolithic combustion support did contact the tube walls locally, hot spotting would be less likely as combustion is distributed throughout the monolith volume, rather than being localized only at the tube wall.

Figure 4 also depicts an outer housing 27 that can be constructed to extend over the entire outer surface of the insulation system 28 or a portion thereof, and which is only depicted over a small segment of the insulation system 28. The insulation system may be constructed from one or more layers of insulation materials, and may be either rigid or flexible. The precise amount and type of insulation employed is dependent upon a variety of factors such as allowable heat loss, maximum surface temperature of the outer housing 27, and the mode of structural support for the reactor. These variables do not materially affect the performance advantages of the reactor of the present invention, and any number of possible insulation configurations are considered within the scope of the present invention. The outer housing 27 also does not materially affect the operation of the reactor and is designed instead based upon factors such as structural requirements, environmental conditions, and aesthetics. Thus, any number of configurations for the outer housing are considered within the scope of the present invention.

Several surprising and unexpected advantages of the reactor of the present invention are apparent when it is compared to the conventional systems.

The first advantage is the great simplification in the construction of the reactor system afforded by combining the steam reforming and water-gas shift reactors and their associated heat transfer functionalities into a single mechanical device. This eliminates the requirement for separate inlet and outlet zones, fittings, and interconnecting plumbing. This advantage is even further evidenced in systems incorporating the feed preheat function and/or the internal catalytic burner. In small hydrogen generation applications (< 15,000 scf/hr or 1 ton per day), this reduction in physical components and interconnects can greatly reduce the cost of the completed system.

A second advantage is the great reduction in heat loss achieved by the reactor of the present invention when compared to the unit process approach of the conventional systems. In part because the number of fittings and interconnecting plumbing is decreased in the novel

reactor of the present invention, the amount of heat transfer surface with the ambient environment is greatly diminished. Consequently, the heat lost to the ambient environment is desirably proportionally reduced. This heat loss can otherwise undesirably form a large energy requirement in conventional small-scale, hydrogen-generating reactors. The reduction in heat loss achieved by the present invention leads to a higher energy efficiency of the reactor and a faster warmup time. Additionally, the low heat loss of the reactor of the present invention allows it to be maintained in a hot condition for extended periods of time without generating hydrogen and without consuming much fuel, which desirably makes "hot standby" of the novel reactor more practical than in conventional reactors.

A third advantage of the reactor of the present invention is its ability to start up from a cold condition more rapidly than conventional reactors. This is believed to be due to both the lower structural weight of the reactor and its lower heat loss when compared to conventional discrete reactors and heat exchangers. The rapid warmup capability allows the reactor of the present invention to be operated intermittently without excessive penalties in warmup time or warmup fuel usage.

Preferably, the present invention is carried out without pretreatment of the fuel feed to the steam reformer for the removal of sulfur and molecular oxygen. Pretreatments which are preferably excluded from the present invention include any or all of partial oxidation, hydrodesulfurization, adsorption, or absorption. Other such pretreatment methods known to one of ordinary skill in the art are preferably excluded as well.

Low-pressure water and hydrocarbon fuel are admitted to separate or combined fluid compression devices; and they are subsequently heated to their vaporization points and admitted to a primary steam-reforming reactor. This steam-reforming reactor is provided with a catalyst which is resistant to poisoning by both sulfur and molecular oxygen, and is preferably based upon catalytically-active group VIIIB metals such as ruthenium, rhodium, iridium, platinum, palladium or combinations thereof supported on a ceramic support of high surface area. In this primary steam-reforming reactor, the vaporized fuel and steam are further heated by a separate stream of hot combustion product which is separated from the reactants by the walls of the reactor, which also form heat exchange surfaces. These heated gases are then encouraged to react by the aforementioned catalyst to form a hydrogen-rich product gas with a composition near its equilibrium value at the reactor outlet conditions. This hydrogen-rich gas is then cooled and passed over a second catalyst which is also sulfur resistant, and is active for the water-gas shift reaction while being substantially-inactive for the reverse of the steam-reforming reaction, the methanation reaction. An example of such a catalyst is a finely divided mixture of oxides of iron and chromium, which is well-known in the art as "high temperature" water-gas shift or "ferrochrome" catalyst. The hydrogen rich gas stream has much of its carbon monoxide converted to carbon dioxide and hydrogen in the water-gas shift reactor, and exits with a carbon monoxide concentration between 0.3% and 4%, at a temperature above 200 °C.

In conventional systems, a further low-temperature water-gas shift reactor is provided, whereas in the system of the present invention no such reactor is provided, as an active, sulfur-tolerant catalyst operable at such low temperatures is not easily made. The product gas mixture is then further cooled either by heat exchange with ambient air or cool water or by quenching

with cool water in an evaporative cooler. Condensed water is then removed from the gas via a separator, and the thus partially-dried gas mixture is admitted to the PSA purification system. In the PSA system, impurities are adsorbed from the gas while the product hydrogen is delivered at a high purity and at an elevated pressure (slightly below the steam reformer pressure). The impurities are then purged with a small portion of the hydrogen product at low pressure and are delivered as a fuel to a catalytic combustor, which is provided with an exit temperature sensor and a means of controlling the rate of admission of air. The rate of air admission is thus controlled such that the exit temperature from the combustor is below the maximum allowable temperature of the reformer metallurgy. This hot combustion product is then ducted to a heat transfer interface in the steam reformer to provide heat for the endothermic reaction therein to proceed. The combustion product, at a reduced temperature, may then be used to heat and vaporize the pressurized water and, if desired, fuel streams.

As described below, the rate of air admission is controlled by a feedback loop based upon the outlet temperature of the catalytic combustor. The calorific value of the low-pressure mixed fuel gas expelled from the PSA system is determined by the degree of hydrogen purity required. A feedback control system based upon a product carbon monoxide sensor based on either infrared or electrochemical principles will be used to set the rate at which the PSA system purges itself of contaminants. When high purity is desired, a high purge rate is employed and the calorific value of the low-pressure gases is high. When less stringent purity is required, the rate of purging may be lower, and the calorific value of the purged gases may be correspondingly lower. Indeed, the purge rate may be reduced to a point where the calorific value of the purge gas is too low to sustain the reactor temperature, at which point unreacted hydrocarbon fuel may be provided from a valve to make up the deficit. Whereas the carbon monoxide concentration is of special significance for fuel cell applications, in other applications it is understood that another impurity may be more critical, and feedback based upon concentrations of that species may accordingly be employed.

Referring to Figure 5, the hydrogen production system of the present invention can process hydrocarbon fuels such as natural gas, town gas, refinery off-gas, propane, liquefied petroleum gas, naphtha, alcohols or any other hydrocarbon fuel with a sulfur content less than 100 parts per million (ppm) by mass. Natural gas or liquified petroleum gas are preferred. More preferably, the sulfur content is less than 75 ppm, most preferably, the sulfur content of the fuel is less than 50 ppm. The second feed to the system is water, which is subsequently chemically reacted with the fuel to yield hydrogen. This water feed must be conditioned to remove particles, organics, and ionized species. This may be achieved using methods apparent to one skilled in the art. The molar ratio of the water to the fuel is such that the ratio of water molecules to carbon molecules is between 2.5:1 and 8:1. More preferably, the ratio is between 3:1 and 5:1.

The water feed to the system is pressurized using an appropriate pump 66 to a pressure greater than the operating pressure of the system, which is preferably 4 atm to 18 atm. The pressurized water is then admitted to a heat exchanger 84 where it is heated by a second fluid, which is the cooled combustion product exhausted from the steam-reforming reactor hot side 60. It must be understood that this heat exchanger may include more than one individual unit, and that alternative strategies may be employed to heat the feed water such as by removing heat from the hot hydrogen-containing gas exiting the water-gas shift reactor 62, or from other high

temperature streams in the system. Irrespective of the exact arrangement of the heat exchange means, sufficient energy is transferred to the water to cause it to vaporize and allow it to be mixed with the fuel at 56.

The fuel is pressurized using compressor 54. This device may be a pump if the fuel is a liquid, and may also be replaced and/or augmented by a steam ejector employing pressure energy stored in the vaporized water to pressurize the fuel. The fuel is mixed with the vaporized water at 56. The resulting pressure of the mixed fuel and water preferably exceeds that of the steam-reforming reactor 58, which is between 4 atm and 18 atm. This requires that sufficient energy be imparted to one or more of the fluids to maintain the resulting mixture in the vapor phase at the steam-reforming reactor inlet. This may require the addition of an evaporator for a liquid fuel, or may be achieved through superheat of the vaporized water.

The steam-reforming reactor includes a high pressure, cold side 58 wherein is disposed a quantity of catalytically active material as well as a lower pressure, hot side 60. The mixed, vaporized fuel and water enter the cold side 58 and are heated by the hot combustion product which flows through the hot side 60. These fluids are prevented from mixing by the shared structure of the reactor, which forms a heat exchange surface, or a plurality of heat exchange surfaces. The pressure of the fluid in the cold side of the reactor is between 4 atm and 18 atm. More preferably, the pressure is between 5 atm and 15 atm. Most preferably, the pressure is between 10 atm and 15 atm. The catalyst disposed in the cold side of the reactor is resistant to both the adsorption of sulfur compounds and oxidation by both steam and molecular oxygen. The catalyst preferably includes an active metal or mixture thereof supported upon a ceramic support material of high surface area. Preferably the catalyst active metal or metals is selected from the group VIIIB metals of the periodic table, incorporated herein by reference. Most preferably the catalyst active metal includes one or more of the following group VIIIB metals singly or in combination; ruthenium, iridium, rhodium, platinum and palladium. The temperature of the reacting mixture is increased in the steam reformer. The exit temperature of the heated reformate, or hydrogen rich mixture, depends upon the fuel, pressure, steam-to-carbon ratio and metallurgy of the reactor. The exit temperature from the cold side 58 is preferably between 500°C and 900°C. More preferably, the temperature is between 600°C and 800°C. Most preferably, the temperature is between 700°C and 800°C.

This heated reformate gas passes from the cold side 58 of the steam reformer to the hot side 62 of the water-gas shift reactor, part or all of which is cooled by cooler, lower pressure air flowing through the cold side of the water-gas shift reactor 64. Like the steam reformer, the water-gas shift reactor is thus provided with one or more heat transfer surfaces for transferring heat between these two fluids. Alternatively, the hot gases may be partially or completely cooled to the water-gas shift reactor temperature before being admitted to its hot side 62. A catalyst active for water-gas shift and inactive for methanation is disposed within the hot side of the water-gas shift reactor 62. This catalyst must also be resistant to poisoning by sulfur compounds. An example of a commercially-available catalyst is a finely divided mixture of oxides of iron and chromium which is formed into pellets or tablets. The gas exiting the water-gas shift reactor hot side 62 is preferably greater than 200°C in temperature. More preferably, the gas is greater than 250°C and less than 400°C in temperature. Most preferably the gas is greater than 275°C and less than 350°C.

The hot, hydrogen rich reformate is then passed through a cooler 68. This is depicted in Figure 5 as being cooled by cool external air from a fan. Alternatively, the cooling may be accomplished via a series of heat exchangers including heating the water feed to the system and cooling with air. Alternatively, the reformate may be cooled by heat exchange with cool water. Alternatively, the reformate may be cooled through the use of an evaporative chiller using directly injected water. These embodiments may also be combined in a variety of configurations apparent to one skilled in the art, which do not in any way limit the scope of the present invention. The reformate exits this cooler 68 at a temperature below 100°C. More preferably, the temperature is between 80°C and 25°C. Most preferably the temperature is between 60°C and 30°C. Because the reformate gas is pressurized, the cooling will cause some portion of the water vapor to condense. This condensed water vapor, and any condensed fuel residuals, is then removed in a condensate separator 74.

The partially dried reformate is then admitted to the Pressure Swing Adsorption (PSA) system 72. PSA systems are known to those skilled in the art. The PSA system 72 removes impurities from the reformate, thus delivering a substantially pure hydrogen product at a pressure slightly lower than the reactor pressure due to pressure drop. The contaminant species are purged from the PSA system 72 using some of the pure hydrogen product. This purge gas is rejected at lower pressure than the hydrogen is delivered as product. It is also possible to provide a vacuum pump to reduce the pressure at which the low-pressure exhaust is rejected to thus improve the performance of the PSA system 72. The average hydrogen purity may be controlled by varying the rate with which the beds in the PSA system 72 are purged. This rate of purging may be controlled via a feedback loop of the present invention which is described herein. The PSA product outlet may optionally be provided with a gas composition sensor 70 for use in the control of the system.

The low-pressure purged gases from the PSA system 72 are fed to the catalytic combustor 78, where they are mixed with the process air which is compressed by the feed compressor 76, and heated by the reformate in the cold side of the water-gas shift reactor 64. The catalytic combustor is provided with an inlet end and an outlet end, with a means of preheat or ignition, a charge of combustion catalyst, and an outlet temperature sensor. The flowrate of air delivered by the feed compressor 76 is regulated such that the temperature of the combusted mixture does not exceed the maximum temperature allowed by the metallurgy of the steam reformer. The strategy for this control is disclosed later in this document. The system is also provided with an auxiliary fuel metering valve 82, which may deliver low-pressure fuel as shown, or may be required to deliver pressurized fuel, to match the pressure utilized in the combustion loop. This valve may be used to deliver fuel during system startup, and to augment the low-pressure reject fuel gas from the PSA system 72 if it is insufficient to supply the steam reformer heat requirements.

The hot combustion product is delivered to the hot side of the steam reformer 60, where it is cooled in exchanging heat with the reformate. It then flows through the water preheater 84 to transfer heat for the purpose of vaporizing the reactants. After leaving the water preheater 84, the combustion product is sufficiently cooled to be exhausted to the atmosphere. This exhaust may be unrestricted, flow through a back-pressure regulator, or flow through a gas turbine or

other work recovering device. Such modifications are included within the scope of the present invention.

Referring to Figure 6, the preferred embodiment of the temperature control scheme for the reactor-combustor system is shown. The control scheme employs a minimum of two temperature sensors shown in Figure 5, the first temperature sensor 80 in the hotter outlet stream of the catalytic combustor and the second temperature sensor 52 in the outlet stream of the colder, steam reforming side of the steam reformer. The temperatures at these two points are preferably measured at repeated intervals, and their values are compared to target values.

If the combustor outlet temperature measured by the sensor 80 is above the preset value, which is dependent upon the fuel, the steam-to-carbon ratio, the reactor pressure, and the reactor design, then the temperature of the heated reformate measured by sensor 52 is checked. If this temperature is below the minimum value consistent with proper performance, then the flowrate of air to the combustor must be increased and the cycle repeated. This change in the airflow may be affected by a variation in the compressor or blower speed, or by the application of a throttling valve. The air to fuel stoichiometry will always be fuel lean in the reformer system of the present invention in order to control the peak temperature to a safe level. If the reformate temperature is above the minimum temperature, the flowrate of the auxiliary fuel must be checked. If this flowrate is zero, then the air flowrate must be increased and the cycle restarted. If the flowrate of auxiliary fuel is not zero, then the flowrate should be decreased and the cycle restarted.

If the combustor outlet temperature does not exceed the maximum temperature, then the reformate temperature must be checked. If the reformate temperature is above the minimum value, then all is well and no changes are required. The control system will then continue to cycle until something disturbs the steady-state condition. If, however, the reformate temperature is below the minimum value, the flowrate of auxiliary fuel must be increased and the cycle repeated.

Other control strategies which achieve the twin aims of maintaining a maximum temperature in the combustion product and a minimum temperature in the reformate will be apparent to one skilled in the art. Modifications to the control strategy of Figure 6 designed to improve the response of the system or to reduce oscillations about the steady state condition may also be envisioned. These alternative and modified control strategies are encompassed within the scope of the present invention.

Figure 7 presents a preferred example of a feedback control strategy for the PSA subsystem based upon the signal from a carbon monoxide sensor. If the carbon monoxide sensor detects a concentration above the maximum value, the purge rate for the PSA system is increased and the control cycle is repeated. If the carbon monoxide concentration is below the maximum value, and above the minimum value, then no action is taken and the control cycle repeats. If the value is below the minimum value then the purge rate is decreased and the control cycle repeats. The minimum contaminant concentration is determined by minimum allowable system efficiency, as running at arbitrarily high purge rates will greatly reduce hydrogen recovery and thus system thermodynamic efficiency. As noted previously, the example of carbon monoxide,

though particularly suitable for fuel cell applications, is not limiting. Feedback control based upon the exit concentrations of other gases may also be employed, and is within the scope of the present invention.

The improved hydrogen generation system of the present invention has many advantages compared to conventional systems, especially for applications requiring less than one ton per day of hydrogen. Preferably, the present invention is used in a reactor system producing less than 1 ton per day of hydrogen, more preferably less than 7/8 ton per day, and most preferably less than 3/4 ton per day.

The improved system of the present invention eliminates partial oxidation of the fuel, sulfur removal (via hydrodesulfurization or other processes), and low temperature water-gas shift. These simplifications reduce system cost relative to conventional systems by eliminating components. It also improves safety and durability by reducing the number of interconnections which may develop leaks in service.

The improved system of the present invention is capable of quicker and simpler startup from a cold or idle condition. This is due to several factors, including the reduced mass of the present system due to the elimination of many components as well as the fact that the rugged catalysts employed in the system of the present invention are insensitive to fuel impurities which require bypassing the feed in conventional systems until full operating temperature is attained. The startup is further simplified as the rugged catalysts do not require inert purging during startup. The rugged catalysts of the present invention also do not require special precautions on shutdown such as inert purging. This simplifies the design of the system further, thus reducing cost and improving safety.

The improved system of the present invention preferably operates in a pressure regime where suitable pressurization equipment is commercially-available and very inexpensive. Conventional systems operate either at low pressure in the steam reformer, with subsequent compression of the reformate product at high cost and complexity, or at very high pressures where small-scale compression equipment is not readily available.

The improved system of the present invention preferably employs active control of the reactor peak temperature. This temperature is limited to a value consistent with extended operation of the reformer. In conventional systems, the peak gas temperatures were often above an acceptable service temperature of the reactor structure, and if any upset in the endothermic catalytic reaction took place the structure might be badly overheated.

Any embodiment of the hydrogen production system of the present invention may be implemented on a computer system. Figure 8 illustrates a preferred computer system 801 upon which an embodiment of the present invention may be implemented. The computer system 801 includes a bus 802 or other communication mechanism for communicating information, and a processor 803 coupled with the bus 802 for processing the information. The computer system 801 also includes a main memory 804, such as a random access memory (RAM) or other dynamic storage device (e.g., dynamic RAM (DRAM), static RAM (SRAM), and synchronous DRAM (SDRAM)), coupled to the bus 802 for storing information and instructions to be executed by processor 803. In addition, the main memory 804 may be used for storing

temporary variables or other intermediate information during the execution of instructions by the processor 803. The computer system 801 further includes a read only memory (ROM) 805 or other static storage device (e.g., programmable ROM (PROM), erasable PROM (EPROM), and electrically erasable PROM (EEPROM)) coupled to the bus 802 for storing static information and instructions for the processor 803.

The computer system 801 also includes a disk controller 806 coupled to the bus 802 to control one or more storage devices for storing information and instructions, such as a magnetic hard disk 807, and a removable media drive 808 (e.g., floppy disk drive, read-only compact disc drive, read/write compact disc drive, compact disc jukebox, tape drive, and removable magneto-optical drive). The storage devices may be added to the computer system 801 using an appropriate device interface (e.g., small computer system interface (SCSI), integrated device electronics (IDE), enhanced-IDE (E-IDE), direct memory access (DMA), or ultra-DMA).

The computer system 801 may also include special purpose logic devices (e.g., application specific integrated circuits (ASICs)) or configurable logic devices (e.g., simple programmable logic devices (SPLDs), complex programmable logic devices (CPLDs), and field programmable gate arrays (FPGAs)).

The computer system 801 may also include a display controller 809 coupled to the bus 802 to control a display 810, such as a cathode ray tube (CRT), for displaying information to a computer user. The computer system includes input devices, such as a keyboard 811 and a pointing device 812, for interacting with a computer user and providing information to the processor 803. The pointing device 812, for example, may be a mouse, a trackball, or a pointing stick for communicating direction information and command selections to the processor 803 and for controlling cursor movement on the display 810. In addition, a printer may provide printed listings of the data structures/information shown in Figures 3 and 4, or any other data stored and/or generated by the computer system 801.

The computer system 801 performs a portion or all of the processing steps of the invention in response to the processor 803 executing one or more sequences of one or more instructions contained in a memory, such as the main memory 804. Such instructions may be read into the main memory 804 from another computer readable medium, such as a hard disk 807 or a removable media drive 808. One or more processors in a multi-processing arrangement may also be employed to execute the sequences of instructions contained in main memory 804. In alternative embodiments, hard-wired circuitry may be used in place of or in combination with software instructions. Thus, embodiments are not limited to any specific combination of hardware circuitry and software.

As stated above, the computer system 801 includes at least one computer readable medium or memory for holding instructions programmed according to the teachings of the invention and for containing data structures, tables, records, or other data described herein. Examples of computer readable media are compact discs, hard disks, floppy disks, tape, magneto-optical disks, PROMs (EPROM, EEPROM, flash EPROM), DRAM, SRAM, SDRAM, or any other magnetic medium, compact discs (e.g., CD-ROM), or any other optical medium,

punch cards, paper tape, or other physical medium with patterns of holes, a carrier wave (described below), or any other medium from which a computer can read.

Stored on any one or on a combination of computer readable media, the present invention includes software for controlling the computer system 801, for driving a device or devices for implementing the invention, and for enabling the computer system 801 to interact with a human user (e.g., print production personnel). Such software may include, but is not limited to, device drivers, operating systems, development tools, and applications software. Such computer readable media further includes the computer program product of the present invention for performing all or a portion (if processing is distributed) of the processing performed in implementing the invention.

The computer code devices of the present invention may be any interpretable or executable code mechanism, including but not limited to scripts, interpretable programs, dynamic link libraries (DLLs), Java classes, and complete executable programs. Moreover, parts of the processing of the present invention may be distributed for better performance, reliability, and/or cost.

The term "computer readable medium" as used herein refers to any medium that participates in providing instructions to the processor 803 for execution. A computer readable medium may take many forms, including but not limited to, non-volatile media, volatile media, and transmission media. Non-volatile media includes, for example, optical, magnetic disks, and magneto-optical disks, such as the hard disk 807 or the removable media drive 808. Volatile media includes dynamic memory, such as the main memory 804. Transmission media includes coaxial cables, copper wire and fiber optics, including the wires that make up the bus 802. Transmission media also may also take the form of acoustic or light waves, such as those generated during radio wave and infrared data communications.

Various forms of computer readable media may be involved in carrying out one or more sequences of one or more instructions to processor 803 for execution. For example, the instructions may initially be carried on a magnetic disk of a remote computer. The remote computer can load the instructions for implementing all or a portion of the present invention remotely into a dynamic memory and send the instructions over a telephone line using a modem. A modem local to the computer system 801 may receive the data on the telephone line and use an infrared transmitter to convert the data to an infrared signal. An infrared detector coupled to the bus 802 can receive the data carried in the infrared signal and place the data on the bus 802. The bus 802 carries the data to the main memory 804, from which the processor 803 retrieves and executes the instructions. The instructions received by the main memory 804 may optionally be stored on storage device 807 or 808 either before or after execution by processor 803.

The computer system 801 also includes a communication interface 813 coupled to the bus 802. The communication interface 813 provides a two-way data communication coupling to a network link 814 that is connected to, for example, a local area network (LAN) 815, or to another communications network 816 such as the Internet. For example, the communication interface 813 may be a network interface card to attach to any packet switched LAN. As another example, the communication interface 813 may be an asymmetrical digital subscriber line

(ADSL) card, an integrated services digital network (ISDN) card or a modem to provide a data communication connection to a corresponding type of communications line. Wireless links may also be implemented. In any such implementation, the communication interface 813 sends and receives electrical, electromagnetic or optical signals that carry digital data streams representing various types of information.

The network link 814 typically provides data communication through one or more networks to other data devices. For example, the network link 814 may provide a connection to a another computer through a local network 815 (e.g., a LAN) or through equipment operated by a service provider, which provides communication services through a communications network 816. In preferred embodiments, the local network 814 and the communications network 816 preferably use electrical, electromagnetic, or optical signals that carry digital data streams. The signals through the various networks and the signals on the network link 814 and through the communication interface 813, which carry the digital data to and from the computer system 801, are exemplary forms of carrier waves transporting the information. The computer system 801 can transmit and receive data, including program code, through the network(s) 815 and 816, the network link 814 and the communication interface 813.

The mechanisms and processes set forth in the present description may be implemented using a conventional general purpose microprocessor programmed according to the teachings in the present specification, as will be appreciated to those skilled in the relevant art(s). Appropriate software coding can readily be prepared by skilled programmers based on the teachings of the present disclosure, as will also be apparent to those skilled in the relevant art(s).

The present invention thus also includes a computer-based product which may be hosted on a storage medium and include instructions which can be used to program a computer to perform a process in accordance with the present invention. This storage medium can include, but is not limited to, any type of disk including floppy disks, optical disks, CD-ROMs, magneto-optical disks, ROMs, RAMs, EPROMs, EEPROMs, flash memory, magnetic or optical cards, or any type of media suitable for storing electronic instructions.

Preferred embodiments of the invention are listed below:

A. A system for the production of hydrogen from hydrocarbon fuel such as natural gas, propane, naphtha, and other hydrocarbons low in sulfur content (< 100 ppm sulfur by mass); wherein the product hydrogen is made substantially pure (>99.99%) by separating impurities using a pressure swing adsorption (PSA) system, wherein no pretreatment of the fuel feed to the steam reformer by the removal of sulfur and molecular oxygen is carried out.

B. The hydrogen production system of A wherein the steam-reforming catalyst is insensitive to sulfur and molecular oxygen, preferably the catalyst active metal comprises one or more of the following group VIIIB metals singly or in combination; ruthenium, iridium, rhodium, platinum and palladium supported upon a high area ceramic support.

C. The hydrogen production system of A wherein the operation of the system is in a mesobaric regime, between 4 and 18 atmospheres, more preferably the pressure is between 5 atm and 15 atm, most preferably the pressure is between 10 atm and 15 atm.

D. The hydrogen production system of A wherein feedback control is employed for the delivery of fuel and or air to a catalytic combustor in proportion such that the peak temperature of the gases entering the primary steam reformer does not exceed a safe maximum temperature determined by the metallurgy of the steam reformer.

E. The hydrogen production system of A where no low temperature water-gas shift reactor is employed, wherein the exit temperature of the high temperature water-gas shift reactor employed is preferably above 200°C, more preferably the temperature is greater than 250°C and less than 400°C , most preferably the temperature is greater than 275°C and less than 350°C.

F. The hydrogen production system of A wherein feedback control of product carbon monoxide, or other impurity, concentration is employed.

G. The hydrocarbon production system of A wherein the pretreatment includes at least one selected from the group including partial oxidation, hydrodesulfurization, adsorption, and absorption.

I. A hydrogen production method, which includes the catalytic steam reforming and subsequent high temperature water-gas shift of low-sulfur (< 100ppm by mass) hydrocarbon fuels to produce hydrogen followed by hydrogen purification with pressure swing adsorption (PSA).

Having now fully described the invention, it will be apparent to one of ordinary skill in the art that many changes and modifications may be made thereto, without departing from the spirit or scope of the invention as set forth herein.

It is therefore to be understood that within the scope of the appended claims, the invention may be practiced otherwise than as specifically described herein.

U.S. Provisional Application No. 60/214,737, filed June 29, 2000, is hereby incorporated by reference in its entirety, the same as if set forth at length.

The entire contents of each of the above-mentioned patents, references and published applications is hereby incorporated by reference, the same as if set forth at length.

CLAIMS:

1. A reactor, comprising:

a unitary shell assembly having an inlet and an outlet;

a flow path extending within said shell assembly from said inlet to said outlet, said flow path having a steam reformer section with a first catalyst and a water-gas shift reactor section with a second catalyst, said steam reformer section being located upstream of said water-gas shift reactor section;

a heating section within said shell assembly and configured to heat said steam reformer section; and

a cooling section within said shell assembly and configured to cool said water-gas shift reactor section.

2. The reactor of Claim 1, wherein said flow path includes a preheat section located upstream of said steam reformer section.

3. The reactor of Claim 2, wherein said preheat section includes a packing material.

4. The reactor of Claim 3, wherein said packing material is a sulfur absorbent bed.

5. The reactor of Claim 1, wherein said flow path includes an adiabatic water-gas shift reactor section located downstream of said water-gas shift reactor section.

6. The reactor of Claim 1, wherein:
said steam reformer section and said water-gas shift reactor section are formed of an array of tubes;
said flow path includes an inlet tube header located upstream of said steam reformer section; and
said flow path includes an outlet tube header located downstream of said water-gas shift reactor section.

7. The reactor of Claim 6, wherein the interior of the tubes is provided with a catalyst in the form of at least one selected from the group consisting of a coating, a monolith, a loose packing of pellets, extrudates, and mixtures thereof.

8. The reactor of Claim 1, wherein said shell assembly includes:
a means of thermal expansion relief;
at least one inlet to said cooling section configured to receive a cooling medium; and
at least one outlet for said cooling section.

9. The reactor of Claim 8, wherein said shell assembly includes:
at least one inlet to said heating section configured to receive a heating medium; and
at least one outlet for said heating section.

10. The integral reactor of Claim 6, wherein said tubes in said array of tubes have an exterior surface configured to aid heat transfer between said heating section and said steam reformer section, and between said cooling section and said water-gas shift reactor section.

11. The reactor of Claim 10, wherein said exterior surface of said tubes are configured with at least one configuration selected from the group consisting of twisted tubes, finned tubes, rifled tubes, plate fins, loose packing material, and combinations thereof.

12. The reactor of Claim 6, further comprising baffles within said shell assembly and provided exterior of said tubes, said baffles being configured to force a heat transfer medium flowing outside said tubes across the array of tubes in a direction substantially normal to a longitudinal axis of said tubes.

13. The reactor of Claim 12, wherein said baffles have a modified surface area.

14. The reactor of Claim 1, further comprising a catalytic burner configured to heat at least one of a heating medium provided within said heating section and a cooling medium provided within said cooling section.

15. The reactor of Claim 14, wherein said catalytic burner is provided within said shell assembly.

16. The reactor of Claim 14, wherein said catalytic burner includes at least one inlet for fuel delivery.

17. The reactor of Claim 14, wherein said catalytic burner includes at least one selected from the group consisting of a means for mixing fuel and heated air, a means for preheating and/or igniting, at least one temperature sensor, and combinations thereof.

18. The reactor of Claim 1, wherein said first catalyst is substantially resistant to poisoning by sulfur and molecular oxygen.

19. The reactor of Claim 1, wherein said second catalyst is substantially resistant to poisoning by sulfur.

20. The reactor of Claim 1, further comprising:

an insulation assembly provided on at least a portion of an exterior of said shell assembly; and

an outer housing provided on an exterior of said insulation assembly.

21. The reactor of Claim 1, further comprising a second flow path defined by said cooling section and said heating section, wherein said cooling section and said heating section are fluidly connected.

22. The reactor of Claim 1, wherein said unitary shell assembly is a pressurized shell assembly.

23. The reactor of Claim 1, wherein said unitary shell assembly is a gas-tight shell assembly.

24. The reactor of Claim 1, wherein said shell assembly further comprises an insulating layer.

25. The reactor of Claim 24, wherein said insulating layer is contiguous or non-contiguous.

26. The reactor of Claim 1, wherein said first and second catalysts are the same or different.

27. The reactor of Claim 1, wherein said first catalyst is in admixture with said second catalyst.

28. The reactor of Claim 1, wherein said second catalyst is in admixture with said first catalyst.

29. The reactor of Claim 1, wherein said shell assembly comprises a plurality of inlets.

30. The reactor of Claim 1, wherein said shell assembly comprises a plurality of outlets.

31. The reactor of Claim 1, wherein said shell assembly comprises a tube-side and a shell-side.

32. The reactor of Claim 31, wherein said tube-side forms a continuous pressure vessel.

33. A reactor for the production of hydrogen from at least one selected from the group consisting of natural gas, propane, liquefied petroleum gas, alcohols, naphtha, hydrocarbon fuels and mixtures thereof, said reactor comprising:

a unitary shell assembly having an inlet and an outlet;

a flow path extending within said shell assembly from said inlet to said outlet, said flow path including a convectively-heated catalytic steam reformer and a convectively-cooled water-gas shift reactor.

34. A method for producing hydrogen, comprising the step of:

feeding at least one fuel selected from the group consisting of natural gas, propane, liquefied petroleum gas, alcohols, naphtha, hydrocarbon fuels and mixtures thereof, into a reactor comprising a unitary shell assembly having an inlet and an outlet, and a flow path extending within the shell assembly from the inlet to the outlet, the flow path comprising a convectively-heated catalytic steam reformer and a convectively-cooled water-gas shift reactor, whereby hydrogen is produced.

35. A method for producing hydrogen from at least one fuel selected from the group consisting of hydrocarbon fuel, natural gas, propane, naphtha, hydrocarbons with < 100 ppm sulfur by mass, and mixtures thereof, comprising:

producing hydrogen by steam reforming said fuel; and

substantially purifying said hydrogen with a pressure swing adsorption (PSA) system;

wherein prior to said producing, no pretreatment of said fuel to remove at least one impurity selected from the group consisting of sulfur and molecular oxygen and mixtures therof is carried out.

36. The method of Claim 35, wherein said steam reforming comprises a steam-reforming catalyst, and wherein said steam-reforming catalyst is insensitive to sulfur and molecular oxygen.

37. The method of Claim 36, wherein said steam-reforming catalyst comprises a catalytically active metal selected from the group consisting of group VIIIB metals, ruthenium, iridium, rhodium, platinum, palladium and mixtures thereof supported upon a ceramic support.

38. The method of Claim 35, which is carried out at a pressure of between 4 and 18 atmospheres.

39. The method of Claim 35, further comprising a feedback control loop for delivering said fuel or air or both to said steam reforming and for controlling a temperature of said fuel or air or both.

40. The method of Claim 35, which does not comprise a low temperature water-gas shift reaction.

41. The method of Claim 40, further comprising, prior to said purifying and subsequent to said steam reforming, a high temperature water-gas shift reaction, and wherein an exit temperature of a product exiting said high temperature water-gas shift reaction is above 200°C.

42. The method of Claim 35, wherein said reforming produces carbon monoxide or at least one impurity or both, and wherein said method further comprises a feedback control loop for controlling a concentration of said carbon monoxide or said impurity or both.

43. The method of Claim 35, wherein said pretreatment is at least one selected from the group consisting of partial oxidation, hydrodesulfurization, adsorption, absorption, and combinations thereof.

Figure 1a

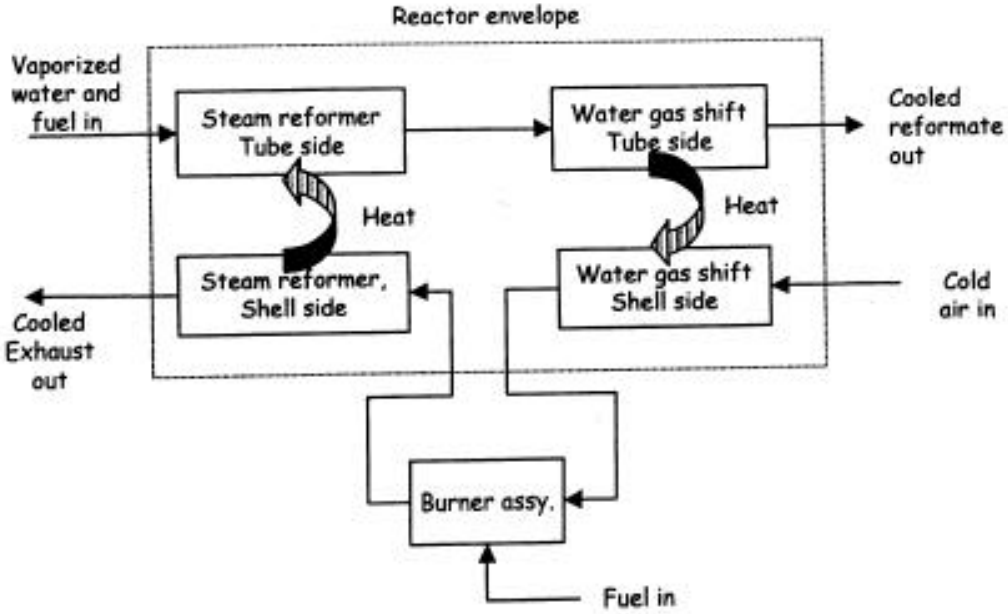
Reactor envelope
Vaporized water and fuel in
Steam reformer Tube side
Water gas shift Tube side
Cooled reformate out
Heat
Heat
Steam reformer, Shell side
Water gas shift Shell side
Cold air in
Cooled Exhaust out
Burner assy.
Fuel in

Figure 1b

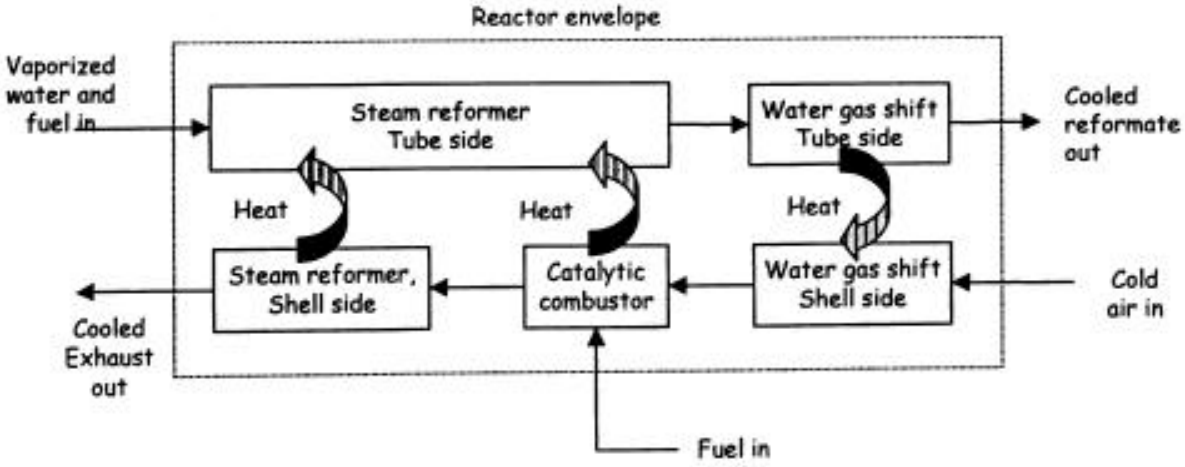
Reactor envelope
Vaporized water and fuel in
Steam reformer Tube side
Water gas shift Tube side
Cooled reformate out
Heat
Heat
Heat
Steam reformer, Shell side
Catalytic combustor
Water gas shift Shell side
Cold air in
Cooled Exhaust out
Fuel in

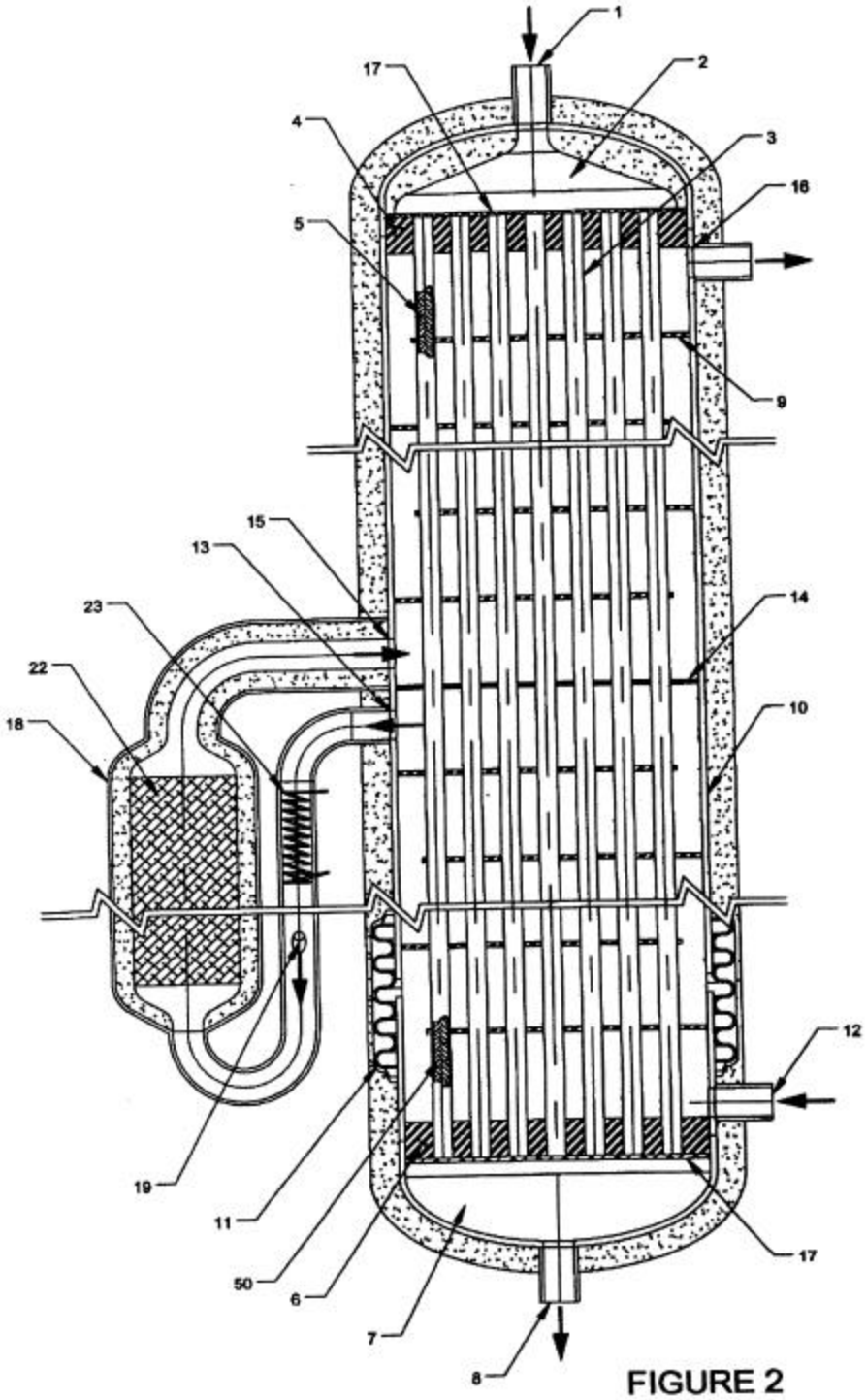

FIGURE 2

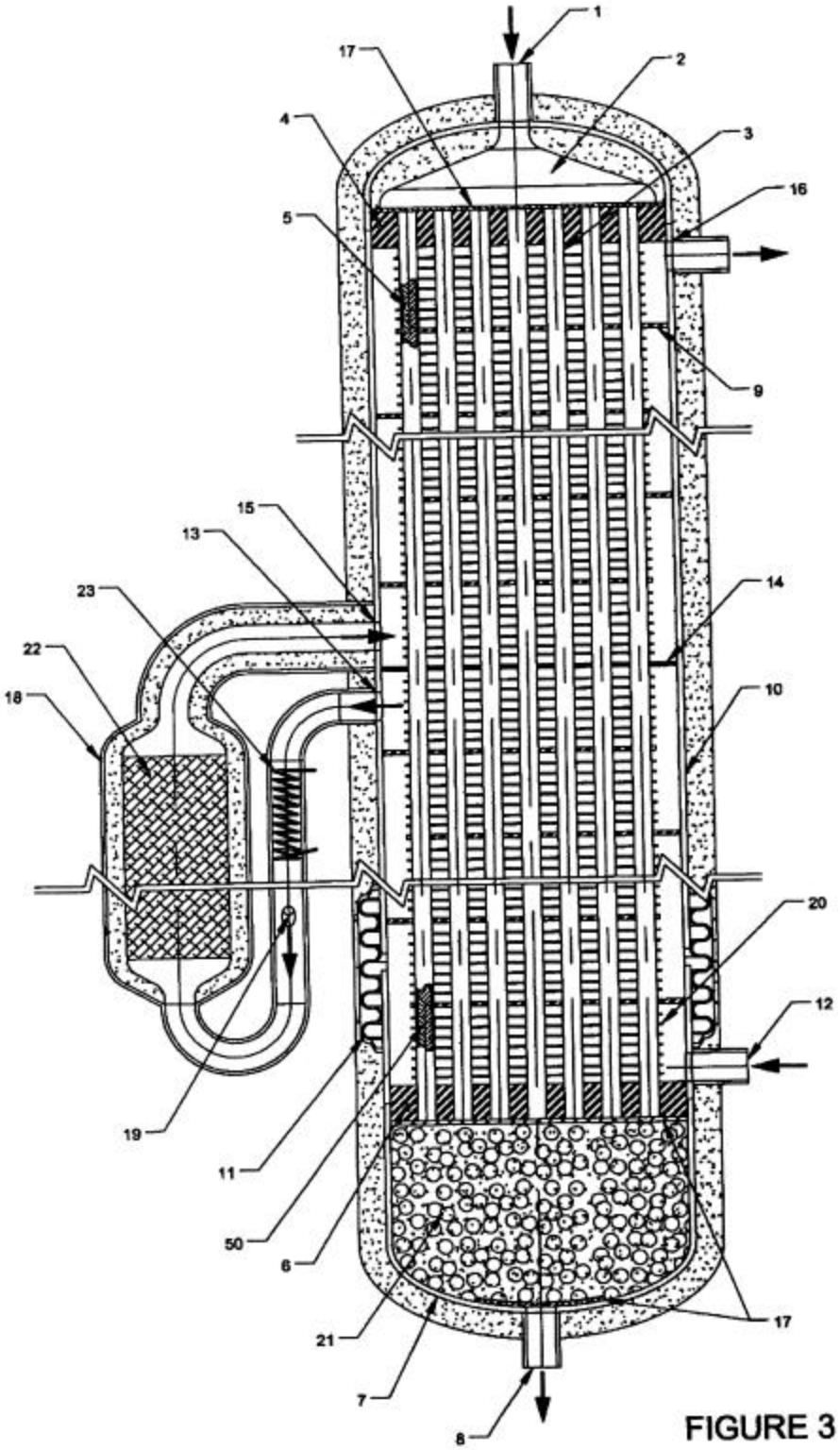

FIGURE 3

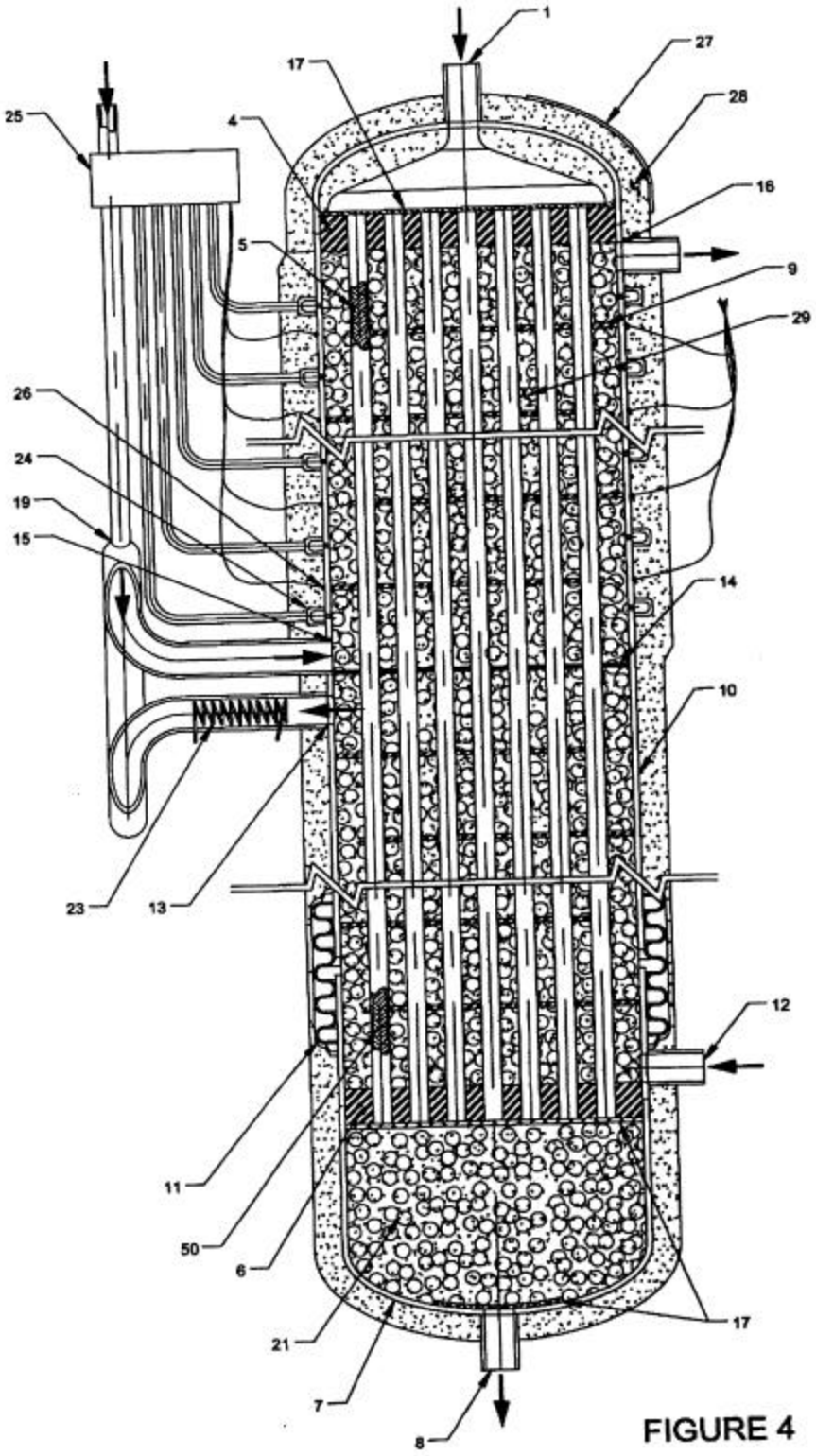

FIGURE 4

Figure 5

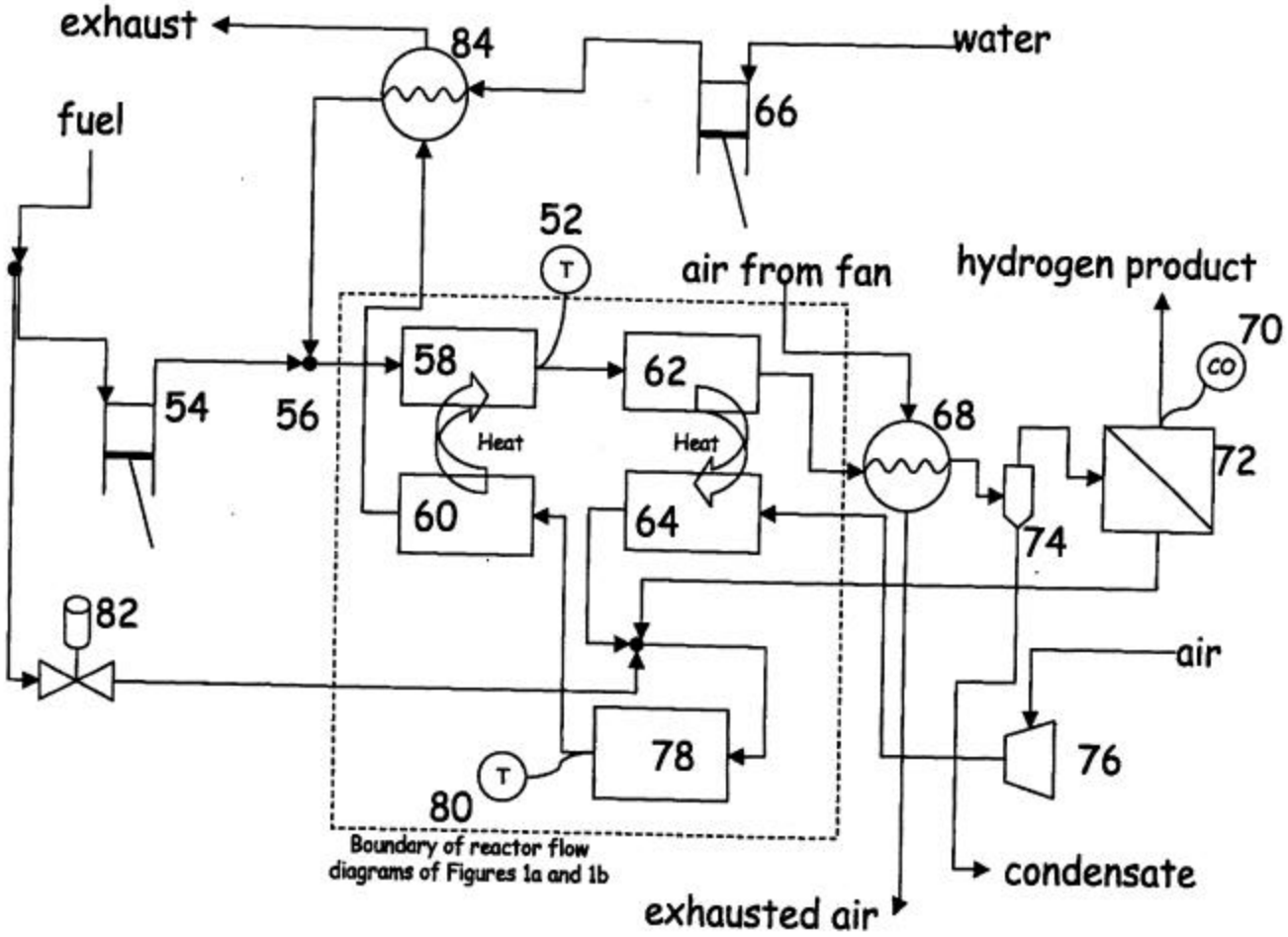
exhaust
84
water
fuel
66
52
T
air from fan
hydrogen product
70
CO
58
62
54
56
Heat
Heat
68
72
60
64
74
82
air
78
76
T
80
Boundary of reactor flow diagrams of Figures 1a and 1b
condensate
exhausted air

FIGURE 6

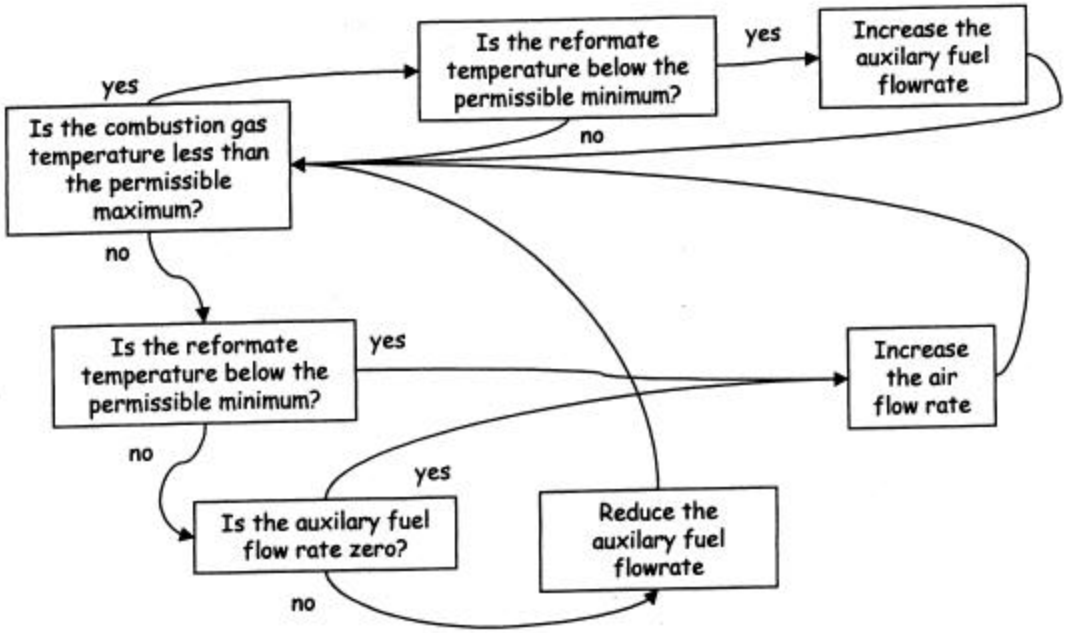
Is the reformate temperature below the permissible minimum?
yes
Increase the auxilary fuel flowrate
yes
Is the combustion gas temperature less than the permissible maximum?
no
no
Is the reformate temperature below the permissible minimum?
yes
Increase the air flow rate
no
yes
Is the auxilary fuel flow rate zero?
Reduce the auxilary fuel flowrate
no

FIGURE 7

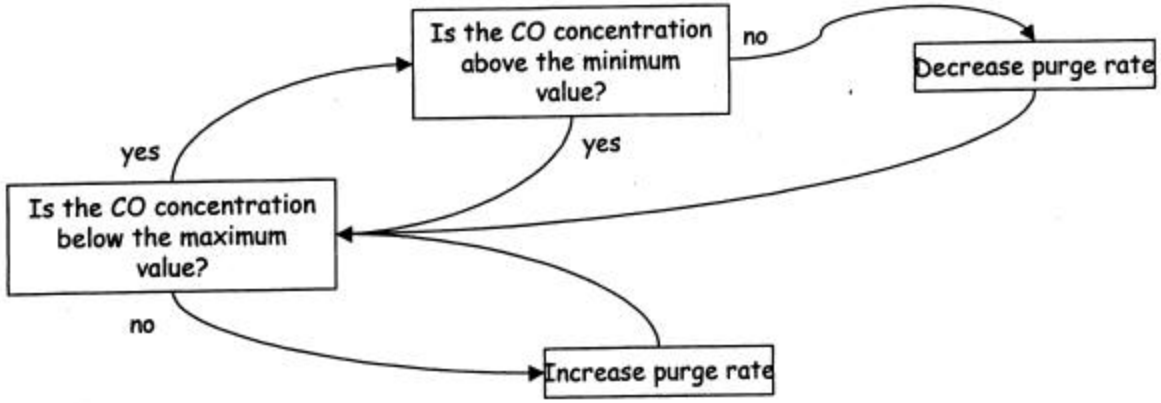
Is the CO concentration above the minimum value?
no
Decrease purge rate
yes
yes
Is the CO concentration below the maximum value?
no
Increase purge rate

FIGURE 8

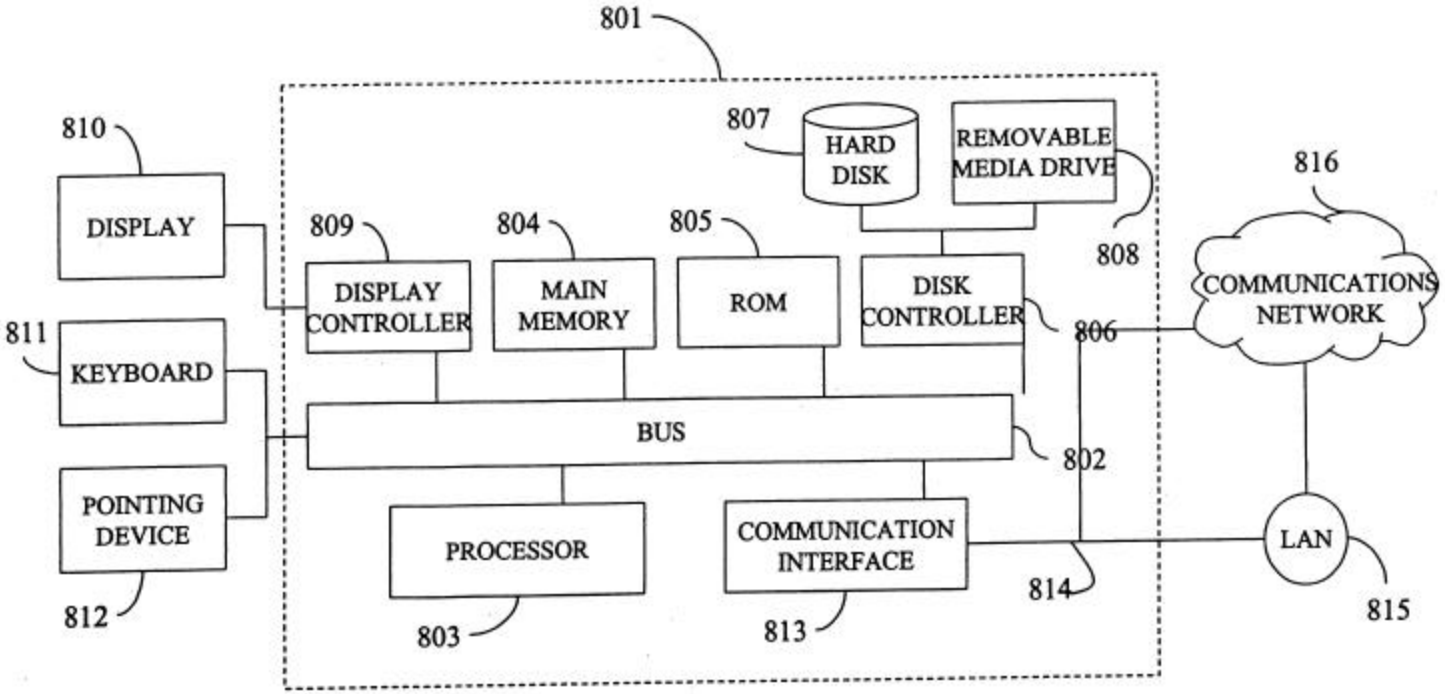
801
810
DISPLAY
807
HARD DISK
REMOVABLE MEDIA DRIVE
816
809
804
805
808
DISPLAY CONTROLLER
MAIN MEMORY
ROM
DISK CONTROLLER
COMMUNICATIONS NETWORK
811
KEYBOARD
806
BUS
802
POINTING DEVICE
PROCESSOR
COMMUNICATION INTERFACE
LAN
814
812
803
813
815

Vita

Franklin D. Lomax, Jr.

Professional Experience:

H2Gen Innovations, Inc., Arlington, VA (February 2001): Director of Development and Chief Engineer. Lead team developing manufacturable small-scale stationary hydrogen generator. Responsible for all engineering aspects of the development program.

Directed Technologies, Inc., Arlington, VA (1995 to 2001):

Principal Engineer. Led design of small-scale stationary hydrogen generator. Designed new catalysts, systems and hardware for hydrogen synthesis. Coordinated activities with partners and subcontractors. Conducted numerous DFMA studies of client prototype and pre-production hardware concepts. Evaluated client power and process systems from a feasibility and economic viability standpoint. Led joint project with Virginia Tech to develop fuel cell components with NSF and state funding.

Lead Engineer. Led design of vehicle hydrogen generator using gasoline fuel for Ford/Mobil fuel reformer development program. Designed, tested and delivered two separate classes of prototype hardware in 18 months. Cooperated with client and teaming partner employees to meet customer-driven product goals. Conducted safety analyses using FMEA techniques. Conducted manufacturability studies using DFMA techniques. Led project to develop fuel cell components.

Staff Engineer. Conducted extensive thermodynamic trade study of gasoline fuel reformer system architectures for Ford/Mobil fuel reformer development program. Designed and evaluated critical mechanical, chemical and electrochemical engineering aspects of fuel cell electric power and propulsion systems and hydrogen infrastructure. Conducted groundbreaking Design For Manufacture and Assembly (DFMA) analyses on critical system components. Prepared detailed technical evaluations of subcontractor fuel cell test results for use in downselect decision. Led development of the corporate laboratory facility. Initiated new research programs from concept definition through proposal preparation to design and fabrication of experimental apparatus.

Center for Neighborhood Technology, Chicago, IL (Summer, 1994): Research Assistant. Conducted detailed economic/technical analysis of proposed municipal incinerator retrofit in light of city-wide waste management program. Evaluated emerging recycling technologies, especially regarding wood wastes. Wrote numerous technical evaluations of proposed waste management facilities throughout Illinois/Indiana.

Princeton University Center for Energy and Environmental Studies, Princeton, NJ (Fall, 1994): Assisted in development of Advanced PRISM energy analysis software.

Education:

Virginia Polytechnic Institute and State University: M.Eng. in Mechanical Engineering with a program focus on process and power systems. Master's project, "Investigation of Steam Reformation of Natural Gas for the Very Small Scale Production of Hydrogen Fuel for Light Duty Vehicles in Appliance-type Refueling Systems."

Princeton University: B.S.E., *magna cum laude*, in Mechanical and Aerospace Engineering with a program focus in energy science. Received a Certificate in Environmental Studies. Conducted senior thesis research through the Princeton Entrepreneurial Engineering (PEP) and Environmental Studies programs, "Design of a Residential-scale, Combined Chemical and Anaerobic, Waste Treatment/Cogeneration System." Admitted to Sigma Xi scientific research society. Successfully lobbied Mechanical Engineering Department for expanded energy science curriculum.